ARRAY GEOMETRY EFFECTS ON VORTEX SHEDDING AND INSTABILITY IN HEAT EXCHANGER TUBE BUNDLES

By

MOHY ELDIN MOHAMED ELKASHLAN

B.Eng. (honors), B.Sc. Math. (honors), M.Eng.

A Thesis

Submitted to the School of Graduate Studies

in Partial Fulfilment of the Requirements

for the Degree

Doctor of Philosophy

McMaster University

VORTEX SHEDDING AND INSTABILITY IN HEAT EXCHANGERS

To my beloved family

DOCTOR OF PHILOSOPHY (1984)
(Mechanical Engineering)

McMASTER UNIVERSITY
Hamilton, Ontario

TITLE: Array Geometry Effects on Vortex Shedding and Instability in Heat Exchanger Tube Bundles

AUTHOR: Mohy Eldin Mohamed ElKashlan,

B.Eng. (honors) (Alexandria University)
B.Sc. Math. (honors) (Alexandria University)
M.Eng. (McMaster University)

SUPERVISOR: Dr. D. S. Weaver

NUMBER OF PAGES: xvi, 270

ABSTRACT

Eight tube arrays were tested to determine the effect of tube pattern and pitch on excitation phenomena in tube arrays in cross-flow. These consisted of two different pitch-to-diameter ratios for each of the four standard heat exchanger tube array configurations. Measurements of vortex shedding frequencies showed that laminar vortex shedding may occur for some tube arrays at low Reynolds numbers and is associated with very high Strouhal numbers. Some arrays showed multiple values of Strouhal numbers at moderate Reynolds numbers, and over a small range of pitch ratios. Quite good agreement is found with some of the published results. Also, an improved correlation of the existing Strouhal numbers is obtained. The effect of tube pattern and pitch on the critical flow velocities at low damping parameter was determined. The results were used with other available results to determine the variation of the reduced velocity with the damping parameter for the different arrays tested.

ACKNOWLEDGEMENTS

The author is indebted to his supervisor Dr. D. S. Weaver, for his sincere guidance during the course of this study.

Thanks are also due to Departmental technicians, Mr. Dave Schick and Mr. Frank Drieman, for their help during this work. The author further wishes to express his appreciation to Mrs. Debbie Harris for the great effort of producing this work on the word processor.

The author gratefully acknowledges the financial support of the Natural Science and Engineering Research Council under Grant A8284.

TABLE OF CONTENTS

Page

LIST OF FIGURES

Page

Page

LIST OF TABLES

LIST OF SYMBOLS

P/d	Pitch ratio.
$V_{u,p,g,gm}$	Upstream, pitch, theoretically determined gap, measured gap velocity, respectively, m/sec.
R_u	Reynolds number based on upstream flow velocity and the outside tube diameter.
f_s	shedding frequency, Hz.
$S_{u,p,g,gm}$	Strouhal number based on upstream flow velocity, pitch velocity, theoretically determined gap velocity, measured gap velocity, respectively.
RMS amplitude	Root mean square value of the amplitude, mm.
V_{cr}	Critical flow velocity, m/sec.
f	Tube natural frequency, Hz.
d	tube diameter, m.
m	Tube mass/unit tube length, kg/m.
δ	logarithmic decrement of damping.
ρ	fluid density, kg/m^3.
$\frac{V_{cr}}{fd}$	Reduced velocity parameter.
$\frac{m\delta}{\rho d^2}$	Mass damping parameter.
K	Instability factor = $(\frac{V_{cr}}{fd}) \;/\; (\frac{m\delta}{\rho d^2})^{0.5}$

CHAPTER 1

INTRODUCTION

Tube and shell heat exchangers such as steam generators, heat exchangers, steam condensers, and coolers are important parts of power and chemical process plants. Practical designs for tube arrays in such components commonly have four standard arrangements, namely: Normal square, Rotated square, Normal triangle, and Parallel triangle. The typical pitch-to-diameter ratios for these arrangements are in the range of 1.2 to 2.0.

Researchers usually divide the flow patterns depending on whether the flow is parallel to or normal to the tube axes. Most of the research in the area of flow induced vibration is more concerned with cross flow due to the destructive amplitudes of vibration which may be produced. However, at the entrance and exit nozzles, where most of the failures are reported, the incident flow direction is often far from ideal due to the presence of baffles, impingement plates, etc.

For cross flow vibrations there are four basic mechanisms:

(1) The tube vibrations result from periodic fluctuations within the flow. These fluctuations are typical of the presence of vortex shedding in the flow and with frequencies proportional to the flow velocity. Vortex

shedding may result in resonant peaks if the shedding frequency coincides with a natural frequency of the tubes.

(2) The fluctuations within the flow are turbulent in which case a behaviour associated with a randomly forced damped vibration arises. The peak tube displacements will rise if the dominant frequency in the force spectrum coincides with a natural frequency of the tubes.

(3) If the vortex shedding frequency coincides with one of the natural frequencies of the gas column in the direction perpendicular to the flow direction and the tube axis, this may result in a transverse acoustic resonance in the heat exchanger shell cavity. This will cause severe tube vibrations if the acoustic frequency is coincident with tube natural frequencies.

(4) Tube vibrations which are fluidelastic in nature and result from the interaction of the tube motion and the interstitial motions of the fluid. In this case the amplitudes of vibration will be significant and will appear at a definite natural frequency of the tube after a certain critical flow velocity. This threshold flow velocity depends upon the geometrical arrangement of the tubes in the array. It is, therefore, very important for

practical applications to determine the relationship between the threshold velocity and pitch-to-diameter ratio for different array geometries.

Flow induced vibration of the tubes may result in tube damage either by fatigue or by impact with each other or the tube supports. This problem is nowadays more common because of the trend towards higher flow velocities and the use of small diameter tubes with large spacing between supports. The severity of the damage and the high cost due to partial or total shutdowns of nuclear power plants are reported by Paidoussis [1].

Research in the area of cross flow induced vibration is expanding very rapidly. Major conferences and symposia have been held [2,3,4,5,6] with hundreds of publications, in order to understand the phenomena of flow induced vibrations in nuclear power plants. The most recent literature survey is given by Paidoussis [7]. The scatter in the published results is still very significant and many unanswered questions remain.

While the phenomenon of vortices being shed from a single cylinder and its effect on the vibratory motion of the cylinder is reasonably well understood, its existence for closely packed tube arrays is questioned, as there is no room for a vortex street, in the usual sense, to form. Owen [8] argued that vortex shedding within a closely packed tube array was impossible and postulated instead a turbulent buffeting mechanism with a peak in the frequency spectrum. Others have suggested that vortex shedding may exist for some but not all tube arrays [9]. The maps of Chen [10] and Fitz-Hugh [11] for Strouhal numbers versus tube spacings for the four standard array geometries, added more confusion. Although they collected their data mainly from the same sources large discrepancies do nevertheless exist between them [7]. Paidoussis [7] argued that the vortex shedding mechanism of Chen and Fitz-Hugh and the turbulent buffeting mechanism of Owen are the same mechanism. Recently, Zukauskas and Katinas [12] proposed formulae for calculating the Strouhal number for in-line and staggered tube arrays. The formulae were based on experimental results from normal square and normal triangular arrays. The proposed formulae do not fit all of their experimental results and other published results. Its applicability to other array geometries is not known. More recently, Murray et al. [13] recommended not to use the Fitz-Hugh maps because the collected data were based on results at resonance and were therefore not reliable.

Tube response amplitudes associated with vortex shedding resonance will likely result in a long term fretting wear and fatigue damage of the tubes at the tube supports. On the other hand, the significantly larger amplitudes associated with fluidelastic instability in tube arrays have caused mid-span leaks due to tube-to-tube clashing and extensive tube damage.

The fluidelastic stability threshold developed by Connors [14] and the extended model by Blevins [15] for a single row of tubes are used very widely as a design guide for multi-row tube arrays. Experimental investigation expanded very rapidly after Connors and Blevins in order to examine the instability for tube arrays of different geometries and spacings and fluid flows other than air [9,16-26].

The fluidelastic excitation in tube arrays is usually correlated in terms of a dimensionless velocity parameter (V/fd) and a dimensionless damping parameter ($m\delta/\rho d^2$). Weaver and Grover [19] showed that the stability boundary for a parallel triangular array is less dependent on the damping parameter than that given by Connors. On the other hand, Weaver and ElKashlan [20] found that the logarithmic decrement of damping δ and the mass ratio $m/\rho d^2$ are not linearly dependent parameters as implied by the use of the so called damping factor. A comparison between fluidelastic instabilities on a parallel triangular array by Weaver and Koroyannakis [26] in air and water flows, showed that the reduced velocity V/fd in water lies considerably below the projection of the curve from data in air. The implication is that the velocity threshold is not a simple function of the square root of the damping parameter.

The importance of the effect of other parameters such as different array geometries and spacings was raised by Hartlen [16] and Soper [17]. The scatter between their results is large. However, Hartlen claimed that his results are not very precise as the experiments were designed to produce general trends and not design data. The recently published theoretical model [27] emphasises again the importance of such parameters.

Current design approaches still rely on the use of Connors' stability formula without taking into consideration the effect of tube array pattern and pitch. The primary purpose of the present research was to study the effect of tube pattern and pitch on excitation phenomena in tube arrays in cross-flow. Two arrays with different pitch-to-diameter ratios for each of the four standard heat exchanger tube array configurations were tested. Measurements were taken for tube response as well as interstitial hot-wire data to examine the fluid mechanics. In addition to providing insights into excitation mechanisms, the results will provide a set of consistent data for evaluating theoretical models.

Although some data do exist for tube arrays of different patterns and pitches, they are inconsistent because of the use of different definitions of the critical velocity for the onset of instability and because of the different experimental equipment used. The only other systematic investigations of pattern and pitch [16], [17] were conducted at higher damping parameters than the present study and, as mentioned above, yielded inconsistent results. However, the results obtained together with those of [16] and [17] were used to determine the variation of the reduced velocity with the damping parameter for the different arrays tested. The arrays were also used to measure the vortex shedding frequencies and determine if they will result in resonance of the tubes in any of the arrays.

The data obtained in this study is used to explain some of the scatter in the published literature for both vortex shedding Strouhal numbers and fluidelastic instabilities. Also, an improved correlation of the existing Strouhal numbers is attempted.

Chapter 2 gives a summary of the available information on the excitation mechanisms of vortex shedding and fluidelastic instabilities. The equipment used for conducting the experiments of the present study is presented in Chapter 3. Descriptions of the test-section, test arrays, and their design are also given in this chapter. The experimental results obtained together with the analysis of these results can be found in Chapter 4. A comparison of the present results with those available from the literature and new vortex shedding correlations are also given in Chapter 4. The conclusions derived from the present research and its contributions are presented in Chapter 5.

It is hoped that the present research programme will develop a better understanding of both vortex shedding and fluidelastic instability phenomena for tube arrays of different patterns and pitches.

CHAPTER 2

A LITERATURE SURVEY

Fluid force components in a turbulent flow or as a result of the interaction of the flow with a structure are the source of flow induced vibrations. The phenomena of flow induced vibration are extremely complicated and have a very wide field of application. Since the problem was recognized, many conferences and symposia were held with hundreds of publications showing different mechanisms responsible for structural vibration and with recommended methods for suppressing their effects.

Of concern in this thesis is the flow induced vibration of cylindrical structures, especially those in heat-exchanger tube arrays.

Four different mechanisms can cause vibration of tubes arrays, these being due to:

1. Vortex shedding from the tubes.
2. Turbulent buffeting; the response of the system to turbulence in the flow.
3. Acoustic resonance.
4. Fluidelastic instability.

Emphasis will be on the first and last mechanisms as these are of more importance for the research conducted in this thesis.

2.1 Vortex Shedding

Vibration may be induced by the periodic force which results from the shedding of vortices in the wake of a bluff body. The nature of this vibration is of the "self-controlled" type because it is associated with periodicity in the flow. If the shedding frequency of those vortices in the wake of the structure reaches the natural frequency of the structure, the later will vibrate in resonance. The vibration is usually stronger for dense fluids like water or highly compressed gases. If this happens, the amplitude of vibration of the structure may build up to the point where it starts to control the magnitude and frequency of the fluid force components. Thus the vortex shedding will be controlled by the rythm of the tube vibration. This is the result of a dynamic feedback mechanism between the motion of the structure and the flow field. More details about this mechanism will be given later in this section.

The problem of vortex shedding has had a fairly long history. A row of vortices was first sketched in the fifteenth century by Leonardo da Vinci in the wake of a bluff body. Description of flow regimes has been summarized by Marris [28] from an earlier work by Foppl [29], Tritton [30], Roshko [31], and others. Marris also presented a survey of the available information on the problem of periodic wakes behind a cylinder and the dynamics of vortex wake flow.

The major regimes of interest for the entire range of Reynolds number are given in Figure 2.1, and obtained from Lienhard [32]. A description of the flow regimes follows.

For an isolated single cylinder at extremely low Reynolds number (<3), the streamlines close behind the cylinder and the flow follows Stokes law. A pair of fixed vortices of the type discussed by Föppl [29] are formed immediately behind the cylinder as the Reynolds number is increased to a value between 5 - 10. This pair of Föppl vortices is separted from the main body of the fluid by the vortex layers which are continuations of the laminar boundary layer of the cylinder after its separation. As the Reynolds number is increased the vortices elongate in the streamwise direction and at a Reynolds number of about 90, one of the Föppl vortices breaks away from the cylinder, leaving the other vortex attached to the cylinder. This creates a wake pressure asymmetry which causes the other vortex to leave the cylinder. This process repeats itself and the state of vortices being shed alternately in the wake is attained.

In an extensive study of the nature of the wake behind a cylinder, Roshko [31] found that for Reynolds numbers less than 150, the resulting vortices are purely viscous, the flow in such vortices is laminar, and the vortex street is preserved for many diameters downstream.

For Reynolds numbers between 150 - 300, the free vortex layers become turbulent prior to their rolling up into vortices. Thus the resulting vortices consist of turbulent fluid. The point at which transition into turbulence in the free vortex layers occurs depends on

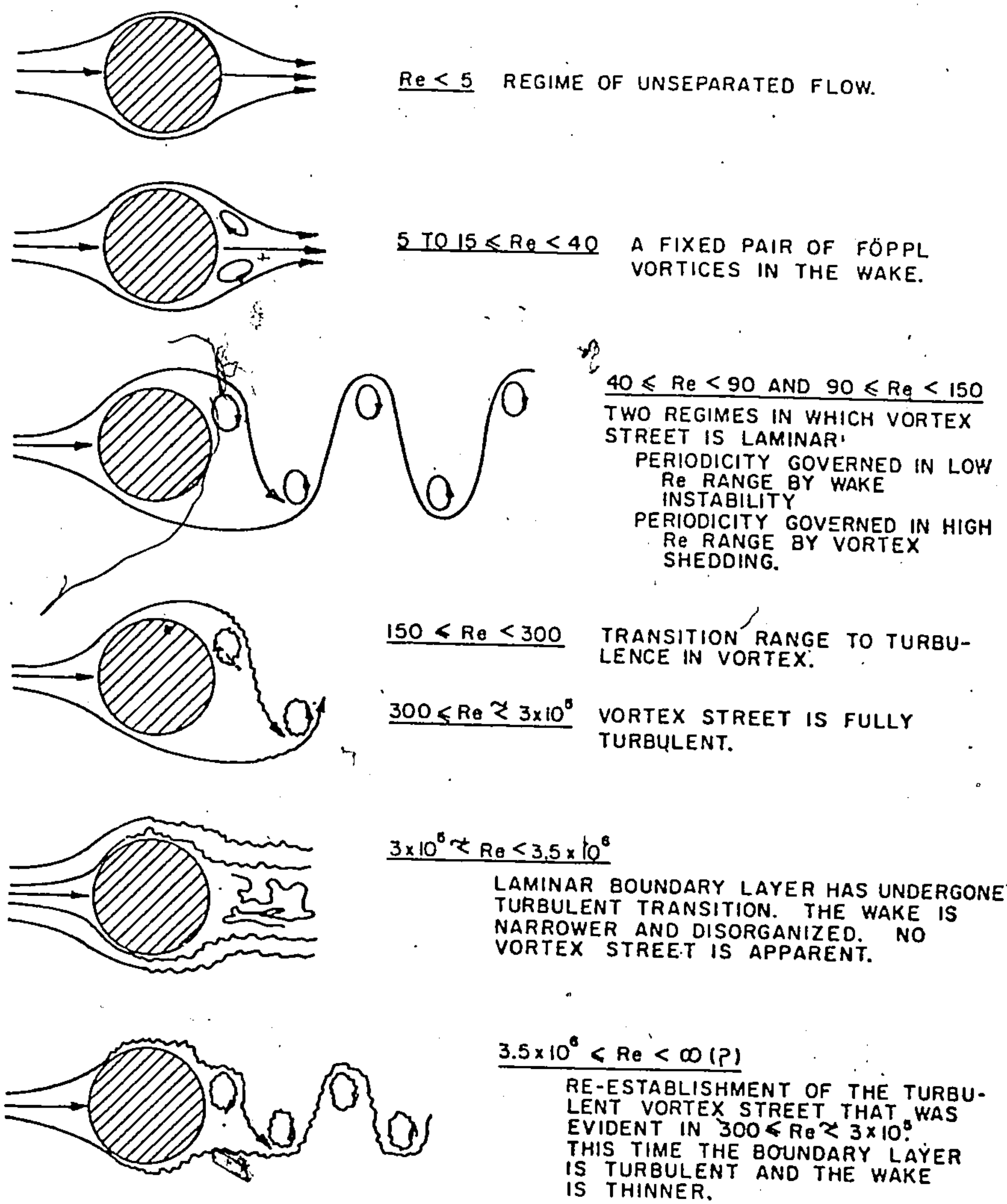

FIGURE 2.1 : FLOW REGIMES ACROSS CIRCULAR CYLINDER FROM LIENHARD [32]

the Reynolds number. This point moves upstream towards the separation point as Reynolds number increases, and at some particular Reynolds number the transition point in the vortex layer reaches the separation point on the cylinder. Roshko gives 50 diameters for the development of a completely turbulent wake.

Shedding of periodic turbulent vortices seems to continue from a Reynolds number of 300 up to about $2x10^5$. At this value, transition in the boundary layer on the cylinder itself occurs, forcing the separation point to move around the cylinder and the wake to become narrow.

Besides the drag force on the cylinder, the unstable shedding of vortices results in a lift force on the cylinder normal to the flow stream. Lienhard [32] gave an excellent summary of most of the available data for drag and lift coefficients for a single cylinder.

Bishop and Hassan [33], Gerrard [34] and Griffin [35] found that a predominantly transverse fluctuating force is exerted on the cylinder which may excite transverse vibration.

The predominant exciting frequency associated with the vortices which cause these transverse fluctuating forces may be predicted by using the Strouhal number, a dimensionless frequency defined as:

$$S = \frac{f_s d}{V}$$

where

f_s = the shedding frequency of the vortices

d = the outside diameter of the cylinder or tube

V = flow velocity

When the tube is exposed to an increasing cross flow velocity, f_s rises linearly such that S is constant. When f_s gets close to f_n, the natural frequency of the cylinder, and only if the response amplitude is sufficiently large, f_s jumps to and remains constant at f_n although the flow velocity is increasing. This phenomenon continues until f_s jumps suddenly to the value given by the constant original value of S before resonance. The range over which f_s is controlled by f_n is termed "lock-in" and demonstrates that there is a feedback mechanism in which the exciting force is controlled by the tube response. Periodic wake shedding could generate periodic forces in tube arrays if such a phenomenon were to occur.

Strouhal numbers for a single cylinder for the Reynolds number range $40 < R_e < 10^7$ are well represented by Lienhard [32] based on the earlier work by many researchers. Strouhal number increases from about 0.12 to a value of 0.2 in the Reynolds number range 40 - 300 and remains constant at this value up to Reynolds number of about $2x10^5$. For a further increase in Reynolds number, the Strouhal number starts to increase again. Relf and Simmons [36], and Fujino [37], found that Strouhal number increases due to the narrowing of the wake of the flow.

In 1946, Spivack [38], studied the effect of changing the spacing between two parallel cylinders on the vortex frequency in the wake and the gap of the two cylinders. The appearance of a second harmonic for all spacings between a gap to diameter ratio of 0 to 5 was reported. A Strouhal number between 0.2 and 0.35 rising in an approximate parabola was obtained in the gap between a gap to diameter ratio of 1 to about 0.5 respectively, followed by a sharp drop attributed to a delay of separation of vortices as the two cylinders get close together. Some of the values obtained were attributed to a jet mechanism in the gap. The Strouhal number was found to be independent of Reynolds number for Reynolds numbers greater than 15,000.

The following results were reported from Marris' paper [28] on research done by Landweber [39] for the flow between a pair of parallel cylinders. For a ratio of the distance between the cylinders to the diameter less than 0.45 a single vortex street wake results and the eddy forces cause cylinders to vibrate as a pair. For a ratio greater than 0.45 and less than 1.5 a double vortex street of alternate vortices is formed in which the vortices from the outer edge of one of the cylinders are in phase with the vortices from the inside edge of the other, and this causes the cylinders to vibrate in phase as one. For a ratio of about 1.5 a double vortex street is formed in which the vortices shed from the outer edges are in phase, and those shed from the inner edge are in phase. This spacing will cause the cylinders to vibrate 180 deg. out of phase. These conditions are valid only as long as the amplitude of vibration is small so that the cylinder motion does not effect the hydrodynamic system.

In an array of tubes, the tubes have a natural frequency f_n, and will be forced to vibrate when the exciting force fluctuates at a frequency f_s which is close to f_n. Strouhal numbers in arrays of tubes are a function of their geometry. Upon predicting both f_n and f_s, designs where these frequencies are close may be avoided.

Grotz and Arnold [40], measured for the first time systematically the vortex shedding frequencies in an in-line tube bank model with various tube spacing ratios. Their results and those of others were used to construct maps of Strouhal numbers for arrays of various geometries. However, it is believed that many of these Strouhal numbers were calculated from data in the lock-in region, and thus these numbers may be too low.

Chen [10], investigated the problem of vortex shedding to add more confirmation to a previously correlated data of his own and other authors. The results are in the form of a curve group between the Strouhal number and the transverse spacing ratio with the longitudinal ratio as a parameter for both in-line and staggered tube-banks. He expected that the formation of vortices in a column will be the faster and thus the frequency of Von Karman vortex street the higher, the shorter the longitudinal distance between two tubes in an in-line array. Also the curve for Strouhal number should rise continuously with increasing transverse spacing ratio for large longitudinal spacing ratio. He also stated that if a flow passes only an isolated single tube, the vortex force exerted on the tube is always perpendicular to the flow direction for the subcritical range of Reynolds number. The separation point of the vortex is practically at maximum span of the circular periphery of the tube, and the tube will be forced to vibrate solely in the transverse direction. But when a tube is surrounded by a series of other parallel tubes the flow streaming past it will be guided by the neighbouring ones and the separation point of vortex will be shifted downstream. The tube will no longer vibrate solely perpendicularly to the flow but also parallel to it. Curves for in-line and staggered arrays are shown in Figure 2.2.

Fitz-Hugh [11] suggested a correlation of most of the available Strouhal numbers available at that time. He also found that the fluid exciting force is neither of a discrete frequency nor it is correlated over the length of the tubes. Tube movement and acoustic resonance produce axial correlation which increase force on the tubes. The maps produced by Fitz-Hugh are shown in Figure 2.3 for staggered and in-line arrays. These maps are divided into areas of approximately constant S and represent the values published by Bauly [41], König and Gregorig [42], Putnam [43] for staggered arrays; Grotz and Arnold [40], Classen and Gregorig [44] for in-line arrays; Chen [10,45], Jaudet and Hutzler [46] for both types of arrays. Fitz-Hugh predicted that tube vibration will occur if $1/3 < f_s/f_n < 3$. He also noted, that the frequency spectrum of the exciting force may change with location in the array and may become broad.

Pettigrew et al. [47] found that, for arrays in liquid flow, lock-in or resonance occur in the first few rows for values of Strouhal numbers greater than 0.3 and less than 0.7. Also for liquid flows, Pettigrew and Gorman [9], found that the Strouhal number is different from one row to the other and it does not exist for some arrays.

However, Grover and Weaver [48] for gaseous flows observed that for Reynolds number higher than 1000, increasing turbulence intensity will suppress any discrete vortex shedding frequency, and that resonance is not a problem for arrays in gaseous flows in the

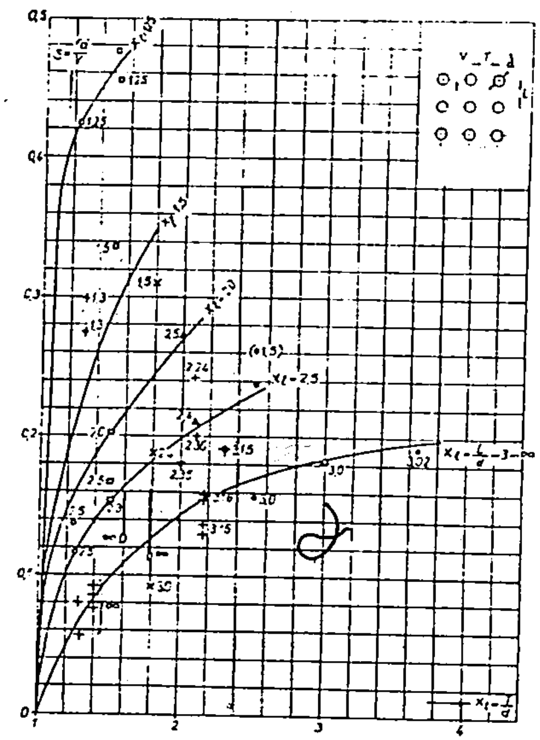

IN-LINE ARRAYS

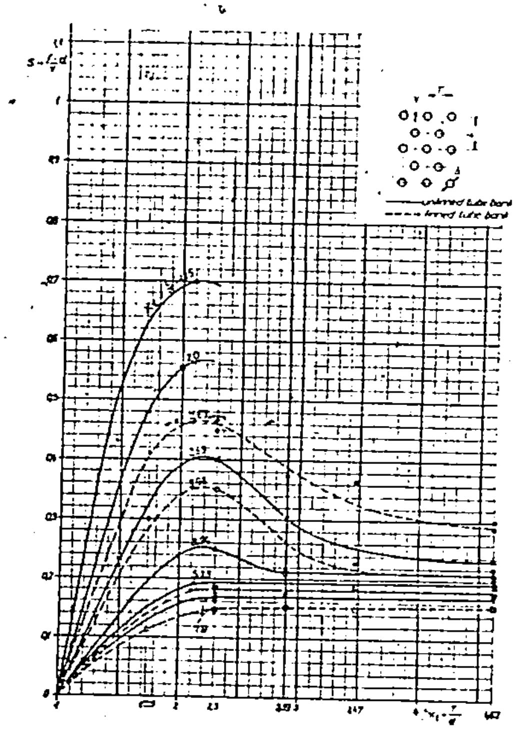

STAGGERED ARRAYS

FIGURE 2.2: CHEN'S MAPS [10] FOR STROUHAL NUMBERS

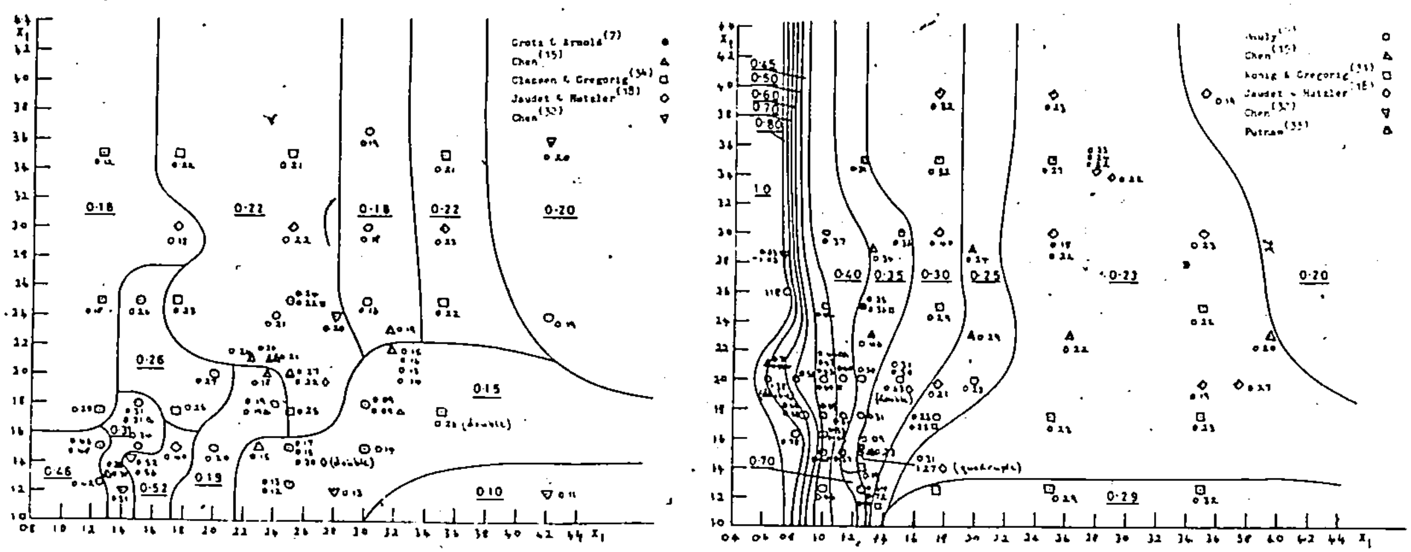

IN-LINE ARRAYS

STAGGERED ARRAYS

FIGURE 2.3: FITZ-HUGH'S MAPS [11] FOR STROUHAL NUMBERS

absence of acoustic reinforcement. Weaver and Lever [49] confirmed the above mentioned observations by Grover and Weaver.

Zukauskas and Katinas [12] studied the phenomenon on large scale models in air and liquid flows of arrays of the normal triangle and square configurations. Hot-wire measurements of the local velocity fluctuations confirmed that tubes in the first rows are subjected to low turbulence levels and uniform velocity profiles, while the inner rows are subjected to high turbulence and nonuniform velocity distributions. In the inner rows, flow turbulence is about 40% and its value is a function of pitch ratios and array geometry. The lower the pitch ratio, the higher the turbulence. Tubes in the leading rows are excited by a narrow spectra while those in the inner rows are by a wide-spectrum pressure fluctuations. Their measurements suggested the following formulae for determining the vortex shedding Strouhal number.

$$S_g = 0.2 + \exp\{ - \frac{(P/d)^{1.8}}{2.3} \}$$

for normal triangular arrays with $P/d \geq 1.15$, and

$$S_g = 0.2 + \exp\{ - \frac{(P/d)^{1.83}}{0.88} \}$$

for normal square arrays with $P/d \geq 1.15$.

Their results are shown in Figure 2.4. However, their results for Strouhal numbers in water flow are less than those in air flow for the same array, probably because of measurements taken at resonance in water flows.

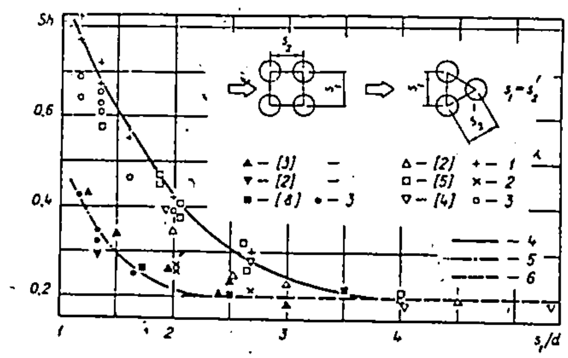

FIGURE 2.4 : ZUKAUSKAS AND KATINAS RESULTS [12]
FOR STROUHAL NUMBERS

Recently Paidoussis [7] plotted the results of Strouhal numbers from Chen [10] and Fitz-Hugh [11] maps, and pointed out that although Chen and Fitz-Hugh draw their data mostly from the same sources, large discrepancies do nevertheless exist between them. Paidoussis also plotted the results of Owen [8]; who studied turbulent buffeting excitation as it will be seen later in this section; and suggested that the vortex shedding of Chen's and Fitz-Hugh's and the buffeting of Owen's are the same exciting mechanism. His plot is shown in Figure 2.5.

Avoiding resonance due to vortex shedding excitation is usually done by keeping the natural frequency of the tube f_n away from the vortex shedding frequency f_s. Another solution is altering the flow regime around the tube so as to prevent any formation of vortices by using splitter plates, helical strakes or perforated shrouds. While these kind of solutions are practical for smoke stacks, cables, etc., they are impractical for tube arrays because of the limited space. Increasing the damping is a third possibility, so as to reduce the vibration amplitude.

While the problem of vortex shedding in tube arrays is not of a great concern for gaseous flows, it has an appreciable effect for arrays in liquid flows because of the much higher dynamic pressures. Also, it is pointed out by Weaver and Koroyannakis [26] and Weaver and Yeung [22,23] that studying these phenomena in liquid flows is rather difficult because it may be coupled with other excitation mechanisms. Weaver and Yeung [23] also predicted that tube amplitudes will be negligibly small for tube arrays with a mass damping parameter greater

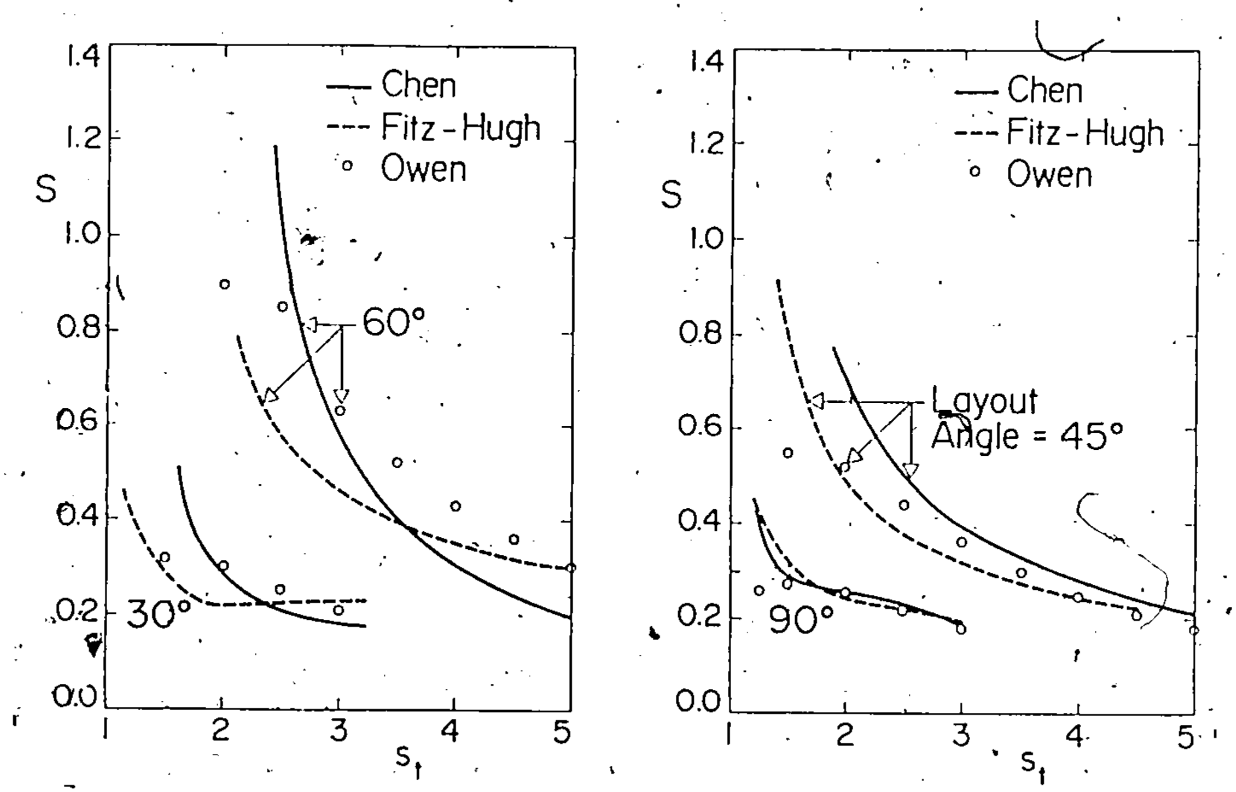

FIGURE 2.5: PAIDOUSSIS'S PLOTS [7] FOR STROUHAL NUMBERS

than 1.0, which explains why no vortex resonance is observed in air. This prediction will vary with tube pattern and P/D ratios. They showed that the Strouhal number is dependent on the approach flow direction between a square array to a rotated square array, and it does not change for triangular arrays. They also reported some cases where vorticity response was not observed at all. Cases where vorticity for some arrays was not observed were also reported in references [9,24].

However, the existence of coherent vortices in tube arrays is still not clear. In the wake of the flow exists a broad band of turbulence. As the flow passes through each row of tubes it will be faced by a resistance which ultimately will convert its pressure energy of mean motion into turbulent energy. Thus the turbulence intensity will increase as the flow moves more deep into the array. Turbulent eddies are associated with randomly fluctuating forces imposed on the tubes. A flexible array will pick-up the frequency in the turbulence which coincides with its natural frequency and amplify it especially if small damping is inherent in the system.

Turbulence buffeting excitation was studied extensively by Owen [8], who based his theory on the fact that sufficiently deep inside an array of tubes the flow is essentially turbulent. The study was for high Reynolds number. As the flow accelerates and decelerates between tube rows, Owen, from energy equilibrium between the rate of dissipation of turbulent energy and the rate at which work is done on the gas by the mean pressure gradient, found an expression for the dominant buffeting frequency in the following form:

$$\xi = \{3.05\ (1 - \frac{d}{T})^2 + 0.28\} \frac{Ud}{LT}$$

where

ξ = buffeting frequency

d = tube diameter

T = lateral tube spacing

L = distance between successive tube rows

U = Mean gas velocity between adjacent tubes

A plot between $\frac{\xi L}{U} \frac{T}{d}$ and $(1 - \frac{d}{T})^2$ with the available experimental results based on acoustic resonance data of Grotz and Arnold [40], and Hill and armstrong [50] showed a good agreement with little scatter.

Owen stated also the following rule:

> "The dominant frequency of vibrations in a bank of tubes, for which the ratio of the diameter to the lateral spacing lies between 0.2 and 0.6, is equal to the interstitial gas velocity divided by twice the distance between successive rows."

Furthermore, if the vortex shedding frequency coincides with one of natural frequencies of the gas column of the heat exchangers in the direction perpendicular to the flow direction and the tube axis, this transverse gas column will be forced to vibrate too. Vibrations of the gas column will be transfered to the outside shell of the heat exchangers and its vibration will radiate an intense noise into the surroundings. The phenomena of transverse acoustic resonance was studied extensively by Chen [10,45,51], Morse [52], Funakawa and Umakoshi [53], and Zdravkovich and Nuttall [54]. While they proposed criteria for excitation, they also recommended methods for eliminating or minimizing its effect. Chen [55] recommended the use of detuning baffles along the flow direction with a length comparable with the sound wave length, while Zdravkovich and Nuttall recommended omitting some tubes from the array to disturb the flow pattern.

2.2 Fluidelastic Instability Mechanism

Fluidelastic instability of tube arrays is a self-excited type of vibration. Oscillations of the tubes due to high velocity flow field result in periodic forces which in turn amplify the tubes' motion. Of course, these periodic forces disappear in the absence of tube motion. Instability will occur when during one vibration cycle the energy absorbed from the fluid forces exceeds the energy dissipated by damping. The flow velocity at which instability will start is termed as "critical flow velocity" or "threshold velocity".

Roberts [56] was the first to discover that self-excited vibrations occur in only the flow direction of a one row tube array. As the flow passes a pair of tubes of alternate motion in the streamwise direction a flow jet will form in the gap between the tubes. The result is a jet-switch or a tube-displacement mechanism in which the fluid forces will amplify the tube motion and result in a dynamic instability.

However, Connors [14] found that the jet-switch mechanism proposed by Roberts [56] is not the one which causes the fluidelastic instability of the tube row but rather that, as one tube starts to vibrate, it will change the flow field around it and obviously around its neighbouring tubes causing them to vibrate too. Steady state fluid force coefficients were then determined according to previously determined relative mode shapes. This together with experimental results for the single row of tubes were used by Connors to derive a semi-empirical criterion for the threshold of fluidelastic instability. The criterion was found to be dependent on the reduced velocity parameter V/fd as a linear function of the square root of the damping parameter $m\delta/\rho d^2$, in the form:

$$\frac{V}{fd} = 9.9 \left(\frac{m\delta}{\rho d^2}\right)^{1/2}$$

where

V = mean flow velocity in the gap between adjacent tubes,

f = tube natural frequency,

d = tube outside diameter,

m = virtual tube mass per unit length (the mass of the tube itself, plus the added mass of the displaced fluid),

δ = logarithmic decrement of damping of tube in still fluid, dimensionless,

and ρ = mass density of the surrounding fluid.

The stability constant 9.9 is a function of the array geometry.

Blevins [15] confirmed Connors' result, that the threshold for fluidelastic instability for a single-tube row was dependent on the reduced critical velocity parameter and the damping parameter for an extended model which includes tube stiffness and damping.

Although the stability boundary by Connors and the extended model by Blevins are used widely as a design guide for predicting the fluidelastic vibrations in heat exchangers, its validity for tube arrays has been questioned. Even the 0.5 exponent in their criterion is in doubt. New studies which include different parameters such as variable damping, mass ratios, array's layout and geometry both experimentally and theoretically have since been completed.

Tube arrays commonly used in practice have four different types of arrangements; namely: normal square, rotated square, parallel triangle, and normal triangle, see Figure 2.6.

Hartlen [16] employed soft plastic tubing for the evaluation of the stability threshold for different array patterns and with three different pitch-to-diameter ratios. His results indicated that the stability threshold for a full array lies below that for a single transverse row indicated earlier by Connors by a factor of 1.5 to 3 and are sensitive to tube pattern and pitch as shown in Figure 2.7. Even the sharpness of threshold is sensitive to tube pattern and damping as it is very sharp for rotated square and gradual for rotated triangular arrays.

The effect of changing the pitch-to-diameter ratios on fluid-elastic instabilities was also studied by Soper [17]. The scatter in the data between the two authors is significant when compared on the basis of the Connors' relationship. They did their experimental work in a different range of the mass damping parameter, and additionally, Hartlen claimed that his results are not so reliable.

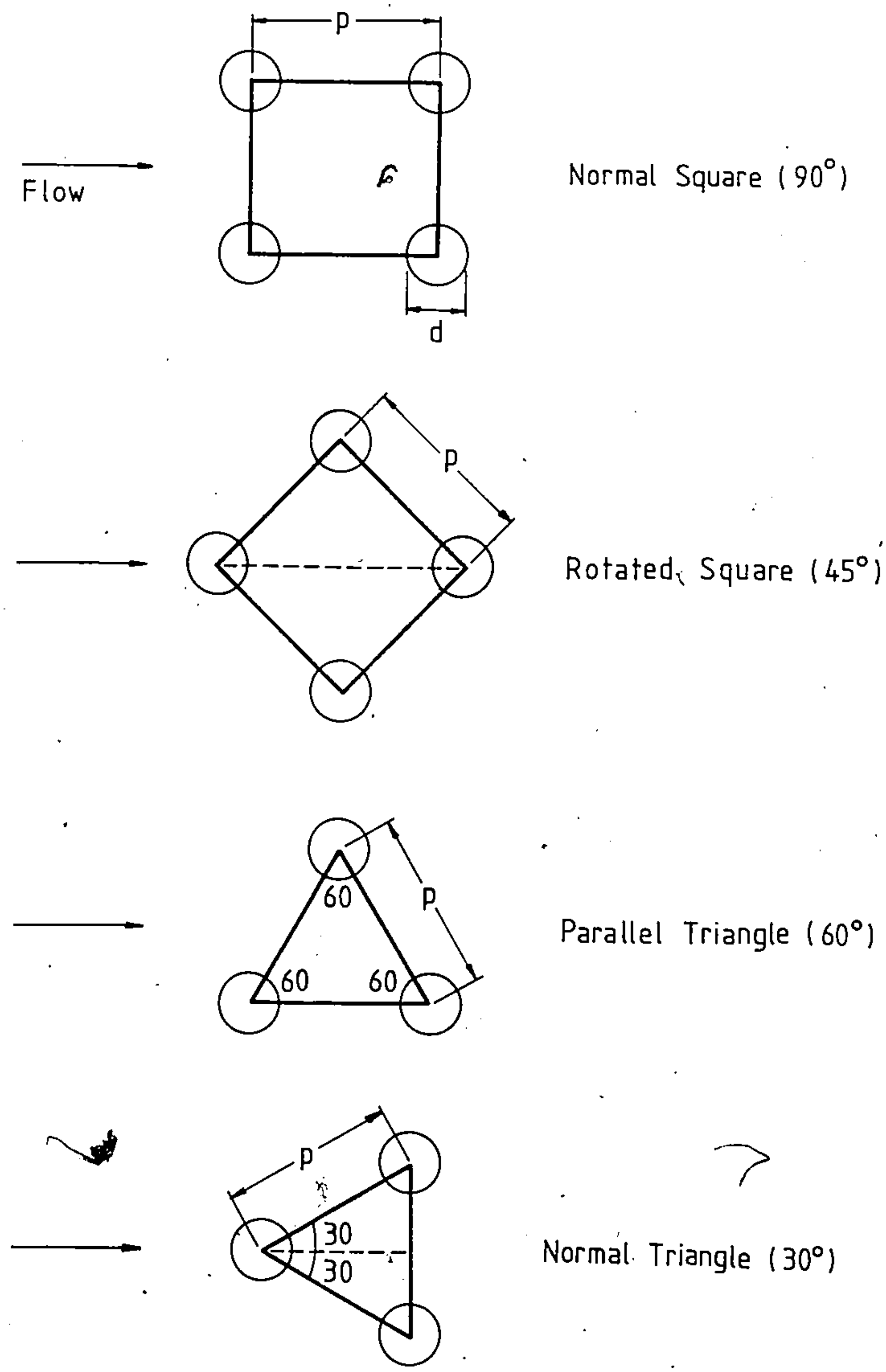

FIGURE 2.6: STANDARD ARRAY CONFIGURATIONS

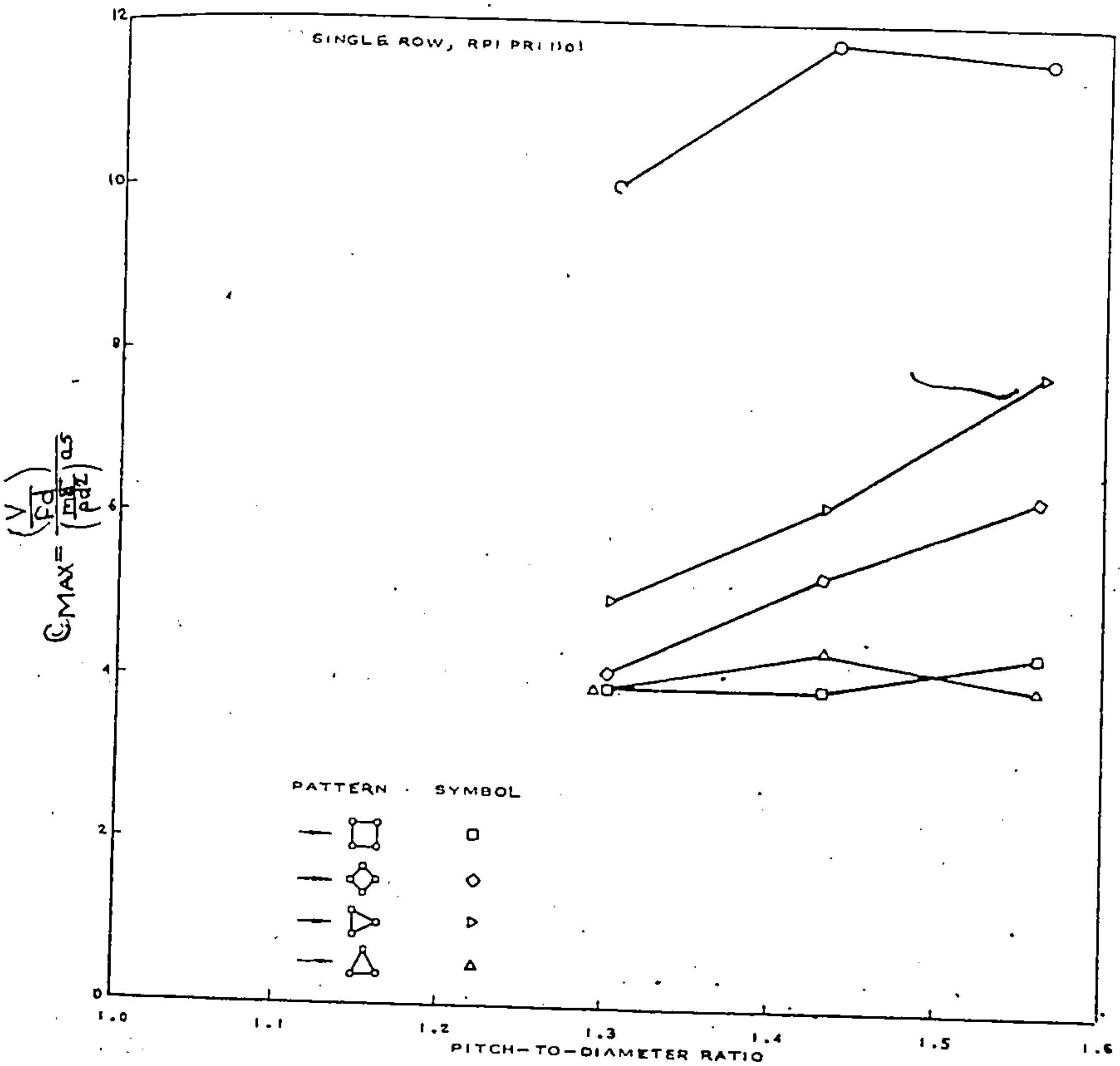

FIGURE 2.7: STABILITY THRESHOLD FOR DIFFERENT ARRAY PATTERNS FROM HARTLEN [16]

Chen [57] included both the effect of Reynolds number R and the spacing ratio x (x_t = T/D or x_l = L/D depending on which is the smallest) for tube arrays, and expressed a formula for the fluid-elastic instability as,

$$\left(\frac{V}{fd}\right) \frac{R}{x} = F\left(\frac{m\delta}{\rho_d{}^2}\right)^{1/2}$$

Later, Chen [58] modified the exponent of R to be 0.25 instead of 1 to give a correlation with the available experimental results. His results show that fluidelastic coupling between elastic vibration of the tubes and the flow path variation owing to the relative movement of the neighbouring tubes, is sensitive to tube spacing ratios. For small tube spacings, mechanisms such as wake swing, jet switch, and jet instability are the sources of excitation. This will be followed by fluidelastic instability. For moderate to large tube spacing ratio, Karman vortex shedding is suggested to be the only source of excitation. He also reported that the dimensionless critical speed increases practically linearly with the spacing ratio for different arrangement groups. The instability criterion is inversely dependent on spacing ratio. The slope of the line governing the relationship between the reduced velocity parameter and the damping parameter increases with increasing the damping parameter. The dimensionless critical speed for single tube rows is higher than for tube banks. There is no general tendency to show whether the in-line tube arrangement or the staggered one is superior with respect to the stability threshold.

Another formula for tube banks with in-line and staggered tube arrangements, was proposed by Gross [59], (quoted for Chen [58]) in the form:

$$\frac{V}{fd} = \frac{4}{K}\left(\frac{m\delta}{\rho_d 2}\right)$$

Note the difference in the value of the instability factor and the exponent of the damping factor with those of the previous formulae.

In a theoretical study Blevins [60] extended his previous model for a single transverse tube row to include tube arrays. He reported that tube array with in-line arrangement (normal square array) is more critical than that with a staggered one (rotated square, normal triangle, and parallel triangular arrays).

While Hartlen [16] showed that a straight line with an exponent of 0.37 for the damping parameter fits Connor's experimental results for a single tube row much better than 0.5, Savkar [61] suggested an exponent of 0.4 as much closer.

Weaver and Grover [19] demonstrated that, for parallel triangular arrays, the stability boundary is less dependent on damping, and, based on varying damping only, suggested a formula of the form,

$$\frac{V}{fd} \quad \alpha \quad \left[\frac{m}{\rho_d 2}\right]^{0.5} \quad \delta^{0.21}$$

Later Weaver and ElKashlan [20], varied $m/\rho d^2$ while keeping δ constant for the same type of arrays of [19], and found that,

$$\frac{V}{fd} \quad \alpha \quad \left[\frac{m}{\rho_d 2}\right]^{0.29} \quad \delta^{0.21}$$

Gibert et al [18], showed that by varying ρ (the fluid density) while keeping δ constant, the reduced critical velocity V/fd will be proportional to the mass ratio factor $m/\rho d^2$ to the power 0.3 which agrees very well with Weaver and ElKashlan.

Recently Weaver and Yeung [23] studied the effect of varying tube mass on fluidelastic instabilities in water flows. They found that critical flow velocities are independent of the mass ratios in water flows. They gave the following formula to determine the added mass coefficient for a tube which is oscillating in a confined space, as,

$$C_m = \frac{\gamma_t}{\gamma_w} [(\frac{f_A}{f_w})^2 - 1]$$

where γ_t and γ_w are the tube and fluid specific gravities respectively, f_A is the tube natural frequency in air, and f_w is the tube natural frequency in the fluid. They also predicted that tube mass has no effect on added mass, but added mass has a great effect on tube dynamics especially when the tubes are light compared to the fluid mass.

Weaver and Koroyannakis [26] showed that in water flows, added mass effects result in less regular response of the tubes than those in air flows. They also showed a reduction in natural frequencies occurs due to added mass and a broadened natural frequency spectrum due to fluid coupling effects.

The effect of approach flow direction on the fluidelastic instability of tube arrays was studied extensively by Weaver and Yeung [21,22]. They found that the approach flow direction from a normal square to a rotated square has no clear effect on the fluidelastic instability, while for only about 8^{o} incident flow angle, the stability threshold for a normal triangle drops substantially to that for a parallel triangle.

In order to simulate the situation in the U-bend region of a heat-exchanger, Weaver and Koroyannakis [25] studied the effect of using assymmetric stiffness (different stiffness in the streamwise direction from that in the transverse direction) on the fluidelastic instability. They found that the reduced velocity will increase by about 20% over that of symmetric stiffness. They also found that changing the direction in which the tube is more stiff would not change this effect.

The effect of partial admission (blockage) was studied by Franklin and Soper [62]. Partial admission was found to increase the critical speed. They also found that upstream turbulence always reduces the critical velocity and has more effect on the first tube row than the last tube row.

Mahrenholtz [63] was able to determine experimentally the unsteady fluid forces for an elastically mounted tube within a tube array. The results show that fluid forces can lead to damped or increasing vibrations of the tubes. Unsteady fluid force coefficients are relatively high in the second tube row, which means that this row is highly susceptible to damage.

In the first few years of studying the phenomenon of fluid-elastic instability in tube arrays, the research was mainly experimental as discussed above. The development of semi-empirical models which characterize the behaviour of the tubes for the onset of instability was attempted by Connors and Blevins and was even restricted to a single tube row. Semi-empirical models for full arrays require measuring experimentally beforehand fluid force coefficients for every tube in the array and for every specified direction of motion. Since the flow regimes differ from one array arrangement to the other, this will require measuring fluid force coefficients for every tube pattern. The next step, is to insert these fluid force coefficients into the equation of motion which is even linearized.

Developing a semi-empirical mathematical model to predict the fluidelastic instability of tube arrays was first attempted by Chen [64,65]. Displacement, velocity and acceleration dependent fluid force coefficients for unsteady fluid forces were used in a linearized equation of motion. Tanaka and Takahara [66,67,68] studied the characteristics of the threshold velocity of normal square arrays with P/d = 1.33 and 2.0 in water flows using a similar approach. Their semi-empirical model was based on inserting in the equation of motion, experimentally determined unsteady fluid dynamic force coefficients. The latter were found to be dependent on reduced flow velocity, tube motion, and the motion of its nearest surrounding neighbours. A stability curve covering the region of their tests was generated and showed good agreement with their experimental results. Through a comparison between the normal square array with P/d = 1.33 and the one with P/d = 2.0, they were able to determine theoretically the behaviour of a normal square array with different pitch-to-diameter ratios. They found that the critical flow velocity increases with the pitch-to-diameter ratio for a normal square array when it is less than 2.0, and level off for values above 2.0. The critical velocities for a U-turn flow is about 85 percent of those in cross flow. For the normal square array with P/d = 1.33 they proposed a stability boundary of the form:

$$\frac{V}{fd} \alpha \left(\frac{m}{\rho_d 2}\right)^{0.5} \delta^{-0.5} \quad \text{for low density flow, and}$$

$$\frac{V}{fd} \alpha \left(\frac{m}{\rho_d 2}\right)^{0.33} \delta^{0.2} \quad \text{for high density flow.}$$

while for the normal square array with P/d = 2.0,

$$\frac{V}{fd} \alpha \left(\frac{m\delta}{\rho_d 2}\right)^{0.75}$$

Later Chen [69,70], further developed his previous unsteady model using the Tanaka-Takahara fluid force coefficients, and extended the stability curve to cover the air flow region. Two instability criterion were proposed, namely: "Fluid-damping-controlled" instability for high density flows, and "Fluidelastic-stiffness-controlled" instability for low density flows.

A quasi-static model for a staggered two-row array was developed by Price and Paidoussis [71] in which the fluid force coefficients were measured statically. The reduced critical velocity for fluidelastic instability is found to have the form:

$$\frac{V}{fd} = 16.9 \left(\sqrt{\frac{T^2 + P^2}{d}} - 1\right)^{1.7} \{1 + (1 + 0.365\frac{m\delta}{\rho d^2})^{0.5}\}$$

where T is the tube pitch in the direction 90° from that associated with the tube pitch P. Their empirically fitted equation for a double row array agreed with the experimental data of Weaver and ElKashlan [20].

Recently Lever and Weaver [27] developed a very simplified model to predict the fluidelastic instabilities of tube arrays. The model is based on a single tube in a shaped flow channel which preserves the basic geometry of the array. They found that the mechanism of instability is due to mass flow redistribution of the free-stream flow which is a result of tube motion and phase lag resulting from the finite fluid inertia. No measured fluid force coefficients are required in their model and it includes the effect of array geometry. While other researchers considered the effect of neighbouring tubes in measuring steady and unsteady fluid forces, Lever and Weaver found that one flexible tube is enough in understanding and providing the mechanism of instability and that the flow field created by the surrounding tubes will result in the instability. Fluid coupling between tubes occurs in the post-stable region. The stability curve produced does not continue from air to water and that for water is considerably below the stability curve for air for the same array.

In common between Tanaka-Takahara, Chen, and Lever and Weaver is that the critical reduced velocity for fluidelastic instability is substantially different between gas and liquid flows. Jumps or discontinuities in the stability curve are predicted by all of them. While these stability curves are in good agreement with some experimental results, a great deal of scatter exists in the available experimental data.

Fluidelastic instabilities in tube arrays can be avoided by limiting the flow velocity across the tubes to a value below the threshold velocity for instability. Reducing the tube response and delaying the fluidelastic instability is by the use of tube supports. Weaver and Schneider [72] demonstrated the use of flat bars as antivibration supports. Small clearances helped to prevent both the out-of-plane and the in-plane modes. They reported that the larger the impact force and/or the support clearance, the greater is likely to be the wear rate. They also pointed out the importance of support effective spacing, support geometry, and tube-to-support clearances.

The effect of detuning as a method for stabilizing fluid-elastic instability was studied by many researchers [15,49,68,70,71]. While detuning produces a stabilizing effect in some cases, it may have no effect in others. Weaver and Lever [49] showed that detuning by up to 3 percent will increase the critical velocity, but increasing the tube-to-tube frequency difference beyond this, will bring the critical velocity down again to its original value.

There is no doubt that a great deal has been accomplished towards understanding the mechanisms responsible for resonance and instability. Still, considerable scatter in the available results does exist, and more careful experimental research is needed to produce reliable and consistent data with which to develop design guides and confirm theoretical models.

CHAPTER 3

EXPERIMENTAL FACILITY AND INSTRUMENTATION

A low speed wind-tunnel facility was available for this research [73]. The average upstream turbulence intensity inside the test-section over the range of operating speeds was only about 0.2%. The velocity distribution is uniform within 1% outside of the boundary layers on the test section walls. The vibration and noise levels of the wind-tunnel are negligibly small. The tunnel was also provided with a speed control unit to control the flow velocity very precisely at all operating speeds so that both vortex shedding and self-excited vibrations phenomena of the tubes can be studied carefully. The tunnel was used to operate in a velocity range from 0 m/sec. to 19.0 m/sec.

As the purpose of this study was mainly to study the effect of changing pitch-to-diameter ratios and arrangements of tube arrays on the fluid excitation mechanisms, the test-section was designed to facilitate the insertion and removal of the array without changing the test-section itself. Acrylic flexible cantilevered tubes mounted on steel rods were used for studying the fluidelastic instabilities, while hot-wire probe arrangement was employed to study the unsteady flow phenomena and mean velocity between the tubes. The designs of the test-section and tube-models are described later in this chapter.

3.1 The Wind-Tunnel

The low speed wind-tunnel was designed and constructed previously by Grover [73] for this type of study and is shown schematically in Figure 3.1. The upstream portion of the wind-tunnel begins with the contraction section which is made of 3.2 mm. birch plywood mounted on oak bulkheads. The length of this section is approximately 1.14 m. The section starts with 1.45 m. square inlet and ends with 0.31 m. square outlet, the contraction ratio being 22:1. The wall contours were so designed to prevent any adverse pressure gradients which might cause boundary layer separation. The purpose of this section is to reduce any spatial irregularities in the velocity distribution and results in low turbulence levels at the test-section.

This contraction is followed by the test-section specifically designed for the present study. This is a box type structure made up of eleven perspex plates bolted together, the thickness of each plate being 19 mm. The nominal internal dimensions of the test-section are 0.31 m. square by 0.82 m. long. The design of the test-section allowed changing the tube array by insertion of the tube arrays into the bottom. The complete design of the test-section is given later in this chapter.

The next section is the 2.59 m. long diffuser section. The main purpose of this section is to decelerate the flow and give an

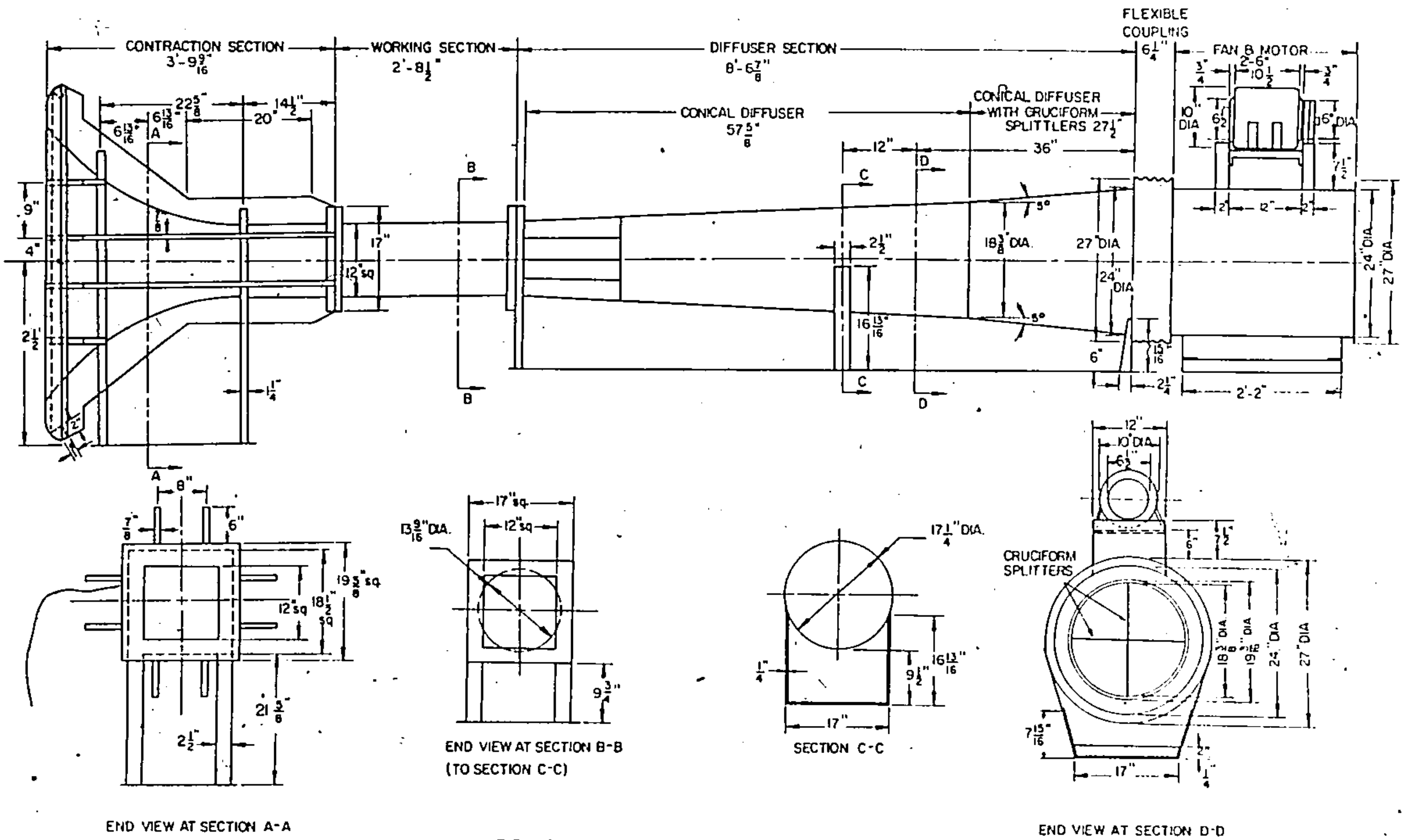

FIGURE 3.1 SCHEMATIC OF THE WIND - TUNNEL DERIVED FROM [73]

efficient conversion of kinetic energy into pressure energy. Its efficiency depends on wall angle, inlet and outlet velocity profiles. The diffuser section is made of 12 gauge mild steel sheets with a square-to-round transition at the front and an included angle for the main body of 6^{o}. At the end of the diffuser, cruciform splitters are installed to afford an increase in the included angle to 10^{o} and thus shorten the overall length.

At the end of the tunnel, the fan and motor assembly are installed. A 0.61 m. vane-axial fan having a maximum rating of 3.8 m^3/sec. at 0.038 m. water static pressure is used. A 10 Hp. D.C. motor is employed to drive the fan. A D.C. motor speed control unit is used to control the speed. The speed control unit and regulator are installed near the end of the tunnel. The motor speed could be kept constant within $\pm$ 1 R.P.M. in the speed range 0 - 500 R.P.M. and within $\pm$ 3 R.P.M. for higher speeds of 500 - 2500 R.P.M. Two different sizes of pulleys are used at the motor shaft to give the desired range of fan speeds.

Between the diffuser section and fan unit a flexible sleeve is fitted to prevent any fan vibration from reaching the test-section.

This wind-tunnel assembly is installed on steel frames such that the middle of the test-section is approximately at eye level.

3.2 The Test-Section

It was desired to design a test-section into which eight tube arrays could be fitted without changing the test-section for every array. These arrays could also be used for future research in water tunnel test-section. After careful consideration of these requirements together with keeping the internal nominal dimensions of the test-section to a 0.31 m. square, it was decided to build a test-section which is made of perspex plates bolted together. Schematic views of the test-section and the dimensions of the plates used are shown in Figure 3.2. A 5.08 cm hole was drilled in the top plate to allow insertion of a hot wire probe between the tubes. The position and size of this hole were chosen so that an acrylic plug fits it and holds the probe centrally between tubes in each array. Another hole was drilled on the upstream part of the top plate for another hot-wire probe used to measure the upstream flow velocity. On the upstream part of the bottom plate a third hole was drilled for a pitot-static tube used in parallel with the hot-wire probe to provide a check on measurement of the upstream flow velocity. The clearing hole on the bottom side allowed insertion of the tube arrays. The plates on the end of the test-section were used to hold the test-section with the contraction section on one side and with the diffuser section on the other side. A photograph of the test-section with one of the tube arrays and the probes in position is shown in Figure 3.3.

The velocity distribution is uniform within 1.0% over the central 80% of the test-section area. Over the range of operation speeds, the average upstream turbulence intensity is about 0.2%. The boundary layer thickness midway through the test section is about 8 mm., while at the tube arrays position is about 9 mm. thick.

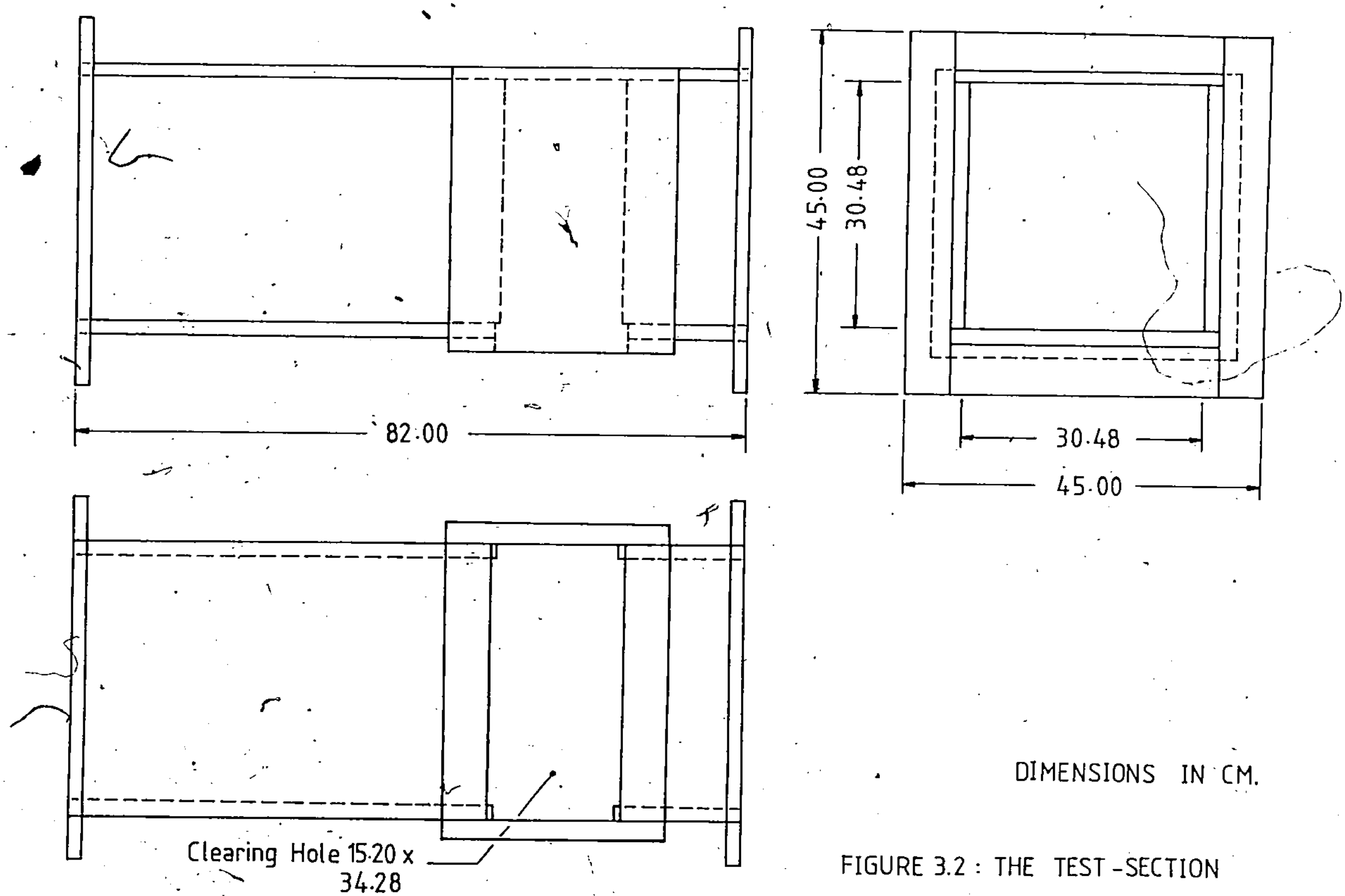

FIGURE 3.2 : THE TEST-SECTION

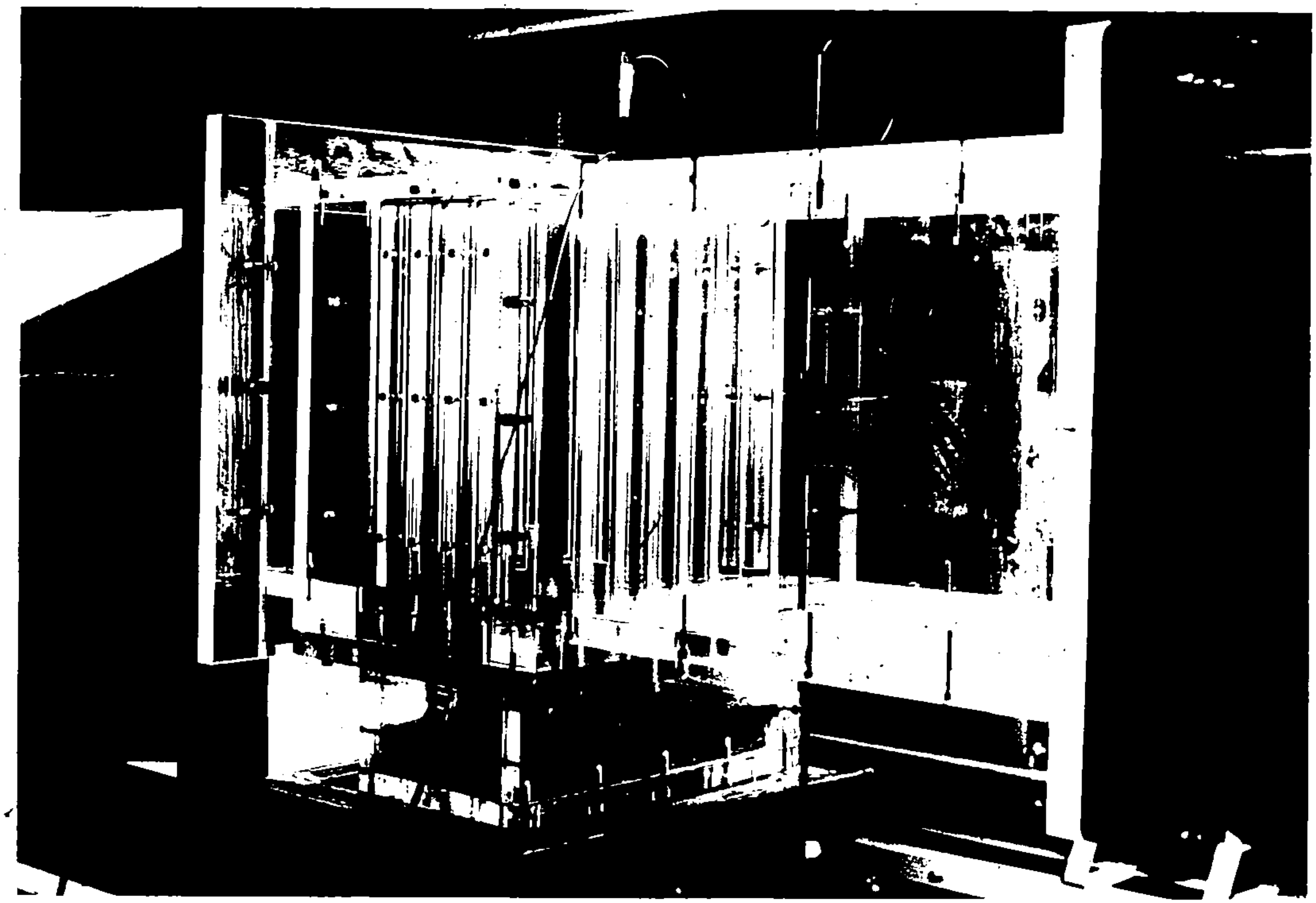

FIGURE 3.3 THE TEST SECTION WITH ONE OF THE TUBE ARRAYS AND THE PROBES IN POSITION.

3.3 The Flexible Tube Model

In previous research conducted by Franklin and Soper [62], they found that a cantilevered tube would have the same characteristic behaviour for fluidelastic instability as that for a simply supported one. This together with the fact that these type of tubes will be more convenient for the intended study, and could be used for flow visualization in water tunnel, were the reasons behind adopting this tube model.

In this tube model:

i) the tube is elastically mounted; the elastic constraint is linear, i.e., restoring action is proportional to tube displacement.

ii) the logarithmic decrement of damping has a single value in all directions.

An acrylic tube was mounted on a stainless steel rod as shown in Figure 3.4. The tube has a flat top and the elastic rod is screwed and glued for about 2.54 cm into the bottom of the tube. The connection was rigid enough to prevent any relative motion between the acrylic tube and the steel rod. The other end of the steel rod was made to be screwed into a steel base which will hold all flexible tubes as will be seen later in this chapter. The acrylic tube with the steel rod weighs 238 grams, while the acrylic tube itself weighs 182 grams. Thirteen such flexible tubes were built. The reason for

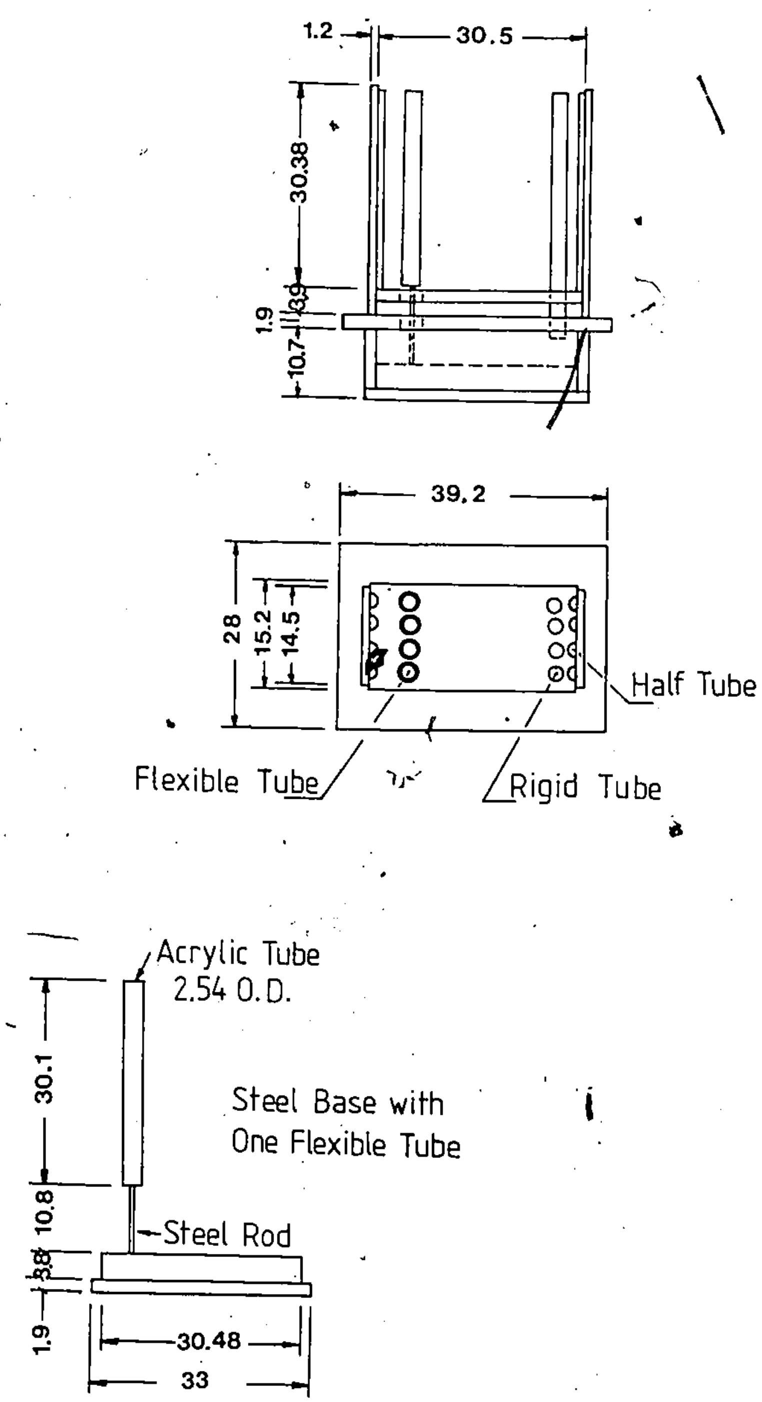

DIMENSIONS IN CM.

FIGURE 3.4 : A TEST-ARRAY

choosing this number will be given later in this chapter. Only two of these flexible tubes were instrumented. On each of these instrumented tubes, four strain gauges were installed near the base with a 90^o difference between them. Each opposite pair were connected to form a half bridge to double the sensitivity of the output in a given direction. The other pair will represent the orthogonal direction. Specifications of strain gauges are given in Appendix A. The calibration showed a linear output for cantilever tip deflections up to those required for tube-to-tube clashing (the calibration was carried on up to a deflection equal to 16% of tube diameter and which is approximately equal to the spacing between tubes for arrays with low P/d used in this study). The procedure and results of this calibration are given in detail in Appendix B.

The output signal from each pair of strain gauges recorded on a Spectral Dynamics 375 Fourier Analyzer through a strain gauge bridge (signal conditioning amplifier) showed no directional variation in effective stiffness of the tube.

3.4 The Test-Arrays

As was mentioned previously, the purpose of the present research is to study the effect of changing the pitch-to-diameter ratio and the geometry of tube arrays on the fluidelastic instability and vortex shedding phenomena. Many factors were taken into consideration in designing and selecting these arrays. First of all, from a previous study [74], it was found that a maximum number of six tube rows are enough to study fluidelastic instability. Tubes in the second, third, and fourth rows are critical in terms of fluidelastic instability [16,74] and vortex shedding response [9,12]. Deep inside the array, the flow is more irregular because of the high turbulence intensities and vortex shedding may not be present [8]. Secondly, all arrays with a reasonable depth should fit in the same test-section.

A 30.48 cm x 14.60 cm x 3.81 cm steel base was used to hold the flexible tubes. The steel base was large and heavy enough and the connection between the steel rod and steel base was sufficiently rigid to allow very little mechanical coupling between tubes.

Preliminary calculations of the possible arrays with integer number of tube rows for section width are represented in Table 3.1. Only those with a reasonable number of tube rows were selected. Two arrays of each of the four different geometries, making a total of eight arrays were believed to be enough for the purpose of the present study. The selected arrays are: normal square arrays with P/d = 1.33, 1.5; rotated square arrays with P/d = 1.414, 1.70; normal triangular arrays with P/d = 1.33, 1.5; and parallel triangular arrays with P/d = 1.375, 1.73. Layout of the tube arrays used for conducting the experiments is shown in Figure 3.5. As can be seen, half tubes were installed along the walls to minimize wall effects. Exact locations of flexible and instrumented tubes will be given in the next chapter. A photograph of seven of these arrays is shown in Figure 3.6. The eighth array was installed in the test-section at the time this photo was taken.

Table 3.1

Possible arrays with integer number of tube rows for section width.

	SQUARE		TRIANGLE	
	Normal	Rotated	Normal	Parallel
P/d	1.714	1.7	1.714	1.73
No. of Tube Rows	3	5	4	6
P/d	1.5	1.414	1.5	1.375
No. of Tube Rows	4	5	4	6
P/d	1.33	1.212	1.33	
No. of Tube Rows	4	6	5	
P/d	1.2		1.2	
No. of Tube Rows	5		5	

□ Selected arrays

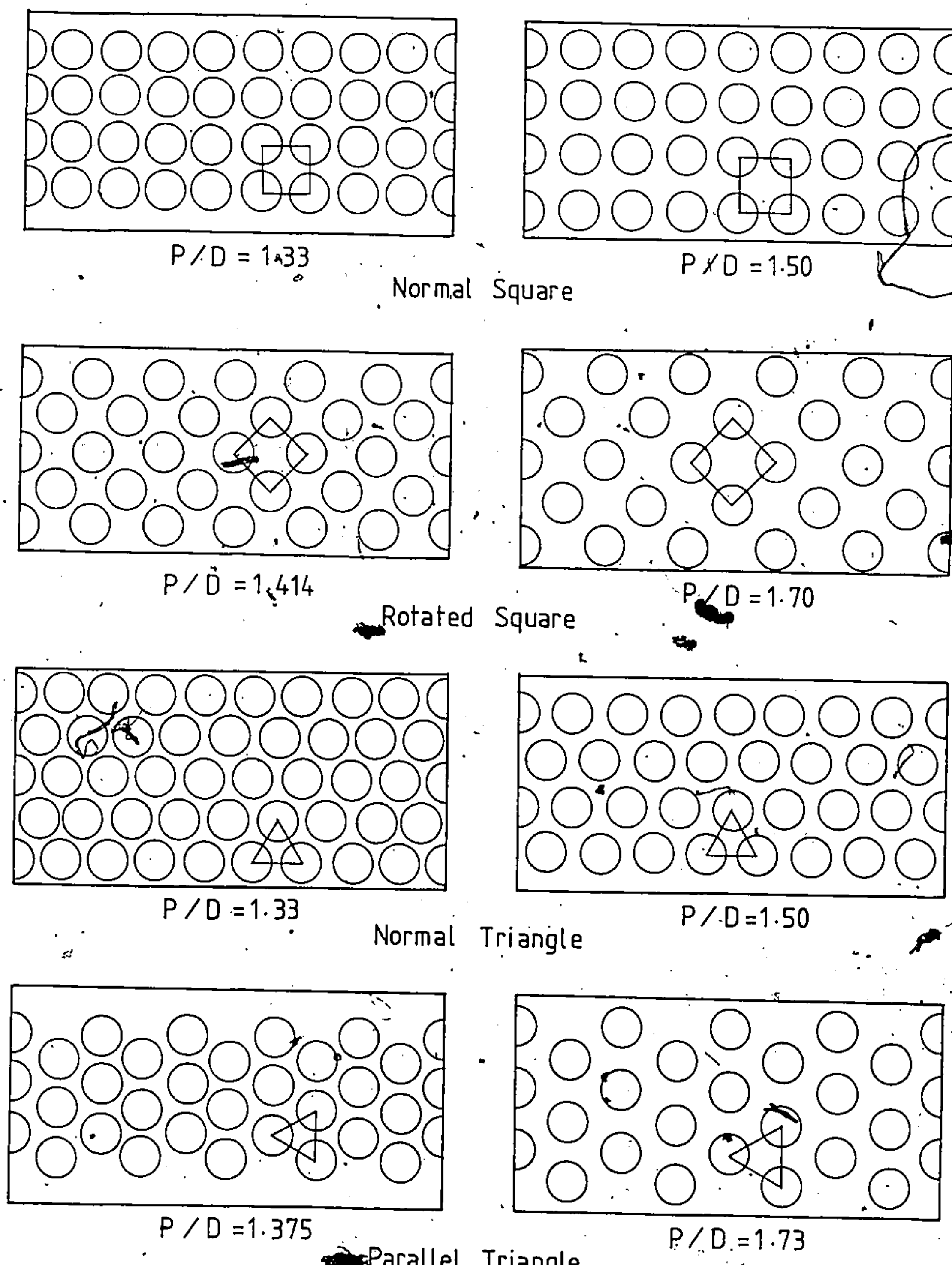

FIGURE [illegible] LAYOUT OF TUBE-ARRAYS

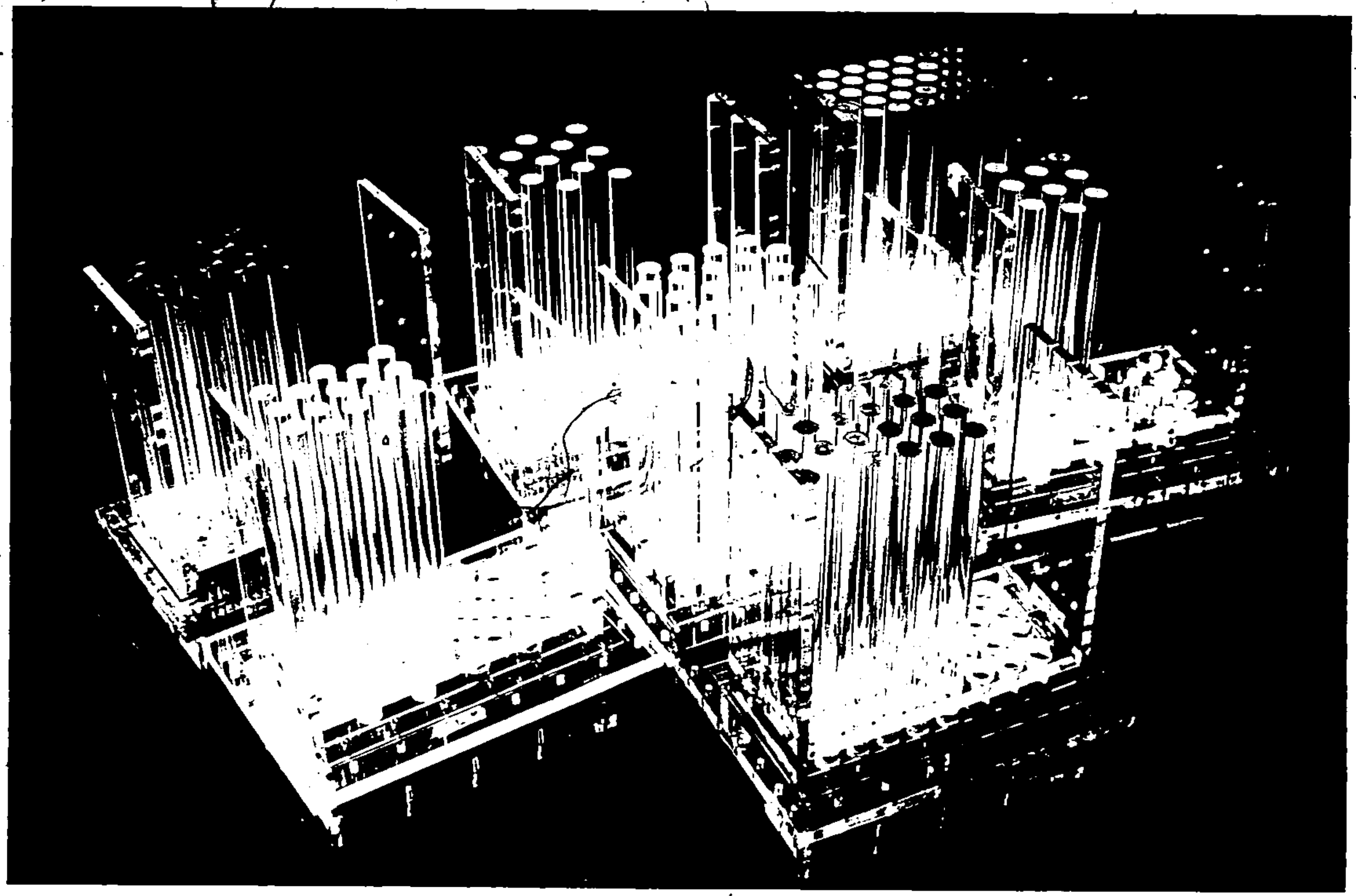

FIGURE 3.6 SEVEN OF THE TUBE ARRAYS.

The reasons for not selecting the rest of the tube arrays seen in Table 3.1 were; for the normal square array with P/d = 1.714 for the obvious reason of small number of tube rows, while on the other hand, for normal square array with P/d = 1.2, rotated square array with P/d = 1.212, and normal triangle array with P/d = 1.2 was basically a judgement call. Although a pitch-to-diameter ratio of 1.2 is a minimum practical pitch ratio, it was thought that the pitch ratios chosen would more likely yield useful results.

3.5 Vortex Shedding Response Equipment

In order to obtain frequency spectra in the flow between tubes for different arrays, it was desired to use a single adaptor for the hot-wire probe for every array. A transparency containing the plan of each array was drawn. From overlapping different transparencies, a plug containing eight holes, a hole corresponding to each array was selected. The size of the hole was made equal to the diameter of the hot-wire probe holder. Its centre is located midway between tube spacing at the minimum gap between tubes, and so that the wire on the hot-wire probe is at the centre-line between tubes. Size and dimensions of the plug are shown in Figure 3.7. Accordingly a hole was drilled on the top plate of the test-section at the required location. The detailed location of the hot-wire probe for every individual tube array will be given in the next chapter. Eight small plugs were made to fit the hot-wire probe holder hole, so that if one of the holes is being used the rest of the holes are closed to prevent any leakage of air into the test-section.

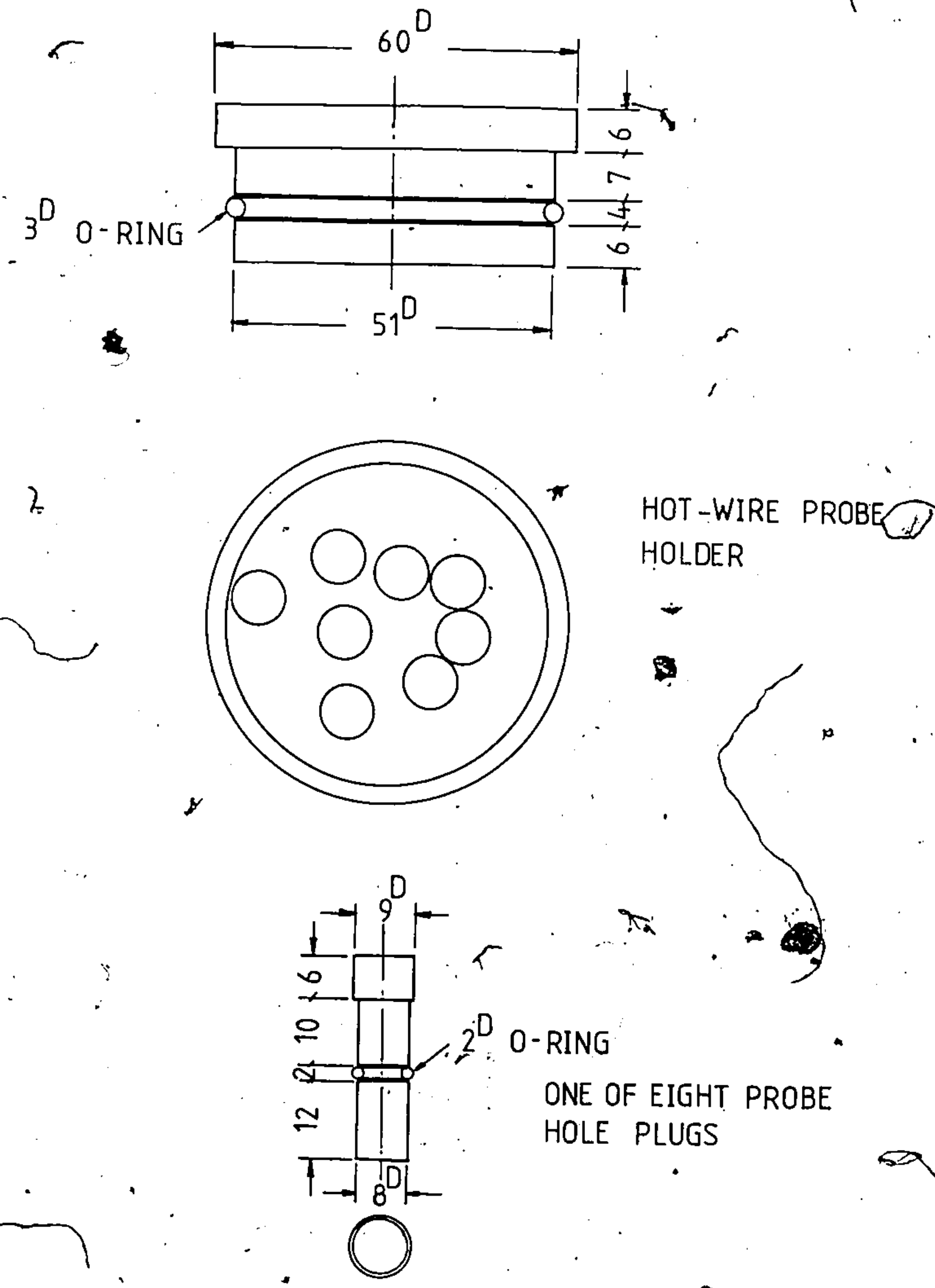

DIMENSIONS IN MM.

FIGURE 3.7 : PLUGS USED TO FACILITATE MEASURING VORTEX SHEDDING FREQUENCIES

3.6 Instrumentation

Tuning of the instrumented tubes was achieved through the output of the strain gauges (Gauge type: CEA-09-032UW-120), which are installed near the fixed end of each tube. The output of the strain gauges is connected to a Conditioning amplifier (Vishay 2310 Signal conditioning amplifier), then viewed on a Fourier analyzer (Spectral Dynamics Model 375-1). The same sequence of instrumentation was used to measure the amplitude of vibration at different flow velocities. Four strain gauges were installed with a 90° difference between them on each of the instrumented tube support rods. As mentioned previously each opposite pair were connected together to double the sensitivity of the output and the output will represent amplitude of vibration in a certain direction. The output from the second pair of strain gauges will give the amplitude of vibration in the orthogonal direction.

An MTI capacitive probe (Type ASP-10) used in conjunction with a distance and vibration meter (MTI AS1000) and the Fourier analyzer were employed to tune the rest of the flexible tubes for each array to the required frequency.

Two different types of instrumentation were employed in order to obtain a reliable and accurate measurement of the upstream flow velocity. All the results for vortex shedding and fluidelastic instability phenomena were obtained with respect to the upstream flow velocity. The first set of instrumentation was a DISA 90° miniature hot-wire probe (DISA type 55P14) in conjunction with a DISA constant-temperature anemometer (DISA type 55A01). In order to read the output voltage from the DISA constant temperature anemometer more accurately, it was displayed on a digital voltmeter (Type HP 3465A). The second set is a pitot-static probe and a manometer.

The minimum gap velocity was measured using another DISA 90^{o} miniature hot-wire probe and a DISA constant-temperature anemometer. The output was also displayed on a digital voltmeter. The same signal of the output from the hot-wire probe and the constant temperature anemometer in the minimum gap was used for computing the flow-field velocity-spectra using the Fourier analyzer.

The output of the strain gauges after being processed through the signal conditioning amplifier was recorded on a U.V. recorder (Visicorder oscillograph, Model 2106). The output on the Kodak line-graph paper was used to check the natural frequency and compute the logarithmic decrement of damping of the instrumented flexible tubes.

The complete instrumentation is shown schematically in Figure 3.8. The photograph in Figure 3.9, shows most of the instruments used in conducting different sets of experiments, while the photograph in Figure 3.10, shows the wind-tunnel and part of the working area. A scaled photograph of the pitot-static probe, DISA 90^{o} miniature hot-wire probe and the MTI capacitive probe is shown in Figure 3.11.

Detailed specifications of all instruments and probes used for conducting the experiments are given in Appendix A. The necessary calibrations and the calibration curves for the strain gauges and the hot-wire probes are given in detail in Appendix B.

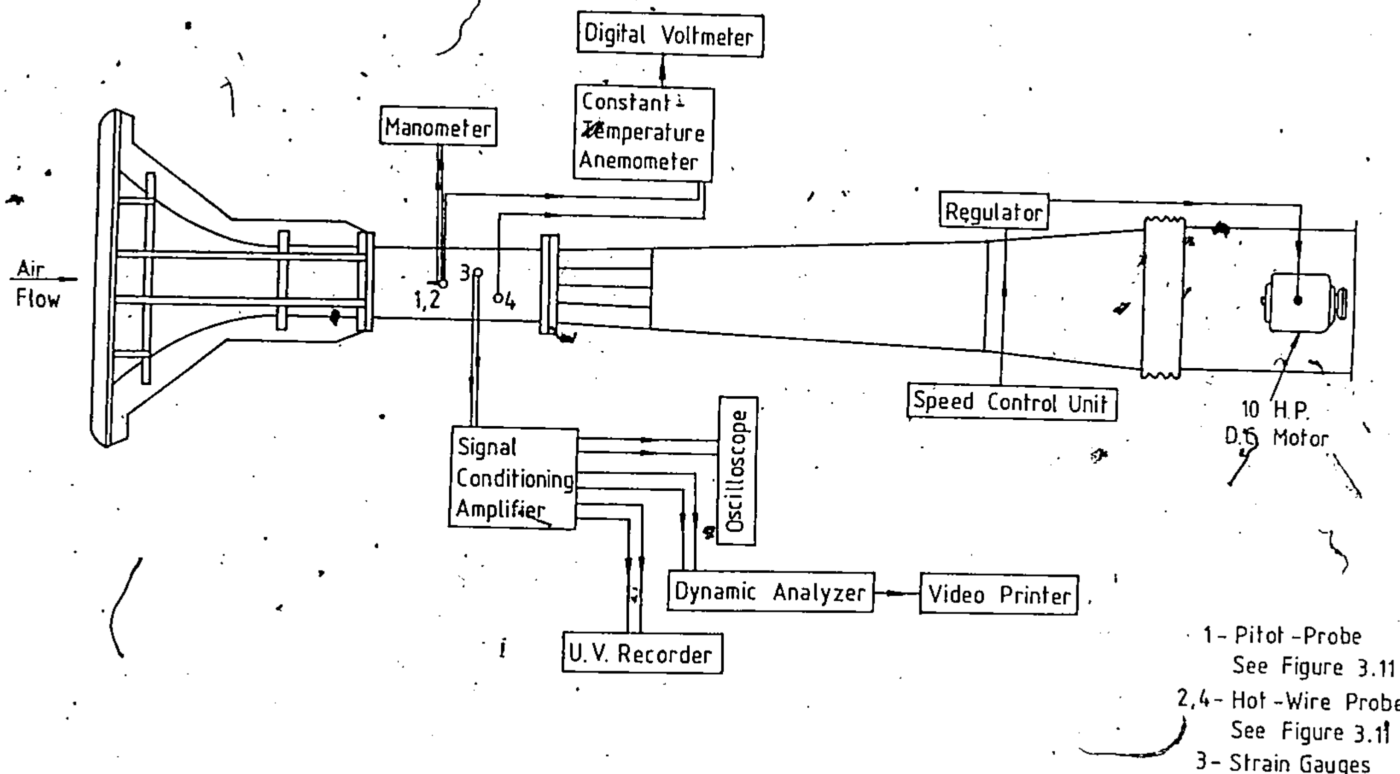

LAYOUT OF THE WORK ARE

FIGURE 3.8

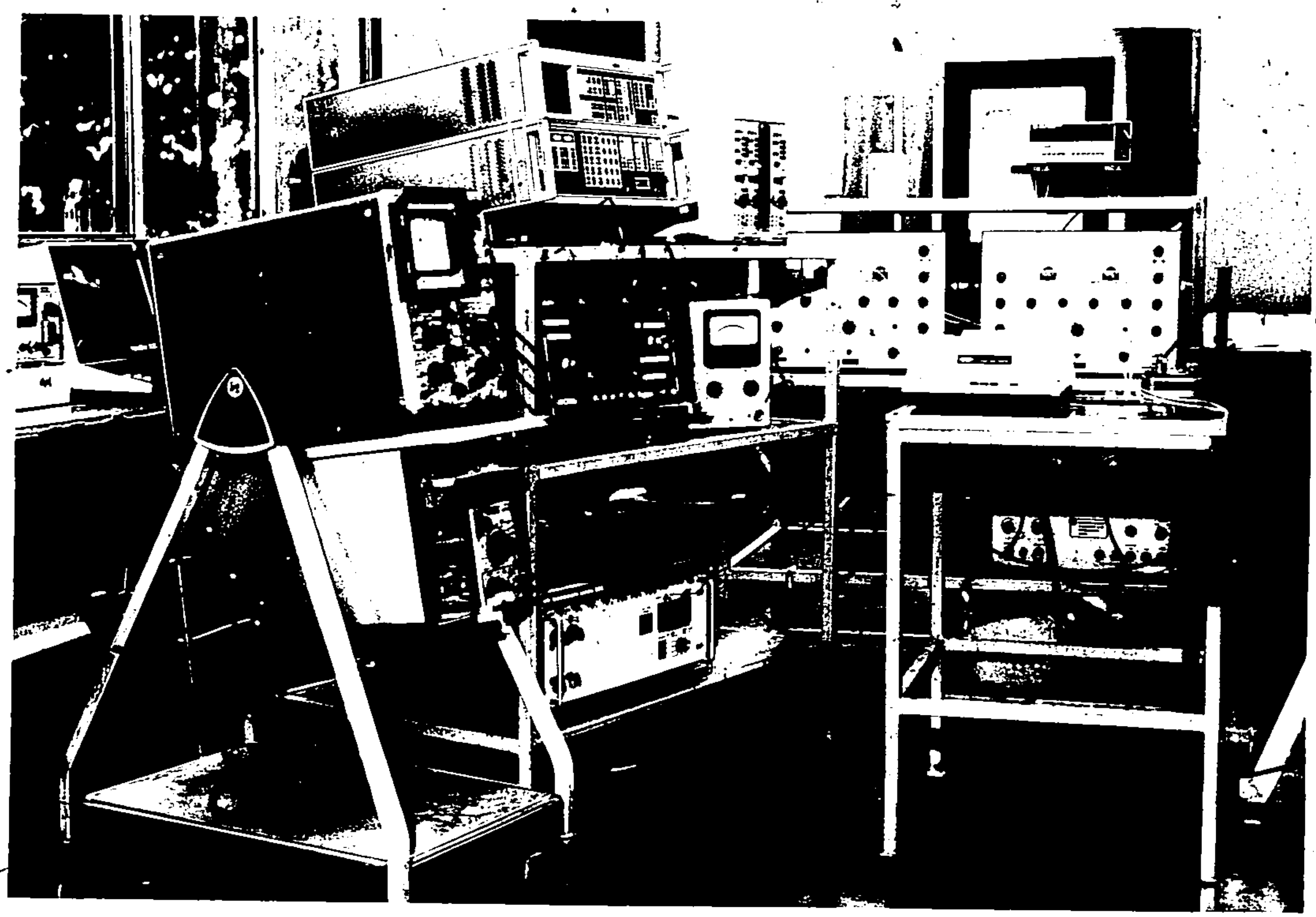

FIGURE 3.9 EXPERIMENTAL EQUIPMENT.

FIGURE 3.10 THE WIND TUNNEL AND PART OF THE WORKING AREA.

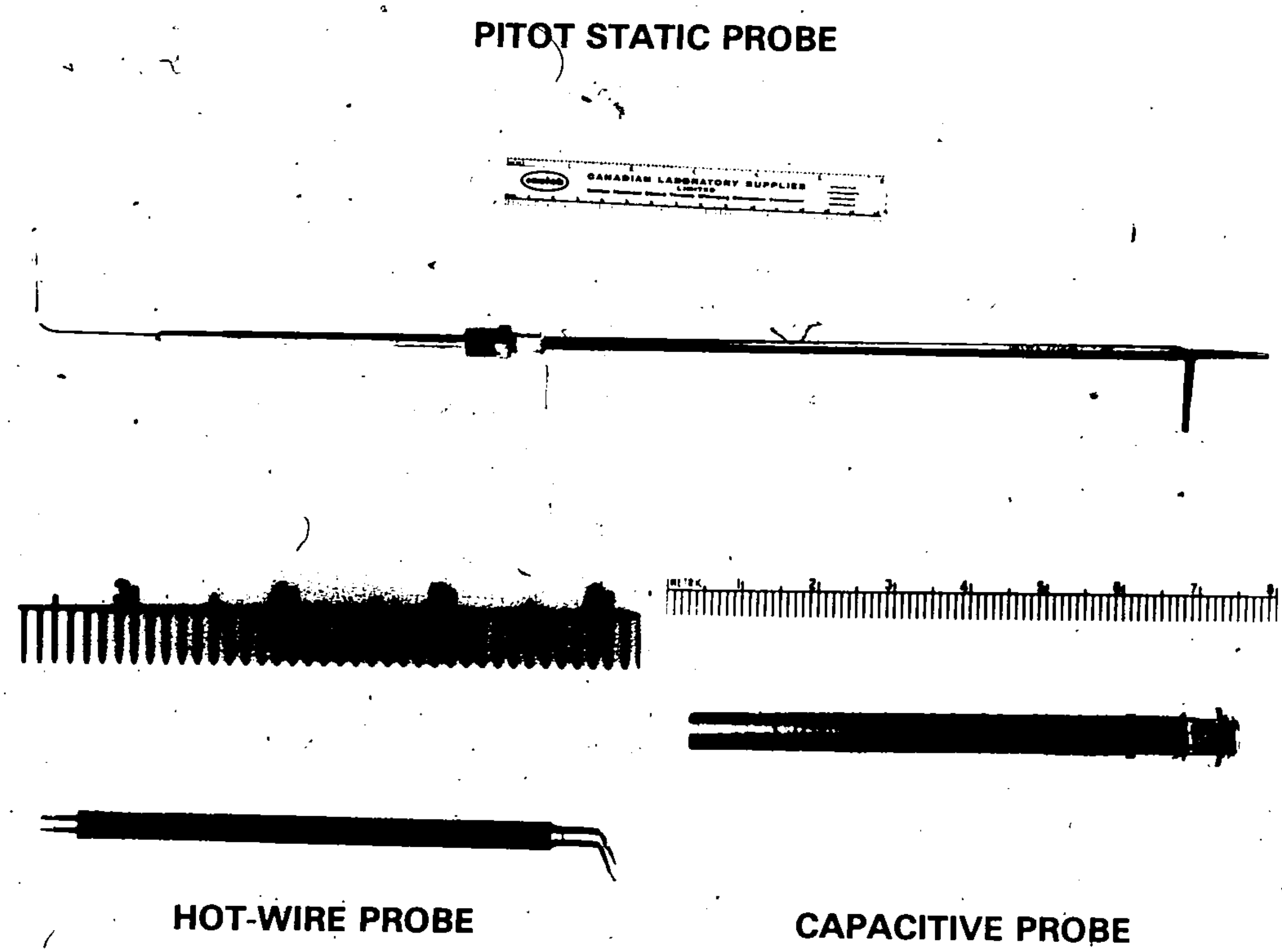

FIGURE 3.11 A SCALED PHOTOGRAPH OF THE PROBES.

CHAPTER 4

EXPERIMENTAL RESULTS AND ANALYSIS

As mentioned in the previous chapter it is intended to set up and carry out sets of experiments to help understand how tube arrays of different pitches and patterns will respond to cross flow excitation. The test-section was so designed to fit all the tube arrays without changing the test-section. Twelve or thirteen flexible tubes were used to study the fluidelastic instability of the arrays. The number of flexible tubes was determined so that the monitored tubes in different rows will always be surrounded by flexible tubes. The number of tube rows selected were sufficient for studying both fluidelastic instability and vortex shedding. A plug with eight holes was designed to hold a hot-wire probe so that the interstitial flow between tubes could be studied for all arrays. The maximum number of tube rows used was six, typical of the result obtained by Weaver and ElKashlan [74]. Only two instrumented tubes were used. They were located in different tube rows, to study the effect of tube location on the critical velocity and amplitude build-up. Each cantilevered instrumented tube had four strain-gauges installed near the fixed end of the tube for vibration pick-up. The exact location of the two instrumented tubes and hot-wire probe used to measure vortex shedding frequencies, for each individual tube array will be given later in this chapter.

4.1 TYPICAL TUBE-RESPONSE AT DIFFERENT FLOW VELOCITIES

An idealized response characteristic of a flexible tube in a tube array to an increasing flow velocity is shown in Figure 4.1. Usually the flexible tube will start to vibrate randomly due to the random excitations of the turbulent pressure fluctuations. These turbulent fluctuations could be from upstream turbulence or due to turbulence generated in the tube bank. Turbulent buffeting excitation usually gives rise to a randomly forced, damped vibration. Amplitudes of vibration will be very small at low flow velocities. Owen [8] suggested that as the flow velocity starts to increase, the amplitudes of vibration will increase in direct proportion to the dynamic head ($1/2\ \rho U^2$), as long as the motion of the tube does not effect the turbulent fluid forces. Southworth and Zdravkovich [75] from experiments on in-line arrays of one and three tube-rows, also reported that the maximum amplitudes due to turbulence excitations are proportional to the square of flow velocities. However, as it will be seen later, in some of the results obtained, the in-line, transverse as well as RMS amplitudes increase almost linearly with flow velocities due to turbulence excitation. The same linear response was also observed by Weaver and Grover [19], and ElKashlan [76]. Tube response for tubes in the leading rows of a tube array will be different from those deep in the array due to increasing turbulent intensities as one progresses deep into the array.

Somewhere along this region the tube may vibrate in resonance due to the periodic shedding of vortices, if the vortex shedding frequency coincides with the natural frequency of the tube.

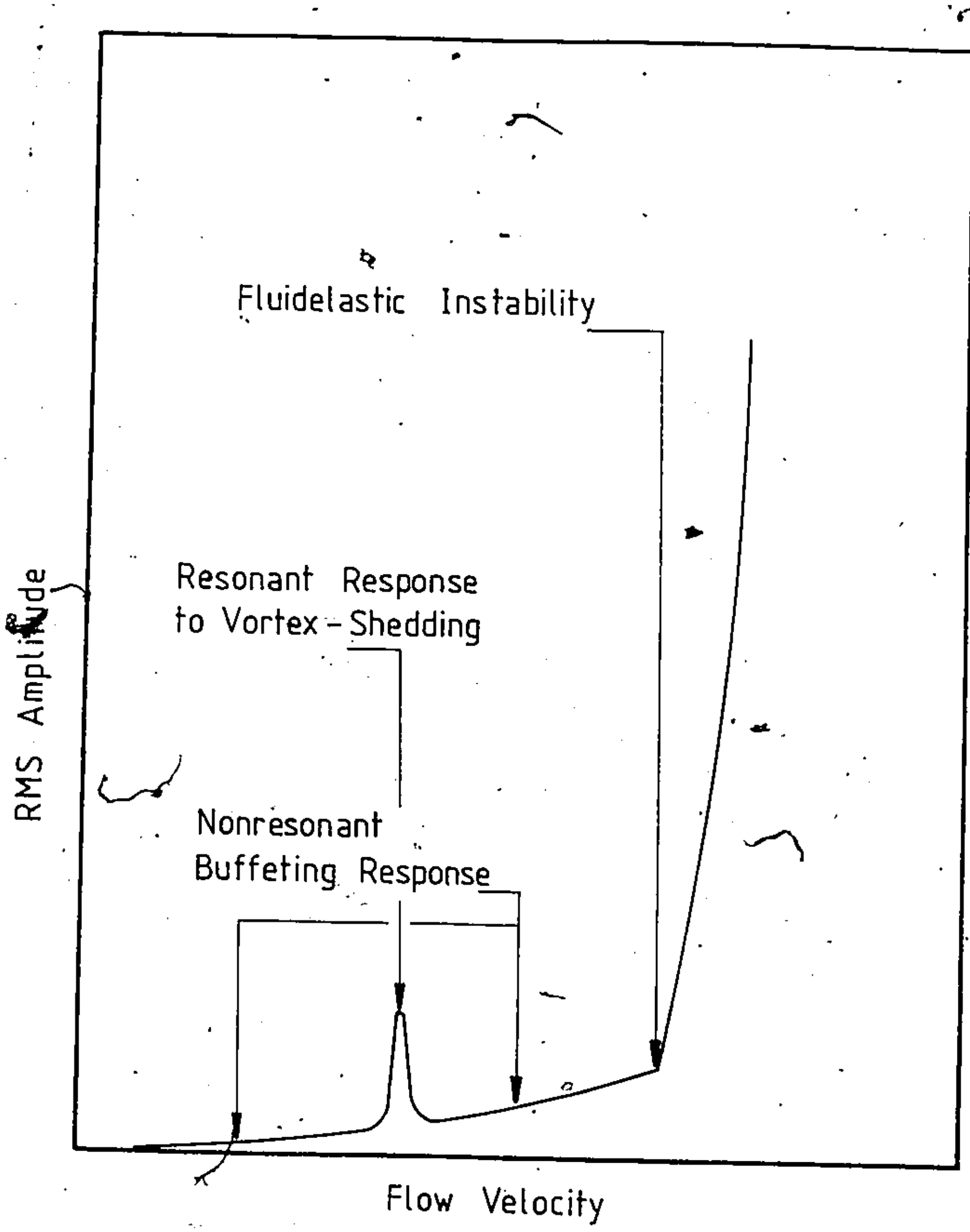

FIGURE 4.1 IDEALIZED RESPONSE OF A TUBE IN AN ARRAY SUBJECTED TO CROSS FLOW.

Amplitudes associated with such resonance are usually higher than those expected with turbulent buffeting. Vortex shedding resonance is usually expected and more important for arrays in water flows than those in air flows. However, for closely packed tube arrays, Owen [8] disputed the existence of vortex shedding. Pettigrew and Gorman [9] reported the existence of vortex shedding for some tube arrays, yet found it did not exist for others. Zukauskas and Katinas [12] reported the existence of vortex shedding for closely packed tube arrays of the normal square and normal triangular configurations, especially for the leading rows. However, Grover and Weaver [48] found that vortex shedding existed in the fifteenth row of a parallel triangular array at low Reynolds numbers, $Re < 1000$.

For further increase in flow velocities, the tube amplitude will keep on building up with a change in its pattern from a random one to an elliptical orbital regular pattern. Amplitudes and direction of motion seem to be a function of array geometry as well as tube location. The flow velocity at which the amplitude response curve changes its slope defines the "critical velocity" or "the threshold velocity". After this velocity any increase in flow velocity will result in much larger tube amplitudes and the array will become unstable. Defining the precise location of the critical velocity may be a problem, especially with arrays associated with a more gradual amplitude build-up. While some groups of researchers define the critical velocity as the point at which a tangent to the curve defining the fluidelastic instability amplitudes intersects the abscissa. Others simply rely on visual observations of the tube response or the flow velocity at which tube-to-tube clashing occurs, or at which tube amplitude is 2% of the tube diameter. However, while the method of visual determination of critical flow velocities may be unconservative especially when amplitude build-up is gradual, other methods may be too conservative. Defining the critical velocity as the point the amplitude-velocity curve changes its slope while observing that the tube response changes from random to regular seems more reliable and is used in the research reported in this thesis. This indicates at least a sudden change in behaviour and that some organized energy transfer mechanism is taking place.

4.2 TUBE FREQUENCY AND DAMPING

To prepare any array for testing, it was necessary to tune all flexible tubes to the same frequency, check the tube's alignment with the rest of the fixed tubes and then measure tube damping. Weaver and Lever [49] found that for a parallel triangular array of tubes, detuning by up to 3% increases the critical flow velocity up to about 40%. Hence, it was considered necessary to tune all flexible tubes to the same frequency if possible or with a difference in frequencies less than 1%. The tuning frequency for the flexible tubes in the array can be determined as the one which will keep the height of the flexible tubes approximately the same as the rest of the fixed tubes. It was found that a frequency of 25.0 Hz will reasonably satisfy this condition. The twelve flexible tubes (except for the normal triangular array with P/d = 1.33 where thirteen flexible tubes were needed) were then tuned in air to a frequency of 25.0 Hz within 1%.

This was done for every tube array, one at a time, as the same set of flexible tubes was used for all tube arrays. Each time the instrumented tubes were transferred to a new array, the operation involved releasing the strain-gauge wires from banana plugs then rewelding them again after the instrumented tubes were installed in the new array. The reason for this was that the strain-gauge wires had to be taken through a hole in the bottom of the tube array as this was the only way to prevent the wires from interfering with the test-section. The two monitored tubes were tuned through the output signal of the strain-gauges. The strain-gauge output is connected to a signal conditioning amplifier then displayed on the spectrum-analyzer. The output signal from each pair of strain-gauges showed no directional variation in effective stiffness of the tube.

The rest of the flexible tubes were tuned using a capacitive probe in conjunction with a distance and vibration meter and the spectrum-analyzer. Alignment of the flexible tubes with the rest of the fixed tubes was very important to maintain the array configuration and did not have any effect on the tuning frequency. An amplitude frequency-spectrum was computed from the output of the strain gauges and is shown in Figure 4.2. The sharp peak at the natural frequency of the monitored tube (25.0 Hz) indicates the excellent linear characteristics of the flexible tube.

The total damping consists of the following:

$\delta = \delta_s$ material damping in vacuo

$+ \delta_j$ joint damping

$+ \delta_f$ quiescent fluid damping

$+ \delta_v$ viscous damping due to flow

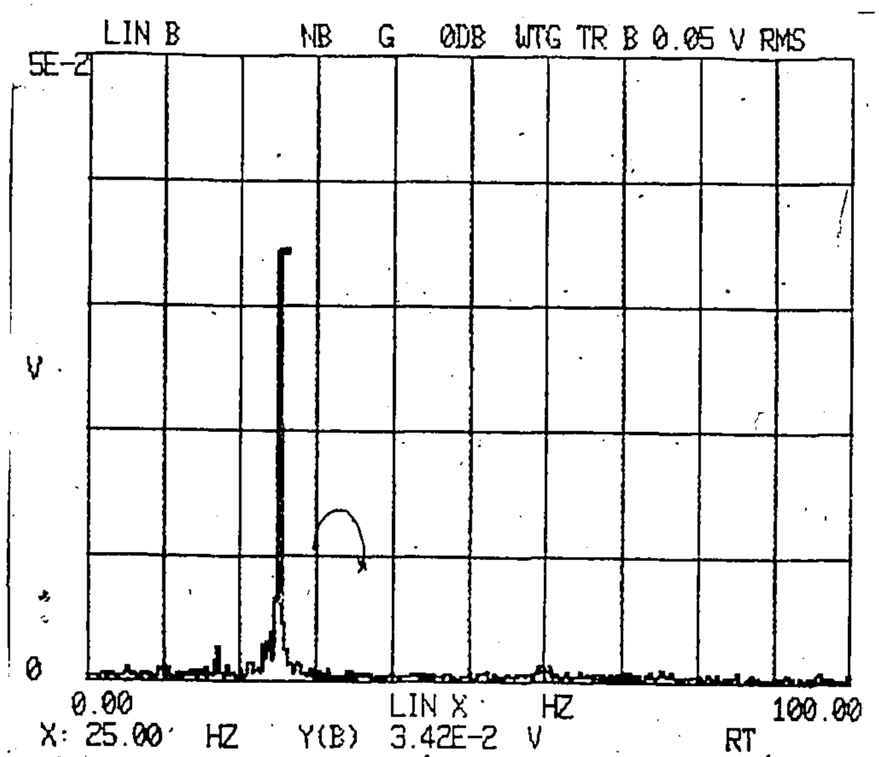

FIGURE 4.2 A TYPICAL FREQUENCY SPECTRUM OF A MOVABLE TUBE IN THE ARRAYS.

The result obtained by Weaver and ElKashlan [20] suggested the use of static damping measured in still fluid for the estimate of the velocity for the onset of instability. The logarithmic decrement of damping in air, was obtained from simple pluck tests using a U-V recorder. The monitored tube was released after displacement from its static equilibrium position and the subsequent amplitude decay was recorded on the U-V recorder. Great care was taken in order to obtain consistent amplitude decay traces. A typical amplitude decay trace recorded for air damping is shown in Figure 4.3. The number of free vibration cycles required for the amplitude to decrease from a particular amplitude to a selected lower amplitude were counted. The logarithmic decrement of damping was calculated and the average value from more than one period on the same trace was calculated. The logarithmic decrement of damping was found to be the same in the two orthogonal directions and for the two monitored tubes and had a value of 0.011 ± 0.001.

The frequency data were observed to be exactly the same during the run of the experiments, while the damping was checked for all arrays before and after the experiments and the value was found to be essentially the same.

Discussion of the response of different tube arrays to vortex shedding and fluidelastic effects will be given separately under these headings below.

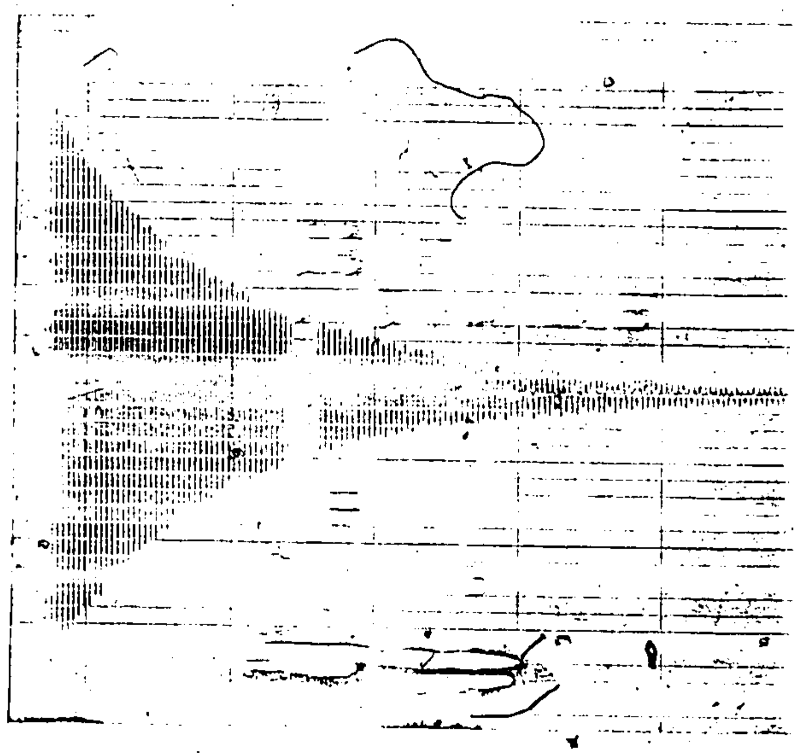

FIGURE 4.3 A TYPICAL AMPLITUDE DECAY TRACE USED FOR CALCULATING FLEXIBLE TUBE DAMPING.

4.3 VORTEX SHEDDING FREQUENCIES

4.3.1 Normal Square Array: P/d = 1.33

The tube array is 4 rows deep with 8 tubes in each row as shown in Figure 4.4. Half tubes are installed along the wall to minimize wall effects. The tubes marked from 1 to 12 are the flexible tubes. The rest of the tubes are rigid tubes. The tube array was inserted into the test section, and the hot-wire probe for measuring the vortex shedding frequencies was inserted in gap between tubes. As shown in Figure 4.4, this hot-wire probe was located between tubes in the third row. The probe was held tightly in position to prevent its motion or rotation during the experiment (by holding the plug carrying it with the top plate of the test-section through a set of small plates and screws).

The response of tubes in the second, third, and fourth rows are not necessarily typical of tubes deep in a similar array, but will be critical in terms of vortex shedding response. Another hot wire probe was inserted upstream of the tube array in the test-section along with a pitot-static probe to measure the upstream velocity (see Figure 3.8). The wind-tunnel fan was started and the experiment begun at some low flow velocity. Due to the fluctuations noticed in the output from the hot-wire probe in the gap between tubes, the upstream hot-wire probe was used to measure the flow velocity. The output from the upstream hot-wire probe at all flow velocities indicated that the flow velocity upstream of the array is steady. At very low flow velocities, no output response was recorded from the pitot static

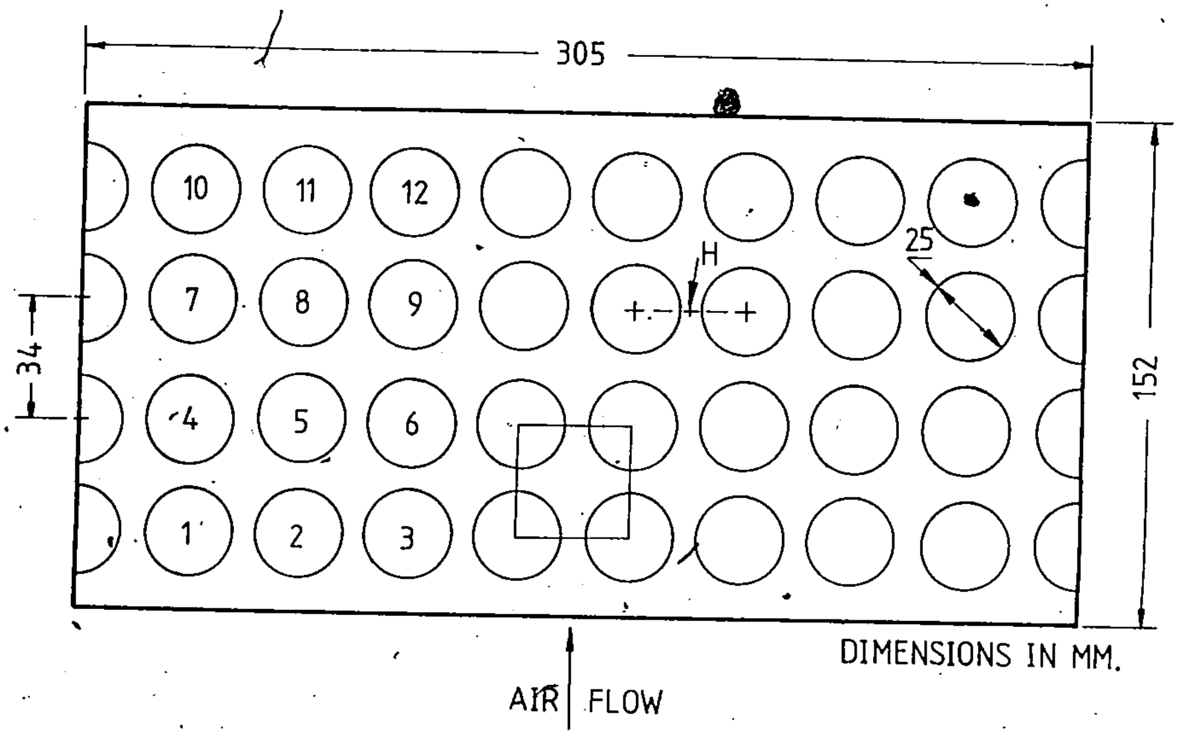

TUBES MARKED 1 - 12 ARE FLEXIBLE TUBES (REST ARE RIGID)

TUBES MARKED 5 and 8 ARE INSTRUMENTED TUBES

H - LOCATION OF GAP HOT-WIRE PROBE

FIGURE 4.4: NORMAL SQUARE ARRAY WITH P/d = 1.33.

probe. On the other hand, the output from the gap hot-wire probe was connected to a DISA constant temperature anemometer and the output signal from this combination was fed into the dynamic analyzer. The dynamic analyzer was used to compute the velocity spectrum of the velocity fluctuations in the gap between tubes in the third row. At an upstream flow velocity of 0.10 m/sec., a concentration of the velocity fluctuations in the flow field was observed in the velocity spectrum at a discrete frequency of 8.75 Hz. No such concentration was observed at lower flow velocities. The velocity spectrum is shown as the top trace in Figure 4.5. In this and all other spectra shown in this thesis, 64 sample averages were taken using the spectrum analyzer. The corresponding Reynolds number based on the upstream flow velocity and the tube outside diameter is $R_u = 170$ (in all further results, the Reynolds number based on the upstream flow velocity and the outside tube diameter will be designated as R_u). If Reynolds number were based on the velocity between adjacent tubes (pitch velocity) the value will be 680. The appearance of a discrete frequency in the flow field is believed to be due to the regular vortex shedding from the tubes in the array. It should be noted that there has been controversy for some years regarding whether or not discrete vortex shedding is possible in closely packed tube arrays. Thus, the phenomenon has variously been referred to as "vorticity shedding", "vortex shedding", "periodic wake shedding" and "turbulence". However, the recent flow visualization studies of Abd-Rabbo [77] have shown that discrete laminar vortex shedding is possible in staggered tube arrays. While discrete vortex shedding was

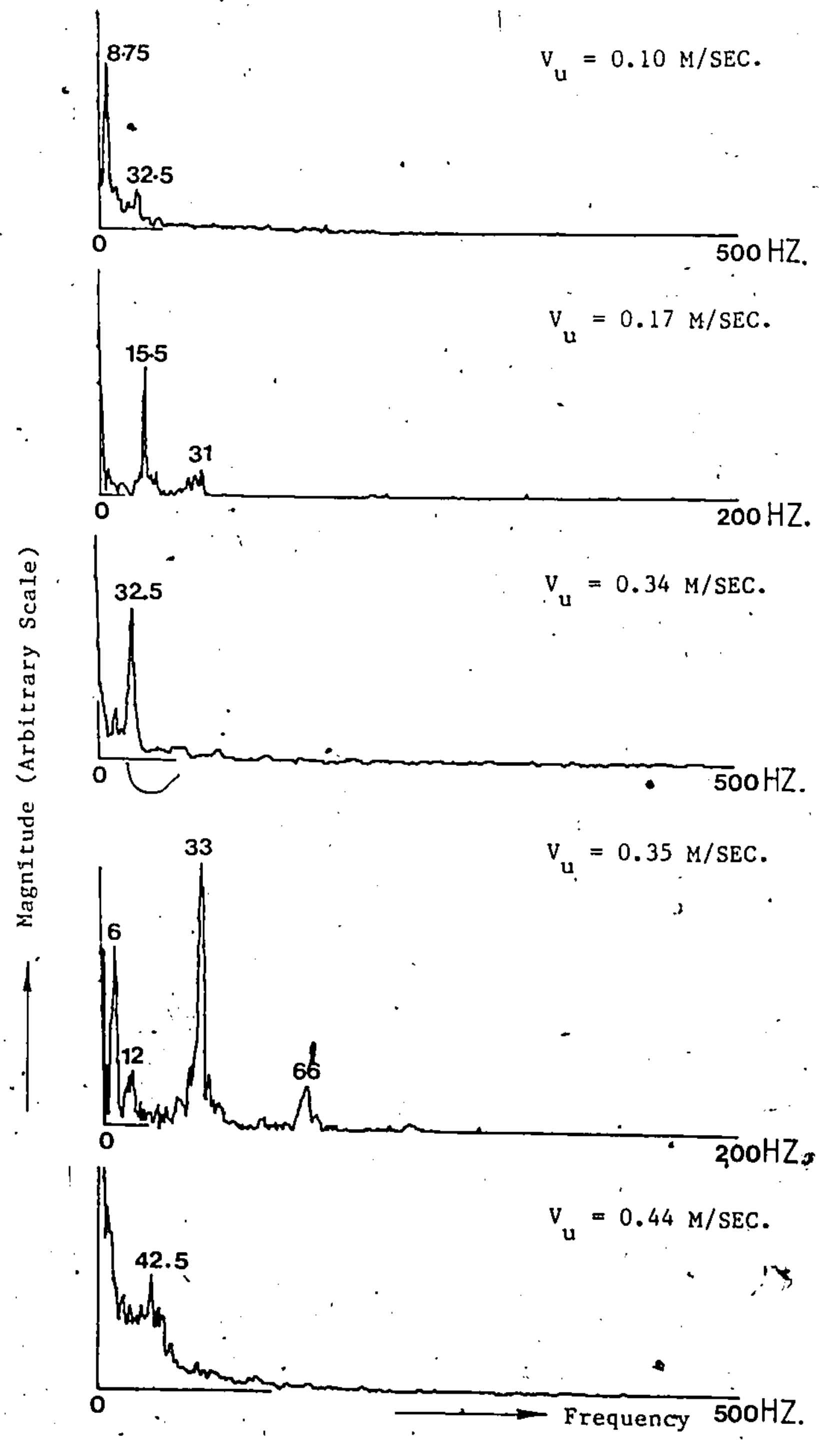

FIGURE 4.5: VELOCITY-SPECTRA FOR THE NORMAL SQUARE ARRAY WITH P/d = 1.33.

not observed for higher Reynolds numbers, there is considerable experimental evidence from both hot wire and tube response data to prove the existence of a discrete excitation phenomenon occuring at a constant Strouhal number for a given array geometry. The associated frequency spectra are not characteristic of turbulence phenomena, the energy being concentrated at a single frequency. For this reason, the phenomenon will be referred to as "vortex shedding" in this thesis.

The corresponding Strouhal number based on the upstream flow velocity and the outside diameter of the tube is $S_u = 2.22$. If the Strouhal number is based on the pitch velocity which is,

$$V_p = \frac{P}{P-d} \quad V_u$$

or the actual gap velocity (see Appendix C), the values will be 0.55 and 0.56 respectively.

With an increase in the flow velocity, the discrete frequency at 8.75 Hz was observed to be shifting to higher frequency. At an upstream flow velocity of 0.17 m/sec., a new velocity spectrum was computed. The spectrum is shown as the second trace in Figure 4.5. As is evident, the velocity fluctuations in the flow field are now concentrated at a discrete frequency of 15.50 Hz, with the appearance of weak signal at double this frequency at 31.0 Hz. The appearance of two vortex shedding frequencies has also been found by Grover and Weaver [48] and others [38,78,79] for flow over tube arrays. A calculated value of Strouhal number based on the corresponding value of the upstream velocity is 2.32.

The wind-tunnel speed was further increased to $V_u = 0.34$ m/sec., which happened to be double the value of the previous speed. The new computed velocity spectrum shown as the third trace in Figure 4.5, shows that the flow energy is concentrated at 32.50 Hz, which is almost double the frequency of the previous result. This indicates that the frequency at which two dimensional cylindrical vortices are shed is a linear function of the flow velocity at least in this range of measurement. The double frequency was not observed with this measurement, but with a slight increase in flow velocity to 0.35 m/sec., the energy peak was shifted slightly to a value of 33.0 Hz and a clear peak at double the frequency at 66.0 Hz. The velocity spectrum computed is shown as the fourth trace in Figure 4.5. The Strouhal numbers based on the upstream flow velocity are 2.43 and 2.40 respectively.

With a further increase in the flow velocity to $V_u = 0.44$ m/sec., a new velocity spectrum was computed as shown by the bottom trace of Figure 4.5. The corresponding Reynolds number based on the upstream flow velocity is $R_u = 740$. It is evident from this spectrum that the excess energy of the regular vortex shedding over the energy associated with the random turbulence in the flow has started to diminish. For a slight increase in the flow velocity, the computed velocity spectra showed complete disappearance of any regular vortex shedding. The experiment was repeated many times up to flow velocity beyond the critical velocity for this particular tube array, i.e. the tube array became unstable, and no discrete frequencies other than those obtained in this flow velocity range were observed.

As can be seen from Figure 4.5, for these low values of Reynolds number (in the range between $R_u = 170$ and $R_u = 740$), the wake has a very pronounced energy corresponding to the vortex shedding, while the turbulence components remain moderate. However, at a Reynolds number higher than $R_u = 740$, the excess energy of the vortices over the broad turbulence spectrum are seen to diminish.

The definition of the different flow velocities used in the literature with the corresponding values for the arrays used in the present research are given in Appendix C. The values of Strouhal numbers based on different flow velocities are given in Table 4.1. Values of the upstream flow velocities with the corresponding Reynolds numbers are also represented in this table. It is seen from this table that for the present array, the different definition of the gap velocity did not affect the value of Strouhal number. A plot of the vortex shedding frequency versus the upstream flow velocity is given in Figure 4.6. It is evident from this figure that the frequency at which vortices are shed is a linear function of the flow velocity over the entire range of measurements which is between Reynolds number of 170 to 740.

From Table 4.1, an average value of the Strouhal number based on upstream flow velocity for the present array will be $S_u = 2.34$. A high value of Strouhal number is usually expected for closely packed tube arrays. No data exists in the Strouhal number maps available in the literature for the present array. Thus, a comparison will be made on the basis of what the maps suggest for the present array. Chen's map [10] on Strouhal numbers for in-line arrays is shown in Figure

TABLE 4.1

Vortex shedding data for normal square array with P/d = 1.33.

V_u	R_u	f_s	S_u	S_{gm}	S_p, S_g
0.10	170	8.75	2.22	0.56	0.55
0.17	290	15.50	2.32	0.58	0.58
0.34	570	32.50	2.43	0.61	0.60
0.35	590	33.00	2.40	0.60	0.60
0.44	740	42.50	2.45	0.61	0.61

V_u = Upstream flow velocity (m/sec.)

R_u = Reynolds number based on upstream flow velocity (dimensionless)

f_s = Vortex shedding frequency (Hz)

S_u = Strouhal number based on upstream flow velocity (dimensionless)

S_{gm} = Strouhal number based on measured gap flow velocity, see Appendix C (dimensionless)

S_p = Strouhal number based on pitch velocity, see Appendix C (dimensionless)

S_g = Strouhal number based on theoretically calculated gap velocity, see Appendix C (dimensionless)

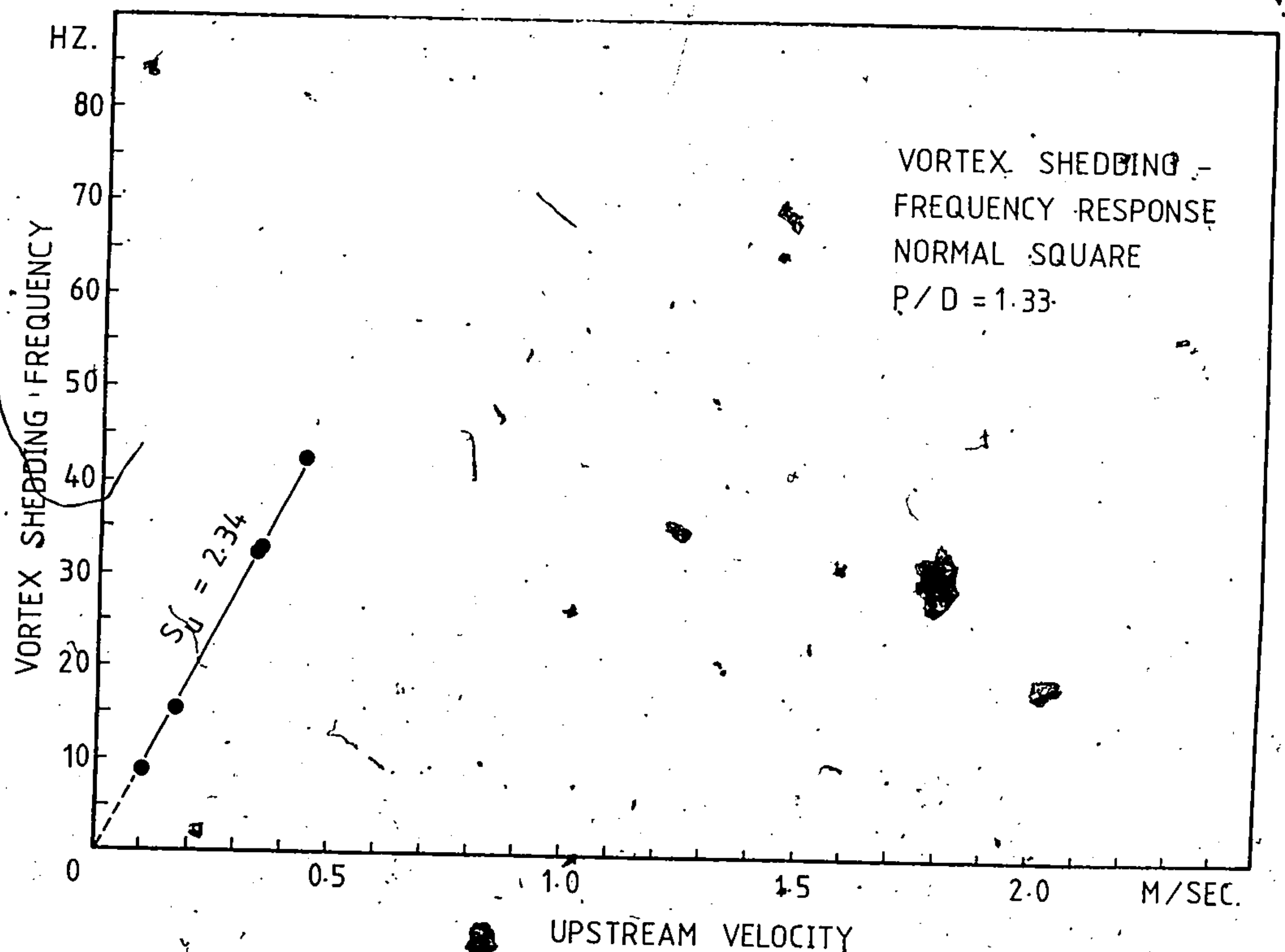
HZ.
80
70
60
50
40
30
20
10
0
VORTEX SHEDDING FREQUENCY
$S_u = 2.34$
VORTEX SHEDDING - FREQUENCY RESPONSE
NORMAL SQUARE
P / D = 1.33
0.5
1.0
1.5
2.0
M/SEC.
UPSTREAM VELOCITY

FIGURE 4.6

4.7. An interpolation of the curves indicate a Strouhal number of $S_g = 0.37$, or $S_u = 1.48$. This value is much lower than that observed (about 58% lower). On the other hand, according to Fitz-Hugh's map [11] (the map for in-line arrays is also shown in Figure 4.7) the expected Strouhal number S_g for the present array would be $S_g = 0.31$, or $S_u = 1.24$. This value is again 89% lower than the Strouhal number found in the present experiment. Pettigrew and Gorman [9] from tests in water flow did not observe any vortex shedding response for a normal square array with P/d = 1.30 (the same geometry and close pitch-to-diameter to the present array). However, recently Zukauskas and Katinas [12] conducted tests on normal square and normal triangular arrays. They observed vortex shedding response for a normal square array with P/d = 1.34. From their tests and a comparison with some of the published results, they proposed the following formula for estimating Strouhal numbers for normal square arrays:

$$S_p = 0.2 + \exp\left\{-\frac{(P/D)^{1.83}}{0.88}\right\}$$

with $P/d \geq 1.15$.

According to this formula $S_p = 0.35$ and so $S_u = 1.4$. Again this value is 67% lower than the value obtained for the present array. Most recently, Weaver and Yeung [23] suggested that normal square arrays of tubes may be excited by every vortex rather than each vortex pair. Accordingly, what is being observed for the present array could be double the value expected from the literature. If half the value obtained from the present experiment were considered, i.e. $S_u = 1.17$.

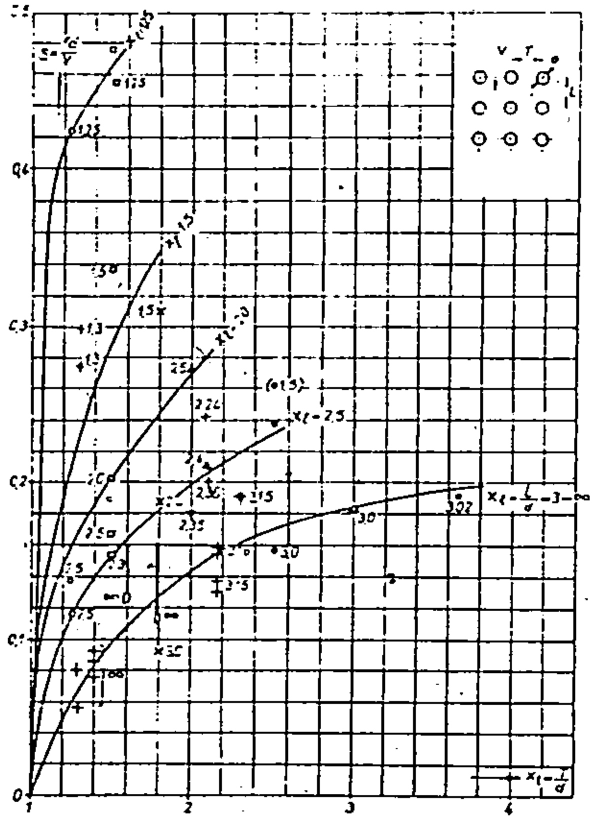

CHEN'S MAP [10]

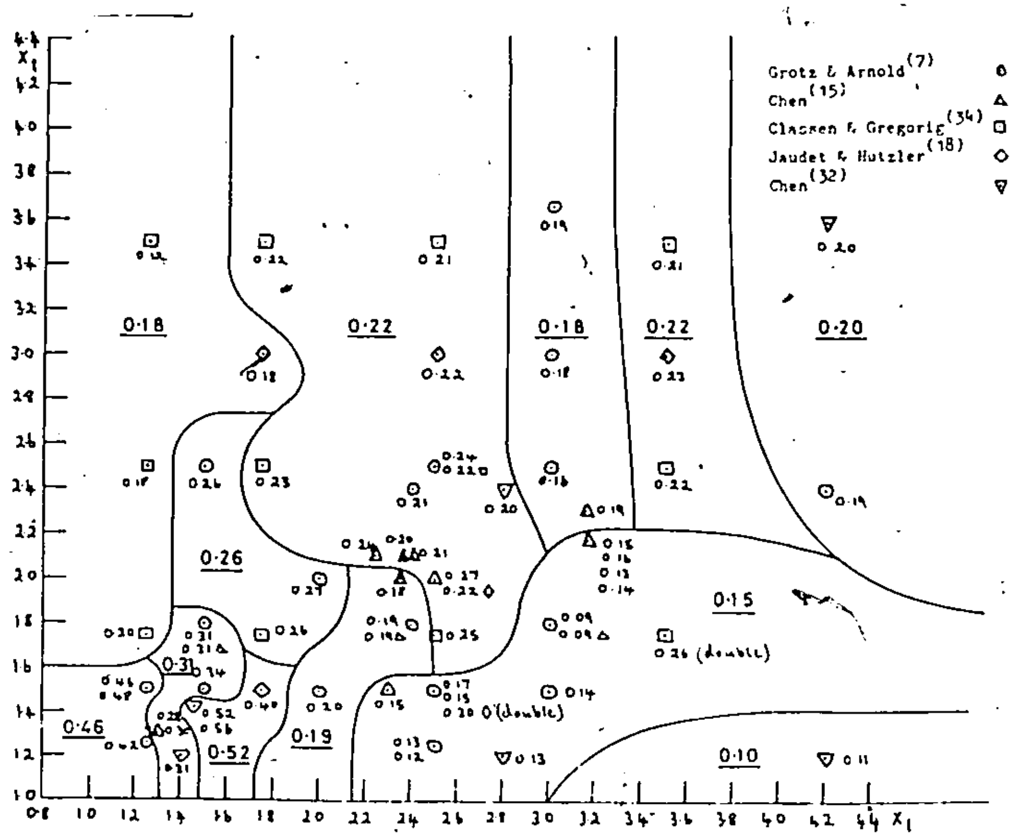

FITZ-HUGH'S MAP [11]

FIGURE 4.7 : GAP STROUHAL NUMBERS FOR IN-LINE ARRAYS

Chen's value will be higher by 26%, while Fitz-Hugh's value will be higher by only 6% and Zukauskas and Katinas' value will be higher by 20%.

It is also important to consider the argument raised by Paidoussis [7], that Owen's predictions of the turbulent buffeting frequencies due to the tube arrays being excited by turbulence in the flow, does not represent anything different but the same vortex shedding frequencies. Owen proposed the following formula for normal square arrays:

$$S_b = [3.05\,(1 - \frac{1}{(P/d)})^2 + 0.28]\,(P/d)^{-2}$$

where S_b is the buffeting frequency = S_p. Accordingly, $S_p = 0.26$, and so $S_u = 1.07$ is expected for the present array. This prediction is less than half the value obtained from the present experiment, and so it shows reasonable agreement if half the present value was considered (only lower by 9%).

While the measurement of vortex shedding frequency was always carried out for the eight arrays tested in the gap between rigid tubes, it is important to observe if the flexible tubes would vibrate in resonance with the vortex shedding. However, no change in the flexible tubes amplitude was observed for the present array. At the same time few experimental results are available in the literature for close arrays to the present array, so no further comparison can be made.

In summary, it can be stated that discrete periodicity characteristic of vortex shedding has been observed for the present normal square array of P/d = 1.33. Strouhal number based on upstream flow velocity is 2.34. Vortex shedding frequencies were observed for the Reynold number range; R_u = 170 - 740. It seems at this point that either the observed frequency is due to every vortex rather than each vortex pair as suggested by Weaver and Yeung [23] or, as will be seen later, for some tube arrays the Strouhal number may be a function of Reynolds number. Higher Reynolds numbers are associated with lower Strouhal numbers. The flexible tubes did not respond in resonance with the presence of vortex shedding.

Before the tube array was removed from the test-section, fluidelastic instability of the array was also studied. The results of this type of self-excited vibration will be given later in this chapter.

4.3.2 Normal Square Array: P/d = 1.5

The normal square array having P/d = 1.5, was also 4 rows deep, but with 7 tubes in each row as shown in Figure 4.8. Positions of the flexible tubes, as well as the instrumented tubes are also shown in this figure. The gap hot-wire probe was located in the gap between tubes in the third row.

The experiment was then started at a low flow velocity. The first concentration of the velocity fluctuations was observed at an upstream flow velocity of 0.25 m/sec. The corresponding Reynolds number is R_u = 420. The velocity fluctuations were concentrated at a discrete frequency of 17.25 Hz. This value is lower than the value

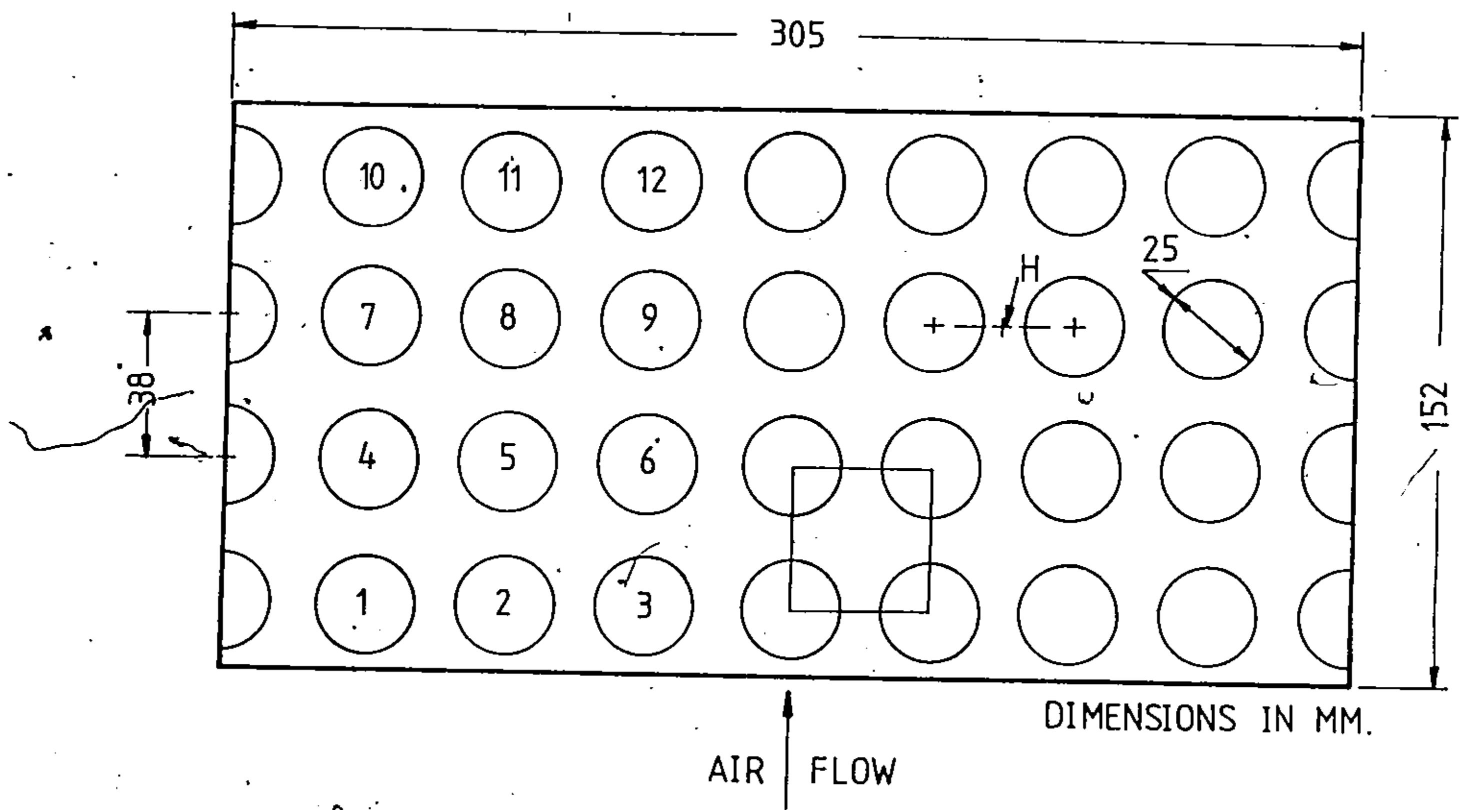

TUBES MARKED 1 - 12 ARE FLEXIBLE TUBES (REST ARE RIGID)
TUBES MARKED 5 AND 8 ARE INSTRUMENTED TUBES
H - LOCATION OF GAP HOT-WIRE PROBE

FIGURE 4.8: NORMAL SQUARE ARRAY WITH P/d = 1.5.

which would be expected using the constant Strouhal number relationship obtained from the previous array. This means that a lower value for Strouhal number is expected for the present array. Based on a flow velocity of 0.25 m/sec., a frequency of 17.25 Hz, and the outside diameter of the tube, the corresponding Strouhal number is 1.75. The computed velocity spectrum is shown in Figure 4.9 (a). As can be seen from this velocity spectrum the appearance of another discrete frequency at 31.25 Hz. Apparently, this value does not represent double the value of the first frequency.

As the flow velocity was increased to V_u = 0.30 m/sec., the discrete frequency of the velocity fluctuations in the flow field was shifted to a higher value of 20.25 Hz. The corresponding Strouhal number is 1.71. The computed velocity spectrum is given in Figure 4.9 (b). Again, no discrete frequency was observed at double the frequency of the original signal, but rather the second frequency which was observed previously at 31.25 Hz is now at 32.25 Hz. It is clear that this second frequency does not follow the constant Strouhal number relationship. More interestingly, the level of energy associated with these two frequencies was noticed to exchange between them. An indication of this energy exchange is shown in Figure 4.9 (c). This velocity spectrum was computed at the same flow velocity but at a different time. A weak signal at double this second frequency can be seen on this spectrum.

With further increase in the wind tunnel speed to V_u = 0.35 m/sec. a new velocity spectrum was computed as shown in Figure 4.9 (d). The energy corresponding to the vortex shedding frequency is at

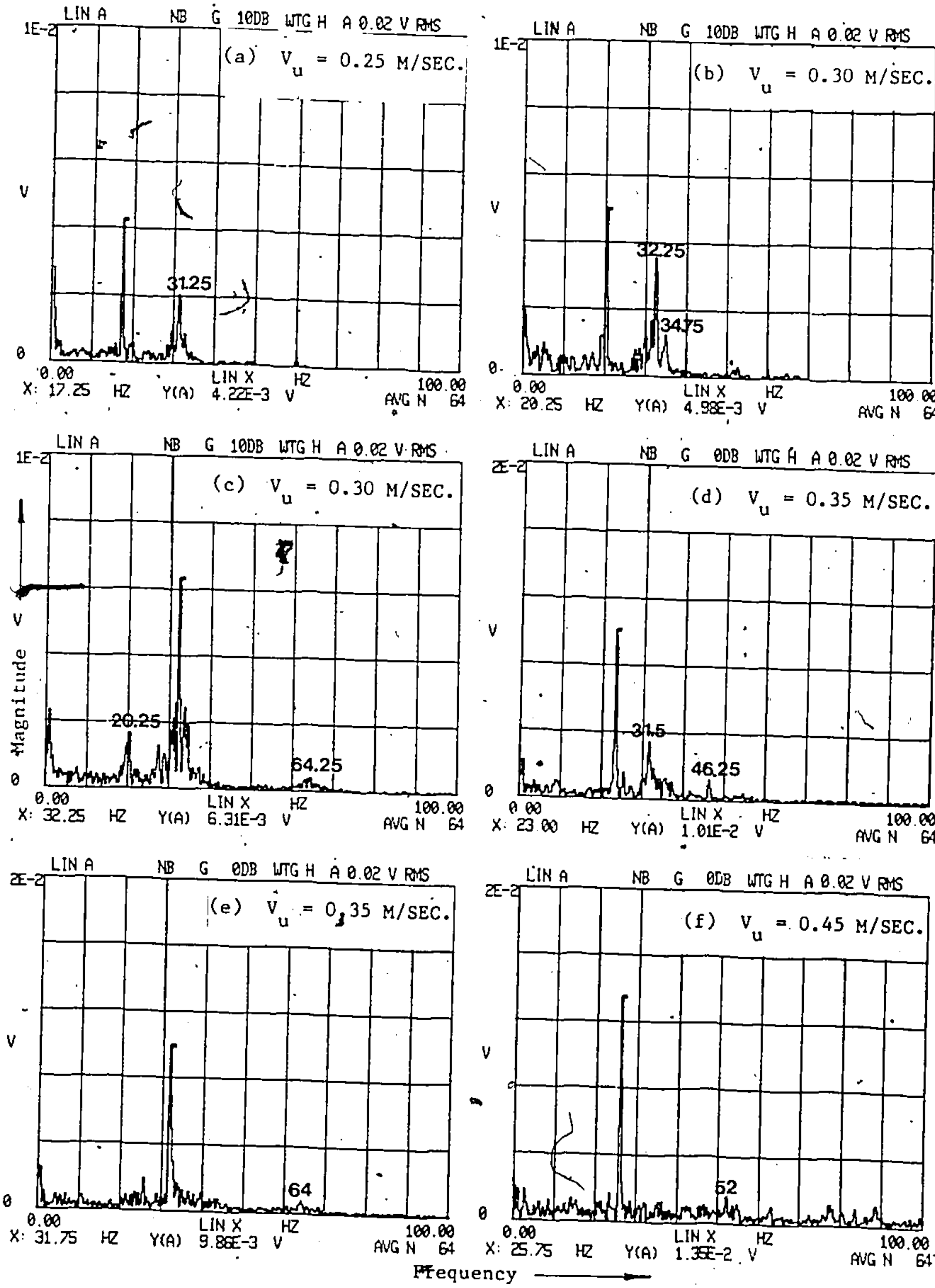

FIGURE 4.9: VELOCITY-SPECTRA FOR THE NORMAL SQUARE ARRAY WITH P/d = 1.5 .

23.0 Hz. The corresponding Strouhal number is 1.67. For the first time appearance of double the frequency can be seen at 46.25 Hz. The second frequency was dropped slightly to a value of 31.5 Hz. An interesting result was obtained when another velocity spectrum was computed at the same flow velocity but at a different instant of time. The new spectrum is given in Figure 4.9 (e). Surprisingly the energy corresponding to the vortex shedding has disappeared completely with the appearance of only the second frequency at 31.75 Hz.

A new velocity spectrum was computed as the flow velocity was increased to a value of V_u = 0.45 m/sec. As can be seen from Figure 4.9 (f), only a discrete frequency at 25.75 Hz with about double this frequency at 52.0 Hz were obtained. The corresponding value of Strouhal number is 1.45. This value is noticably lower than the value of Strouhal number obtained from the previous velocity spectra, the new value being lower by 19%. The corresponding Reynolds number is R_u = 760. However, at the same flow velocity but at a different time, another velocity spectrum was computed. This velocity spectrum is given in Figure 4.10 (a). As can be seen the discrete frequency at 25.75 Hz has disappeared completely, giving a rise to another well pronounced discrete frequency at 36.25 Hz. The reason behind this kind of behaviour is not understood. However, it seems that the flow becomes unstable at this value of Reynolds number. The value of Strouhal number is 2.04. This value is higher than the originally estimated value of Strouhal number for the present array by about 19%.

The flow velocity was then increased to V_u = 0.50 m/sec. The same behaviour was obtained as shown in Figures 4.10 (b) and 4.10 (c).

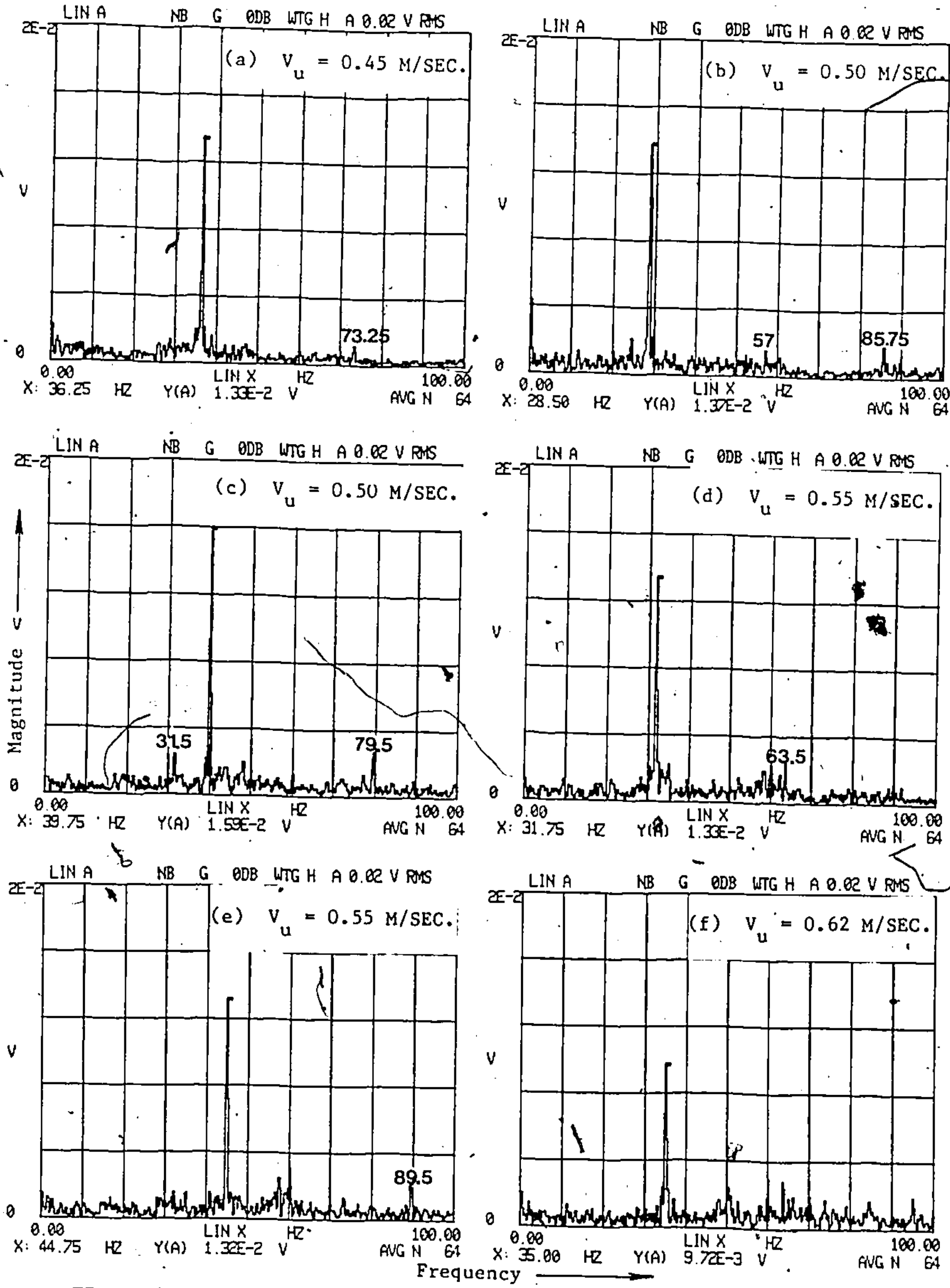

FIGURE 4.10: CONTINUED VELOCITY-SPECTRA FOR THE NORMAL SQUARE ARRAY WITH P/d = 1.5.

The new discrete frequency at 28.50 Hz gives a value of Strouhal number of 1.45, while the second frequency at 39.75 Hz gives a Strouhal number of 2.02. These new values of Strouhal number seem to follow closely the constant Strouhal number relationship with the previous numbers.

As the wind tunnel speed was increased to $V_u = 0.55$ m/sec., the concentration of the velocity fluctuations in the flow field was shifted to higher discrete frequencies of 31.75 Hz, and 44.75 Hz. The velocity spectra are given in Figures 4.10 (d) and 4.10 (e). Again, the corresponding Strouhal numbers are 1.47 and 2.07, respectively. Note the appearance of the double frequencies at 63.50 Hz and 89.50 Hz, respectively.

Four more velocity spectra were computed at an upstream flow velocity of 0.62 m/sec. and 0.67 m/sec. respectively. The velocity spectra are shown in Figures 4.10 (f) and 4.11 (a), (b) and (c). The corresponding Strouhal numbers are 1.43, 2.04, and 1.42, 2.01 respectively. Note that the level of energy associated with the last two spectra started to decrease compared with the previous ones. However, as the flow velocity was increased to higher values ($R_u >$ 1130), no discrete frequencies were obtained as the flow becomes more turbulent.

Vortex shedding frequencies were plotted versus the upstream flow velocity as shown in Figure 4.12. As can be seen from this figure, three values of Strouhal numbers were obtained. All frequencies for these Strouhal numbers seem to follow the constant Strouhal number relationship. Different frequencies at different

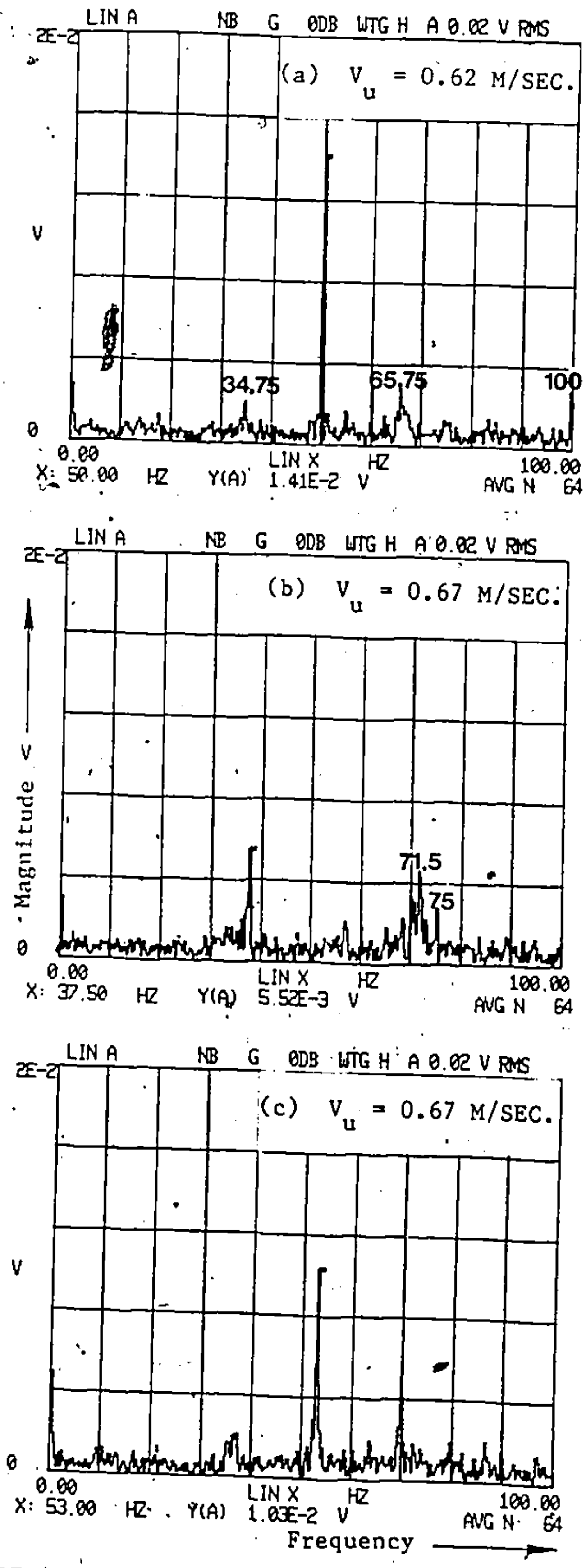

FIGURE 4.11: CONTINUED VELOCITY-SPECTRA FOR THE NORMAL SQUARE ARRAY WITH P/d = 1.5.

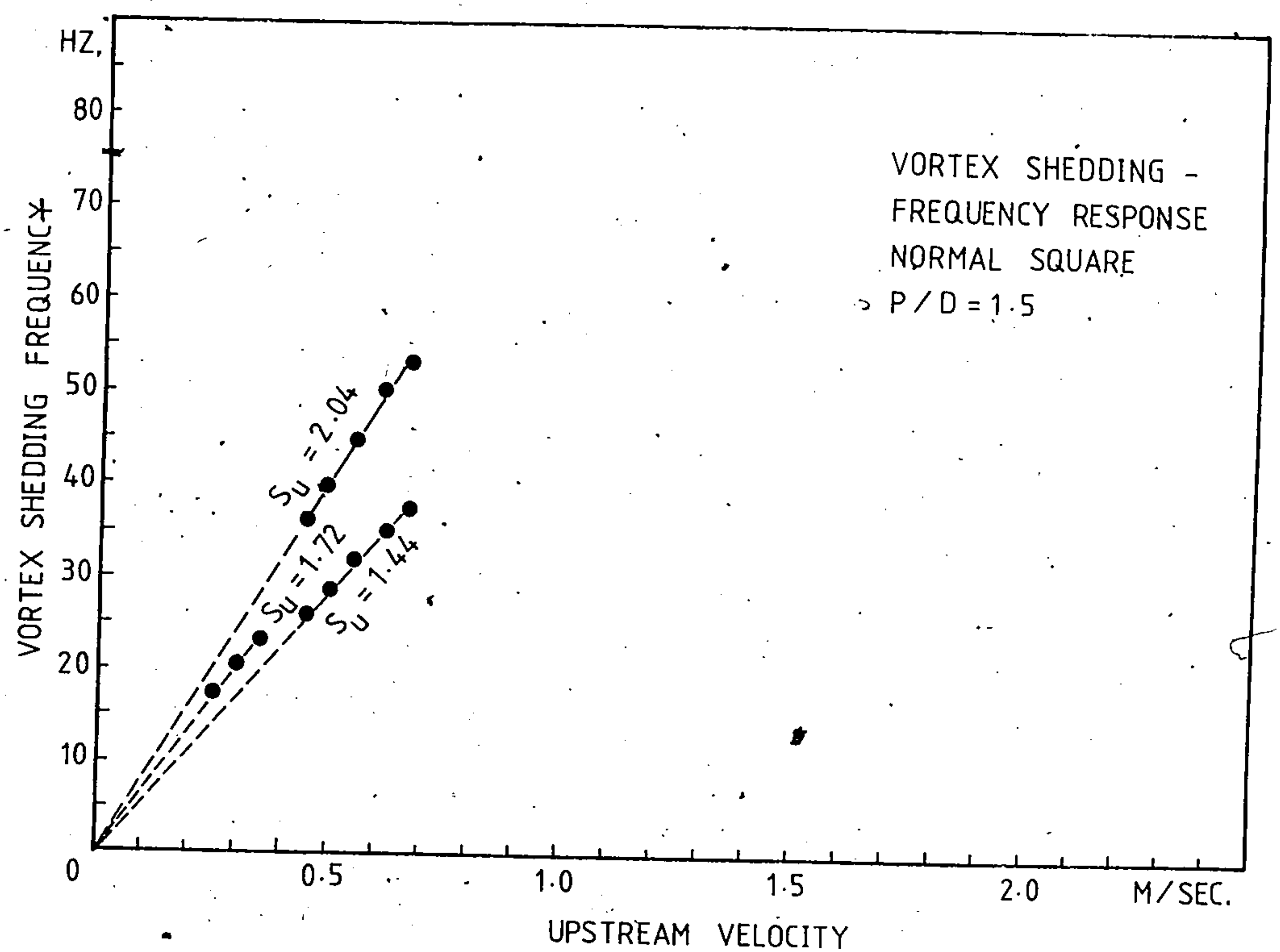
VORTEX SHEDDING -
FREQUENCY RESPONSE
NORMAL SQUARE
P / D = 1·5
HZ,
80
70
60
50
40
30
20
10
0
VORTEX SHEDDING FREQUENCY
0·5
1·0
1·5
2·0
M/SEC.
UPSTREAM VELOCITY
Su = 2.04
Su = 1.72
Su = 1.44

FIGURE 4.12

upstream flow velocities with the corresponding Reynolds numbers are tabulated in Table 4.2. Also given in this Table are the values of Strouhal numbers based on different definitions of flow velocities (see Appendix C). According to the definition of flow velocities for normal square arrays, we can see from the table that $S_p = S_g$. Because the measured ratio between the experimentally determined gap flow velocity and the upstream flow velocity was higher by 14% than that calculated on geometrical basis, the gap Strouhal number S_{gm} is lower by 14% than S_g or S_p. An average value of Strouhal number based on the upstream flow velocity is $S_u = 1.72$, for the Reynolds number range from $R_u = 420$ to $R_u = 590$. For Reynolds number between $R_u = 760$ and $R_e = 1130$, two values of Strouhal number were obtained for the present array with average values of $S_u = 1.44$ and $S_u = 2.04$.

There are few data existing in the literature for the Strouhal number of the present array (normal square with P/d = 1.5). Grotz and Arnold [40] obtained a value of $S_u = 1.02$. This value is lower than the lowest value obtained for the present array ($S_u = 1.44$) by 41% and exactly half the highest value of $S_u = 2.04$. Unfortunately, the range of Reynolds number in which Grotz and Arnold obtained their results is not available. On the other hand, Chen's map [10] (see Figure 4.7) gives a value of $S_u = 0.87$. Again, this value is 66% lower than the value of $S_u = 1.44$. However, Chen drew his map at a much higher Reynolds number range of $R_u = 0.5 - 2 \times 10^4$. Fitz-Hugh's map [11] (also given in Figure 4.7) predicts a value of $S_u = 0.93$. This value is lower than the value of $S_u = 1.44$ by 55%. Zukauskas and Katinas formula [12] gives a value of $S_u = 0.88$ for the Reynolds number range

TABLE 4.2

Vortex shedding data for normal square array with P/d = 1.5.

V_u	R_u	f_s	S_u	S_{gm}	S_p, S_g
0.25	420	17.25	1.75	0.51	0.58
0.30	510	20.25	1.71	0.50	0.57
0.35	590	23.00	1.67	0.49	0.56
0.45	760	25.75	1.45	0.42	0.48
		36.25	2.04	0.60	0.68
0.50	840	28.50	1.45	0.42	0.48
		39.75	2.02	0.59	0.67
0.55	930	31.75	1.47	0.43	0.49
		44.75	2.07	0.61	0.69
0.62	1050	35.00	1.43	0.42	0.48
		50.00	2.04	0.60	0.68
0.67	1130	37.50	1.42	0.42	0.47
		53.00	2.01	0.59	0.67

between $R_u = 3.3 \times 10^3$ to $R_u = 6.7 \times 10^4$. Again, this value is lower than the value of $S_u = 1.44$ by 64%. Owen's formula [8] gives a value of $S_u = 0.83$. While this value agrees with the values represented up till now, it is again much lower than the lowest value obtained for the present array. It is also important to note that a better agreement is obtained with the above published results if half the present results were considered. However, Weaver and Yeung [21] predicted a value for S_u which is higher than $S_u = 1.10$ obtained at an approach flow direction of 20^o to the normal square array and for R_u = 750 - 1150. If this value was considered, it agrees with the value S_u = 1.44 obtained for the present array (only lower by 31%). However, most recently, Weaver and Yeung [23] from their experiments in water flow for the Reynolds number range $R_u = 2.0 - 2.70 \times 10^3$ predicted a value of $S_u = 1.8$ for the present array. This value agrees very well with the value $S_u = 1.72$ obtained from the present experiment in air flow in the Reynolds number range $R_u = 420 - 590$ (only higher by 5%). On the other hand, the values for Strouhal number obtained by Pettigrew and Gorman [9] for a normal square array with P/d = 1.47, in water flows were between $S_u = 1.28$ and $S_u = 1.97$ (depending on tube location). These values agree very well with the three values obtained for the present array. Their results were obtained in the Reynolds number range $R_u = 2.0 - 4.2 \times 10^3$. Finally, data by Fitzpatrick [80] also gives 3 Strouhal numbers of S_u = 0.78, 0.98 and 1.33 for in-line array with transverse spacing of 1.73 and longitudinal spacing of 1.5. These values show good agreement with the present results when taken into account the effect of transverse spacing.

In summary, it can be said that vortex shedding frequencies were observed for a normal square array with P/d = 1.5, in the Reynolds number range, between R_u = 420 to R_u = 1130. Three values for Strouhal number were obtained. The values as based on the upstream flow velocity are S_u = 1.44, S_u = 1.72 and S_u = 2.04. These three values which were obtained for the first time from hot-wire probe measurement in air flow, showed a better agreement with some of the published results for water flows at slightly higher values of Reynolds number. It should be noted that the results in water flow were obtained from off-resonance tube response, rather than interstitial flow velocity fluctuations.

Discussion

Vortex shedding frequencies for normal square arrays with P/d = 1.33 and 1.5 showed Strouhal numbers which are much higher than those available in literature. The same behaviour was also observed by Weaver and Yeung [23] for a normal square array with P/d = 1.5. They reported that the reason behind this behaviour may be the result of measuring every vortex rather than each vortex pair. High Strouhal numbers were also reported by Pettigrew and Gorman [9] for a normal square array with P/d = 1.47 in water flow. However, they did not mention any reason regarding this behaviour. Unfortunately, they have not observed any vortex shedding response for a normal square array with P/d = 1.3. On the other hand, Strouhal numbers may even be slightly different from one tube row to another as was reported by Pettigrew and Gorman. However, for the normal square array with P/d =

1.5, three values of Strouhal number were obtained. While these values were obtained for an array in air where no tube response was observed, they agree with the above mentioned results in water and where significant amplitude tube vibrations were observed. The fact that the constant Strouhal number excitation was observed for somewhat higher Reynolds numbers in water than in air may be due to the fact that the tubes in water were flexible. This could result in some fluid-structure coupling, the tube motion thereby sustaining the vortex shedding to higher Reynolds numbers than possible for the rigid tubes in air.

Many attempts were made to correlate the existing data for normal square arrays with different pitch-to-diameter ratios. The collected data for Strouhal numbers which is based on the pitch velocity (see Appendix C) versus the pitch-to-diameter ratios are shown in Figure 4.13. The figure includes the results of Owen [8], Pettigrew and Gorman [9], Chen [10], Fitz-Hugh [11], Zukauskas and Katinas [12], Weaver and Yeung [23], Grotz and Arnold [40], and the present results. The scatter in the data is large especially at low values of pitch-to-diameter ratios. As can be seen from this figure, Fitz-Hugh's map [11] gives the same value of Strouhal number for many arrays of different pitch-to-diameter ratios. Also, it is seen that Owen's formula [8] shows that Strouhal number decreases with decreasing pitch-to-diameter ratios below about P/d = 1.7. Also, the value of Strouhal number should be the same as that for a single cylinder (S = 0.2) as P/d reaches a value of 3 or higher. Owen's formula predicts a decreasing value of Strouhal number for P/d > 3.

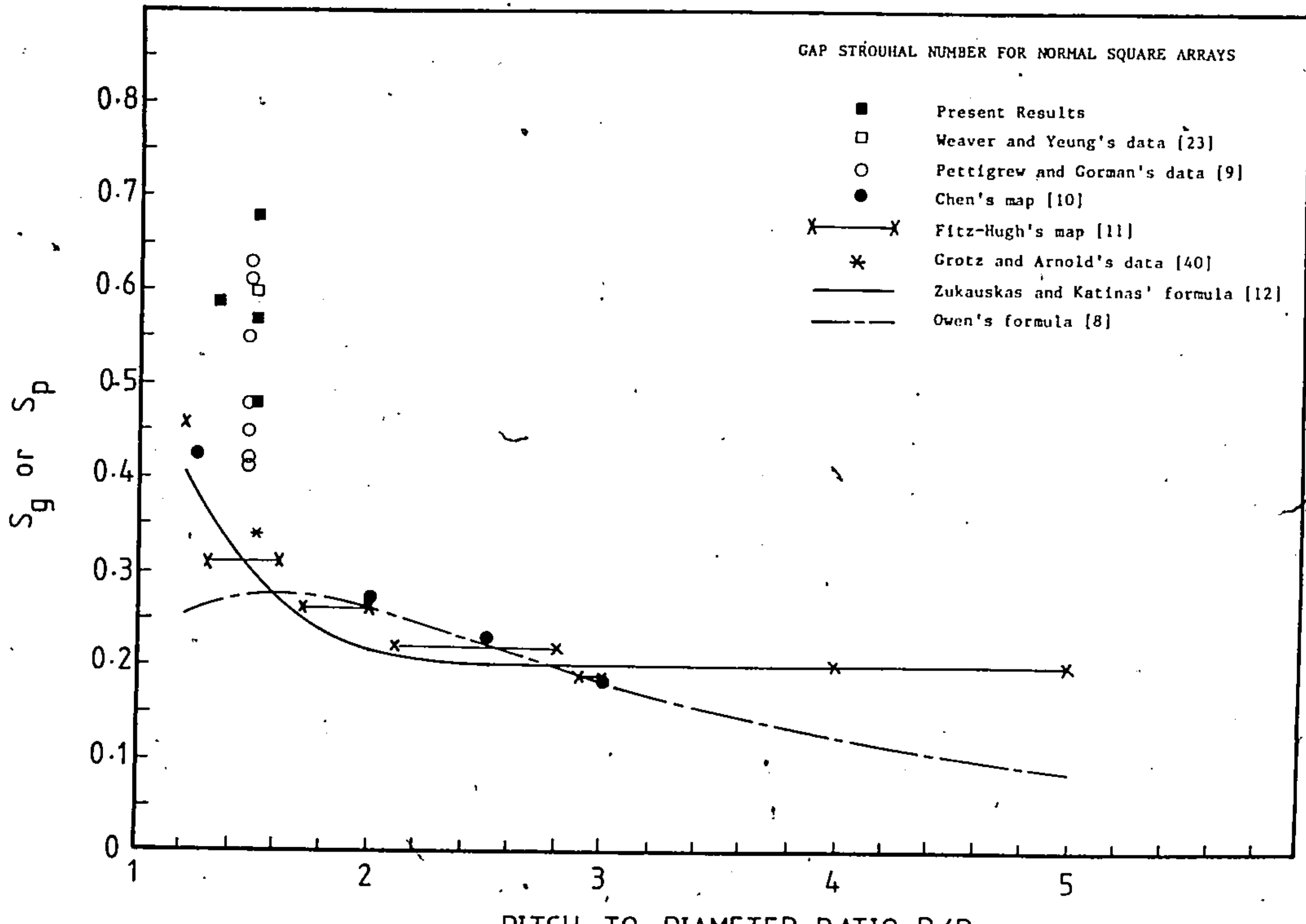
GAP STROUHAL NUMBER FOR NORMAL SQUARE ARRAYS
Present Results
Weaver and Yeung's data [23]
Pettigrew and Gorman's data [9]
Chen's map [10]
Fitz-Hugh's map [11]
Grotz and Arnold's data [40]
Zukauskas and Katinas' formula [12]
Owen's formula [8]
0.8
0.7
0.6
0.5
0.4
0.3
0.2
0.1
0
S_g or S_p
1
2
3
4
5
PITCH-TO-DIAMETER RATIO P/D

FIGURE 4.13

The large scatter in the data of Figure 4.13, was the reason behind replotting Strouhal numbers but on the basis of the upstream flow velocity instead of the pitch velocity. The new plot is given in Figure 4.14. Interestingly, the decay in Strouhal number with decreasing the pitch-to-diameter ratio predicted by Owen's formula, shows now the reverse. The reason behind that is the ratio between the pitch velocity and the upstream flow velocity defined as

$$\frac{V_p}{V_u} = \frac{P}{P-d}$$

It is easy to see that as the pitch-to-diameter ratio gets smaller the ratio V_p/V_u increases rapidly. Owen's predictions also improve for larger pitch ratios. It would appear that the velocity used by Owen in his formula was incorrect. Also shown in this plot are the results of Gregorig and Classen [44]. The plot also shows the difference between Zukauskas and Katinas formula [12] and their experimental results. The argument which Paidoussis [7] raised about Owen's turbulent buffeting mechanism as being the vortex shedding mechanism seems to be true especially for P/d > 1.5 and at high values of Reynolds number. However, Paidoussis raised another point about the maps of Chen [10] and Fitz-Hugh [11] as being based on data from mainly the same sources but large scatter exists between them. The plot in Figure 4.14 shows only minor differences if any between their points. The reason behind Paidoussis' observation was that some but not all of Fitz-Hugh's data points were used.

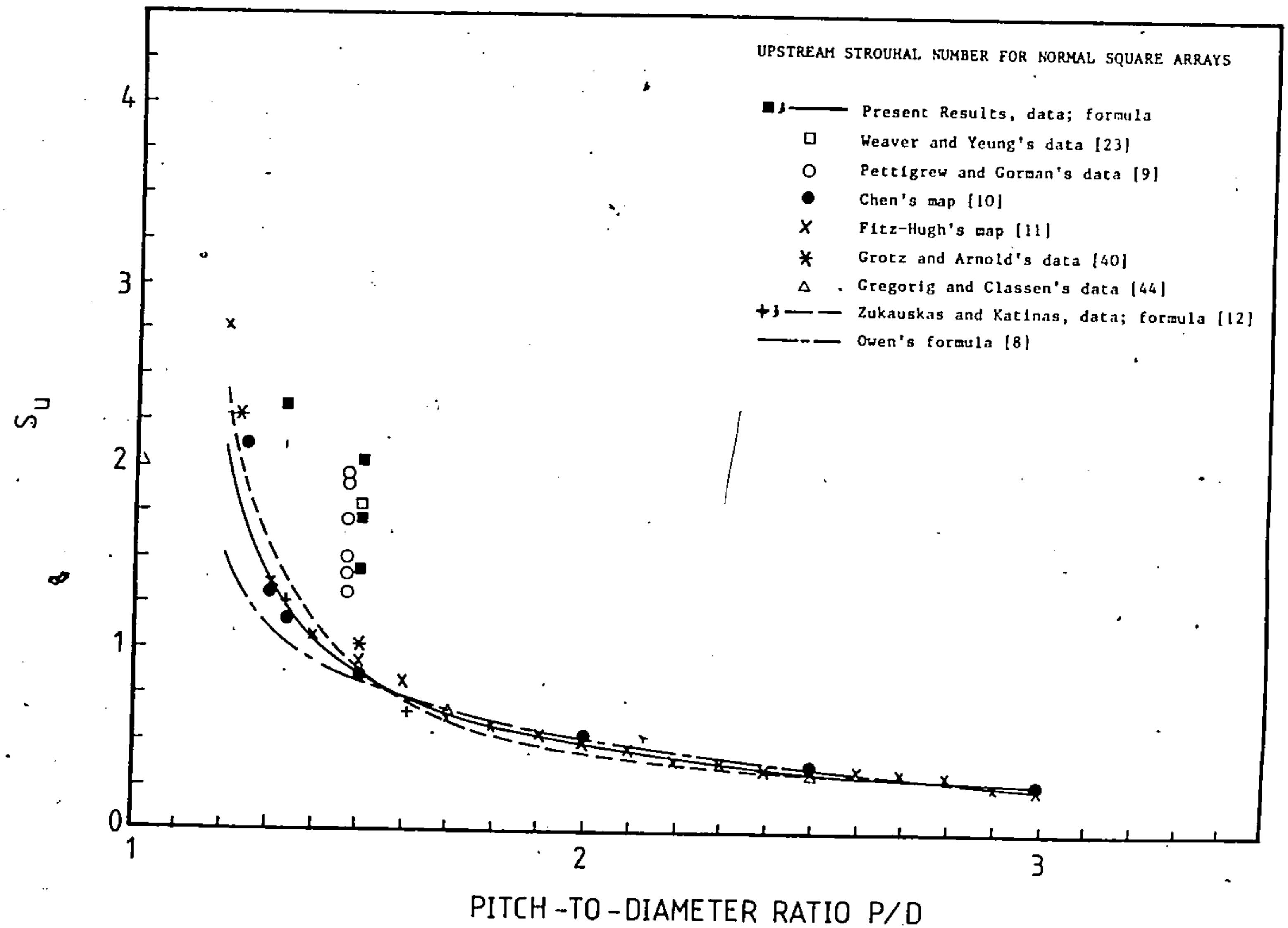
UPSTREAM STROUHAL NUMBER FOR NORMAL SQUARE ARRAYS
Present Results, data; formula
Weaver and Yeung's data [23]
Pettigrew and Gorman's data [9]
Chen's map [10]
Fitz-Hugh's map [11]
Grotz and Arnold's data [40]
Gregorig and Classen's data [44]
Zukauskas and Katinas, data; formula [12]
Owen's formula [8]
S_u
0
1
2
3
4
PITCH-TO-DIAMETER RATIO P/D

FIGURE 4.14

After many long trials, a best fit through the results in Figure 4.14 for Strouhal numbers at high Reynolds numbers was obtained. The best fit which was a combination of a logarithmic and power-law is given by the solid-curve in Figure 4.14. The equation which represents this curve has the form,

$$S_u = -1 + \exp\left\{\frac{[(P/d)-1]^{-0.66}}{2.5}\right\}$$

The difference between this equation and any of the available data for $P/d \geq 1.4$ is within about $\pm 12\%$, except for $P/d = 1.5$ where the difference is $\pm 16\%$. Note that the present results are not included in this equation as it is believed at this point that the phenomenon is Reynolds number dependent as will be discussed later in this Chapter under overview. For $P/d = 1.3$ the difference is $\pm 22\%$. The highest difference of $\pm 36\%$ is for $P/d = 1.2$. Further study is needed to confirm other results for normal square arrays with $P/d = 1.2$ at high Reynolds numbers.

It is hoped that the new equation will serve as a reasonable design guideline against vortex shedding response for normal square arrays expecially for water flows where the phenomenon is more important due to the high amplitudes associated with it.

4.3.3 Rotated Square Array; P/d = 1.414

The rotated square array with $P/d = 1.414$ is shown in Figure 4.15. The array is 5 rows deep with 6 tubes in every row including

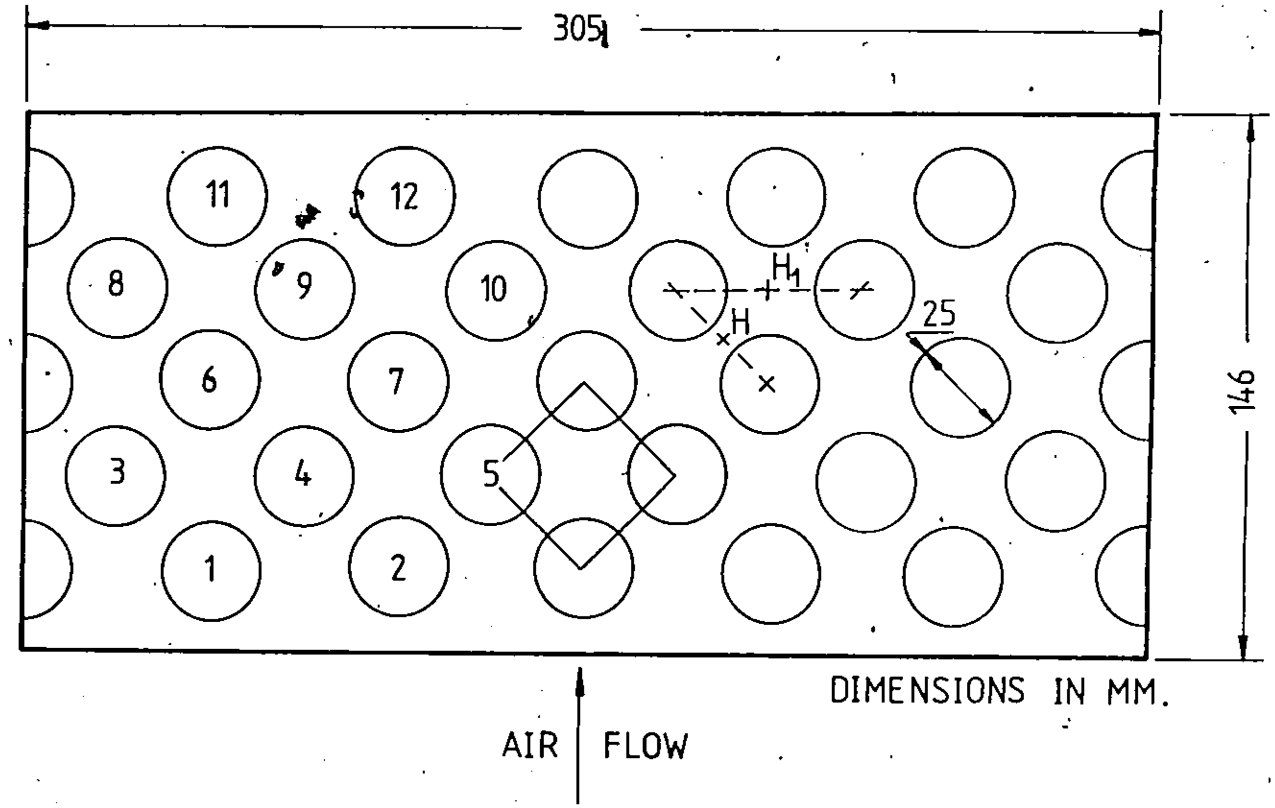

TUBES MARKED 1 - 12 ARE FLEXIBLE TUBES (REST ARE RIGID)
TUBES MARKED 4 AND 9 ARE INSTRUMENTED TUBES
H AND H1 - LOCATION OF GAP HOT-WIRE PROBE

FIGURE 4.15: ROTATED SQUARE ARRAY WITH P/d = 1.414.

the half tubes. The hot-wire probe was located in the position marked "H" between the third and fourth row as shown in Figure 4.15.

The first velocity spectrum was computed at an upstream flow velocity of $V_u = 0.11$ m/sec. No discrete frequencies were observed below this flow velocity. The velocity spectrum is shown in Figure 4.16 (a). As can be seen, a strong very clear discrete frequency at 7.00 Hz was obtained. Also, obtained was the appearance of a few harmonics at 14.0 Hz, 21.0 Hz, 28.0 Hz and 35.0 Hz. The appearance of more than the second harmonic was not observed with the previous arrays or reported before. The discrete frequency at 7.00 Hz, gives a Strouhal number based on the upstream flow velocity of $S_u = 1.69$. The corresponding Reynolds number based on the tube outside diameter is $R_u = 180$.

As the flow was increased to $V_u = 0.15$ m/sec. the discrete frequency shifted to 10.25 Hz. The velocity spectrum is given in Figure 4.16 (b). The corresponding Strouhal number is $S_u = 1.73$. No other harmonics were obtained in this case. Note also that the level of energy associated with this discrete frequency is lower than the one with the frequency of 7.0 Hz in the first velocity spectrum. However, the discrete frequency of the velocity fluctuations went up to 12.75 Hz as the flow velocity was increased to $V_u = 0.19$ m/sec, as shown in Figure 4.16 (c). The upstream Strouhal number is $S_u = 1.75$.

At an upstream flow velocity of $V_u = 0.20$ m/sec, a new velocity spectrum was computed and given in Figure 4.16 (d). Three discrete frequencies are seen at 11 Hz, 13.25 Hz, and 15.25 Hz. However, the level of energy associated with the discrete frequency at

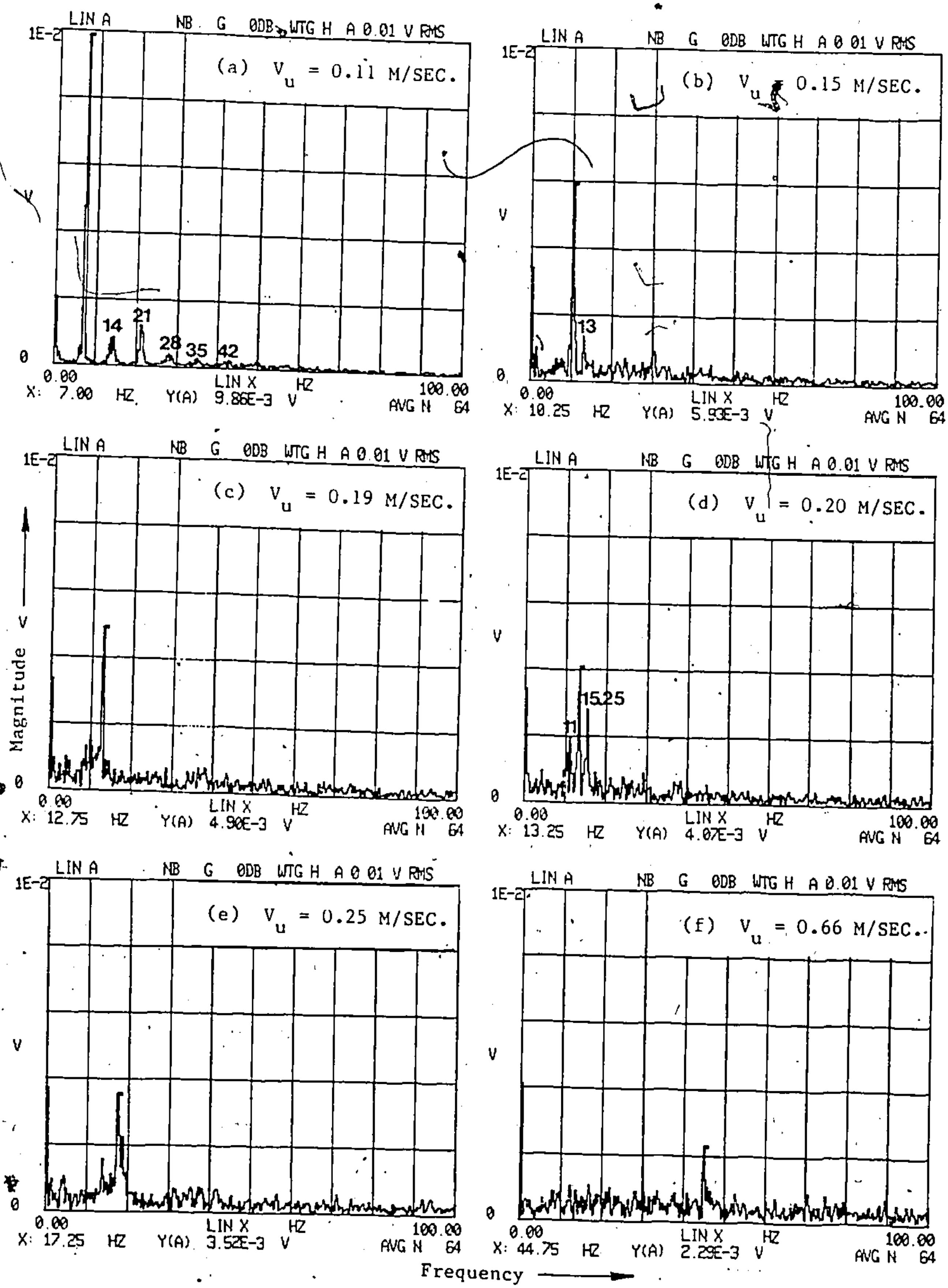

FIGURE 4.16 VELOCITY-SPECTRA FOR THE ROTATED SQUARE ARRAY WITH P/d = 1.414.

13.25 Hz was the highest, and showed that it followed the constant Strouhal number relationship more than the other frequencies. The frequency of 13.25 Hz gives a value of Strouhal number, $S_u = 1.72$.

As many as 9 more velocity spectra were also computed at different upstream flow velocities in the velocity range between V_u = 0.25 m/sec. to V_u = 0.66 m/sec. Due to the similarity of the obtained spectra, only the first and last spectra are given as shown in Figures 4.16 (e) and 4.16 (f). However, the only difference between them is that the level of energy associated with the vortex shedding frequency decays as the flow velocity becomes higher and the background turbulence intensities increase as the flow velocity increases. However, no discrete frequency of the velocity fluctuations was obtained with flow velocities higher than V_u = 0.66 m/sec. The corresponding Reynolds number is R_u = 1120. All discrete frequencies, upstream flow velocities, and the corresponding Reynolds numbers are given in Table 4.3. Also given in this table are the Strouhal numbers based on different definitions of flow velocities used in the literature (see Appendix C). From Table 4.3 the average values for Strouhal numbers are $S_u = 1.73$, $S_{gm} = 0.60$, $S_p = 0.50$, $S_g = 0.72$. It is very important to see that a difference between S_g, S_p is of the order of 0.22. Such a difference may be one of the reasons behind some of the scatter in the published data. Hot-wire probe measurement in position "H_1", (see Figure 4.15) showed that flow velocities are about one-half those measured in position "H". This shows the importance of mislocating the hot-wire probe for flow velocity measurement. The vortex shedding frequencies were plotted versus the

TABLE 4.3

Vortex shedding data for rotated square array with P/d = 1.414.

V_u	R_u	f_s	S_u	S_{gm}	S_p	S_g
0.11	180	7.00	1.69	0.59	0.49	0.70
0.15	250	10.25	1.73	0.60	0.51	0.72
0.19	310	12.75	1.75	0.61	0.51	0.72
0.20	330	13.25	1.72	0.60	0.50	0.71
0.25	410	17.25	1.79	0.63	0.52	0.74
0.30	510	21.25	1.77	0.62	0.52	0.73
0.34	580	23.75	1.76	0.61	0.51	0.73
0.40	680	27.50	1.74	0.61	0.51	0.72
0.45	770	30.75	1.72	0.60	0.50	0.71
0.51	860	34.25	1.72	0.60	0.50	0.71
0.52	880	35.25	1.71	0.60	0.50	0.71
0.60	1010	40.25	1.70	0.59	0.50	0.70
0.66	1120	44.75	1.71	0.60	0.50	0.71

upstream flow velocities as shown in Figure 4.17. All frequencies followed the constant Strouhal number relationship in the Reynolds number range, R_u = 180 to R_u = 1120.

In the following a comparison between S_u of the present array and what is available in the literature will be made on the basis of the ratio between theoreticaly determined gap velocity and the upstream flow velocity, which is

$$V_g/V_u = \frac{\sqrt{2}}{2} \frac{P}{P-d}$$

The reason is that using the ratio P/P-d gives higher values of flow velocities than those actually seen and is not a physically meaningful flow velocity for this array geometry.

Chen [10] has the only available data point on his map (see Figure 4.18) for a staggered array with P/d = 1.414. According to Chen, S_u = 1.55. This value is slightly lower than the value obtained for the present array (12% lower). On the other hand Owen's formula [8] gives a value of S_u = 1.26. This value is much lower than the present value (37% lower). Values from Fitz-Hugh's map [11] (see Figure 4.18) which agrees with Owen's formula for staggered arrays predicts a value of S_u = 1.09, which is lower than the present value by 59%. Zukauskas and Katinas formula [12], which was obtained for normal triangular arrays shows good agreement when applied for rotated square arrays as will be seen later in this section under discussion. According to their formula the value of S_u will be 1.56. This value agrees with Chen's result and only lower by 11% than the result obtained for the present array. However, it is also important to

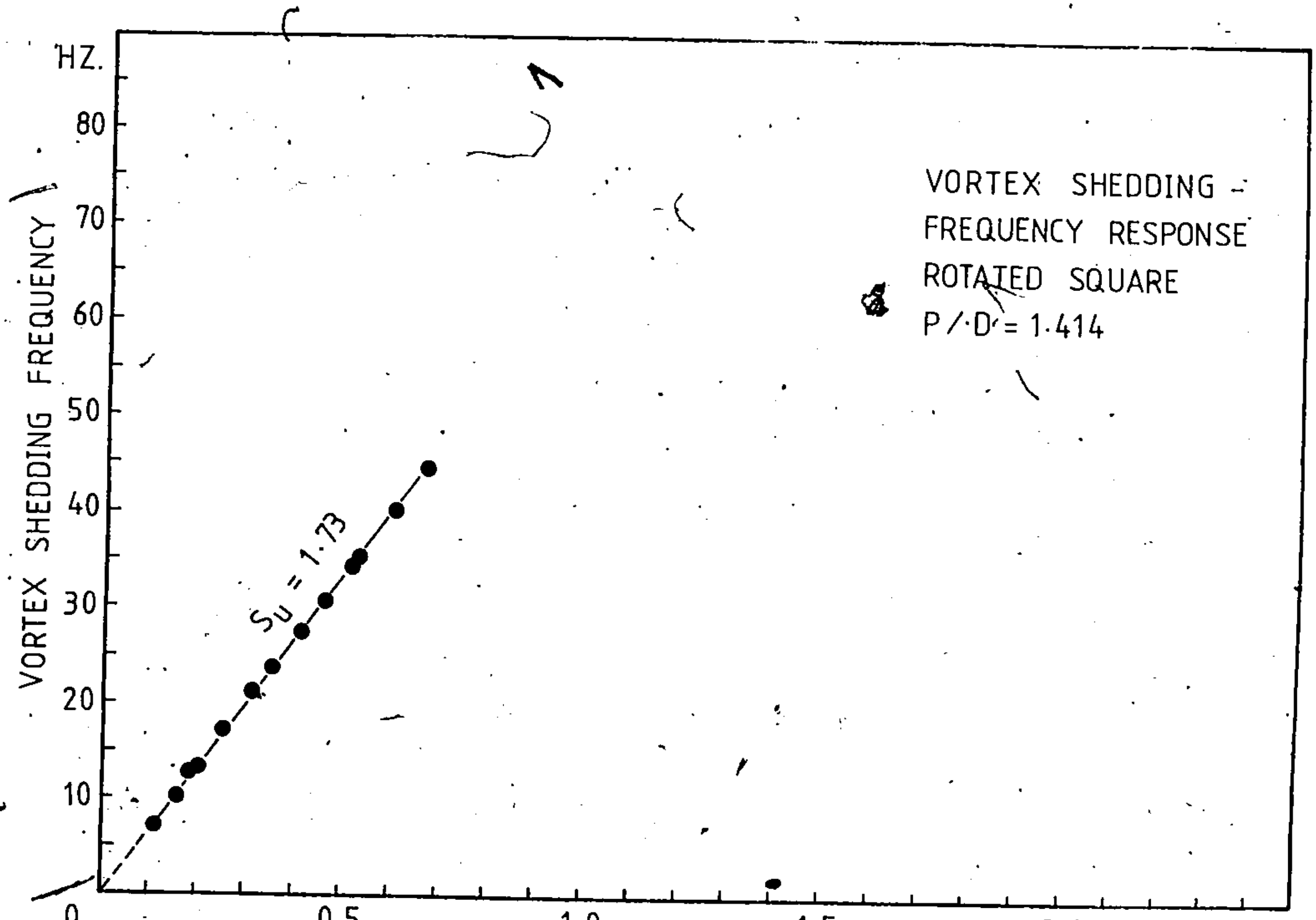

UPSTREAM VELOCITY

FIGURE 4.17

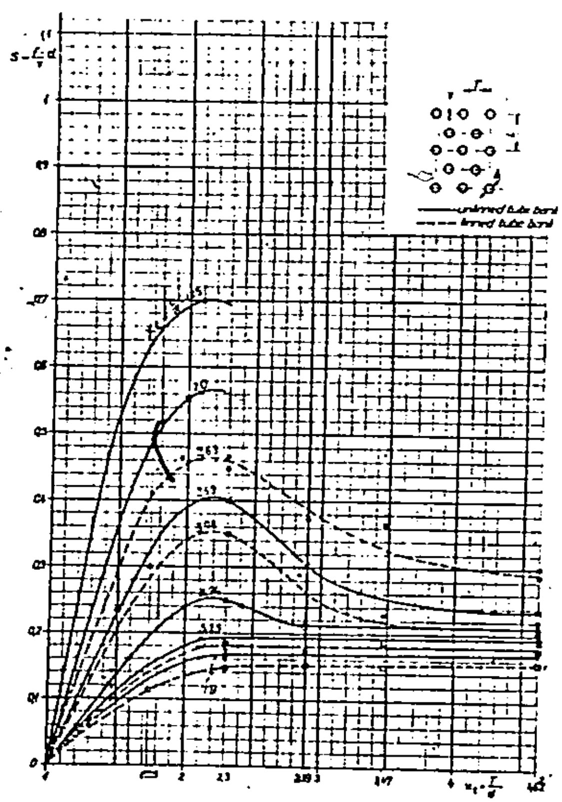

CHEN'S MAP [10]

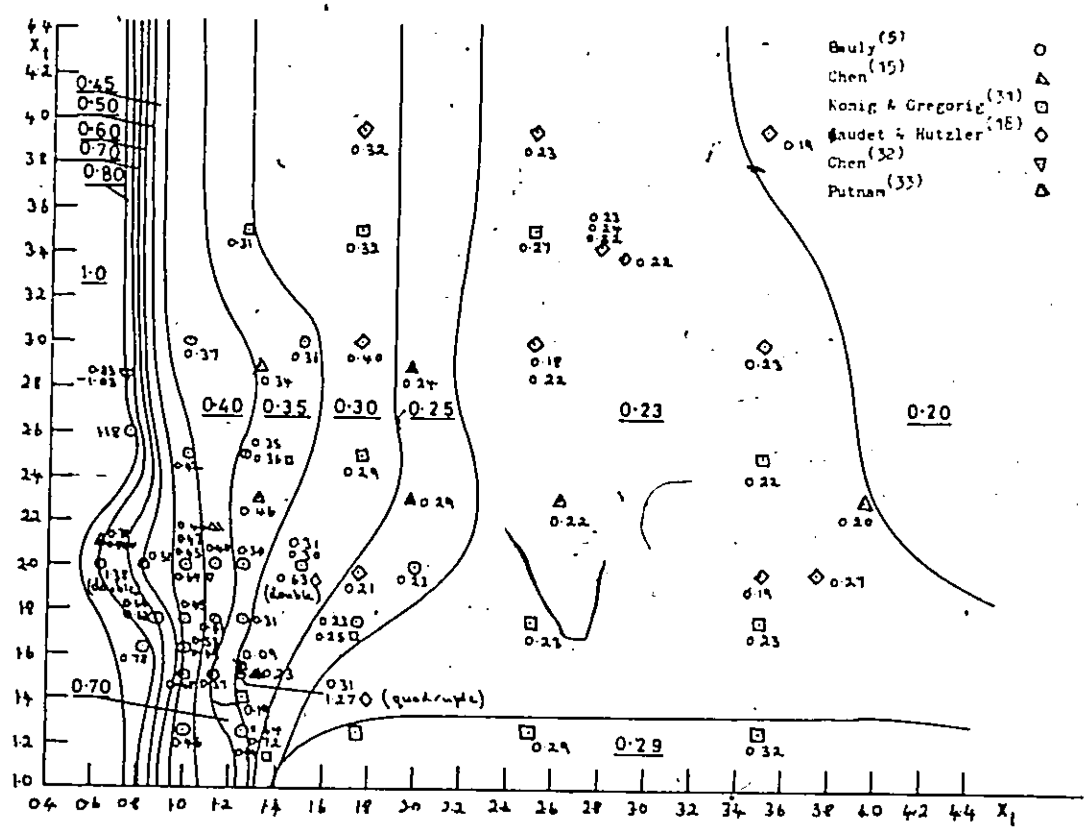

FITZ-HUGH'S MAP [11]

FIGURE 4.18: GAP STROUHAL NUMBERS FOR STAGGERED ARRAYS

indicate that if the ratio V_p/V_u = P/P-d was used, only Owen and Fitz-Hugh predictions will become much closer to the present result. Their values will be S_u = 1.78, 1.54 respectively. Owen's value will be higher than the present value of S_u = 1.73 by only 3%. On the other hand the Fitz-Hugh value will be lower by 12%.

In summary it can be said that for a rotated square array with P/d = 1.414, strong and clear discrete frequencies which represent vortices shed from the tubes were obtained. This flow periodicity was observed in the Reynolds number range between R_u = 180 to R_u = 1120 with a value of the upstream Strouhal number S_u = 1.73. This value agrees with some but not all data in the literature. While the values published in literature are for high values of Reynolds number, the value obtained for the present array was obtained for the first time at low values of Reynolds number. It seems that according to Chen [10] and Fitz-Hugh [11], the phenomenon of flow periodicity repeats itself at high values of Reynolds number, while according to Owen [8], it takes a different form.

4.3.4 Rotated Square Array; P/d = 1.7

The rotated square array with P/d = 1.7 is shown in Figure 4.19. The array is 5 rows deep with only 5 tubes in every row including the half tubes. After inserting the tube array into the test-section, the hot-wire probe was put between the third and fourth row as shown in Figure 4.19.

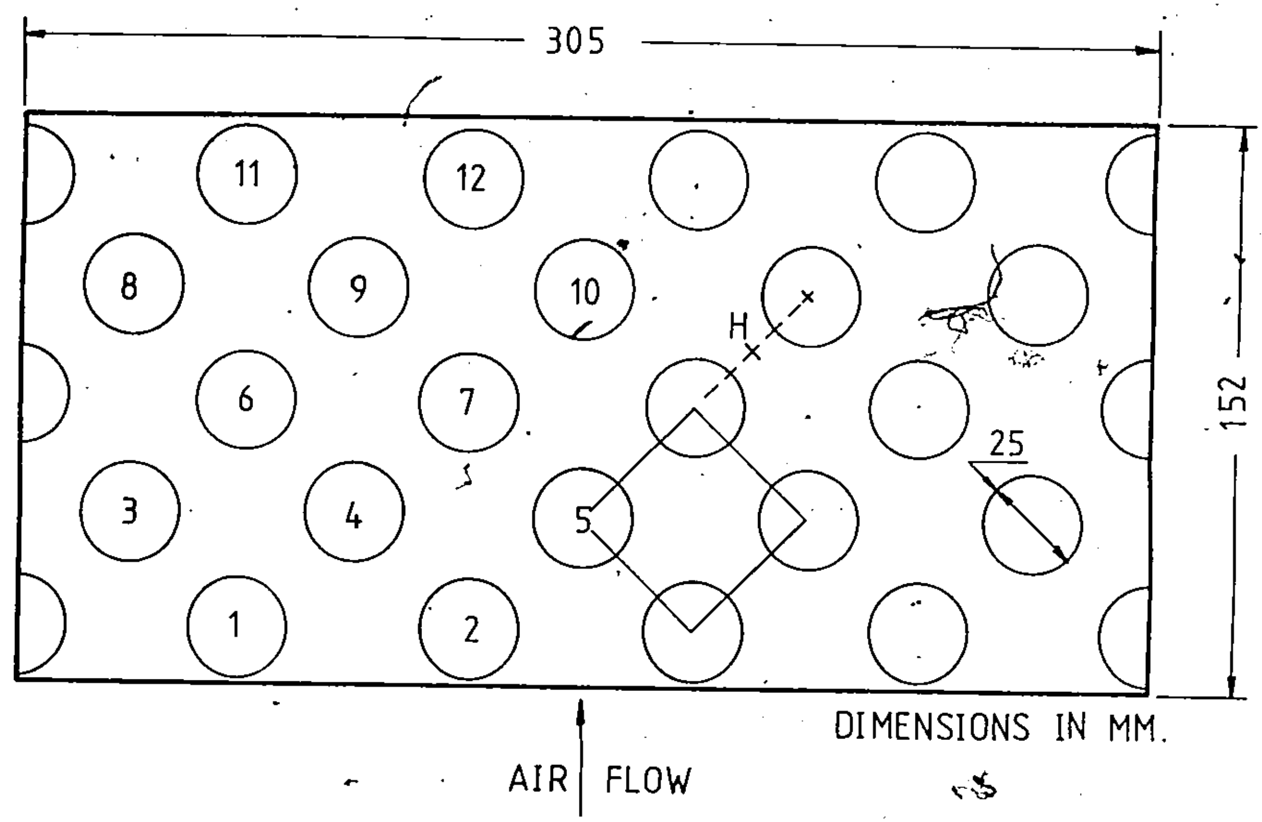

TUBES MARKED 1 - 12 ARE FLEXIBLE TUBES (REST ARE RIGID)

TUBES MARKED 4 AND 9 ARE INSTRUMENTED TUBES

H - LOCATION OF GAP HOT-WIRE PROBE

FIGURE 4.19: ROTATED SQUARE ARRAY WITH P/d = 1.7.

At an upstream flow velocity V_u = 0.40 m/sec., concentration of the velocity fluctuations in the flow were observed. The velocity spectrum was computed and is shown in Figure 4.20 (a). As can be seen the velocity fluctuations are concentrated at a discrete frequency of 14.0 Hz. Another discrete frequency was also obtained at double the original frequency at 28.0 Hz. The discrete frequency at 14.0 Hz gives a value of the upstream Strouhal number of S_u = 0.89. The value of Reynolds number based on this upstream flow velocity and the outside tube diameter is R_u = 670. As the flow velocity was increased to V_u = 0.48 m/sec., the discrete frequency shifted to 16.0 Hz with the appearance of double this frequency at 32.0 Hz as shown in Figure 4.20 (b). The corresponding Strouhal number is S_u = 0.85. By the time the flow velocity had increased to V_u = 0.57 m/sec., the discrete frequency was up to 19.0 Hz with the appearance of double this frequency at 38.0 Hz, see Figure 4.20 (c). The value of Strouhal number is again S_u = 0.85. The appearance of the second harmonic disappeared as the flow velocity was increased to V_u = 0.67 m/sec. The velocity spectrum is shown in Figure 4.20 (d). The corresponding Reynolds number is R_u = 1130. The discrete frequency at 23.0 Hz, gives a value of Strouhal number of S_u = 0.87.

Some interesting results were obtained as the flow velocity was increased to V_u = 1.10 m/sec. The corresponding Reynolds number is R_u = 1850. The computed velocity spectrum which is shown in Figure 4.20 (e), showed two discrete frequencies at 25.0 Hz and 37.0 Hz. The discrete frequency at 25.0 Hz gives a value of upstream Strouhal number of S_u = 0.58. This value of S_u is lower than the value

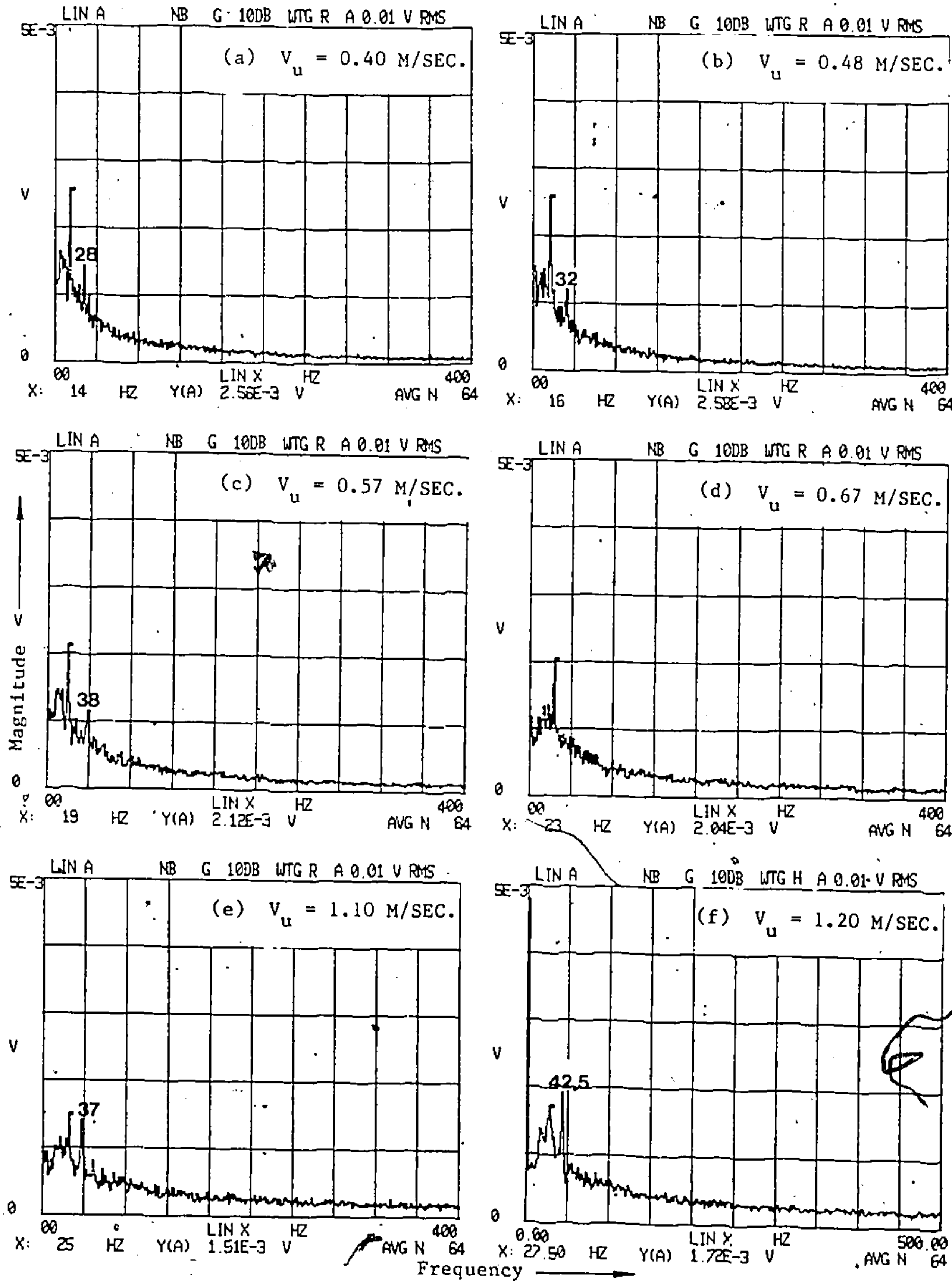

FIGURE 4.20: VELOCITY-SPECTRA FOR THE ROTATED SQUARE ARRAY WITH P/d = 1.70.

obtained from the previously computed spectra. However, the discrete frequency at 37.0 Hz gives a value of $S_u = 0.85$. This means that the latter discrete frequency follows the constant Strouhal number relationship. The level of energy associated with the two frequencies is essentially the same. However, the second frequency does not seem to be associated with an arbitrary eddy in the flow as will be seen from the coming results.

Four more velocity spectra were computed in the velocity range from $V_u = 1.20$ m/sec. to $V_u = 2.70$ m/sec. They are given in Figures 4.20 (f) and 4.21. The appearance of two discrete frequencies was obtained except at the last flow velocity of $V_u = 2.70$ m/sec. Only one discrete frequency which followed the lower value of S_u was obtained. The corresponding Reynolds number is $R_u = 4550$. However, from the previous results, both frequencies were following a constant Strouhal number relationship. No discrete frequencies were observed for flow velocities higher than $V_u = 2.70$ m/sec. All vortex shedding frequencies, upstream flow velocities, Reynolds numbers, and the corresponding Strouhal numbers based on different definitions of flow velocities (see Appendix C) are given in Table 4.4. From this table the average value for Strouhal numbers are $S_u = 0.87, 0.58$; $S_{gm} = 0.42, 0.28$; $S_p = 0.36, 0.24$; $S_g = 0.51, 0.34$. Vortex shedding frequencies versus upstream flow velocities are given in Figure 4.22.

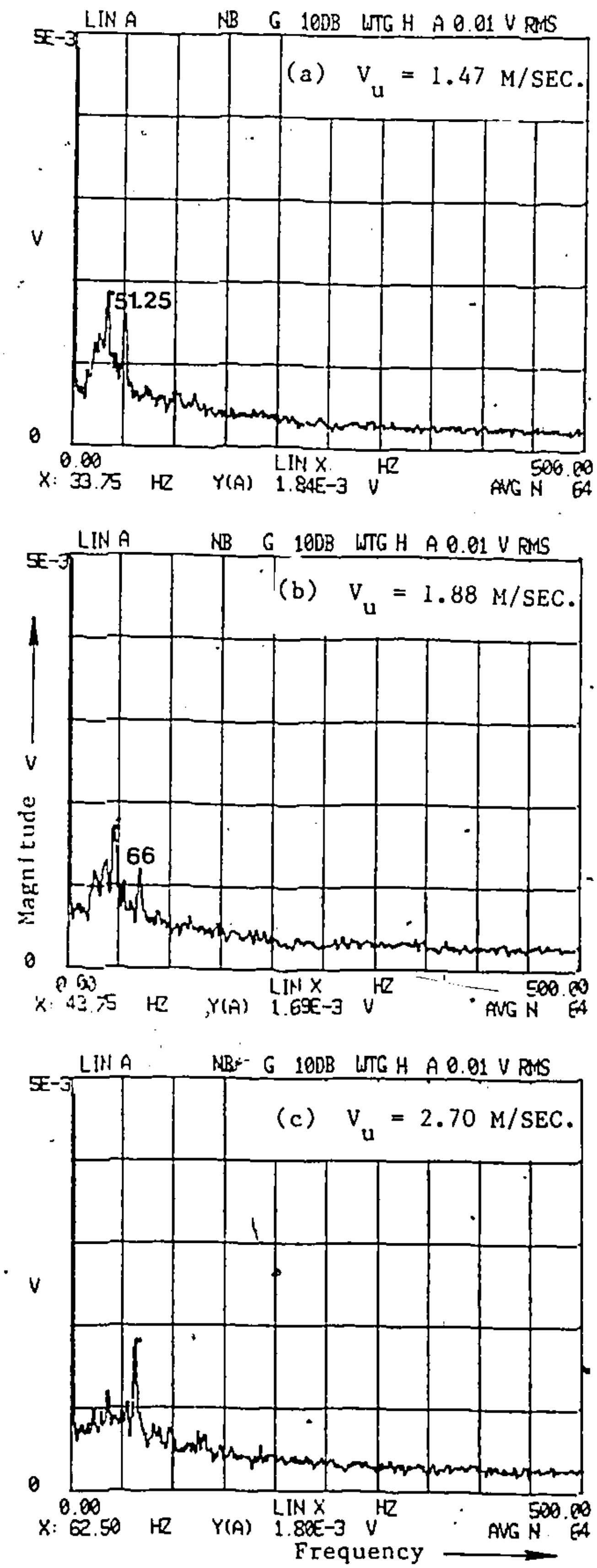

FIGURE 4.21: CONTINUED VELOCITY-SPECTRA FOR THE ROTATED SQUARE ARRAY WITH P/d = 1.70.

TABLE 4.4

Vortex shedding data for rotated square array with P/d = 1.7.

V_u	R_u	f_s	S_u	S_{gm}	S_p	S_g
0.40	670	14.00	0.89	0.43	0.37	0.52
0.48	810	16.00	0.85	0.41	0.35	0.50
0.57	960	19.00	0.85	0.41	0.35	0.50
0.67	1130	23.00	0.87	0.42	0.36	0.51
1.10	1850	25.00	0.58	0.28	0.24	0.34
		37.00	0.85	0.41	0.35	0.50
1.20	2020	27.50	0.58	0.28	0.24	0.34
		42.50	0.90	0.43	0.37	0.52
1.47	2480	33.75	0.58	0.28	0.24	0.34
		51.25	0.89	0.43	0.37	0.52
1.88	3170	43.75	0.59	0.28	0.24	0.34
		66.00	0.89	0.43	0.37	0.52
2.7	4550	62.50	0.59	0.28	0.24	0.34

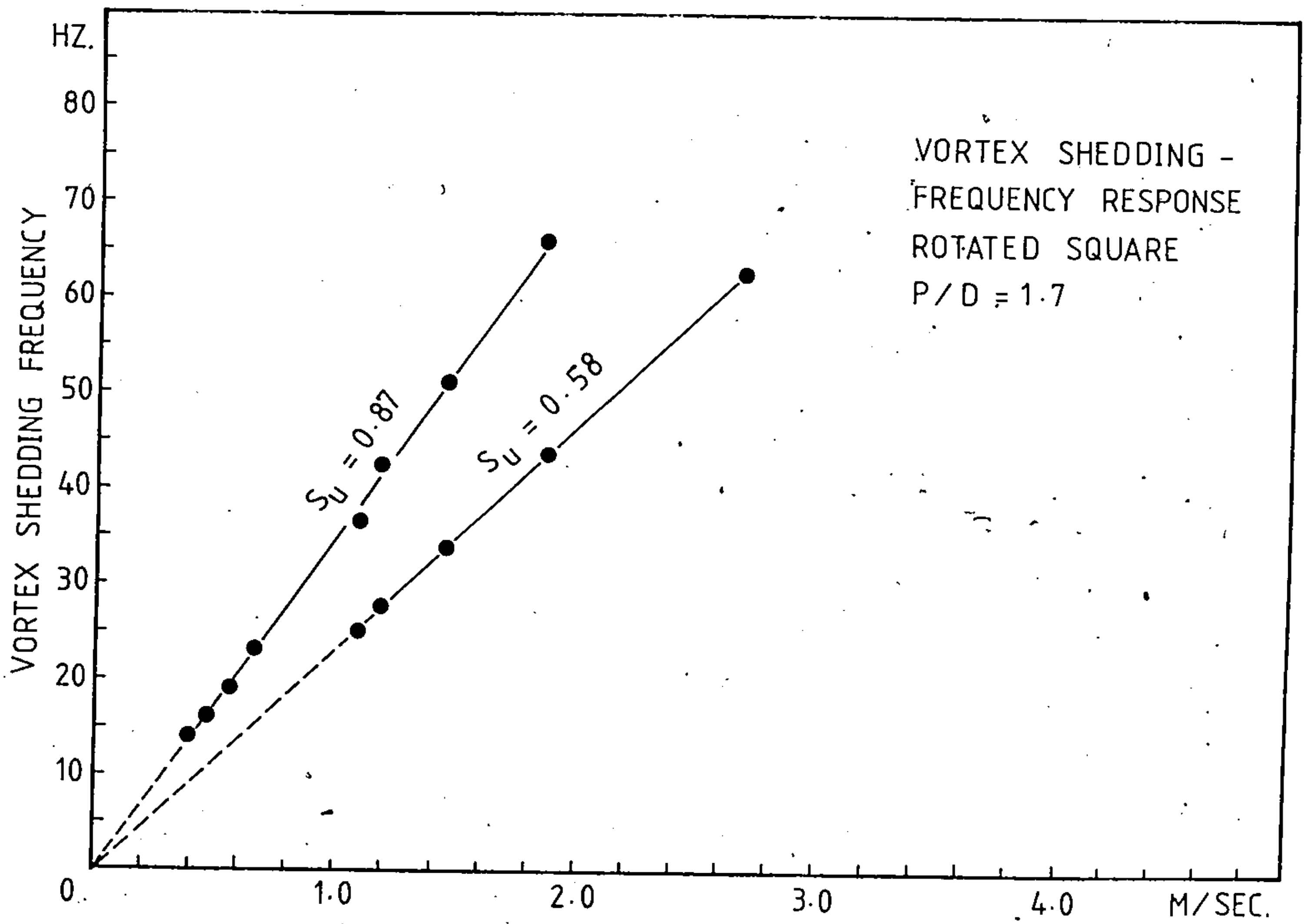

UPSTREAM VELOCITY

FIGURE 4.22

The frequencies of flow periodicity are seen to follow well the constant Strouhal number relationship.

There are no experimental data in the literature for the rotated square array with P/d = 1.7, tested here. However, comparison will be made with the existing formulae and maps on the basis of using the ratio between theoretically determined gap velocity and upstream flow velocity to convert the existing predictions for Strouhal numbers into upstream Strouhal numbers. Preliminary calculations indicated that using this ratio will give better results. Chen's map [10] on Strouhal number for staggered tube arrays is shown in Figure 4.18. Although no data point exists in the map for the present array, an interpolation of the curves indicate a Strouhal number of $S_u = 0.77$. This value lies between the Strouhal numbers of $S_u = 0.87$, $S_u = 0.58$ obtained for the present array. Fitz-Hugh's map [11] for staggered tube arrays which is shown also in Figure 4.18, predicts a value which lies on the boundary between $S_u = 0.60$, $S_u = 0.69$. The first value is higher than the lower value obtained for the present array by only 3%, while the second value is higher by 19%. Owen's formula [8], predicts a value of $S_u = 0.79$ which is lower than the value $S_u = 0.87$ by only 10%. Again, Zukauskas and Katinas formula [12] for normal triangular arrays was used to determine a value for the present array. The formula gives a value of $S_u = 0.9$. This value is higher than the present value of $S_u = 0.87$ by only 3%.

In summary it can be stated that vortex shedding was observed for the first time in the Reynold's number range R_e = 670-4550, for a rotated square array with P/d = 1.7. Two values of Strouhal numbers were obtained, which are $S_u = 0.87$ for $670 \leq R_u \leq 3170$, and $S_u = 0.58$ for $1850 \leq R_u \leq 4550$. Formulae and maps which exist in the literature, but for much higher values of Reynolds numbers predicted value which agree with the present values within a difference of 3 - 19%.

Discussion

Vortex shedding was observed for rotated square arrays with pitch-to-diameter ratios of 1.414 and 1.70, at low values of Reynolds numbers. No experimental data points exist in the literature for these two arrays, except one data point for the rotated square array with P/d = 1.414. Formulae and maps available in the literature are based on data points from other arrays and at much higher values of Reynolds numbers. Theoretically determined gap velocity V_g was used to convert the present results of upstream Strouhal numbers S_u into the corresponding gap Strouhal numbers S_g. This gap flow velocity is a more physically meaningful flow velocity than the pitch velocity V_p especially for rotated square and parallel triangular arrays. However, the ratio V_p/V_u was used only with the results of Pettigrew and Gorman [9] as they indicated clearly that their results were based on this ratio. Strouhal numbers S_g obtained from the present study with those existing in the literature for rotated square arrays with different pitch-to-diameter ratios are shown in Figure 4.23. As can be seen, the present results cover a wide range, which include the published expectations for the rotated square arrays tested in the present study. Owen's formula [8] shows that for P/d < 1.4, Strouhal

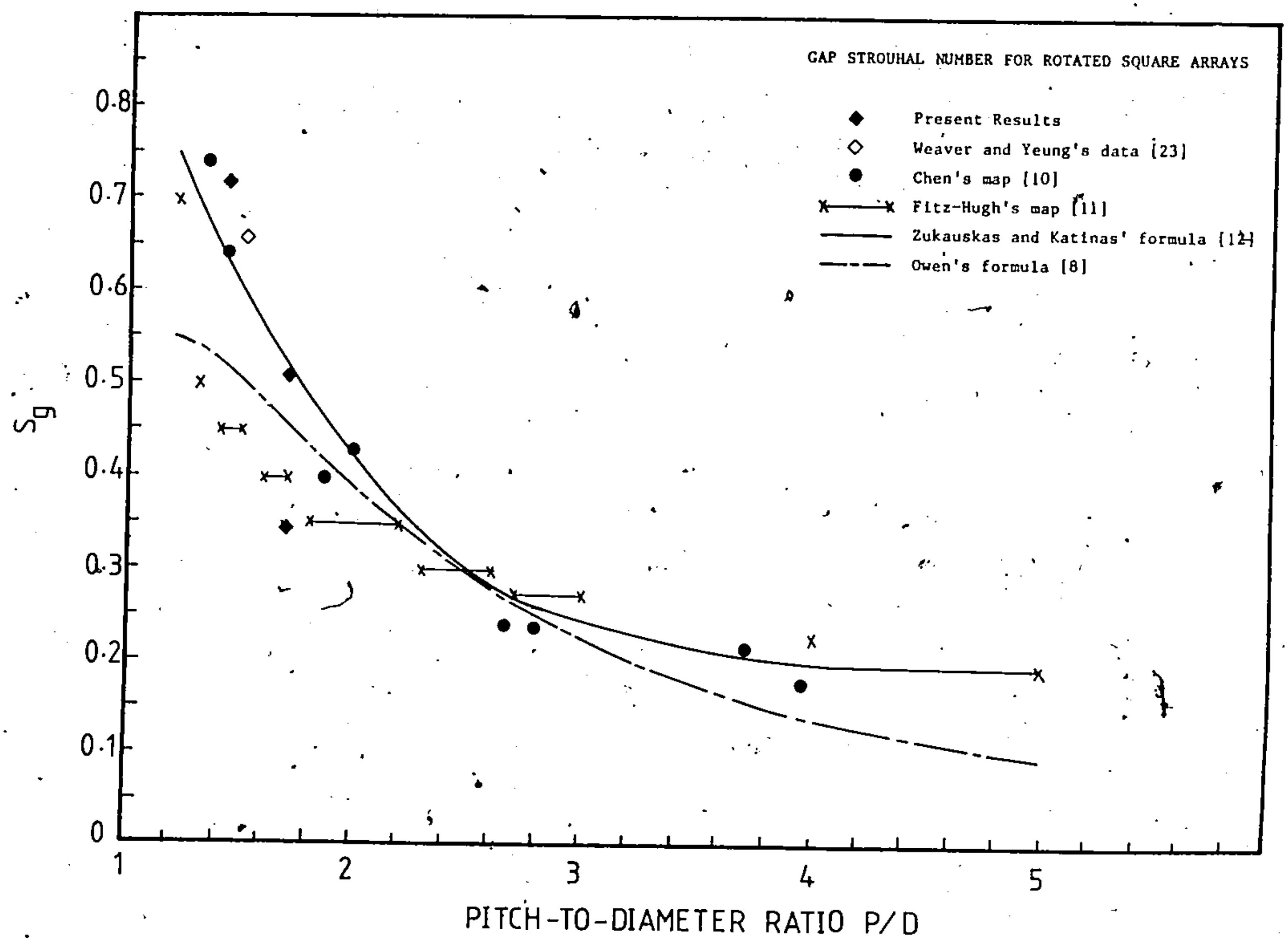
GAP STROUHAL NUMBER FOR ROTATED SQUARE ARRAYS
Present Results
Weaver and Yeung's data [23]
Chen's map [10]
Fitz-Hugh's map [11]
Zukauskas and Katinas' formula [12]
Owen's formula [8]
0.8
0.7
0.6
0.5
0.4
0.3
0.2
0.1
0
S_g
1
2
3
4
5
PITCH-TO-DIAMETER RATIO P/D

FIGURE 4.23

numbers start to decrease. Also for $P/d > 3.3$, Strouhal numbers decay to value below that ($S=0.2$) for a single cylinder. Fitz-Hugh's map [11] and Zukauskas and Katinas formula [12] for Strouhal number reach the value of a single cylinder for $P/d > 4.0$. Upstream Strouhal numbers converted on the basis of using the ratio V_g/V_u, are shown in Figure 4.24. Also included in this figure are the results of Pettigrew and Gorman [9]. Owen's results are better represented in this way as can be seen from Figure 4.24. In addition, the published results are seen to collapse better than those given in Figure 4.23.

A best curve fit was attempted to contain the present results and the published results. The curve is a combination of logarthmic and power-laws and given as the solid line in Figure 4.24. The equation which represents this curve has the form:

$$S_u = -1 + \exp \left\{ \frac{(P/d - 1)^{-0.75}}{2.38} \right\}$$

The equation covers the range of pitch-to diameter ratios from 1.2 up to 3.0.

Attempts were made to plot the results of normal square arrays with the rotated square arrays. The plot showed that they mainly collapse for pitch-to-diameter ratios > 2. This result is not surprising since all arrays should asymptote to the value of a single cylinder ($S = 0.20$) for large P/d. The difference becomes wider as P/d decreases below 2.0. However, the plot showed also that the Strouhal numbers for an ideal normal square array does not represent that of an ideal rotated square array.

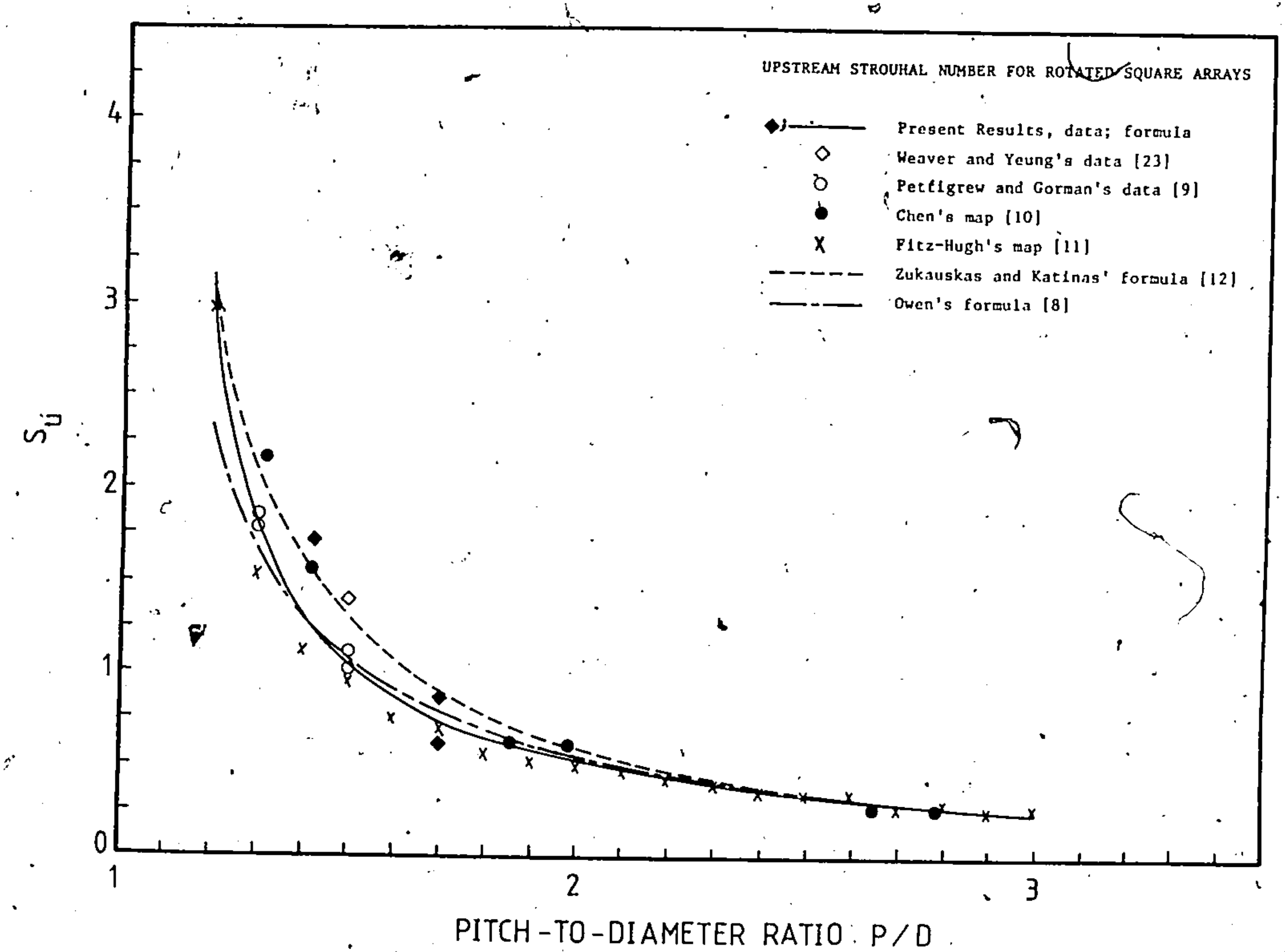
UPSTREAM STROUHAL NUMBER FOR ROTATED SQUARE ARRAYS
Present Results, data; formula
Weaver and Yeung's data [23]
Petfigrew and Gorman's data [9]
Chen's map [10]
Fitz-Hugh's map [11]
Zukauskas and Katinas' formula [12]
Owen's formula [8]
S_u
0
1
2
3
4
1
2
3
PITCH-TO-DIAMETER RATIO P/D

FIGURE 4.24

4.3.5 Normal Triangular Array; P/d = 1.33

The normal triangular array with P/d = 1.33 used in the present study is shown in Figure 4.25. The array is 5 rows deep with 9 tubes in each row including the half tubes which were installed along the walls to minimize wall effects. As can be seen from this figure, it was the only array where thirteen flexible tubes were used. The hot-wire probe was inserted in the gap between the third and the fourth row as shown in Figure 4.25.

As was always the case with vortex shedding measurements, the experiment began at some low flow velocity. At an upstream flow velocity of V_u = 0.08 m/sec., the first concentration of the velocity fluctuations were observed. No discrete frequencies were observed below this velocity. The velocity spectrum given in Figure 4.26 (a), show a discrete frequency at 15.0 Hz, which gives a value of upstream Strouhal number of S_u = 4.76. This value is much higher than any value obtained from the square arrays. This demonstrates that the flow periodicity is dependent on array geometry. The value of Reynolds number based on the upstream flow velocity and the outside tube diameter is R_u = 130. As the flow velocity was increased to V_u = 0.09 m/sec, the strength of this flow periodicity was noticed to increase as shown in Figure 4.26 (b). The discrete frequency was 18.75 Hz with the appearance of the third and fifth harmonics at 56.0 Hz and 93.25 Hz, respectively. The corresponding Strouhal number is S_u = 5.01.

With a very slight increase in flow velocity to V_u = 0.10 m/sec. the discrete frequency shifted to 20.0 Hz with the appearance

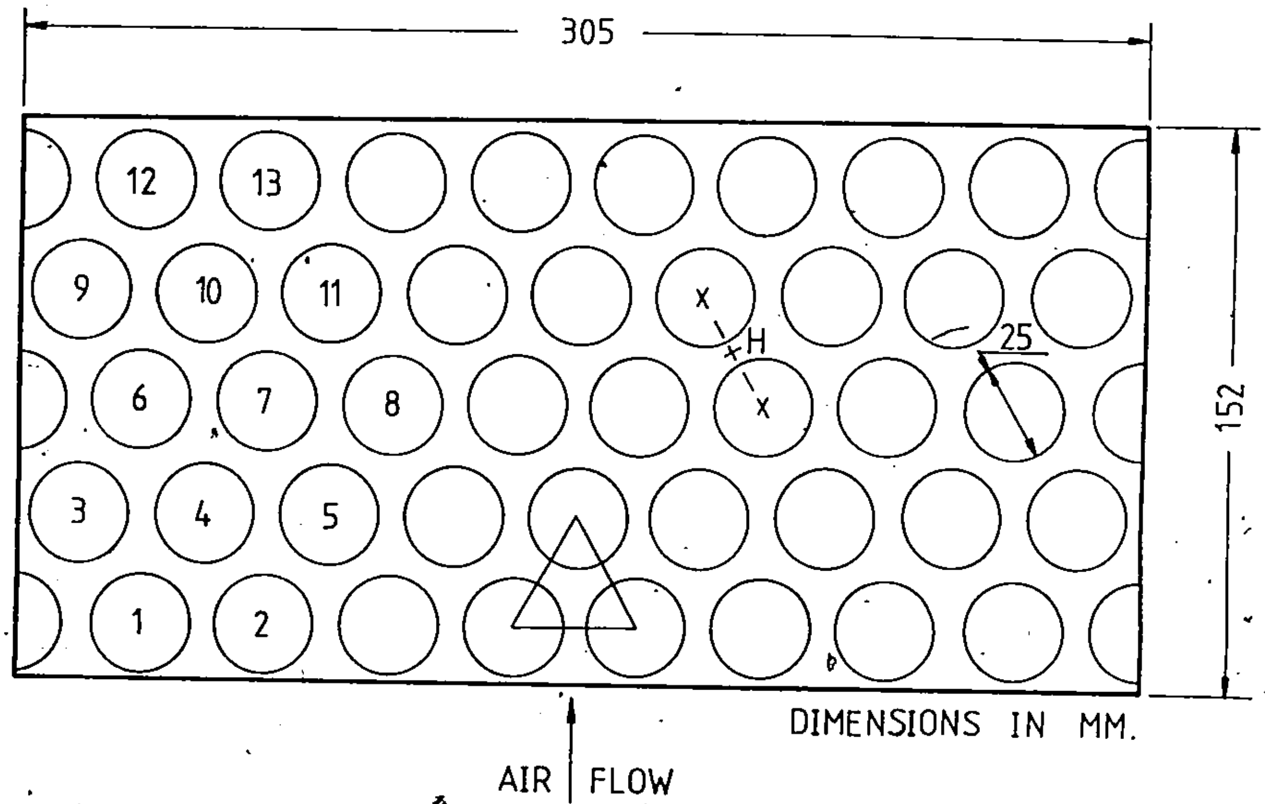

TUBES MARKED 1 - 13 ARE FLEXIBLE TUBES (REST ARE RIGID)

TUBES MARKED 4 AND 7 ARE INSTRUMENTED TUBES

H - LOCATION OF GAP HOT-WIRE PROBE

FIGURE 4.25: NORMAL TRIANGULAR ARRAY WITH P/d = 1.33.

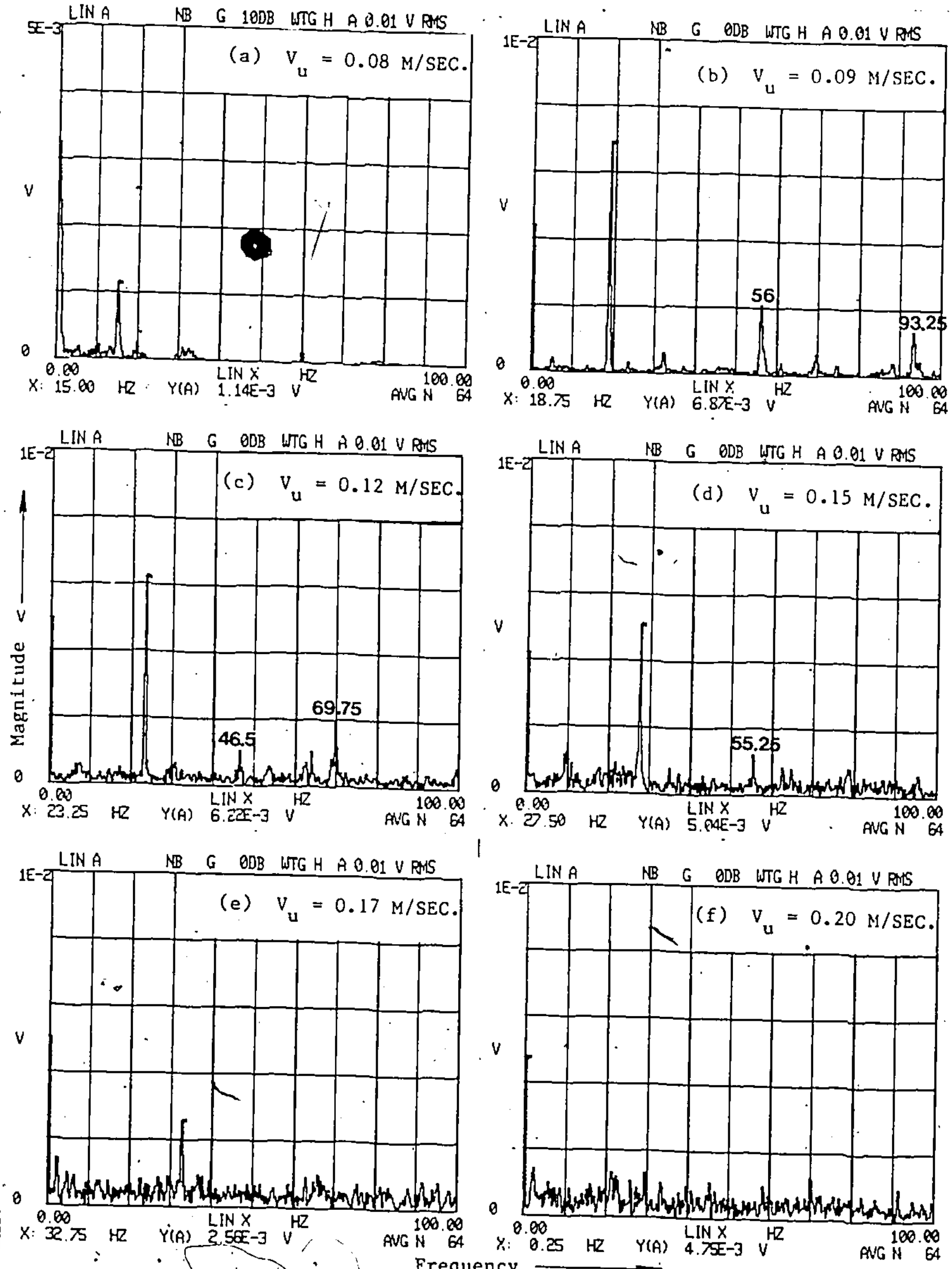

FIGURE 4.26: VELOCITY-SPECTRA FOR THE NORMAL TRIANGULAR ARRAY WITH P/d = 1.33.

of the second, third, and fourth harmonics at 40.0 Hz, 60.0 Hz and 80.0 Hz, respectively. The value of Strouhal number is $S_u = 5.08$.

Six more velocity spectra were computed in the flow velocity range 0.12 m/sec. to 0.20 m/sec. The first, third and last two spectra are given in Figure 4.26 (c) - (f). As can be seen from the last spectra, the discrete frequency disappeared completely for flow velocities higher than $V_u = 0.17$ m/sec., i.e. for $R_u > 290$. All discrete frequencies with the corresponding flow velocities, Reynolds numbers, and the Strouhal numbers based on different definitions of flow velocity (see Appendix C) are given in Table 4.5. From this table the average values of Strouhal numbers are $S_u = 4.89$, $S_{gm} = 1.01$, and S_p or $S_g = 1.21$. Vortex shedding frequencies are plotted versus the upstream flow velocity as shown in Figure 4.27. The frequencies are seen to follow the constant Strouhal number relationship, with a value $S_u = 4.89$, in the Reynolds number range $R_u = 130 - 290$.

The scatter in the published Strouhal number data for normal triangular arrays is larger than arrays of other geometries. This scatter is even large at high values of pitch-to-diameter ratios although it is expected that the Strouhal number will approach that of a single cylinder. However, Chen's map [10] which is shown in Figure 4.18, does not provide any data point for the present array. According to Paidoussis [7], extrapolation of Chen's map will provide a higher value than that obtained for the present array. Owen's formula [8] predicts a value of $S_u = 0.92$, which agrees with the value given by Fitz-Hugh's map [11] (also shown in Figure 4.18) which is $S_u = 0.93$. Both values are about 1/5 that obtained for the present array.

TABLE 4.5

Vortex shedding data for normal triangular array with P/d = 1.33.

V_u	R_u	f_s	S_u	S_{gm}	S_p, S_g
0.08	130	15.00	4.76	0.98	1.18
0.09	160	18.75	5.01	1.03	1.24
0.10	170	20.00	5.08	1.05	1.26
0.12	200	23.25	4.92	1.02	1.22
0.13	220	24.50	4.79	1.00	1.19
0.15	240	27.50	4.82	1.00	1.20
0.16	270	30.50	4.84	1.00	1.20
0.17	290	32.75	4.89	1.01	1.21

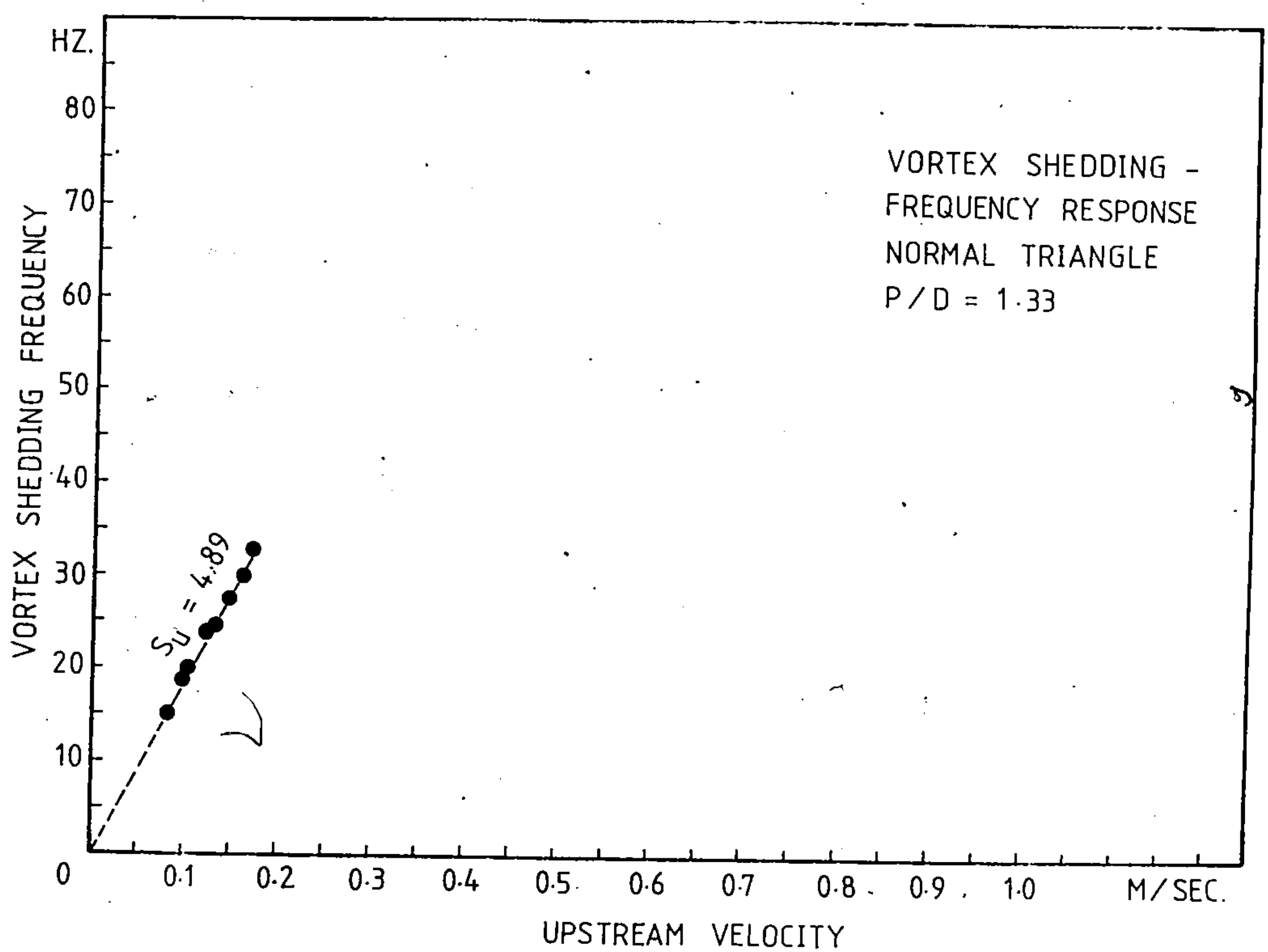

HZ.
80
70
60
50
40
30
20
10
0
0.1
0.2
0.3
0.4
0.5
0.6
0.7
0.8
0.9
1.0
M/SEC.
VORTEX SHEDDING FREQUENCY
UPSTREAM VELOCITY
VORTEX SHEDDING - FREQUENCY RESPONSE
NORMAL TRIANGLE
P / D = 1.33
$S_U = 4.89$

FIGURE 4.27

On the other hand, Zukauskas and Katinas' formula [12] predicts a value of $S_u = 2.76$. This value is 77% lower than the value obtained for the present array but about triple that given by Owen and Fitz-Hugh. Pettigrew and Gorman [9] from a study on a similar array in water flow observed no vortex shedding resonance for tubes beyond the first row up to the downstream row. They provided values of Strouhal numbers for the first row and the downstream row which range between $S_u = 1.21$ to $S_u = 1.93$. However, their values for normal triangular arrays are confusing as they provide for a normal triangular array with P/d = 1.36 values of Strouhal number between $S_u = 1.70$ to $S_u = 2.53$. Higher pitch-to-diameter ratios are expected to lead to lower Strouhal numbers.

In summary, it can be stated that at a very low Reynolds number ($R_e = 130 - 290$) vortex shedding from a normal triangular array with P/d = 1.33 was observed. A value of upstream Strouhal number of $S_u = 4.89$ was obtained. It may be argued that the present result suggests that Strouhal number may be higher at low values of Reynolds numbers than those expected from the literature and which were obtained at much higher values of Reynolds number. However, the present result together with Chen's expectations [10], suggests that the increase in Strouhal number at low pitch-to-diameter ratio may be steeper than that predicted from the literature.

4.3.6 Normal Triangular Array; P/d = 1.5

Normal triangular array with P/d = 1.5 is shown in Figure

4.28. As can be seen from this figure, the array was only 4 rows deep with 8 tubes in each row including the half tubes. The twelve marked tubes are the flexible tubes. The hot-wire probe was inserted into the gap between tubes in the third and fourth row as shown in Figure 4.28.

The wind-tunel was run at some low speed. At an upstream flow velocity, V_u = 0.25 m/sec., a clear peak at 15.00 Hz representing a concentration of the velocity fluctuations in the flow field was obtained. The computed velocity spectrum, shown in Figure 4.29 (a) shows also the appearance of the second, third, and fourth harmonics at 30.0 Hz, 45.0 Hz and 60.0 Hz respectively. The corresponding Strouhal number and Reynolds number (both based on the upstream flow velocity, and the outside tube diameter) are S_u = 1.52, and R_u = 420. No discrete frequencies were observed below this value of Reynold's number.

As the flow velocity was increased to V_u = 0.30 m/sec., the discrete frequency shifted to f_s = 17.50 Hz, with the appearance of its harmonics up to the sixth as shown in Figure 4.29 (b). The corresponding Strouhal number is S_u = 1.48.

With a slight increase in flow velocity to V_u = 0.36 m/sec., the discrete frequency appeared at 21.25 Hz with as many as four harmonics. Upstream Strouhal number in this case is S_u = 1.50.

Two more velocity spectra were computed at flow velocities of V_u = 0.40 m/sec. and 0.48 m/sec. Only the second spectrum is given in Figure 4.29 (c). Note the level of energy associated with the discrete frequency of 27.50 Hz, as compared with the first two

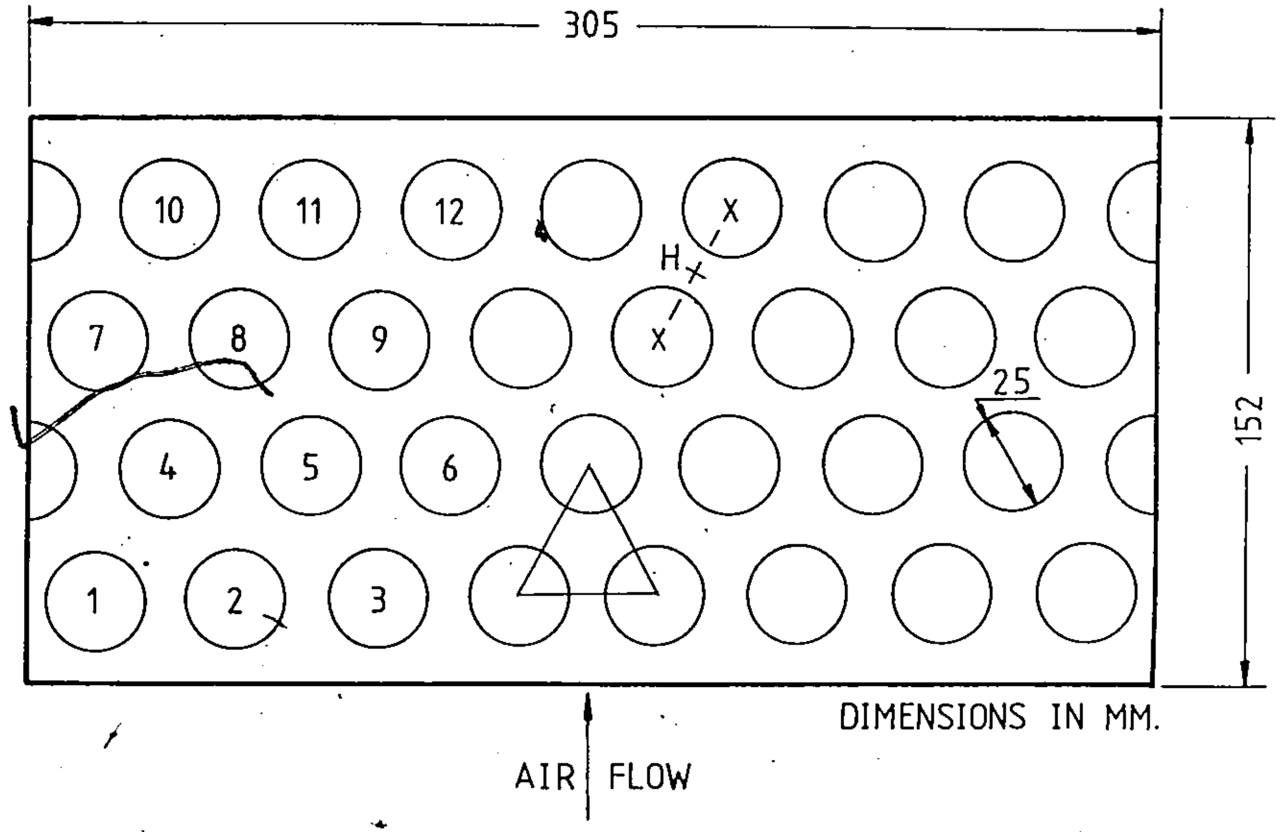

TUBES MARKED 1 - 12 ARE FLEXIBLE TUBES (REST ARE RIGID)

TUBES MARKED 5 AND 8 ARE INSTRUMENTED TUBES

H - LOCATION OF GAP HOT-WIRE PROBE

FIGURE 4.28: NORMAL TRIANGULAR ARRAY WITH P/d = 1.5.

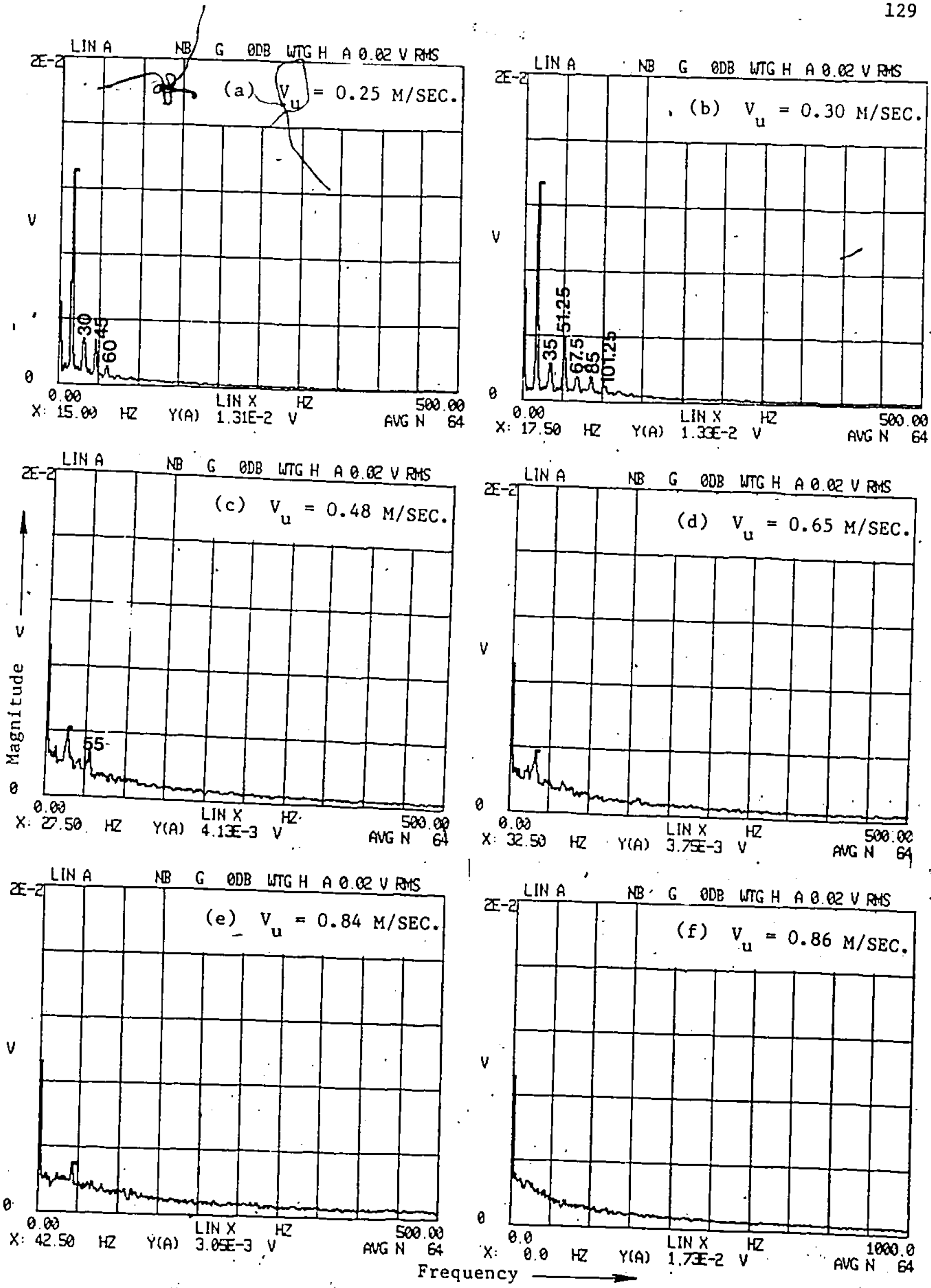

FIGURE 4.29: VELOCITY-SPECTRA FOR THE NORMAL TRIANGULAR ARRAY WITH P/d = 1.50.

spectra. The discrete frequencies obtained gave values of Strouhal numbers of $S_u = 1.51$, and $S_u = 1.46$, respectively. Apparently both values of Strouhal numbers are consistent with values obtained above. The flow velocity at $V_u = 0.48$ m/sec. gives a value of Reynolds number of $R_u = 810$.

The wind-tunnel speed was then increased to $V_u = 0.65$ m/sec. The corresponding number is $R_u = 1100$. The computed velocity spectrum, shown in Figure 4.29 (d), shows concentration of the velocity fluctuations at 32.50 Hz. This frequency gives a lower value of Strouhal number of $S_u = 1.27$. This low value of Strouhal number was also obtained at upstream flow velocities of $V_u = 0.77$ m/sec. and $V_u = 0.84$ m/sec. The velocity spectrum at $V_u = 0.84$ m/sec. is shown in Figure 4.29 (e). The Strouhal numbers were the same for both velocities and have a value of $S_u = 1.28$. The Reynolds number for the flow velocity of $V_u = 0.84$ m/sec., is $R_u = 1420$. No discrete frequencies were observed for higher flow velocities (see Figure 4.29 (f) for the spectrum at $V_u = 0.86$ m/sec.). The appearance of more than one value of Strouhal number for normal triangular arrays was also reported by Pettigrew and Gorman [9] for P/d = 1.33, 1.36, 1.54 and 1.57, and by Zukauskas and Katinas [12] for P/d = 2.0 and 2.68. The vortex shedding frequencies, upstream flow velocities, and the corresponding Reynolds numbers, and Strouhal numbers based on different definitions of flow velocities (see Appendix C) are given in Table 4.6. From this table the average values of the Strouhal number for the present array are $S_u = 1.49$, 1.28; $S_{gm} = 0.49$, 0.42; and S_p, $S_g = 0.50$, 0.43. The results showed that the measured gap velocity

TABLE 4.6

Vortex shedding data for normal triangular array with P/d = 1.5.

V_u	R_u	f_s	S_u	S_{gm}	S_p, S_g
0.25	420	15.00	1.52	0.50	0.51
0.30	510	17.50	1.48	0.49	0.49
0.36	610	21.25	1.50	0.49	0.50
0.40	670	23.75	1.51	0.50	0.50
0.48	810	27.50	1.46	0.48	0.49
0.65	1100	32.50	1.27	0.42	0.42
0.77	1300	38.75	1.28	0.42	0.43
0.84	1420	42.50	1.28	0.42	0.43

V_{gm} is essentially the same as the pitch velocity V_p and the theoretically determined gap velocity V_g. Therefore for the present array $S_{gm} = S_p = S_g$. The vortex shedding frequencies were plotted versus the steady upstream flow velocity as shown in Figure 4.30. As can be seen, both sets of vortex shedding frequencies followed the constant Strouhal number relationship with two values of Strouhal numbers.

Attempts were also made in order to compare the present results with data published in the literature. Chen's map [10], again does not provide any data for the present array. According to Paidoussis' [7], extrapolation of Chen's curves produces a value of about $S_u = 1.8$. This value is higher than the value $S_u = 1.49$ obtained for the present array by 21%. Again, values of S_u provided by Owen's formula [8] and Fitz-Hugh's map [11] are much lower than other published results. Both authors provide values of about $S_u = 0.70$. This value is lower than the low value of $S_u = 1.28$ obtained for the present array by 83%. The recent formula by Zukauskas and Katinas [12] predicts a value of $S_u = 1.82$. This value of Strouhal number agrees well with Chen's value and is higher than the present value of $S_u = 1.49$ by 22%. Most recently, Weaver and Yeung [23] conducted experiments in water flows on a similar array and obtained a value $S_u = 1.59$ in the Reynolds number range $R_u = 1.5 - 6.1 \times 10^3$. This value agrees with the present value $S_u = 1.49$ only being higher by 7%.

In summary, vortex shedding for a normal triangular array with $P/d = 1.5$ was observed in the Reynolds number range $R_u = 420\text{-}1420$. Two values of Strouhal numbers were obtained. These values are $S_u =$

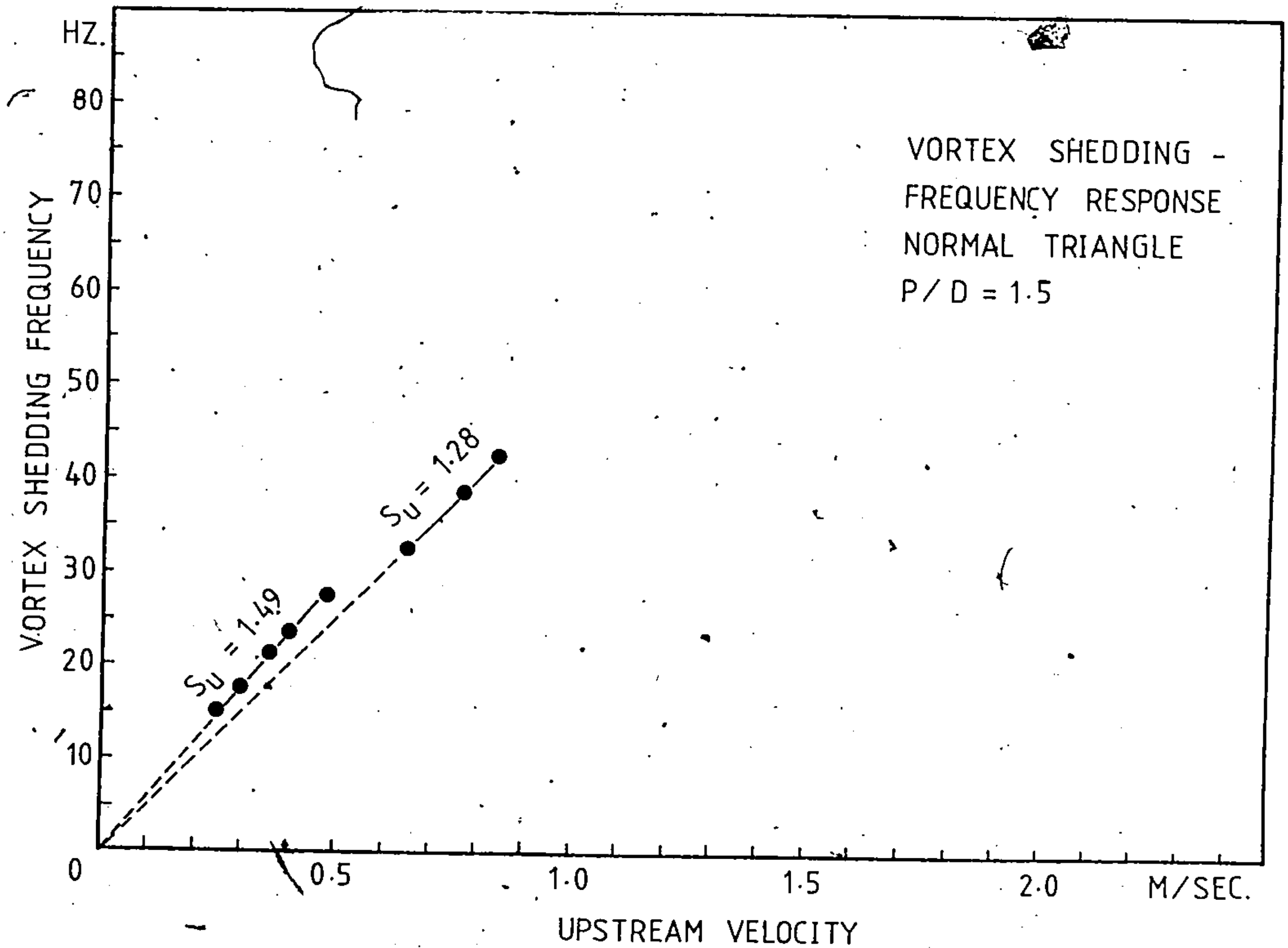
VORTEX SHEDDING -
FREQUENCY RESPONSE
NORMAL TRIANGLE
P / D = 1·5
Su = 1·28
Su = 1·49
HZ.
80
70
60
50
40
30
20
10
0
0·5
1·0
1·5
2·0
M/SEC.
VORTEX SHEDDING FREQUENCY
UPSTREAM VELOCITY

FIGURE 4.30

1.49, 1.28. The value S_u = 1.49 agrees very well with some of the published results for a similar array. No vortex shedding resonance was observed for this array.

Discussion

Two normal triangular arrays were tested, having pitch-to-diameter ratios of 1.33, 1.5. Vortex shedding from both arrays was observed. Strouhal numbers obtained for the normal triangular array with P/d = 1.33 suggest that the increase in Strouhal number with decreasing pitch-to-diameter ratios is much steeper than what is published in the literature. Extrapolation of Chen's curves [10] is the only result which comes close to this result, and even predicts higher value. Other publsihed results are lower than the present value by 77% or more.

Two values of Strouhal number were obtained for the normal triangular array with P/d = 1.5. The higher values agree very well with the only data point obtained by Weaver and Yeung [23] from a similar array in water. However, the appearance of more than one value of Strouhal number for the normal triangular arrays was also reported by other investigators but with arrays of different pitch-to-diameter ratios. The results of different published formulae and maps together with present results are given in Figure 4.31. Also, represented in this figure is the result of Weaver and Yeung [23]. Owen's formula [8], again shows decay in Strouhal number with decreasing P/d below about 1.6. Also for P/d > 2.4, the Strouhal number decreases below that of a single cylinder. The results were

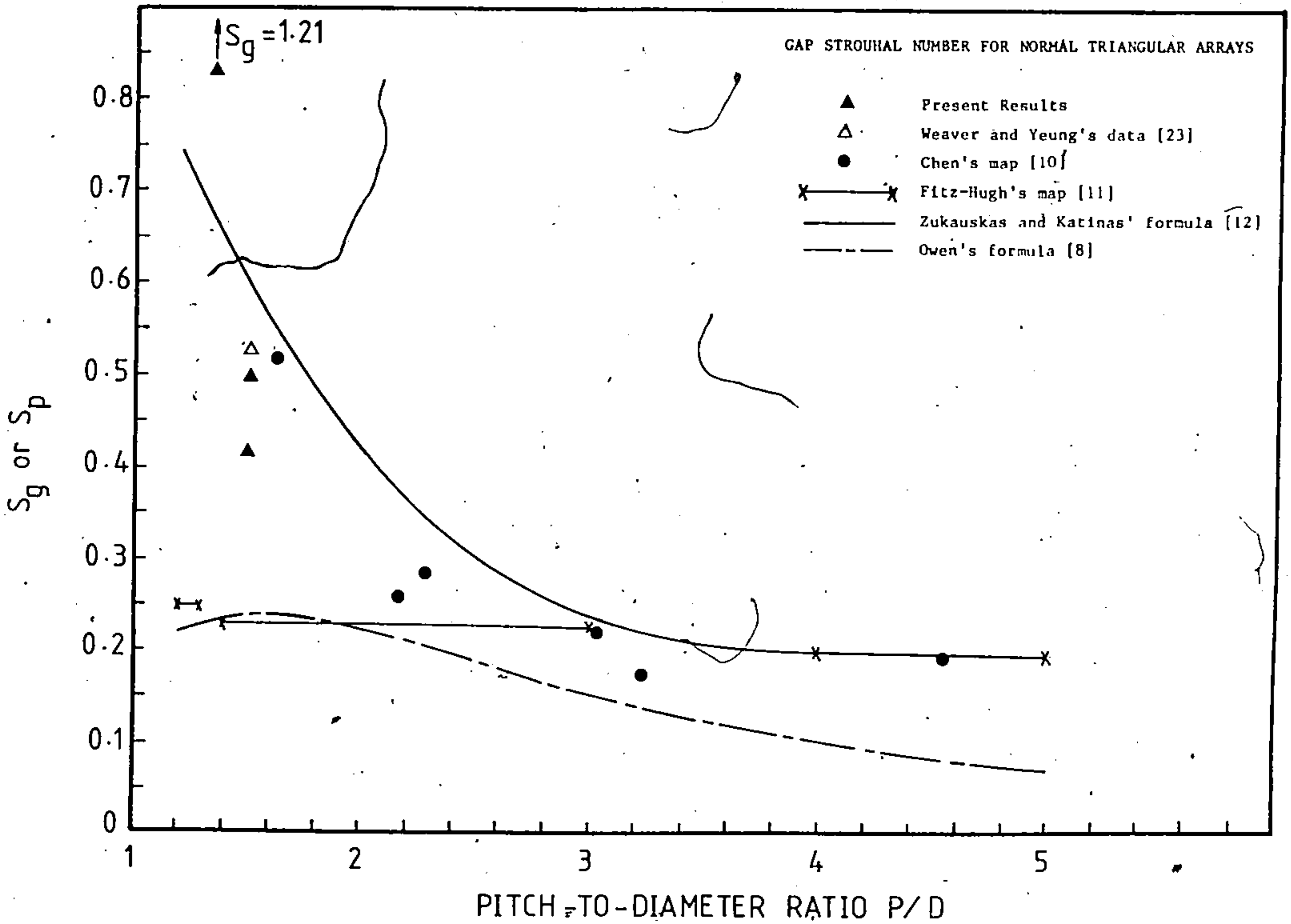
GAP STROUHAL NUMBER FOR NORMAL TRIANGULAR ARRAYS
Present Results
Weaver and Yeung's data [23]
Chen's map [10]
Fitz-Hugh's map [11]
Zukauskas and Katinas' formula [12]
Owen's formula [8]
$S_g = 1.21$
S_g or S_p
0.8
0.7
0.6
0.5
0.4
0.3
0.2
0.1
0
1
2
3
4
5
PITCH-TO-DIAMETER RATIO P/D

FIGURE 4.31

also plotted on the basis of upstream flow velocities as shown in Figure 4.32. Included in this figure are the results of Borges [81] and Heinecke [82]. As can be seen from this figure, the results of Owen and Fitz-Hugh lie below all other published results. It may be that this is due to these data being based on results from acoustic resonance. Strouhal numbers from resonance are lower than the correct values due to the fact that the vortex shedding frequency will be controlled by the tubes natural frequency while the flow velocity is increasing. Also seen in this figure is apparently that the values of Strouhal numbers obtained by Zukauskas and Katinas [12] in water flows are lower than those from air flows. From a second peak in the velocity spectrum for a normal triangular array with P/d = 2.0, they obtained a value of Strouhal number which came close to those predicted by Owen and Fitz-Hugh.

However, for the normal triangular arrays the scatter in the published data is larger than arrays with other configurations. The present results suggest that actual Strouhal numbers are much higher than those given by Owen and Fitz-Hugh. Also the increase in Strouhal numbers with decreasing pitch-to-diameter ratios is steeper than that predicted from the literature.

4.3.7 Parallel Triangular Arrays; P/d = 1.375

The parallel triangular array with P/d = 1.375 used to conduct the present experiment is shown in Figure 4.33. As can be seen, the array is 6 rows deep with only 5 tubes in every row including the half tubes. The hot-wire probe was inserted into the gap between the fourth and the fifth rows as shown in Figure 4.33.

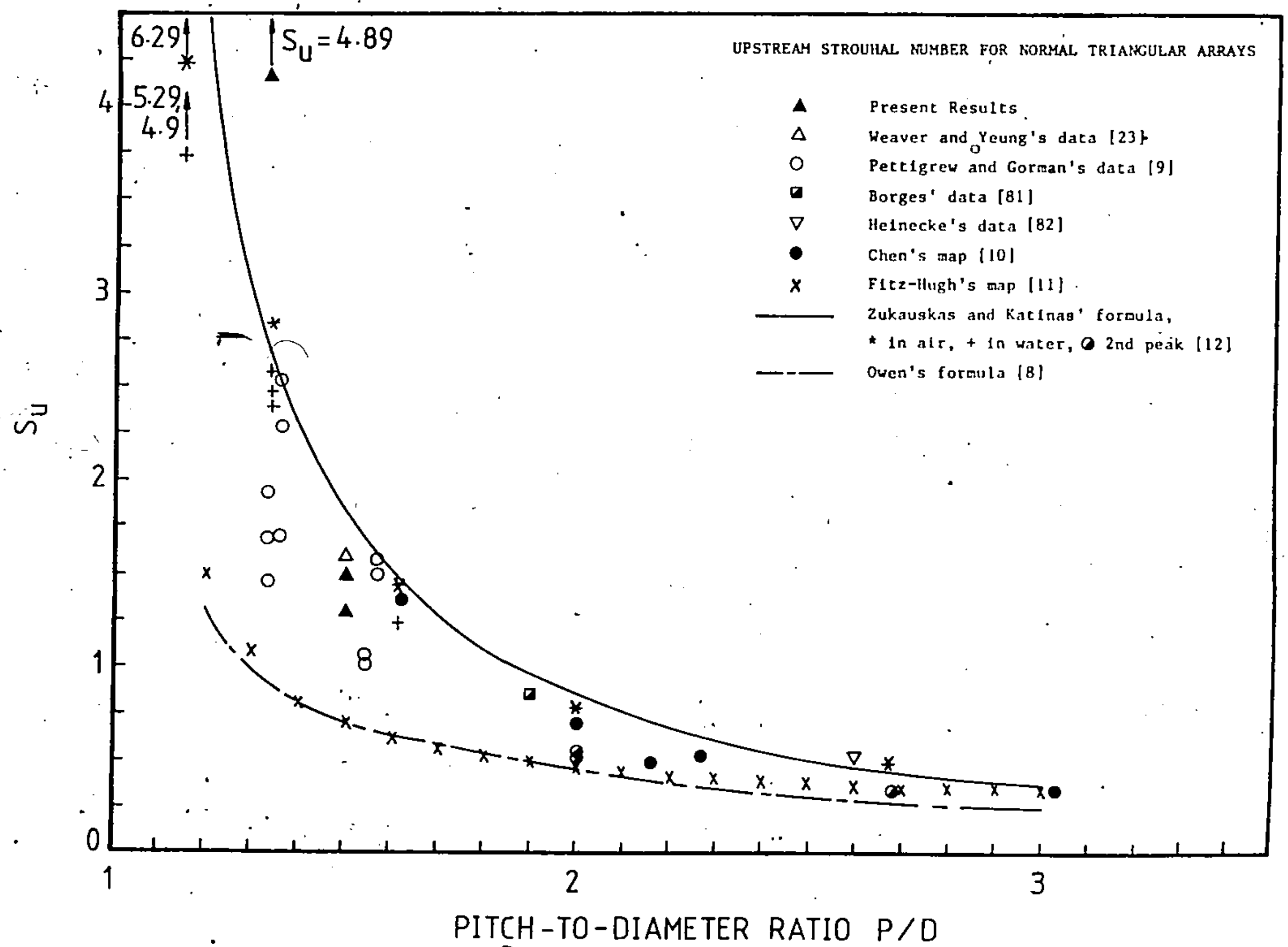
UPSTREAM STROUHAL NUMBER FOR NORMAL TRIANGULAR ARRAYS
Present Results
Weaver and Yeung's data [23]
Pettigrew and Gorman's data [9]
Borges' data [81]
Heinecke's data [82]
Chen's map [10]
Fitz-Hugh's map [11]
Zukauskas and Katinas' formula,
* in air, + in water, 2nd peak [12]
Owen's formula [8]
$S_u = 4.89$
6.29
5.29
4.9
S_u
PITCH-TO-DIAMETER RATIO P/D

FIGURE 4.32

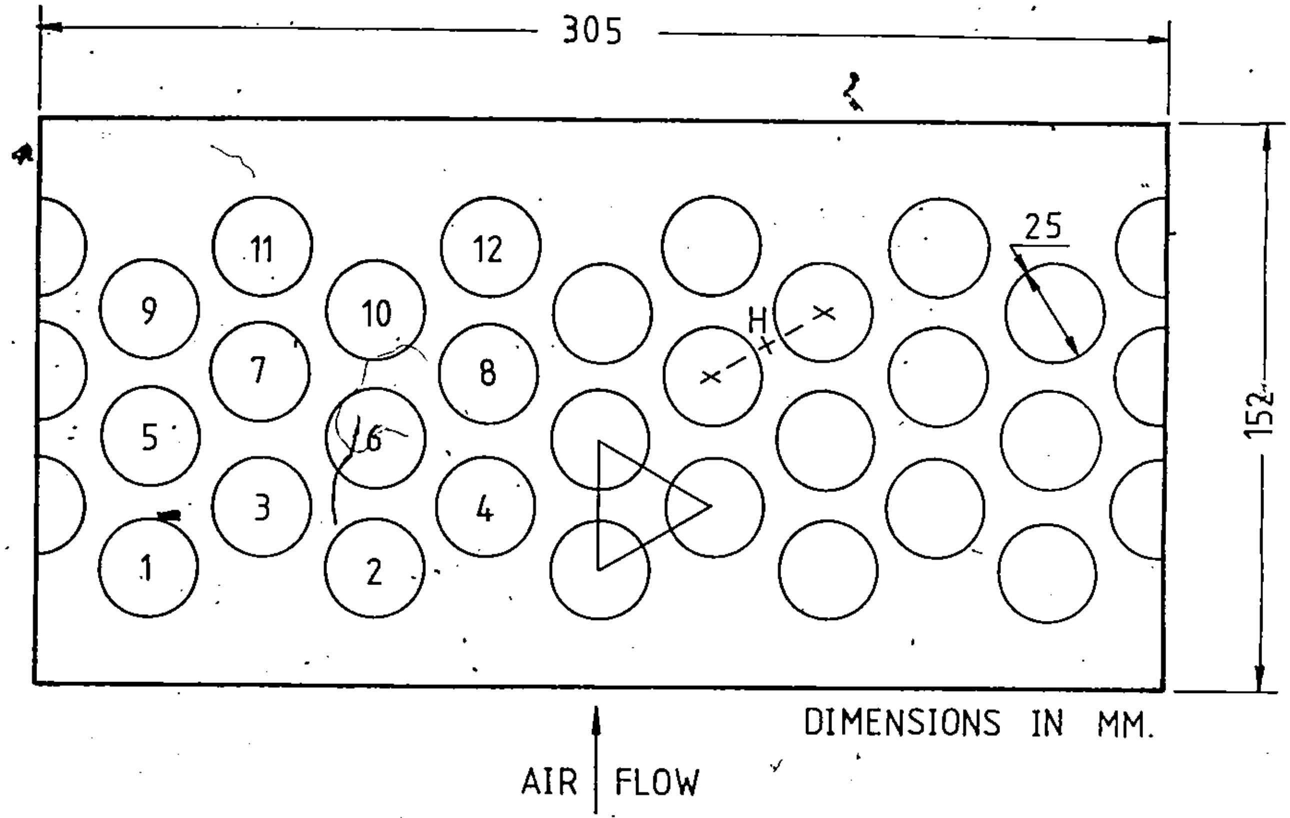

TUBES MARKED 1 - 12 ARE FLEXIBLE TUBES (REST ARE RIGID)

TUBES MARKED 6 AND 7 ARE INSTRUMENTED TUBES

H - LOCATION OF GAP HOT-WIRE PROBE

FIGURE 4.33: PARALLEL TRIANGULAR ARRAY WITH P/d = 1.375.

The experiment began by running the wind-tunnel at low flow velocities. The appearance of the first concentration of the velocity fluctuations was at a discrete frequency of 50.0 Hz and an upstream flow velocity of V_u = 0.58 m/sec. The velocity spectrum is given as the first trace in Figure 4.34. The corresponding Reynolds number (based on the outside tube diameter) is R_u = 980. Note that both frequency and flow velocity are high compared with what was seen with other arrays. However, vortex shedding frequencies are expected to increase in direct proportion with the flow velocity. The observed discrete frequency gives a value of upstream Strouhal number of S_u = 2.19.

At an upstream flow velocity of V_u = 0.68 m/sec., the computed velocity spectrum showed that the discrete frequency was up to 58.0 Hz. The corresponding Strouhal number is S_u = 2.17. The appearance of the second harmonic was only observed when the wind-tunnel speed was increased to V_u = 0.72 m/sec. The computed velocity spectrum is given as the second trace in Figure 4.34. As can be seen the velocity fluctuations are concentrated at 62.5 Hz, with the appearance of the second harmonic at 126 Hz. The corresponding Strouhal number is S_u = 2.20.

Four more velocity spectra were computed up to an upstream flow velocity of V_u = 1.15 m/sec. The last two spectra are shown by the third and fourth traces in Figure 4.34. The corresponding Reynolds number is R_e = 1940. No discrete frequencies were observed for higher values of Reynolds number. All vortex shedding frequencies f_s, upstream flow velocities V_u, and the corresponding values of

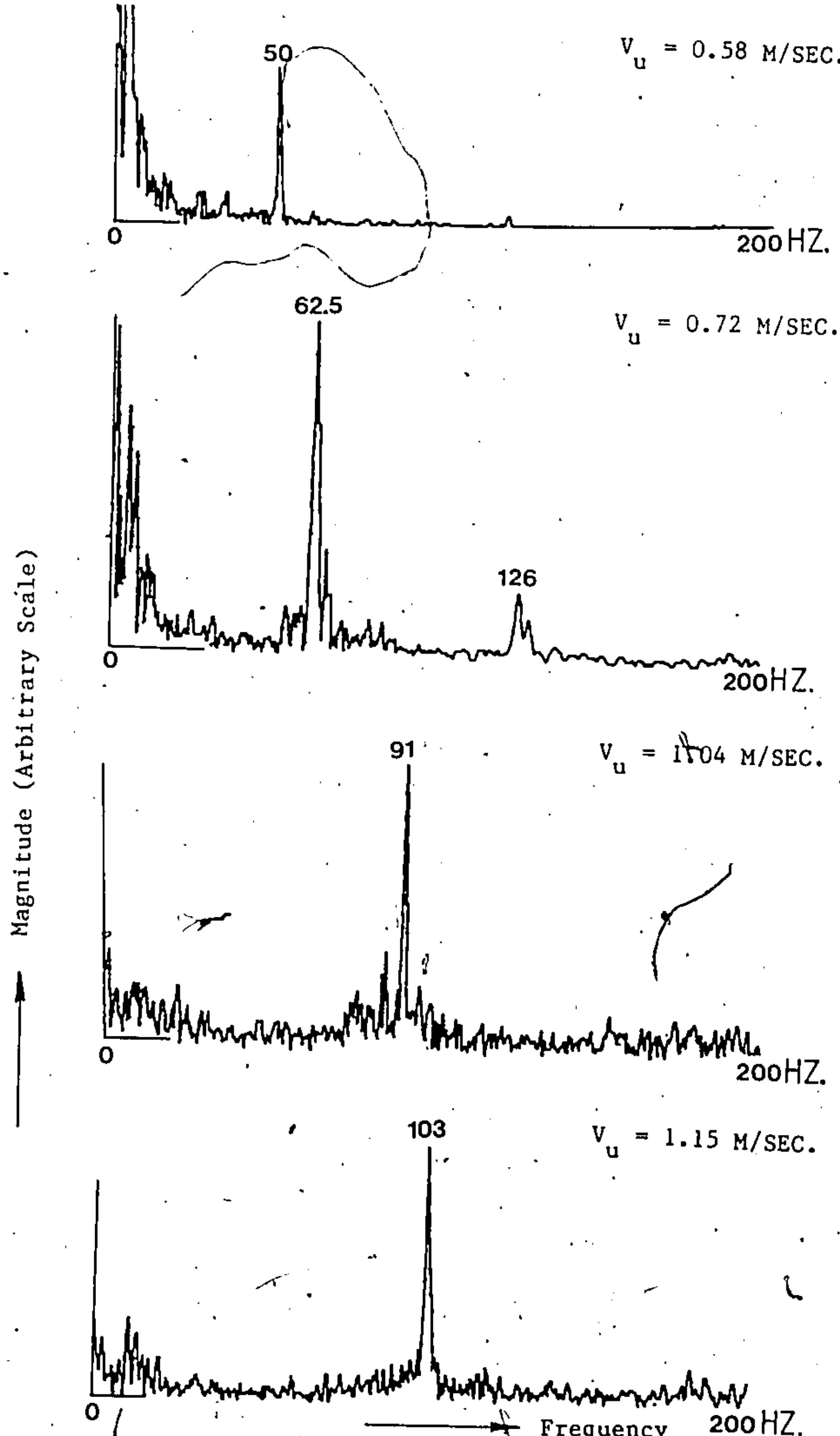

FIGURE 4.34: VELOCITY-SPECTRA FOR THE PARALLEL TRIANGULAR ARRAY WITH P/d = 1.375.

Reynolds numbers R_u, Strouhal numbers based on different definitions of flow velocities (see Appendix C) are given in Table 4.7. From the table, the average values of Strouhal numbers are S_u = 2.21, S_{gm} = 0.60, S_p = 0.60, and S_g = 0.70. There is no difference between S_{gm} and S_p because the measurement showed that the measured gap velocity is equal to the pitch velocity for a parallel triangular array with P/d = 1.375. The vortex shedding frequencies were plotted versus the upstream flow velocities as shown in Figure 4.35. As can be seen, the vortex shedding frequencies are increasing in direct proportion with the flow velocities with a constant value of Strouhal number, S_u = 2.21.

Not many data are available in the literature for the present array. Chen's map [10] does not give a direct data point for the present array (Chen's map for staggered tube arrays is shown in Figure 4.18). Interpolation of the curves will give a value for the upstream Strouhal number of S_u = 2.40. This value is in reasonable agreement with the present value of S_u = 2.21 (only higher by 9%). Fitz-Hugh's map [11] (also shown in Figure 4.18) provides a value of S_u = 3.17. This value is higher than the present value by 43%. However a better interpretation of Fitz-Hugh will be given later in the discussion. Owen's formula [8] predicts a value of S_u = 2.53. This value is higher than the present value by 14%. A similar array was also tested in air flows by Grover and Weaver [48] and by Weaver and Lever [49]. They obtained a value of upstream Strouhal number of about S_u = 2.63 for R_u < 330. This value is again higher than the present value by 19%. The recent formula by Zukauskas and Katinas [12] for normal

TABLE 4.7

Vortex shedding data for parallel triangular array with P/d = 1.375.

V_u	R_u	f_s	S_u	S_{gm}	S_p	S_g
0.58	980	50.00	2.19	0.59	0.60	0.69
0.68	1150	58.00	2.17	0.59	0.59	0.68
0.72	1210	62.50	2.20	0.59	0.60	0.69
0.85	1430	73.50	2.20	0.59	0.60	0.69
0.96	1620	84.00	2.22	0.60	0.61	0.70
1.04	1750	91.00	2.22	0.60	0.61	0.70
1.15	1940	103.00	2.27	0.61	0.62	0.72

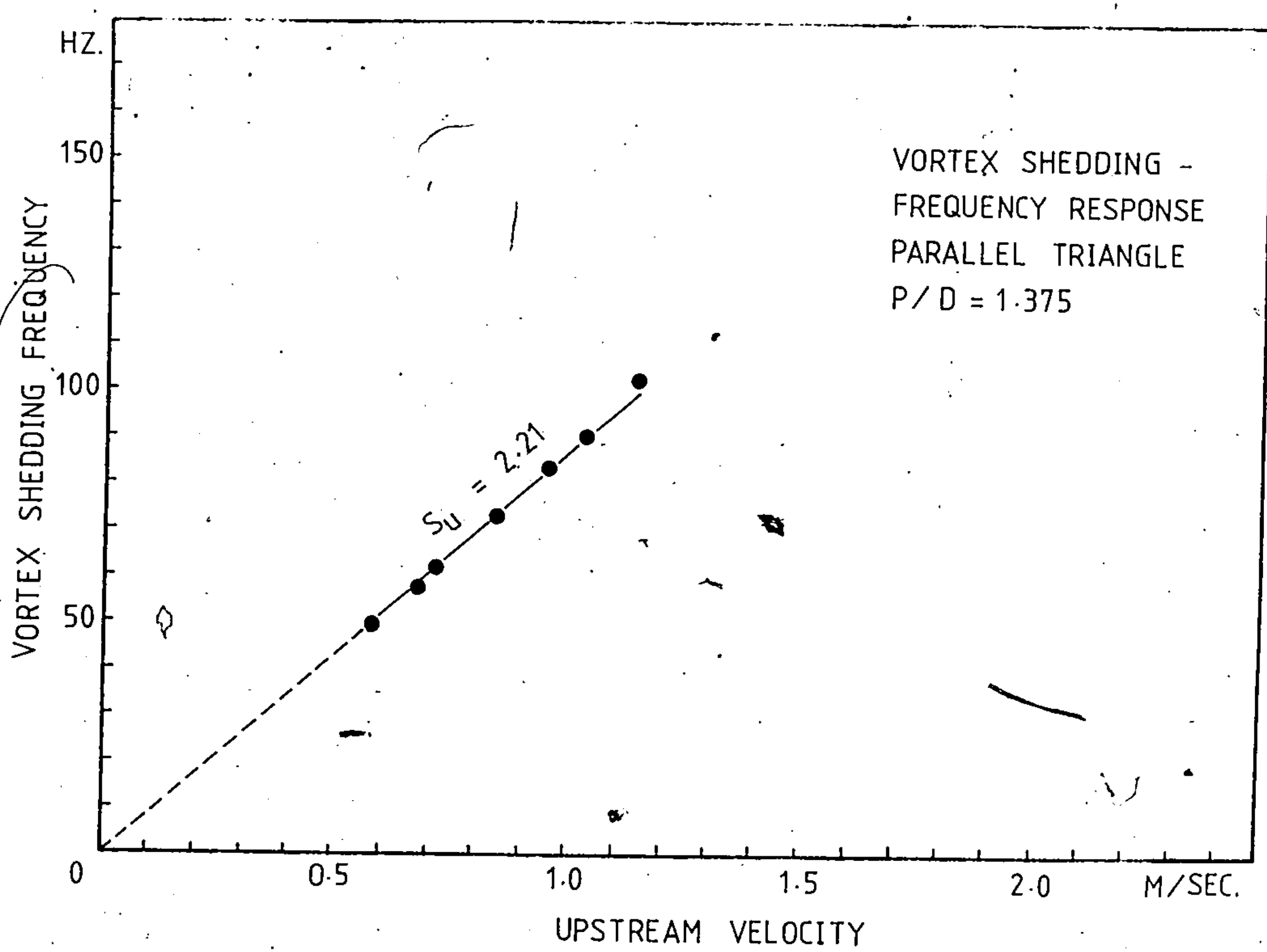
HZ.
150
100
50
0
VORTEX SHEDDING FREQUENCY
0.5
1.0
1.5
2.0
M/SEC.
UPSTREAM VELOCITY
VORTEX SHEDDING -
FREQUENCY RESPONSE
PARALLEL TRIANGLE
P/ D = 1.375
Su = 2.21

FIGURE 4.35

triangular arrays was used to interpret results for parallel triangular arrays. The formula gives a value of $S_u = 2.10$. This value gives a better agreement with the present value, being lower by only 5%. An excellent agreement was obtained as the present result was compared with that obtained by Weaver and Kogoyannakis [25] from a similar array in water flows. They reported a value of $S_u = 2.25$, and was obtained in the Reynolds number range, $R_u = 2.6 - 4.0 \times 10^3$. This value is less than 2% higher than the present value.

In summary, it can be said that vortex shedding was observed for a parallel triangular array with P/d = 1.375 in the Reynolds number range $R_u = 980 - 1940$. No data point for Strouhal number is available in the literature in the same range of Reynolds number. A value of upstream Strouhal number of $S_u = 2.21$ was obtained. This value showed a good agreement with some and not all the published data for a similar array. Vortex shedding frequencies were higher than the natural frequency of the flexible tubes so no vortex shedding resonance was expected.

4.3.8 Parallel Triangular Array; P/d = 1.73

The second parallel triangular array used for testing had a pitch-to-diameter ratio of 1.73. The array is 6 rows deep with only 4 tubes in every row including the half tubes, as shown in Figure 4.36. The hot-wire probe was inserted in the gap between the third and the fourth rows, as shown by the position marked 'H' in figure 4.36.

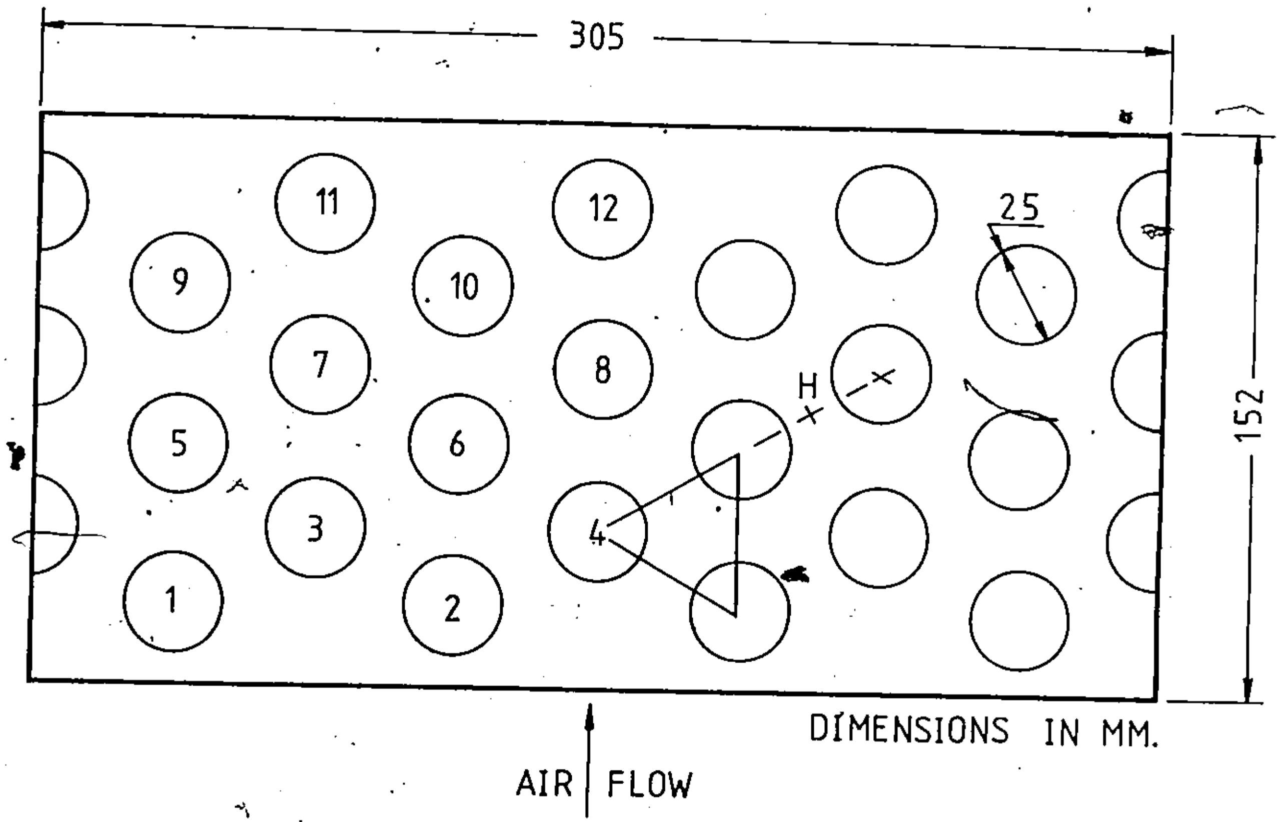

TUBES MARKED 1 - 12 ARE FLEXIBLE TUBES (REST ARE RIGID)

TUBES MARKED 6 AND 7 ARE INSTRUMENTED TUBES

H - LOCATION OF GAP HOT-WIRE PROBE

FIGURE 4.36: PARALLEL TRIANGULAR ARRAY WITH P/d = 1.73.

The appearance of velocity fluctuations was first observed at an upstream flow velocity of $V_u = 0.32$ m/sec. The corresponding Reynolds number is $R_e = 540$. The computed velocity spectrum is given as the first trace in Figure 4.37. As can be seen, the concentration of the velocity fluctuations is at a discrete frequency of 16.25 Hz, and with the appearance of a weak discrete frequency at double the original frequency at 32.50 Hz. The level of energy associated with these frequencies was less than those observed with the first parallel triangular array tested. The upstream Strouhal number will be $S_u = 1.29$. This value is almost half that obtained for the parallel triangular array with P/d = 1.375. This indicates how steep the reduction in Strouhal numbers with the increase in pitch-to-diameter ratio for parallel triangular arrays.

As the flow velocity was increased to $V_u = 0.38$ m/sec., the discrete frequency shifted to $f_s = 18.75$ Hz. The corresponding Strouhal number is $S_u = 1.25$. No appearance of a second harmonic was obtained, as shown by the second trace in Figure 4.37. The appearance of a second harmonic was obtained as the flow velocity was increased to $V_u = 0.45$ m/sec. The computed velocity spectrum is shown by the third trace in Figure 4.37. The discrete frequency at 23.75 Hz represents a value of Strouhal number of $S_u = 1.34$.

Four more velocity spectra were computed for flow velocities up to $V_u = 1.02$ m/sec. The corresponding Reynolds number is $R_u = 1720$. No discrete frequencies were observed for higher flow velocities. Only the second and last spectra are shown as the last two traces in Figure 4.37. The observed vortex shedding frequencies

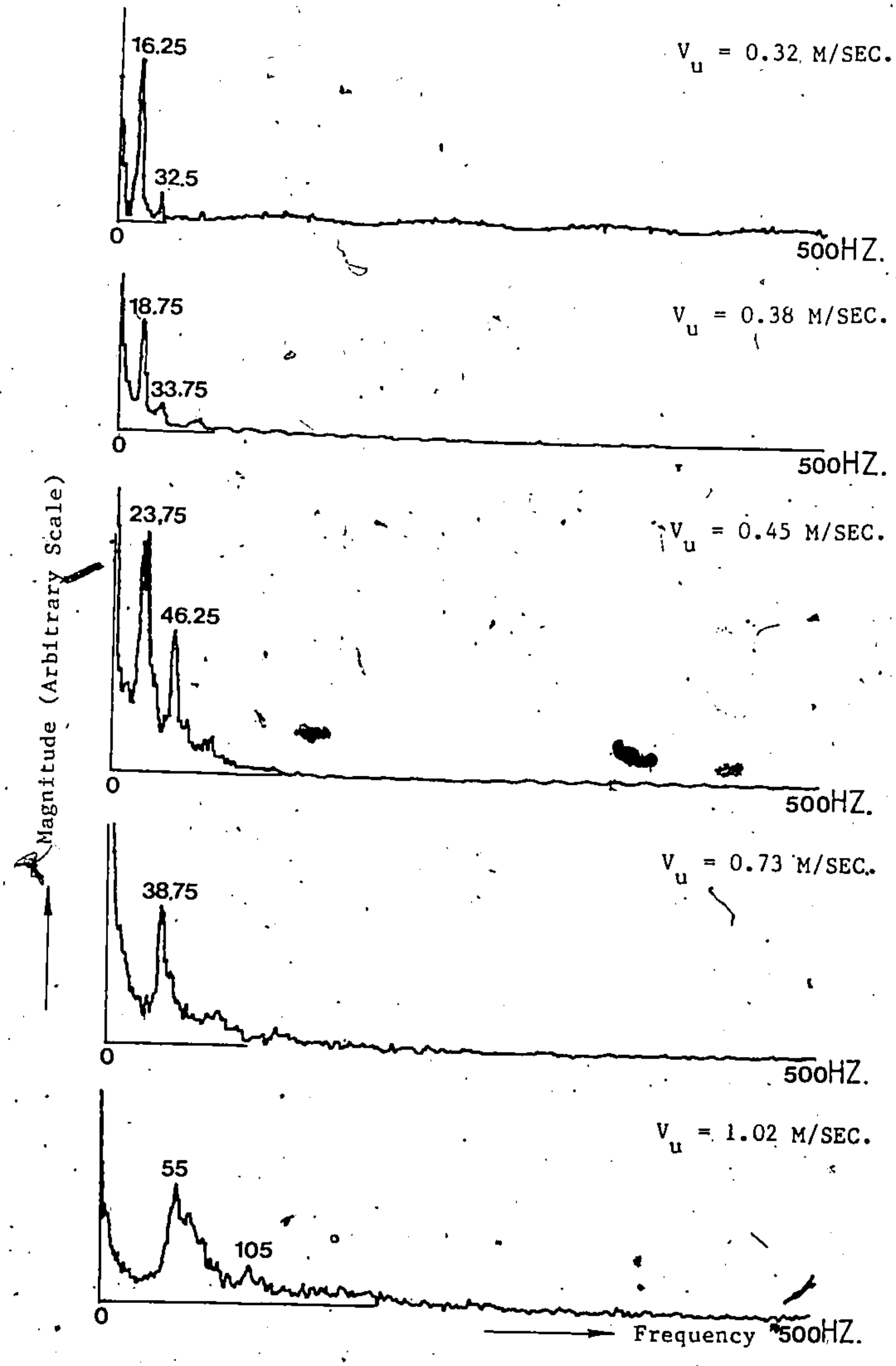

FIGURE 4.37: VELOCITY-SPECTRA FOR THE PARALLEL TRIANGULAR ARRAY WITH P/d = 1.73.

f_s, together the upstream flow velocities V_u, and the corresponding Reynolds numbers R_u, are given in Table 4.8. Also given in this table are the Strouhal numbers based on different definitions of flow velocities (see Appendix C). From Table 4.8, the average values of Strouhal numbers are $S_u = 1.32$, $S_{gm} = 0.58$, $S_p = 0.56$, and $S_g = 0.64$. The vortex shedding frequencies were also plotted versus the upstream flow velocities as shown in Figure 4.38. The figure shows that the shedding frequencies are increasing in a direct proportion with the flow velocities with a constant value of Strouhal number, $S_u = 1.32$.

No data exists in the literature for a parallel triangular array with P/d = 1.73. Chen's map [10] (shown in Figure 4.18) does not provide any direct data point for the present array. However, interpolation of the curves will provide a value of $S_u = 1.25$. This value is in a good agreement with the present value of $S_u = 1.32$ being lower by only 6%. Fitz-Hugh's map [11] (shown also in Figure 4.18) suggests a value $S_u = 1.03$. This value is lower than the present value by 28%. Owen's formula [8] gives a value of $S_u = 1.29$. This value is very close to the present value being lower by only 2%. Again, Zukauskas and Katinas formula [12] was used to interpret results for parallel triangular arrays. The formula gives a value of $S_u = 1.05$. This value is in a good agreement with Fitz-Hugh's value, and lower than the present value by 26%.

In summary, vortex shedding was observed for a parallel triangular array with P/d = 1.73, in the Reynolds number range R_e = 540 - 1720. An upstream Strouhal number of $S_u = 1.32$, was obtained. On the basis of using the ratio between theoretically determined gap

TABLE 4.8

Vortex shedding data for parallel triangular array with P/d = 1.73.

V_u	R_u	f_s	S_u	S_{gm}	S_p	S_g
0.32	540	16.25	1.29	0.57	0.54	0.63
0.38	640	18.75	1.25	0.55	0.53	0.61
0.45	760	23.75	1.34	0.59	0.56	0.65
0.60	1010	31.25	1.32	0.58	0.56	0.64
0.73	1230	38.75	1.35	0.59	0.57	0.66
0.80	1350	42.50	1.35	0.59	0.57	0.66
1.02	1720	55.00	1.37	0.60	0.58	0.67

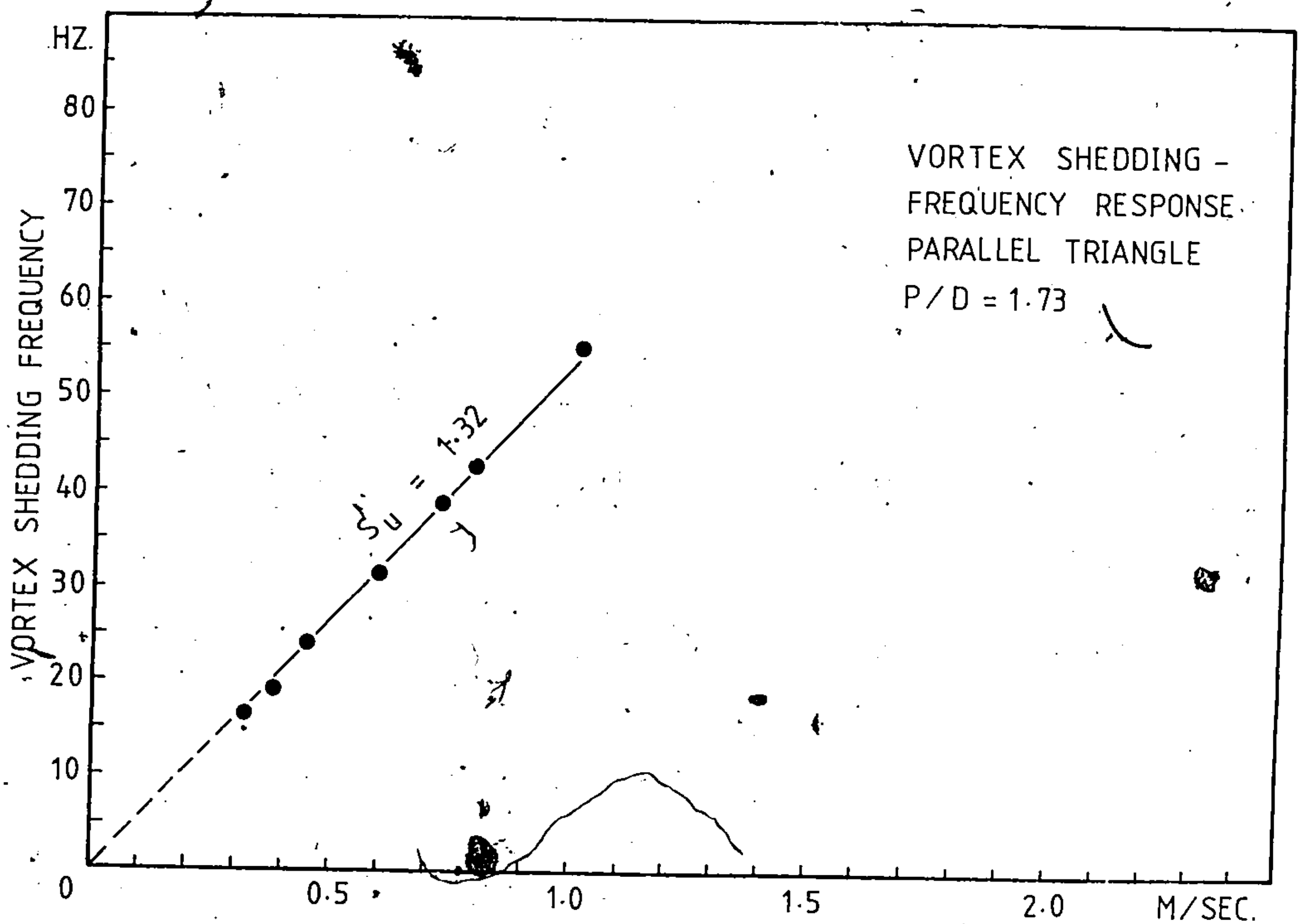
VORTEX SHEDDING -
FREQUENCY RESPONSE
PARALLEL TRIANGLE
P / D = 1·73
S_u = 1·32
HZ.
80
70
60
50
40
30
20
10
0
VORTEX SHEDDING FREQUENCY
0.5
1.0
1.5
2.0
M/SEC.
UPSTREAM VELOCITY

FIGURE 4.38

velocity and the upstream velocity, maps and formulae available in the literature were used for predicting values of the upstream Strouhal number for the present array. A good agreement was obtained with some of the available information. No vortex shedding resonance of the flexible tubes was observed for the present array.

Discussion

Two staggered arrays of the parallel triangular configuration were tested, having pitch-to-diameter ratios of 1.375 and 1.73. Only one value of the upstream Strouhal number for each array was obtained. Both values were obtained in different ranges of Reynolds than those available in the literature. However, few experimental data are available in the literature for the parallel triangular array with P/d = 1.375 and none for P/d = 1.73. Strouhal numbers from different maps and formulae available in the literature for parallel triangular arrays as a function of pitch-to-diameter ratio are plotted in Figure 4.39. As can be seen from this figure, Zukauskas and Katinas formula [12] when used for parallel triangular arrays shows good agreement with other published information. Also, the decay in Strouhal numbers with decreasing P/d due to Owen's formula [8] which was seen with other configurations does not occur with the parallel triangular arrays, with the exception that the formula still predicts values of Strouhal numbers which are below that for a single cylinder for high values of P/d. However, upstream Strouhal numbers were plotted as can be seen in Figure 4.40 up to P/d = 3, where this problem with Owen's formula does not appear. The figure shows that Zukauskas and Katinas

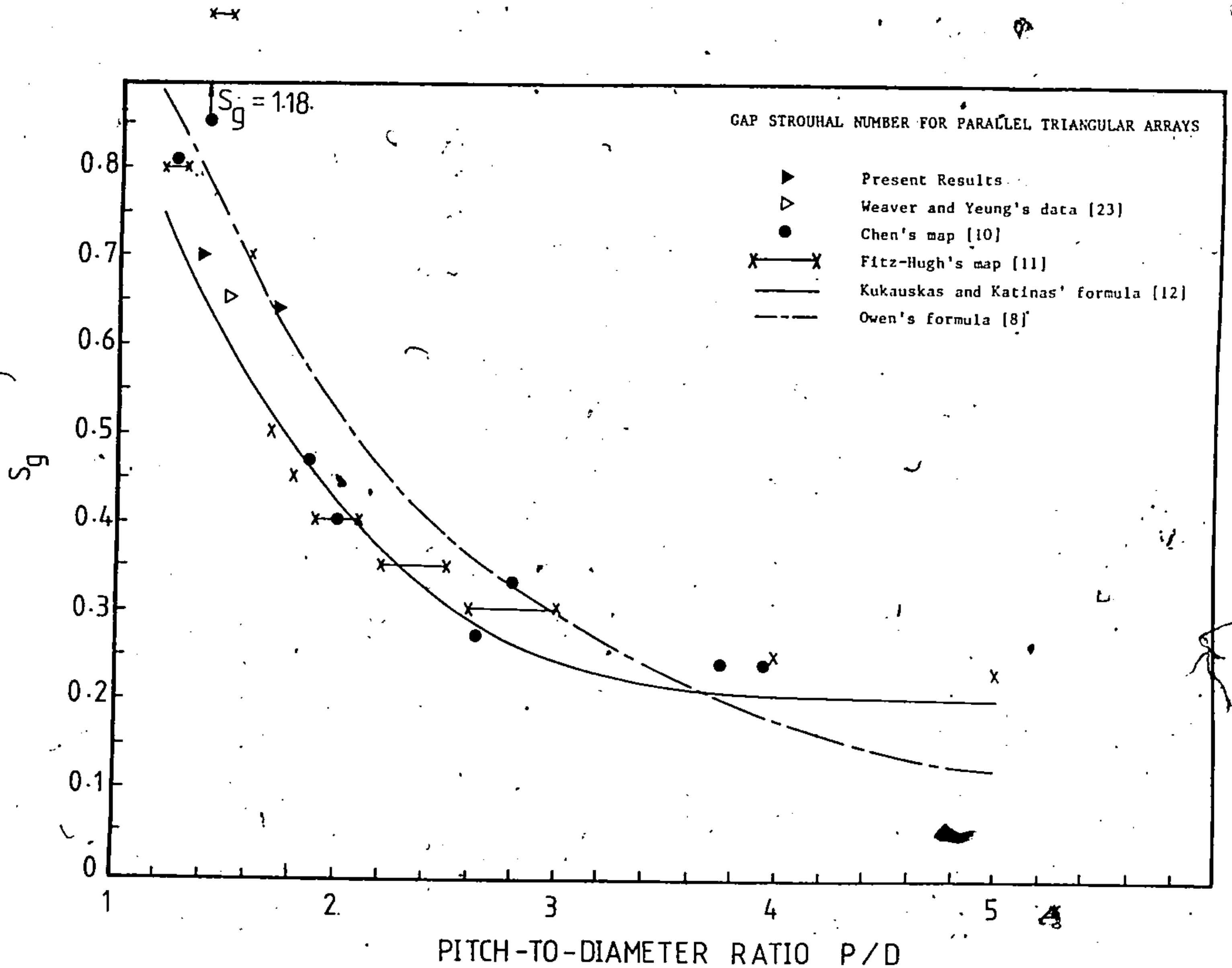
GAP STROUHAL NUMBER FOR PARALLEL TRIANGULAR ARRAYS
Present Results
Weaver and Yeung's data [23]
Chen's map [10]
Fitz-Hugh's map [11]
Kukauskas and Katinas' formula [12]
Owen's formula [8]
$S_g = 1.18$
S_g
0.8
0.7
0.6
0.5
0.4
0.3
0.2
0.1
0
1
2
3
4
5
PITCH-TO-DIAMETER RATIO P/D

FIGURE 4.39

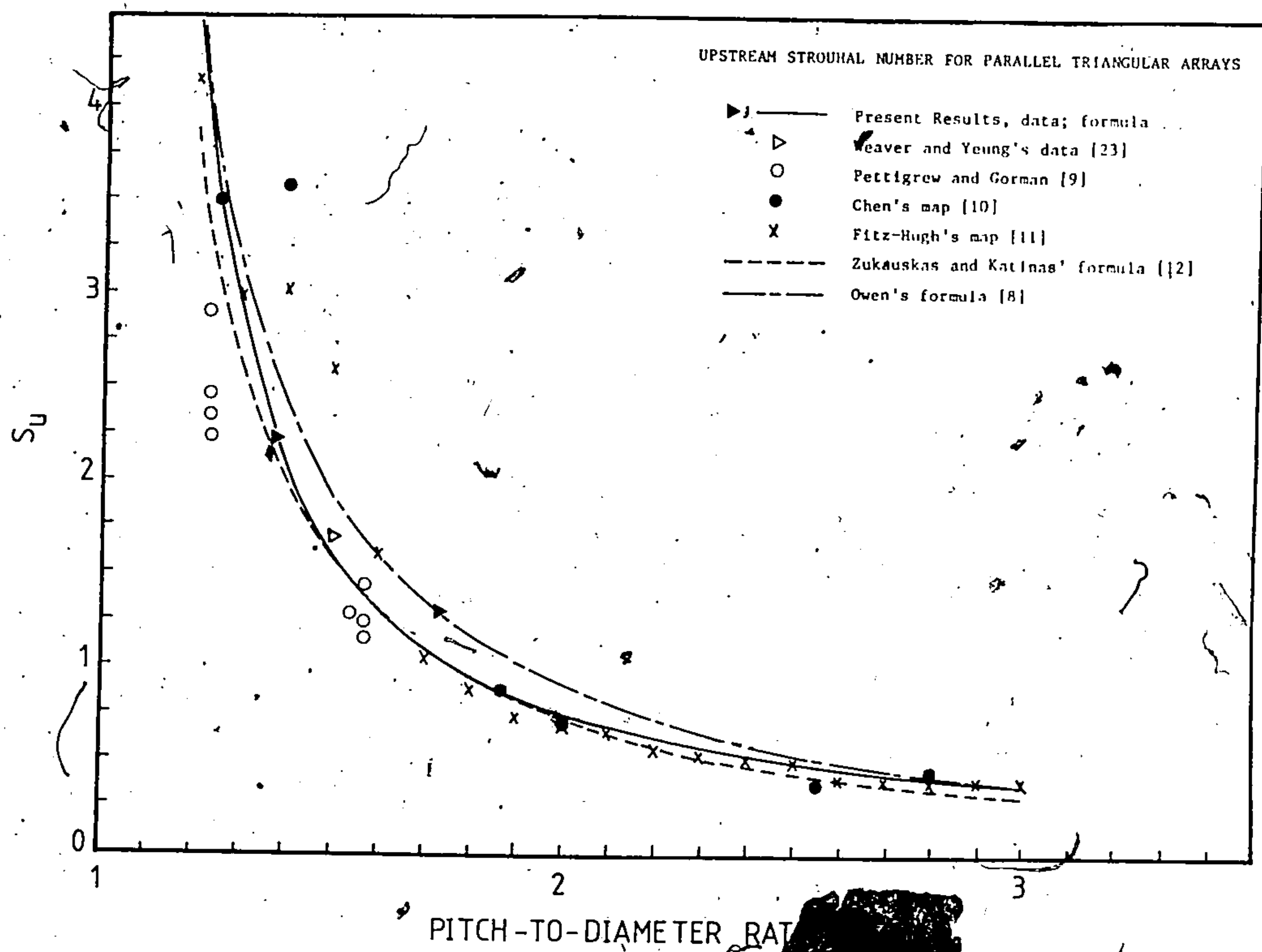
UPSTREAM STROUHAL NUMBER FOR PARALLEL TRIANGULAR ARRAYS
Present Results, data; formula
Weaver and Yeung's data [23]
Pettigrew and Gorman [9]
Chen's map [10]
Fitz-Hugh's map [11]
Zukauskas and Katinas' formula [12]
Owen's formula [8]
S_u
0
1
2
3
4
1
2
3
PITCH-TO-DIAMETER RAT

FIGURE 4.10

formula shows a good agreement with the values obtained from the maps of Chen [10] and Fitz-Hugh [11] for most of the values of P/d. However, as can be seen from Figure 4.40, if Chen's point for P/d = 1.4, and Fitz-Hugh's points for P/d = 1.4, 1.5 and 1.6 were excluded from the plot, their results will be in better agreement with the rest of the published data. Also, their results will be in better agreement with the present results for both arrays. Pettigrew and Gorman's data points [9] are in good agreement with other published results if only the maximum values they provided were considered. Their lower data are probably the result of being taken at tube resonance.

A best fit curve through all these published results, including the present results was attempted. This curve was also a combination of logarithmic and power-laws. The curve obtained is represented by the solid line in Figure 4.40. The formula which represents this curve has the form:

$$S_u = -1 + \exp \left\{ \frac{(P/d - 1)^{-0.75}}{1.79} \right\}$$

The formula is in reasonable agreement with the published results for most of the values of P/d.

Attempts were also made to collapse the results for the normal and parallel triangular arrays. Unfortunately, the attempts were unsuccessful because of the wide scatter associated with the normal triangular arrays.

4.3.9 Overview

Strouhal numbers for the different tube arrays tested in the present study and the corresponding Reynolds number (based on upstream flow velocities and the outside tube diameter) are summarized in Table 4.9. At very low flow velocities, the convective heat transfer from the hot wire probe will influence the probe readings. The DISA manual states that reasonable results may be obtained at low flows by extrapolation of the King's Law curve $(\text{Volt})^2$ versus $(\text{Velocity})^{1/2}$ to the zero flow axis (static flow value) (see Appendix B). Under conditions of very low flows, one might expect velocity errors of the order of $\pm 10\%$. However, the lack of scatter in the Strouhal curves and the consistency in the Strouhal numbers suggest considerably smaller errors in velocity measurement. At any rate, reasonable errors in the magnitude of the flow velocity measurements will not affect the principal conclusions drawn from the experimental results.

An overall assessment can be made of the above results when consideration is taken of a recent flow visualization study by Abd-Rabbo [77]. This showed that laminar vortex shedding occured at low Reynolds numbers in the first three rows of a rotated square array with a pitch ratio of 1.414. The Strouhal number was found to have a value between $S_u = 2.2 - 2.6$ in the Reynolds number range $140 < R_u < 230$. For higher Reynolds numbers, the tube response showed a substantially smaller Strouhal number of $S_u = 1.4$. However, no discrete wake phenomena were observed, the flow visualization being obscured by turbulence. On the other hand, a square array with a pitch ratio of 1.5 showed no laminar vortex shedding. Only large resonance response was obtained at double the Strouhal number reported in the literature.

TABLE 4.9

Summary of Vortex Shedding Data.

Array Geometry	P/d	R_u	S_u	S_{gm}	S_p	S_g
Normal	1.33	170-740	2.34	0.59	0.59	0.59
Square	1.50	420-590	1.72	0.50	0.57	0.57
		760-1130	1.44,2.04	0.42,0.60	0.48,0.68	0.48,0.68
Rotated	1.414	180-1120	1.73	0.60	0.50	0.72
Square	1.70	670-3170	0.87	0.42	0.36	0.51
		1850-4550	0.58	0.28	0.24	0.34
Normal	1.33	130-290	4.89	1.01	1.21	1.21
Triangle	1.50	420-810	1.49	0.49	0.50	0.50
		1100-1420	1.28	0.42	0.43	0.43
Parallel	1.375	980-1940	2.21	0.60	0.60	0.70
Triangle	1.73	540-1720	1.32	0.58	0.56	0.64

It would appear then that certain arrays produce laminar vortex shedding at low Reynolds numbers and this is associated with high Strouhal numbers. At higher Reynolds numbers, turbulence develops in the arrays but discrete excitation persists and is associated with substantially lower Strouhal numbers. Additionally, some arrays show multiple Strouhal numbers at moderate Reynolds numbers and over a range of pitch ratios. However, it is difficult to state the precise ranges of Reynolds numbers over which the vortex shedding phenomenon exists. These ranges will be affected by ambient turbulence levels. As turbulence levels increase with increasing row depth for the first four rows at least, the laminar vortex shedding will terminate at lower Reynolds numbers for the deeper tube rows [77]. It is also likely that the Reynolds number ranges depend on tube motion. Vortex shedding may persist to higher Reynolds numbers if reinforced by small tube motions. Thus, one would expect vortex shedding to occur at higher Reynolds numbers in a flexible tube array exposed to water flow than for a rigid tube array or a flexible tube array exposed to a gas flow.

Laminar Vortex Shedding

In view of the above, the high Strouhal numbers obtained from the present study for the normal square arrays with pitch ratios of 1.33 and 1.5 may be attributed to laminar vortex shedding. For the normal square array with pitch ratio of 1.33, the Strouhal number was found to be $S_u = 2.34$ in the Reynolds number range $R_u = 170 - 740$. However, for the normal square array with pitch ratio of 1.5, three values for the Strouhal number were obtained, these being $S_u = 1.72$ for $R_u = 420 - 590$, and $S_u = 1.44, 2.04$ for $R_u = 760 - 1130$. For this particular array, Weaver and Yeung [23] from off-resonance tube response in water flow predicted a value of $S_u = 1.8$ in the Reynolds number range $R_u = 2.0 - 2.70 \times 10^3$. On the other hand, the values for Strouhal number obtained by Pettigrew and Gorman [9] for a normal square array with P/d = 1.47, in water flows were between S_u = 1.28 and S_u = 1.97 (depending on tube location). These values were obtained in the Reynolds number range $R_u = 2.0 - 4.2 \times 10^3$. As mentioned above, higher Reynolds numbers could be expected for a flexible tube array exposed to water flow. However, these results show higher Strouhal numbers than those reported in the literature.

The appearance of Strouhal numbers which are almost double the results published in the literature for the normal square arrays tested in the present study warns of the fact that vortex shedding could be expected at half the flow velocities expected from the Strouhal numbers reported in the literature.

Another interesting result was obtained for the normal triangular array with pitch ratio of 1.33. A very high Strouhal number of S_u = 4.89 was obtained at very low Reynolds number range of R_u = 130 - 290. Again, it seems likely that laminar vortex shedding is the reason behind this high Strouhal number. The increase in Strouhal numbers for the normal triangular arrays at very low pitch ratios may not be quite as steep as previously suggested. Furthermore, the only result which is close to the present result is based on an extrapolation of Chen's map [10] as reported by Paidoussis [7]. There is significant evidence to show that extrapolation of these results will not provide such a high value for Strouhal number, as demonstrated by the results shown in Figure 4.32.

The results for this normal triangular array together with those for the normal square arrays tested in the present study suggest that laminar vortex shedding could be expected for Reynolds numbers R_u < 1100, for these particular patterns. These Reynolds numbers are not likely to produce a sufficient dynamic head to cause tube vibration in any practical heat exchanger. The question that arises is which other tube arrays produce laminar vortex shedding and which do not. Again, the recent study by Abd-Rabbo [77] shows that laminar vortex shedding occured in the Reynolds number range of $140 < R_u < 230$ for a rotated square array with pitch ratio of 1.414. However, many more tests will be required to establish the range of flows for which laminar vortex shedding may occur in other configurations.

Multiple Strouhal Numbers

The present results show multiple Strouhal numbers for the following arrays: normal square with $P/d = 1.5$, for $420 < R_u < 1130$, rotated square with $P/d = 1.7$ for $670 < R_u < 4550$, and the normal triangular with $P/d = 1.50$ for $420 < R_u < 1420$. No multiple Strouhal numbers were obtained for either of the parallel triangular arrays tested in the present study. There are not many results available in the literature showing this kind of behaviour. Data by Fitzpatrick [80] also gives 3 Strouhal numbers of $S_u = 0.78$, 0.98, and 1.33 for an in-line array with transverse spacing of 1.73 and longitudinal spacing of 1.5. Although Fitzpatrick's configuration was somewhat different from the present study, the numbers reported compare reasonably with the current results for the normal square array with pitch ratio of 1.5 when account is taken of the effect of transverse spacing. Higher transverse spacings are expected to produce lower Strouhal numbers. The reported results by Pettigrew and Gorman [9] show more than one value of Strouhal number for the following arrays: normal square with $P/d = 1.47$, normal triangular with $P/d = 1.33$ and 1.57, and the parallel triangular with P/d = 1.23, 1.57. They obtained their results in water flow for Reynolds number range $R_u = 2.0 - 4.2 \times 10^3$. Their results are shown in Figures 4.14, 4.32 and 4.40. The present results showed significant unsteadiness for the normal square array with pitch ratio of 1.5 in the Reynolds number range $R_u = 760 - 1130$. However, it appears that multiple Strouhal numbers occur for arrays of pitch ratios around 1.5 and for the Reynolds number range $400 < R_u < 5000$.

There is now considerable evidence to show that certain tube array patterns have multiple Strouhal numbers over a range of small pitch ratios. It follows that in cases where there are multiple Strouhal numbers, it is not valid to try to fit a single curve through the data as has been commonly attempted. Further research is necessary to define these curve branches and to determine if one of the Strouhal numbers is more dominant or if all are equally likely to excite acoustic or tube resonance. It would also appear that the best fit drawn from the results in Figure 4.14, and 4.24 may only be valid at high Reynolds numbers. However, there is some scatter in the data reported in the literature due to the distortion resulting from tube or acoustic resonance. An example of this distortion is the results reported by Pettigrew and Gorman [9] for tube resonance. The results are clearly below the expected values for similar arrays as shown in Figures 4.14, 4.24, 4.32, and 4.40. It would also appear that, even if this misleading data were adjusted some scatter will remain.

<u>Owen's Phenomenon</u>

There is now considerable ~~evidence to~~ show that a discrete phenomenon characteristic of vortex shedding exists for closely packed tube arrays. Examples of the existence of this discrete periodicity are the present results, the results reported by Weaver and Yeung [23], and Abd-Rabbo [77]. This excitation phenomenon is not broad band as the one reported by Owen [8]. This implies that Owen's turbulent buffeting is a different phenomenon and is not valid at least for early tube rows. The phenomenon associated ~~with~~ buffeting can exist deep inside arrays where the flow is expected to be more turbulent as shown by Fitzpatrick and Donaldson [83]. Also, the present results show clearly, the wrong flow velocity was used by Owen in his equation. Upstream flow velocity or the proper transverse pitch velocity as suggested [83] must be used to correctly correlate his equation with other published results, depending on whether the Strouhal number is based on upstream or gap velocity.

4.4 FLUIDELASTIC INSTABILITIES

The fluidelastic excitation mechanism is the most important mechanism for tube arrays due to the high amplitudes of vibration associated with it. The severity of the damage due to these high amplitudes is well documented [1]. Tube arrays in a cross flow of a gas generally start to vibrate abruptly when the flow velocity reaches a certain threshold. Reliable data for these threshold velocities (also known as critical velocities) for tube arrays is very important at the design stage. These critical velocities are functions of many parameters such as tube stiffness, damping, mass, and the fluid density. Also, one of the most important parameters is the geometrical arrangement of the tubes in the arrays, as well as the pitch-to-diameter ratios for different array geometries. Surprisingly, the tube pattern and pitch has not had too much attention in the past, and this probably accounts for much of the scatter in the published results. Recently, tube geometry began to be included in the fluid-elastic stability equation. Apparently, the only systematic studies of tube pattern and pitch are those reported by Hartlen [16], and Soper [17]. Hartlen, reported that his results are unreliable, mainly because of the problems involved in conducting the experiments, especially the lack of equipment for precisely determining the critical velocities. On the other hand, Soper's results were for higher values of the damping parameter. The experiments reported here were conducted for a damping parameter which is lower than those used by Hartlen, and in the hope of obtaining more reliable and consistent results. Also, it is hoped that the results will be helpful in understanding the importance of other parameters which affect the critical flow velocities.

The present results will be considered under separate headings for different geometries and pitch-to-diameter ratios. However, before representing these results, a general description of the procedure followed during testing of the arrays will be given.

Procedure for Testing:

As mentioned previously, all flexible tubes in any array were tuned to a natural frequency of 25.0 Hz within 1%. The tube array was used first for obtaining the vortex shedding frequencies, then it was used for obtaining the critical flow velocities before transferring the flexible tubes to another array. After getting the vortex shedding data, the wind tunnel was turned off, and the experiment begun again at some low flow velocity. This flow velocity was well in the stable region of the tube array. This was done by running the wind tunnel at different flow velocities until the tube was observed visually to be unstable and before recording any data an approximate value for the critical velocity was obtained. The wind tunnel was turned off again and the experiment begun at a much lower flow velocity than that after which the array becomes unstable. The upstream hot-wire probe as well as the pitot-static tube were used for measuring the upstream flow velocity, while the amplitude response data were obtained from the strain gauge transducers using the Spectral Dynamics 375 Fourier analyzer. The instrumented tube was connected first to the analyzer through a conditioning amplifier. For every small increment in the flow velocity, the amplitude response data for the in-line and transverse motions of the tube were recorded after waiting for an interval of time of about 10 minutes to allow for a steady state to be reached. The response amplitudes recorded were the result of 64 sample averages which were found from a preliminary test to be sufficient to achieve a steady state and to give a reproducible data. The experiment was repeated for every increment in the flow velocity until the tube was observed to be well into the unstable region. Due to the fact that, with increasing the flow velocity, tubes exhibiting steady orbits would sustain orientation changes in their orbits or it might become unsteady due to any nonlinearities in the source of excitation, the displacement of coordinate direction will increase or decrease accordingly. Therefore the concept of a resultant RMS amplitudes was also used in this study and which is defined as follows:

$$\text{RMS amplitudes} = \sqrt{(\text{in-line amplitudes})^2 + (\text{transverse amplitudes})^2}$$

RMS amplitudes together with the in-line and transverse amplitudes were plotted for every tube tested. These tube amplitudes are the values of the tube tip deflection in mm. Due to the fact that for every array, two tubes were tested, the complete process was repeated for the second monitored tube. The above outlined procedure will be followed with every array tested.

In making the RMS amplitude measurements, 64 sample averages were found to produce good experimental repeatability. In 10 repeated experiments at a particular flow, the standard deviation was found to be 3%. The flow velocity was measured upstream of the tube bundle using both pitot probe and hot wire anemometer. Comparison of the data indicates out of 8 measurements, a maximum difference of ±4%.

4.4.1 Normal Square Array; P/d = 1.33

The normal square array with P/d = 1.33 is shown in Figure 4.4. The two flexible tubes marked 5 and 8 in the second and third rows, respectively, were the instrumented tubes. The in-line, transverse, and RMS tube amplitudes obtained for tube No. 5 in the second row were plotted as shown in Figure 4.41. As can be seen from this figure, the increase in tube amplitude was in proportion with the flow velocity in the stable region. In this region amplitudes are much less than 1% of a tube diameter. Numerical values of vibration amplitudes in this region showed that the in-line amplitudes are slightly higher than those in the transverse directions. However, as the flow velocity begins to reach the critical velocity, amplitudes in

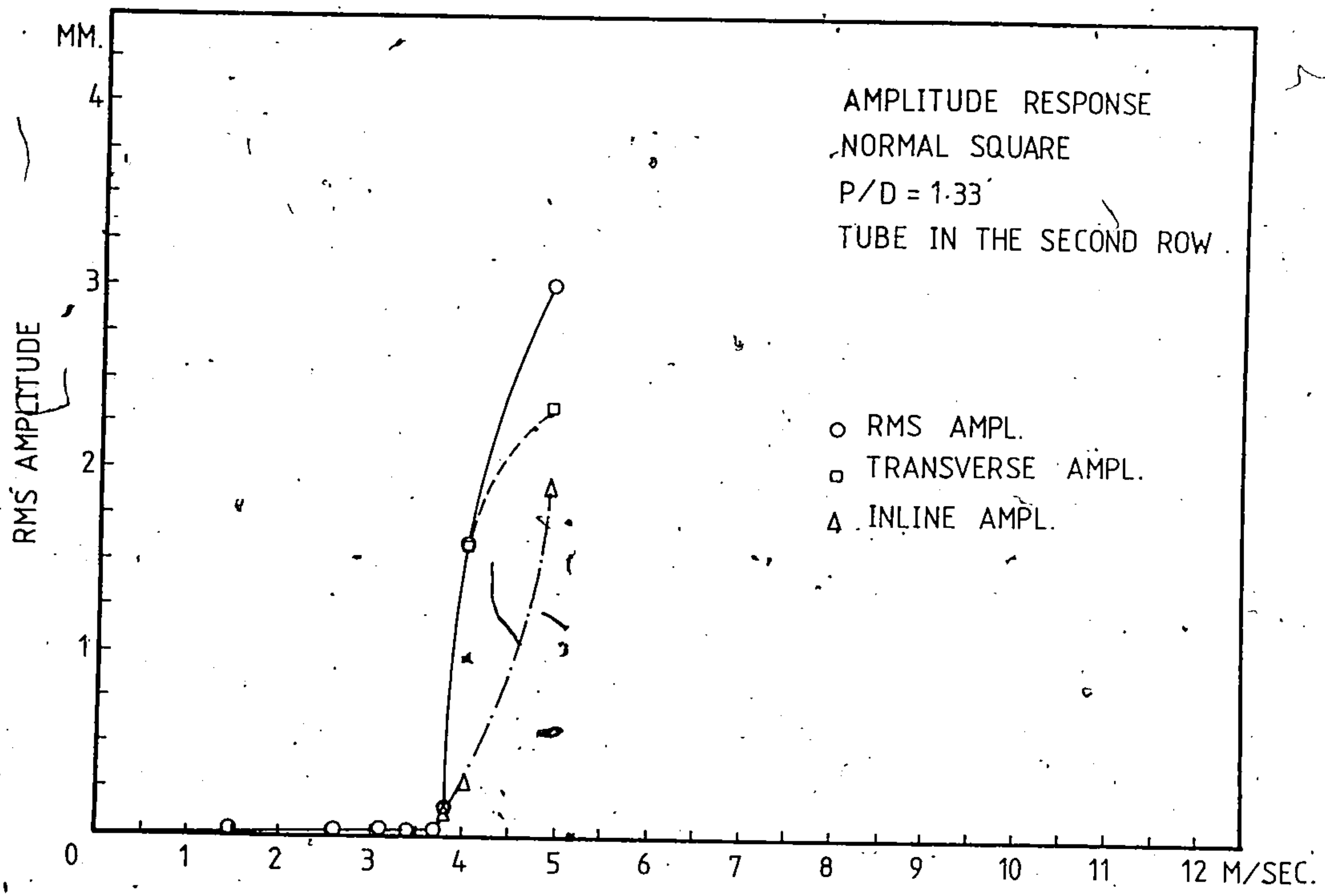
AMPLITUDE RESPONSE
NORMAL SQUARE
P/D = 1·33
TUBE IN THE SECOND ROW
RMS AMPL.
TRANSVERSE AMPL.
INLINE AMPL.
MM.
RMS AMPLITUDE
0
1
2
3
4
5
6
7
8
9
10
11
12 M/SEC.
UPSTREAM VELOCITY

FIGURE 4.41

the transverse direction start to become higher than those in the in-line direction. As our approach for determining the critical flow velocity is defined as the flow velocity after which tube amplitudes will increase rapidly for any small increment in the flow velocity, a value of V_{cr} = 3.70 m/sec., will be the critical velocity for the present array. As can be seen from Figure 4.41, a sharp increase in tube amplitudes was obtained. This sharp increase gives a well defined critical velocity. In the unstable region, amplitudes in the transverse direction kept on increasing higher than those in the in-line direction.

The results obtained for the second monitored tube, tube No. 8, in the third row were plotted as shown in Figure 4.42. The two monitored tubes exhibited the same behaviour in the stable region. Also, as can be seen from Figure 4.42, no change in the critical flow velocity between the second and the third row was obtained. The only difference between these two monitored tubes occurred in the unstable region. Amplitudes in the in-line direction were higher for the tube in the third row over those in the transverse direction. This means that while the tube in the second row was moving mainly in the transverse direction, tube in the third row is whirling with a larger amplitude component in the in-line direction.

4.4.2 Normal Square Array; P/d = 1.5:

The normal square array with P/d = 1.5 is shown in Figure 4.8. The tubes numbered 5 and 8 were the instrumented tubes, located in the second and third row respectively. Note that these two instrumented

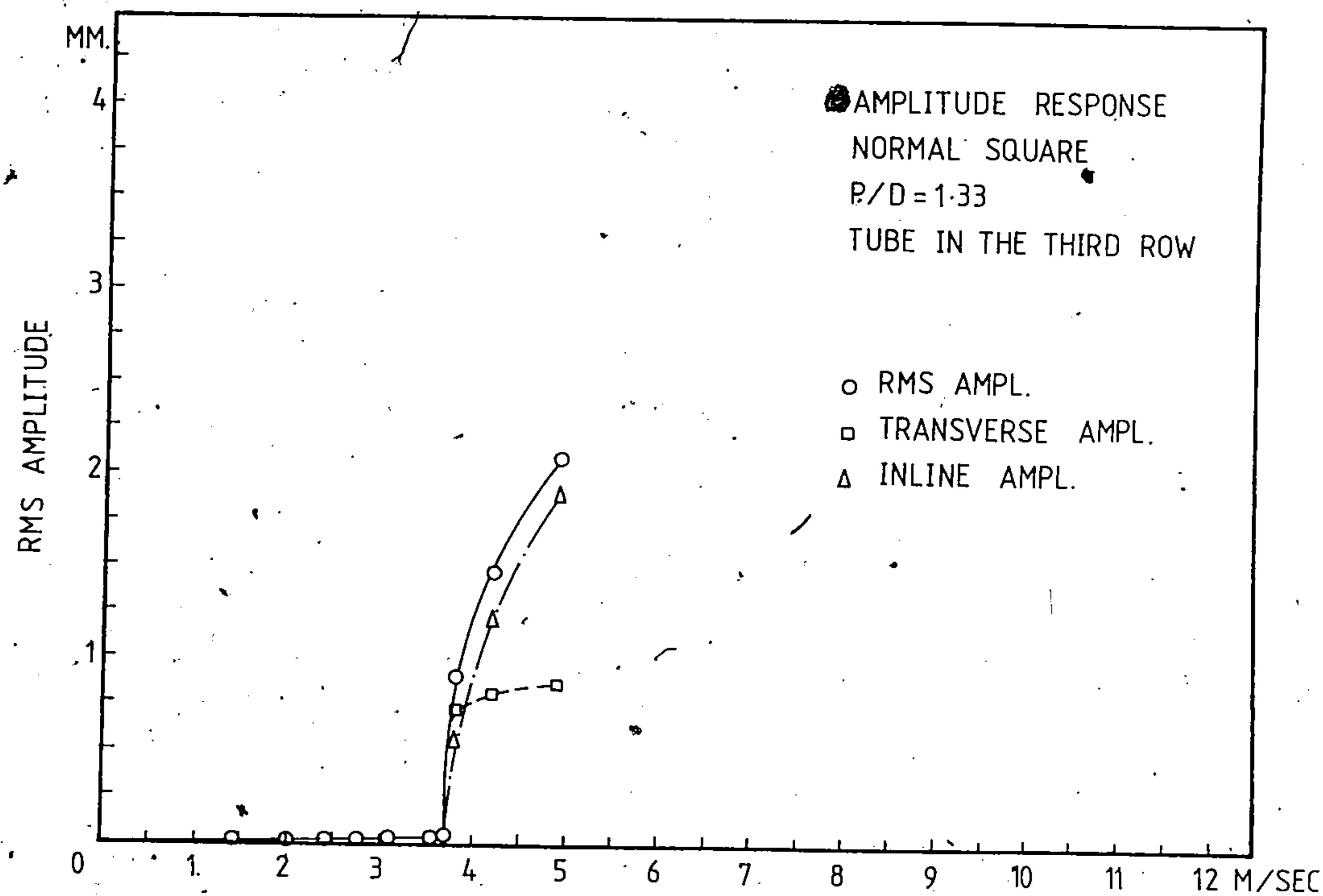
AMPLITUDE RESPONSE
NORMAL SQUARE
P/D = 1·33
TUBE IN THE THIRD ROW
RMS AMPL.
TRANSVERSE AMPL.
INLINE AMPL.
RMS AMPLITUDE
MM.
0
1
2
3
4
1.
2
3
4
5
6
7
8
9
10
11
12 M/SEC.
UPSTREAM VELOCITY

FIGURE 4.42

tubes are surrounded by flexible tubes to account for any fluid coupling from the surrounding tubes. The same feature was chosen for all the arrays tested in this thesis, although it was found by Weaver and Grover [19] and Lever and Weaver [27] that one flexible tube in otherwise rigid array will have nearly the same critical velocity.

In-line, transverse, and RMS amplitudes obtained for tube No. 5 in the second row were plotted versus the upstream flow velocities as shown in Figure 4.43. Again, the tube showed a linear increase in the tube tip deflection with increasing flow velocity in the stable region. However, amplitudes in the transverse direction were slightly higher than those in the in-line direction in this region. This is contrary to what was observed in the normal square array with P/d = 1.33. The same behaviour was also obtained as the tube came into the unstable region. In-line amplitudes, as can be seen from Figure 4.43, were higher for this array than those in the transverse direction. Note that the increase in the tube amplitude around the critical velocity is more gradual for the present array. However, the increase in tube amplitude in the transverse direction show that the tube takes off at a flow velocity of V_{cr} = 3.50 m/sec. If this value was chosen as the critical velocity, this will mean that the increase in pitch-to-diameter ratio from P/d = 1.33 to P/d = 1.5 resulted in a slight decrease in the critical velocity; i.e., normal square array with P/d = 1.5 is more critical than that with P/d = 1.33.

The results obtained for tube No. 8 in the third row were plotted as shown in Figure 4.44. In the stable region, amplitudes in the in-line direction were slightly higher for this tube over those in

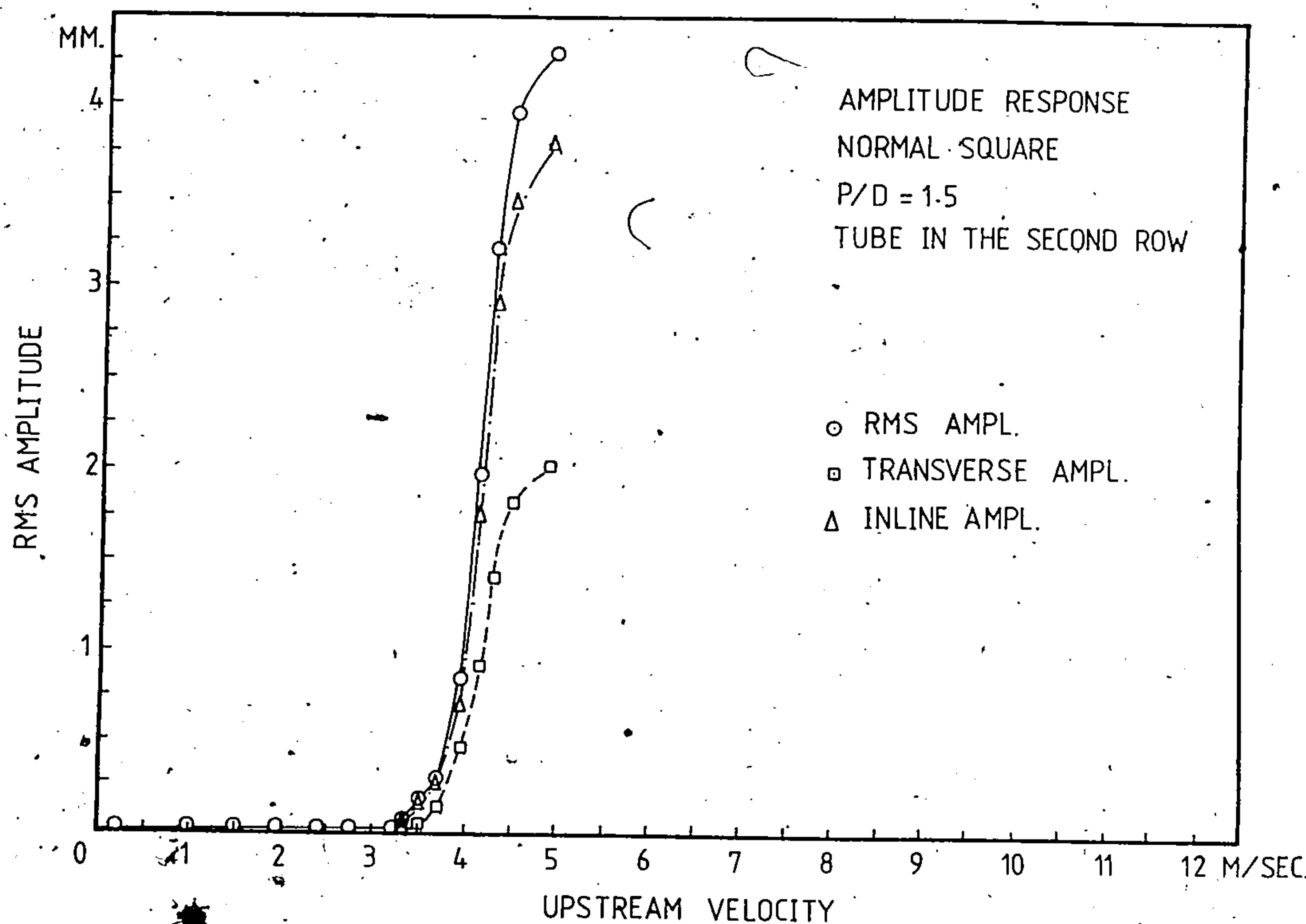
AMPLITUDE RESPONSE
NORMAL SQUARE
P/D = 1·5
TUBE IN THE SECOND ROW
RMS AMPL.
TRANSVERSE AMPL.
INLINE AMPL.
RMS AMPLITUDE
MM.
0
1
2
3
4
5
6
7
8
9
10
11
12 M/SEC.
UPSTREAM VELOCITY

FIGURE 4.43

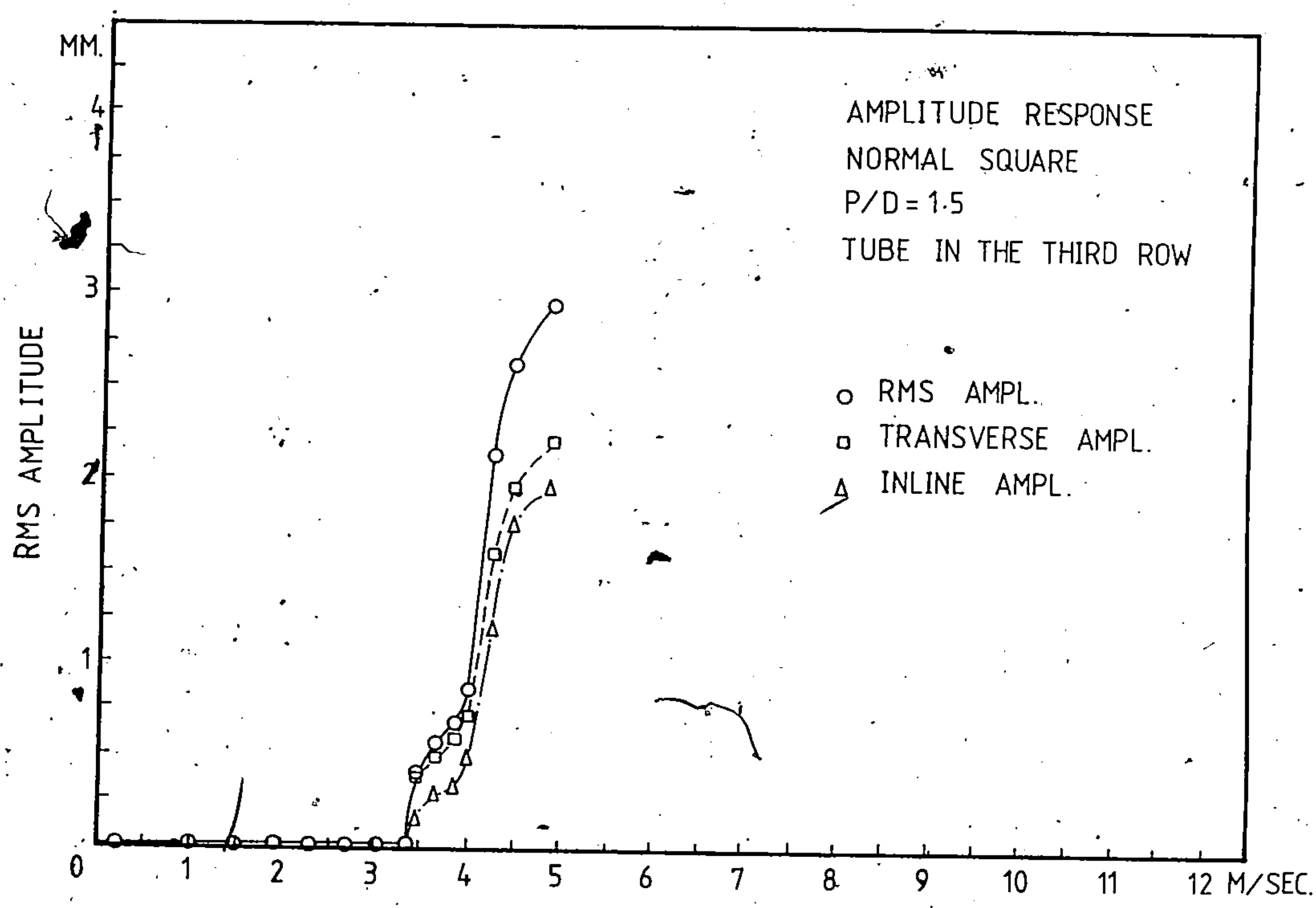
AMPLITUDE RESPONSE
NORMAL SQUARE
P/D = 1.5
TUBE IN THE THIRD ROW
RMS AMPL.
TRANSVERSE AMPL.
INLINE AMPL.
MM.
RMS AMPLITUDE
0
1
2
3
4
5
6
7
8
9
10
11
12 M/SEC.
UPSTREAM VELOCITY

FIGURE 4.44

the transverse direction. A better defined critical velocity of V_{cr} = 3.35 m/sec. was obtained for this tube. This means that the tube in the third row was more critical than that in the second row. Above the critical velocity, amplitudes in the transverse direction were slightly higher than those in the in-line direction with smaller amplitudes than those obtained for the tube in the second row. So, while the tube in the second row was whirling with a larger amplitude in the in-line direction, the tube in the third row was whirling with a larger amplitude in the transverse direction. This is contrary to what was obtained for the normal square array with P/d = 1.33.

The tube response (for tube No. 8 in the third row) as seen on the oscilloscope screen was photographed at a number of flow velocities and has been reproduced in Figure 4.45. The first three pictures show the tube response at flow velocities lower than the critical velocity. In this region the tube response is random in character and the amplitudes are very small. The first picture was taken at a flow velocity where the vortex shedding frequency f_s, coincides with the natural frequency of the tube. No vortex shedding resonance was observed. The fourth picture was taken at a flow velocity slightly higher than the critical velocity. As can be seen the amplitudes were higher in the transverse direction with the tube moving in a figure of eight pattern. As the flow velocity was increased, the tube maintained the same pattern, until the flow velocity reached V_u = 3.90 m/sec. The response became more regular and the tube moved in an oval-shaped orbit. However, the tube did not maintain this orbit for a long time but started to change its response

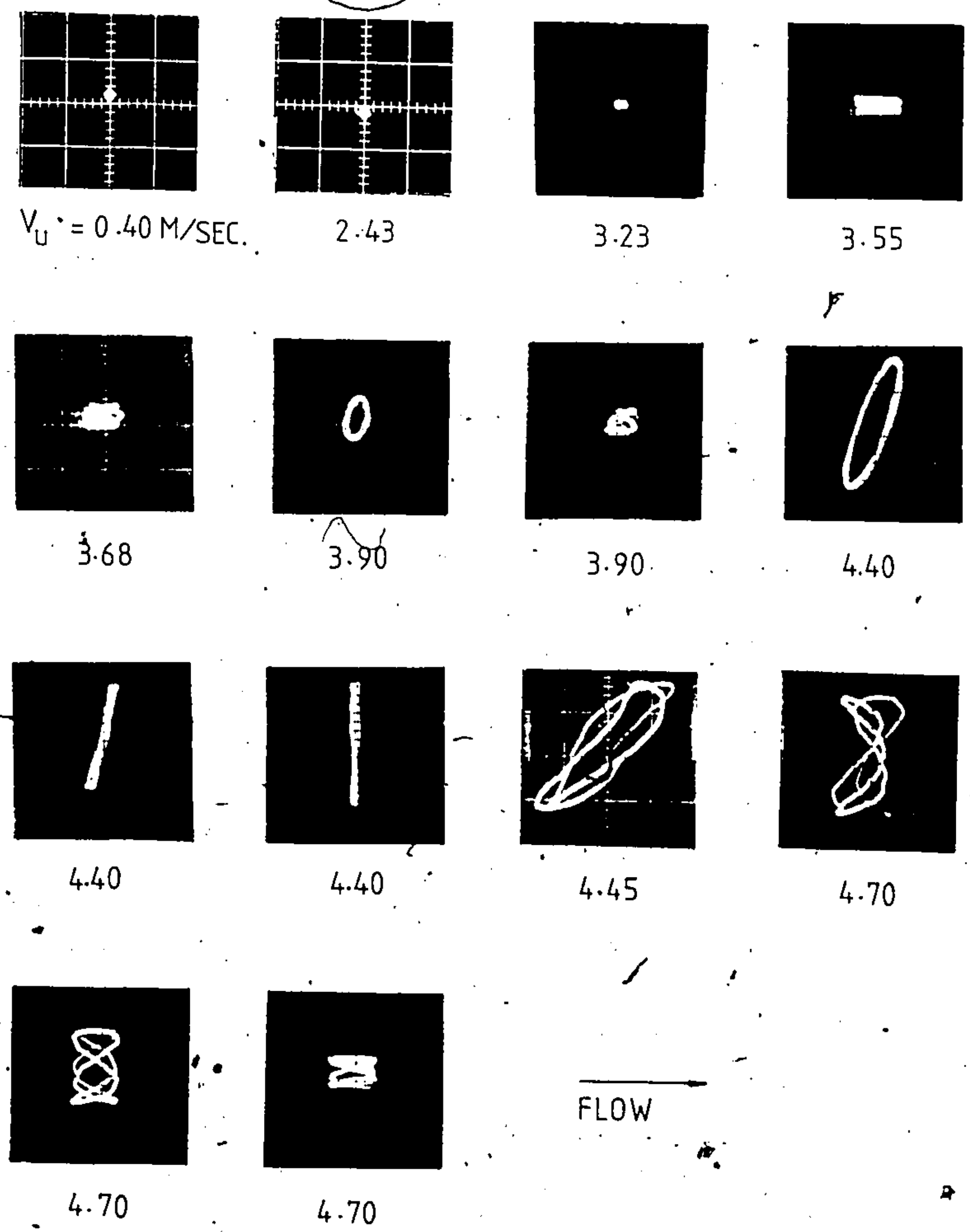

FIGURE 4.45: TUBE RESPONSE IN THE THIRD ROW OF A NORMAL SQUARE ARRAY WITH P/D = 1.5.

with time between this orbit and the 8-shaped pattern. Tube amplitudes kept on building up as the flow velocity increases, as can be seen from the next few pictures. Notice the change in tube response for the same flow velocity but at different instants of time. Such changes in orbital patterns of tubes and amplitude modulations are characteristic of unstable fluidelastic response in tube arrays.

In summary, two arrays of the normal square configuration were tested to determine their fluidelastic instabilities. The arrays had pitch-to-diameter ratios of 1.33 and 1.5. The critical velocity for the array with smaller P/d is higher by about 10% than the value for the array with larger P/d. The velocity threshold is quite sharp for the array with the smaller pitch ratio and, while reasonably well defined, is less so for the larger pitch ratio.

4.4.3 Rotated Square Array; P/d = 1.414:

The rotated square array with P/d = 1.414 is shown in Figure 4.15. Tubes marked number 4 and 9 in the second and fourth row respectively, were the instrumented tubes.

In-line, transverse, and RMS amplitudes of the tube tip for tube No. 4 in the second row were plotted versus upstream flow velocity as shown in Figure 4.46. A linear increase in tube amplitudes was also obtained in the stable region. In this region, amplitudes in the transverse direction were slightly higher over those in the in-line direction. As can be seen from Figure 4.46, a well defined critical velocity at V_{cr} = 6.10 m/sec. was obtained for this

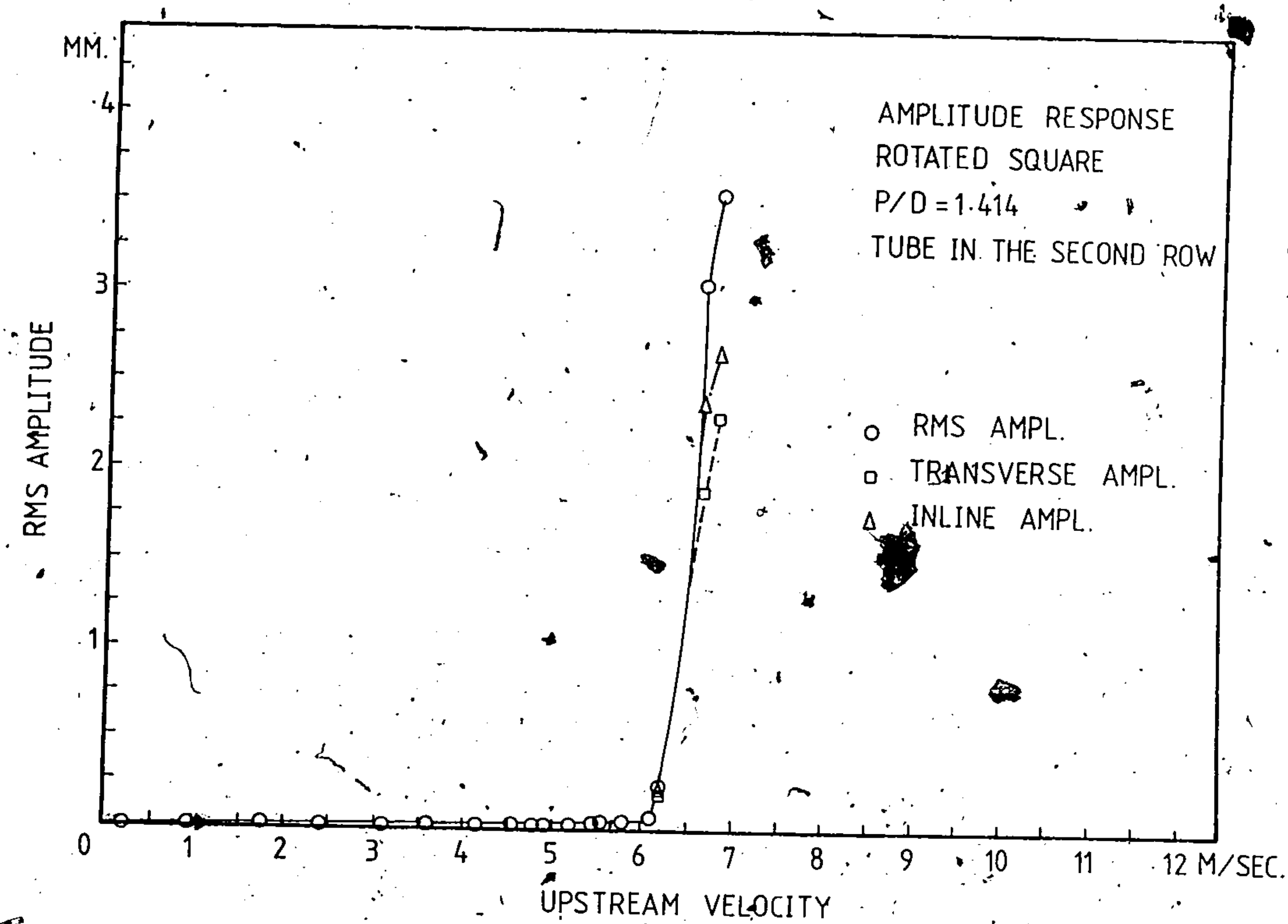
AMPLITUDE RESPONSE
ROTATED SQUARE
P/D = 1.414
TUBE IN THE SECOND ROW
RMS AMPL.
TRANSVERSE AMPL.
INLINE AMPL.
MM.
RMS AMPLITUDE
0
1
2
3
4
5
6
7
8
9
10
11
12 M/SEC.
UPSTREAM VELOCITY

FIGURE 4.46

tube. Around the critical velocity, vibration amplitudes were slightly higher in the transverse direction. However, as the flow velocity is increased further, the vibration became slightly higher in the in-line direction.

The results obtained for the second monitored tube, tube No. 9 in the fourth row, were plotted as shown in Figure 4.47. The amplitudes were slightly higher in the in-line direction in both the stable and unstable regions. The increase in tube amplitudes were somewhat more gradual for this tube. Careful determination of the critical velocity shows that the tube in the fourth row, has essentially the same critical velocity as the tube in the second row. However, tube tip amplitudes were lower than the tube in the second row. Both tubes show that vibration amplitudes in the unstable region are higher in the in-line direction.

4.4.4 Rotated Square Array; P/d = 1.7:

The rotated square array with P/d = 1.7, is shown in Figure 4.19. The instrumented tubes were the tubes number 4 and 9 in the second and fourth rows, respectively. In-line, transverse, and RMS amplitudes recorded for tube No. 4 in the second row were plotted versus the upstream flow velocities as shown in Figure 4.48. In the stable region, the increase in tube amplitude was slightly nonlinear as can be seen in the response curve. Also, the tube amplitudes are slightly higher in the transverse direction at low flow velocities, then become quite small before reaching the critical velocity. This

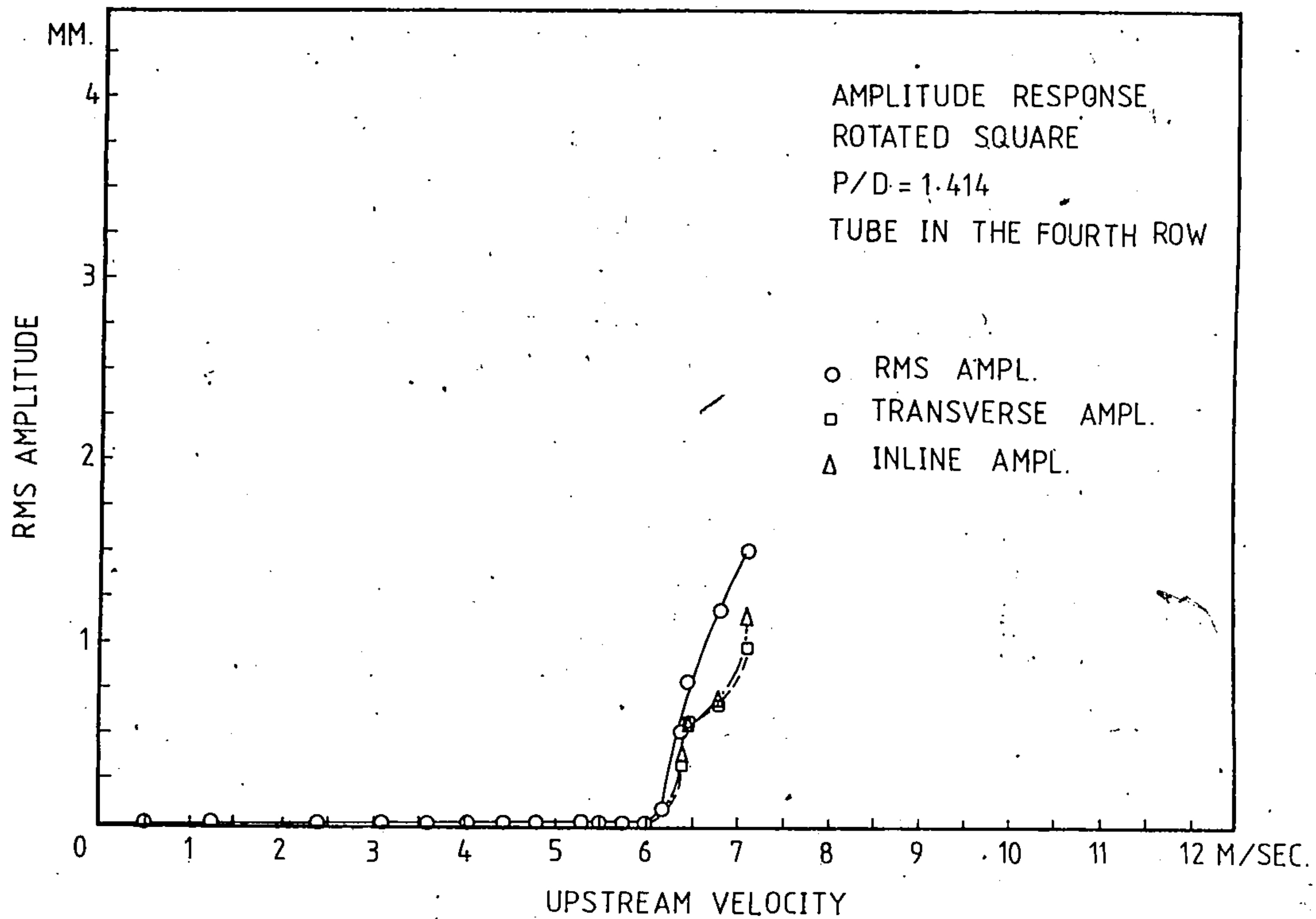
MM.
4
3
2
1
0
RMS AMPLITUDE
AMPLITUDE RESPONSE
ROTATED SQUARE
P/D = 1·414
TUBE IN THE FOURTH ROW
RMS AMPL.
TRANSVERSE AMPL.
INLINE AMPL.
1
2
3
4
5
6
7
8
9
10
11
12 M/SEC.
UPSTREAM VELOCITY

FIGURE 4.47

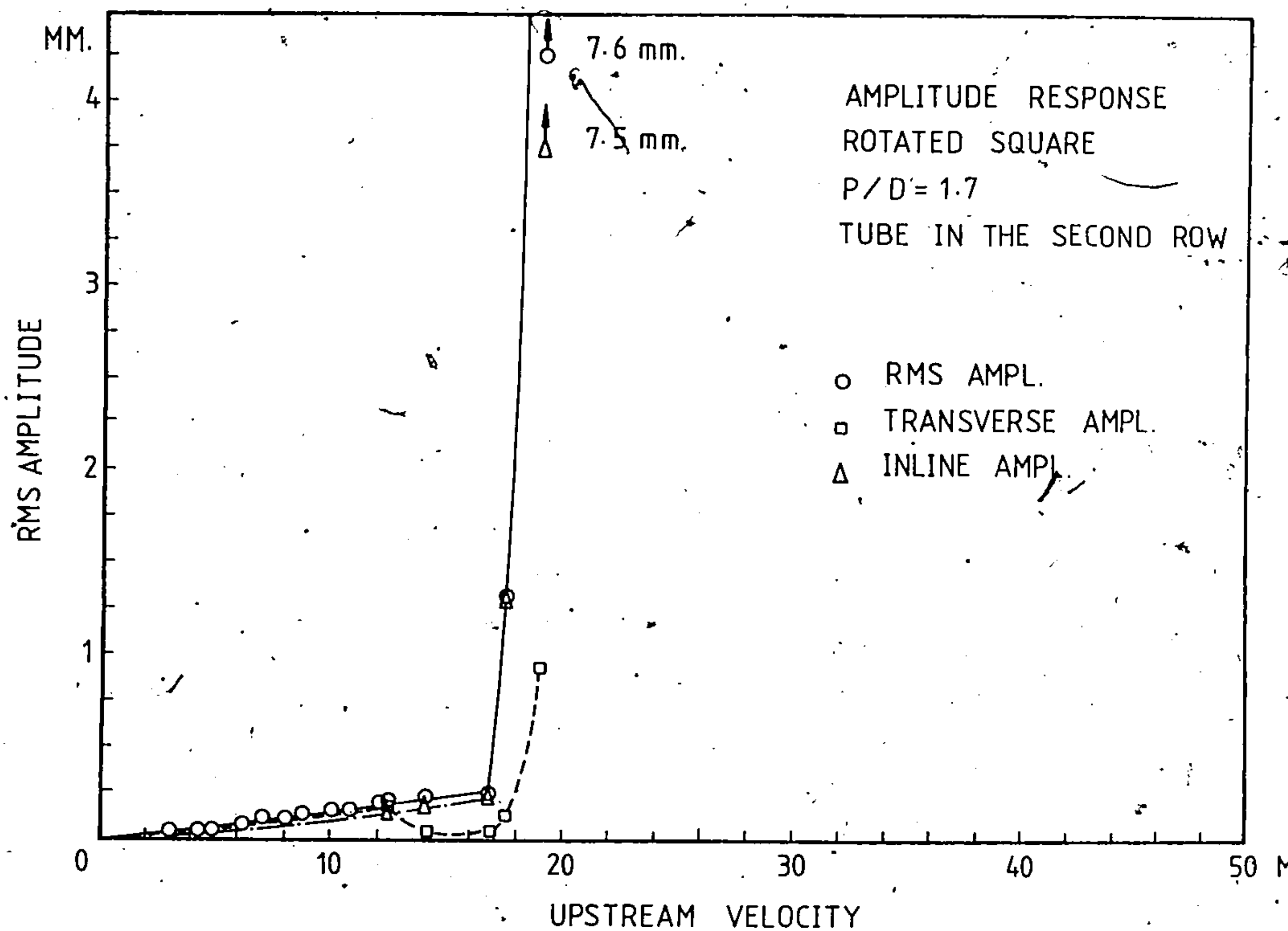
MM.
RMS AMPLITUDE
7·6 mm.
7·5 mm.
AMPLITUDE RESPONSE
ROTATED SQUARE
P / D = 1·7
TUBE IN THE SECOND ROW
RMS AMPL.
TRANSVERSE AMPL.
INLINE AMPL.
UPSTREAM VELOCITY
M/SEC.

FIGURE 4.48

means that the stability threshold is associated with nearly pure streamwise tube motion, as can be seen from Figure 4.48. Sharp increases in the in-line and RMS amplitudes were obtained at the critical velocity. This provides a well defined critical velocity of V_{cr} = 16.90 m/sec. In-line and RMS amplitudes at the critical velocity are about 1% of the tube diameter.

Tube tip amplitudes obtained for the second monitored tube, tube No. 9 in the fourth row, were plotted as shown in Figure 4.49. This tube had the same behaviour as the tube in the second row except that the amplitudes were slightly higher in the stable region and lower in the unstable region. A well defined critical velocity at the slightly higher value of V_{cr} = 17.10 m/sec., was obtained for the tube in the fourth row. However, the results from both tubes show that the increase in tube amplitudes which is mainly in the in-line direction is sharp for the rotated square array with P/d = 1.7 at the critical velocity.

In summary, critical velocities were determined for two rotated square arrays, one with a relatively small pitch-to-diameter ratio of 1.414 and the second with larger pitch-to-diameter ratio of 1.70. The critical velocity for the array with small P/d is about 1/3 that for the array with larger P/d. Both arrays showed sharp increase in RMS tube amplitudes above the critical velocity. The peculiar dip in transverse tube response at the critical velocity for the larger pitched array is not understood and has not been observed before.

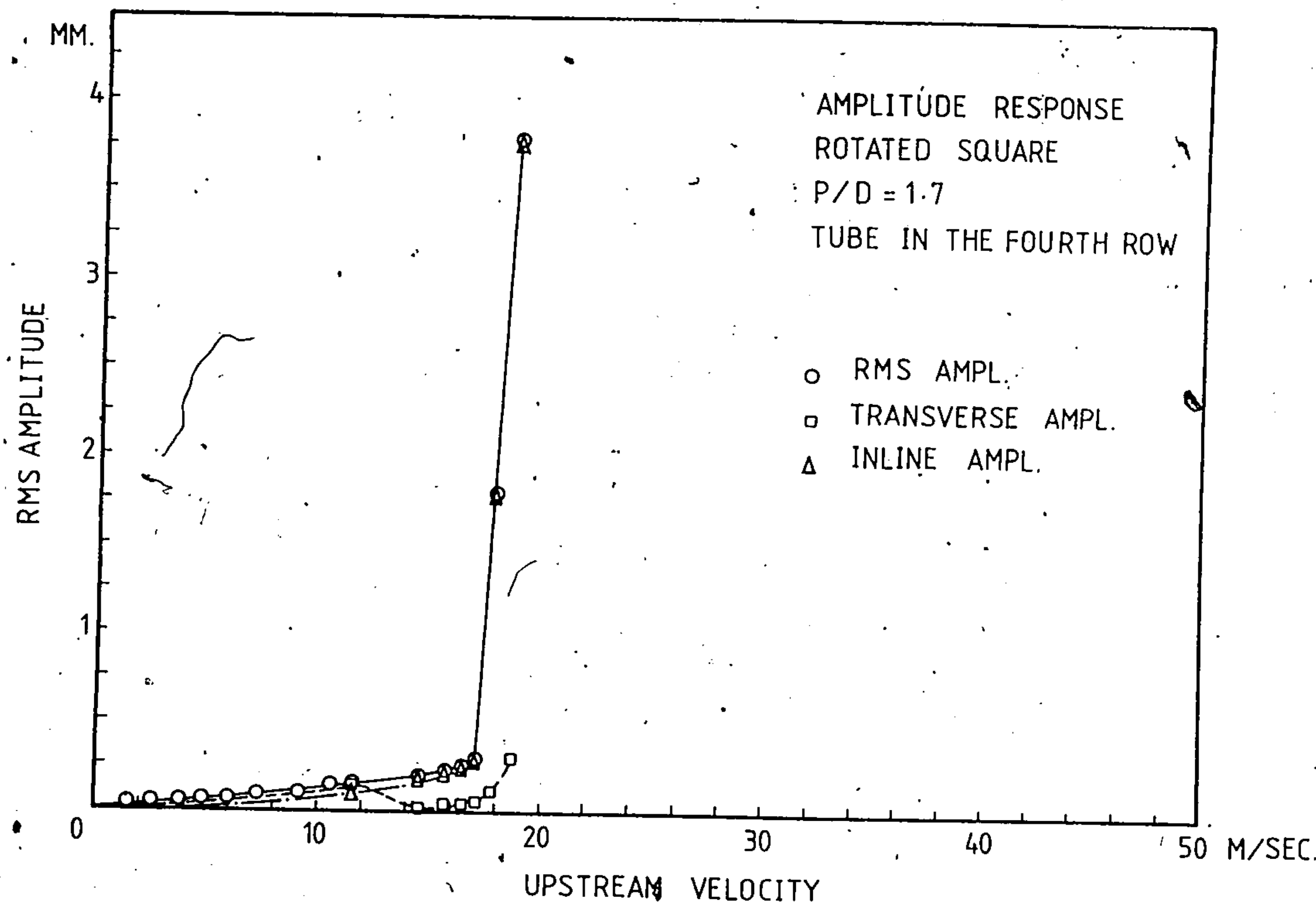
MM.
4
3
2
1
0
RMS AMPLITUDE
10
20
30
40
50 M/SEC.
UPSTREAM VELOCITY
AMPLITUDE RESPONSE
ROTATED SQUARE
P/D = 1·7
TUBE IN THE FOURTH ROW
RMS AMPL.
TRANSVERSE AMPL.
INLINE AMPL.

FIGURE 4.49

4.4.5 Normal Triangular Array; P/d = 1.33:

The normal triangular array with P/d = 1.33 used for conducting the present experiment is shown in Figure 4.25. This is the only array where thirteen flexible tubes were needed, so that the instrumented tube will be surrounded by flexible tubes. The two marked tubes No. 4 and 7 in the second and third rows, respectively, are the instrumented tubes.

In-line, transverse and RMS tube tip amplitudes were obtained for tube No. 4 in the second row and plotted versus upstream flow velocity as shown in Figure 4.50. As can be seen from this figure, a linear increase in tube tip amplitudes was obtained with the increase in flow velocity in the stable region. In this region, tube tip amplitudes were higher in the in-line direction over those in the transverse direction. The increase in tube tip amplitudes was gradual around the critical velocity, with the amplitudes becoming higher in the transverse direction and into the unstable region. The increase in the transverse as well as the RMS amplitudes show that the tube is becoming unstable at a flow velocity of V_{cr} = 2.60 m/sec.

The results obtained for the second monitored tube; tube No. 7 in the third row, were plotted as shown in Figure 4.51. In-line amplitudes were higher in the whole range of flow velocity measurement. A well defined critical velocity at V_{cr} = 2.60 m/sec. was obtained for the present tube. This means that for the normal triangular array with P/d = 1.33, tubes in the second and third row have essentially the same critical velocity.

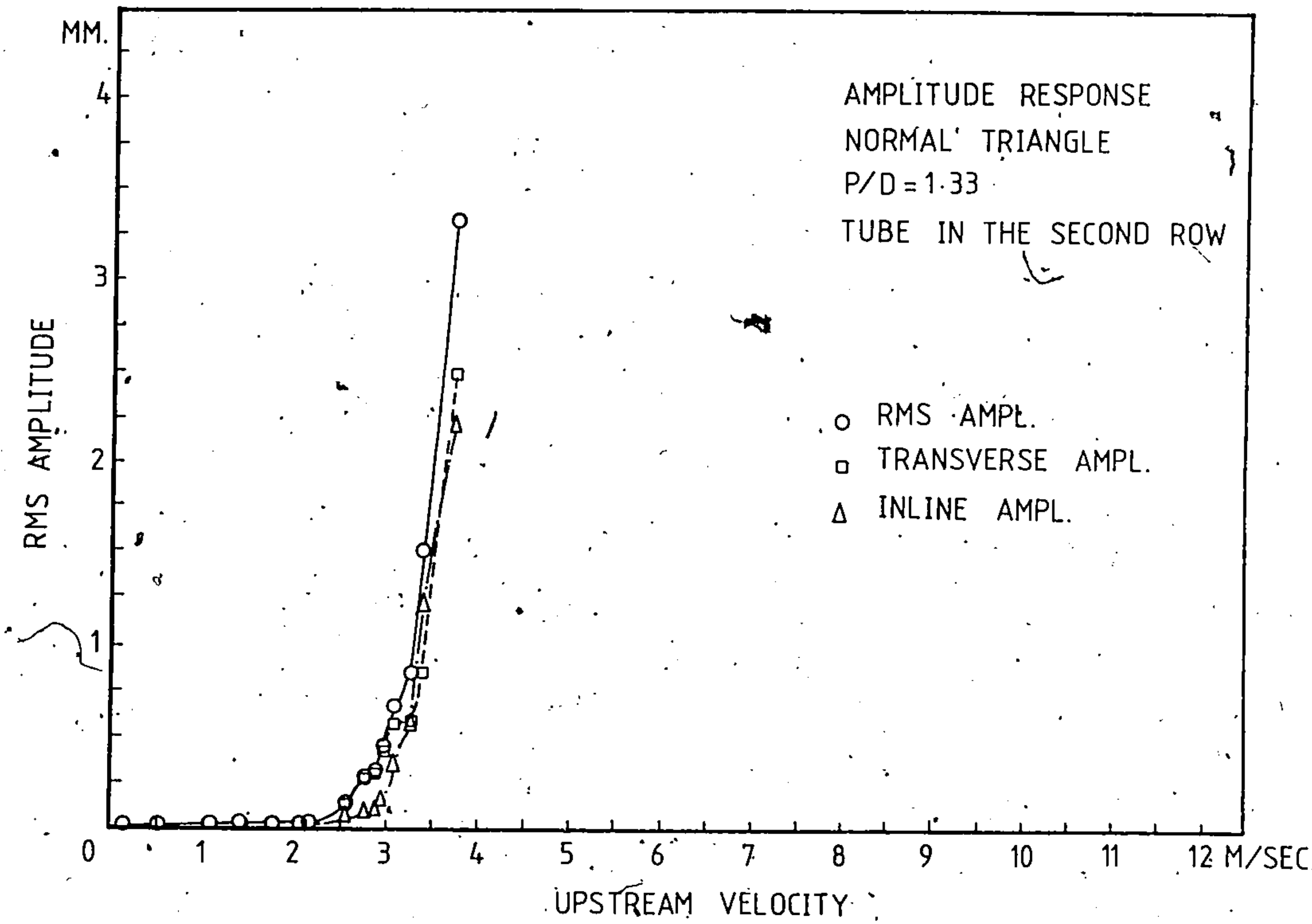
AMPLITUDE RESPONSE
NORMAL TRIANGLE
P/D = 1·33
TUBE IN THE SECOND ROW
RMS AMPL.
TRANSVERSE AMPL.
INLINE AMPL.
MM.
RMS AMPLITUDE
0
1
2
3
4
5
6
7
8
9
10
11
12 M/SEC.
UPSTREAM VELOCITY

FIGURE 4.50

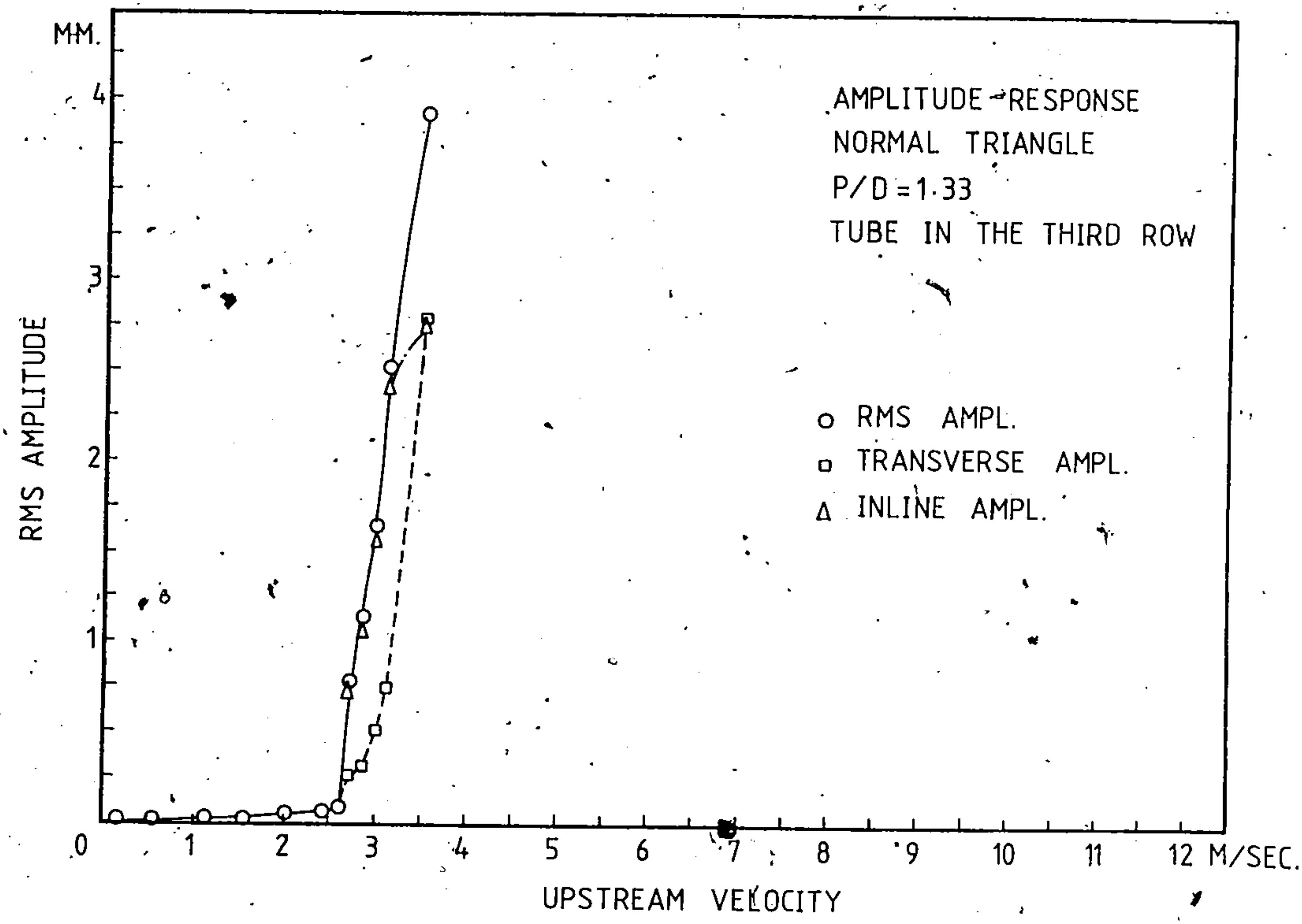
MM.
RMS AMPLITUDE
0
1
2
3
4
5
6
7
8
9
10
11
12 M/SEC.
UPSTREAM VELOCITY
AMPLITUDE - RESPONSE
NORMAL TRIANGLE
P/D = 1·33
TUBE IN THE THIRD ROW
○ RMS AMPL.
□ TRANSVERSE AMPL.
Δ INLINE AMPL.

FIGURE 4.51

4.4.6 Normal Triangular Array; P/d = 1.50

The normal triangular array with P/d = 1.5 is shown in Figure 4.28. Tubes marked 5 and 8 in the second and third rows, respectively, were the instrumented tubes. In-line, transverse, and RMS tube tip amplitudes were obtained for tube No. 5 in the second row and plotted versus the upstream flow velocity as shown in Figure 4.52. As can be seen from this figure, although the tube is responding to turbulence in the flow in the stable region, amplitudes are increasing linearly with the flow velocity. The amplitudes in the transverse direction are higher than those in the in-line direction for the whole range of flow velocity measurement. A well defined critical velocity at V_{cr} = 4.75 m/sec. is obtained for the present tube. However, the increase in tube tip amplitudes was not very rapid in the post stable region.

The amplitude-velocity response curve obtained for the second monitored tube, tube No. 8 in the third row, was plotted as shown in Figure 4.53. As can be seen from this figure the vibration amplitudes were mainly in the transverse direction. A gradual increase in tube tip amplitudes was obtained around the critical velocity. The increase in the transverse as well as the RMS amplitudes show that the present tube is taking off at a flow velocity of about V_{cr} = 5.00 m/sec. This value appears slightly higher than that obtained for the tube in the third row. However, both results show that the tubes tested are primarily oscillating in the transverse direction.

In summary the critical velocities for normal triangular arrays with P/d = 1.33 and 1.5 were determined. The critical velocity

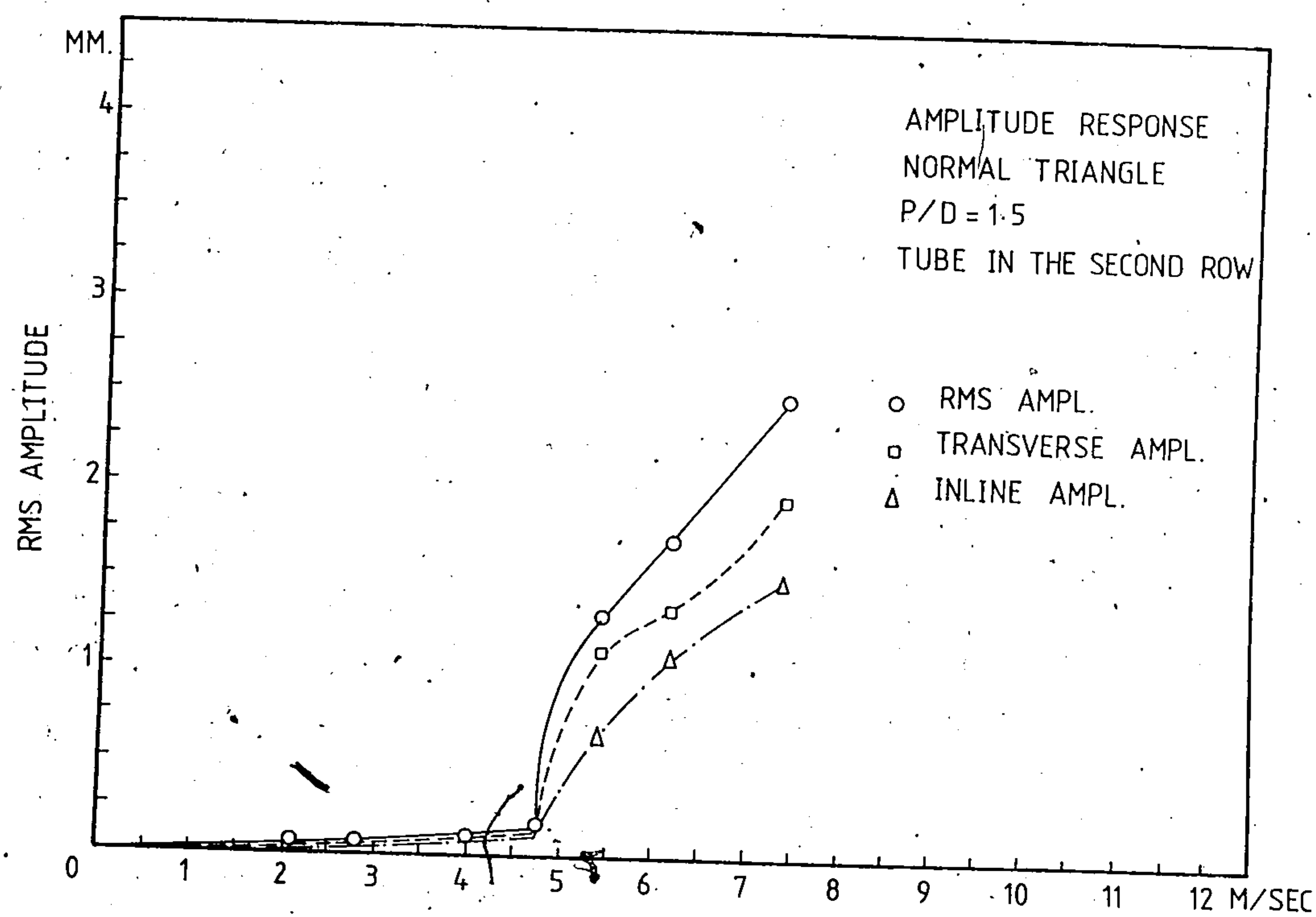
MM.
4
3
2
1
0
RMS AMPLITUDE
AMPLITUDE RESPONSE
NORMAL TRIANGLE
P/D = 1·5
TUBE IN THE SECOND ROW
RMS AMPL.
TRANSVERSE AMPL.
INLINE AMPL.
1
2
3
4
5
6
7
8
9
10
11
12 M/SEC.
UPSTREAM VELOCITY

FIGURE 4.52

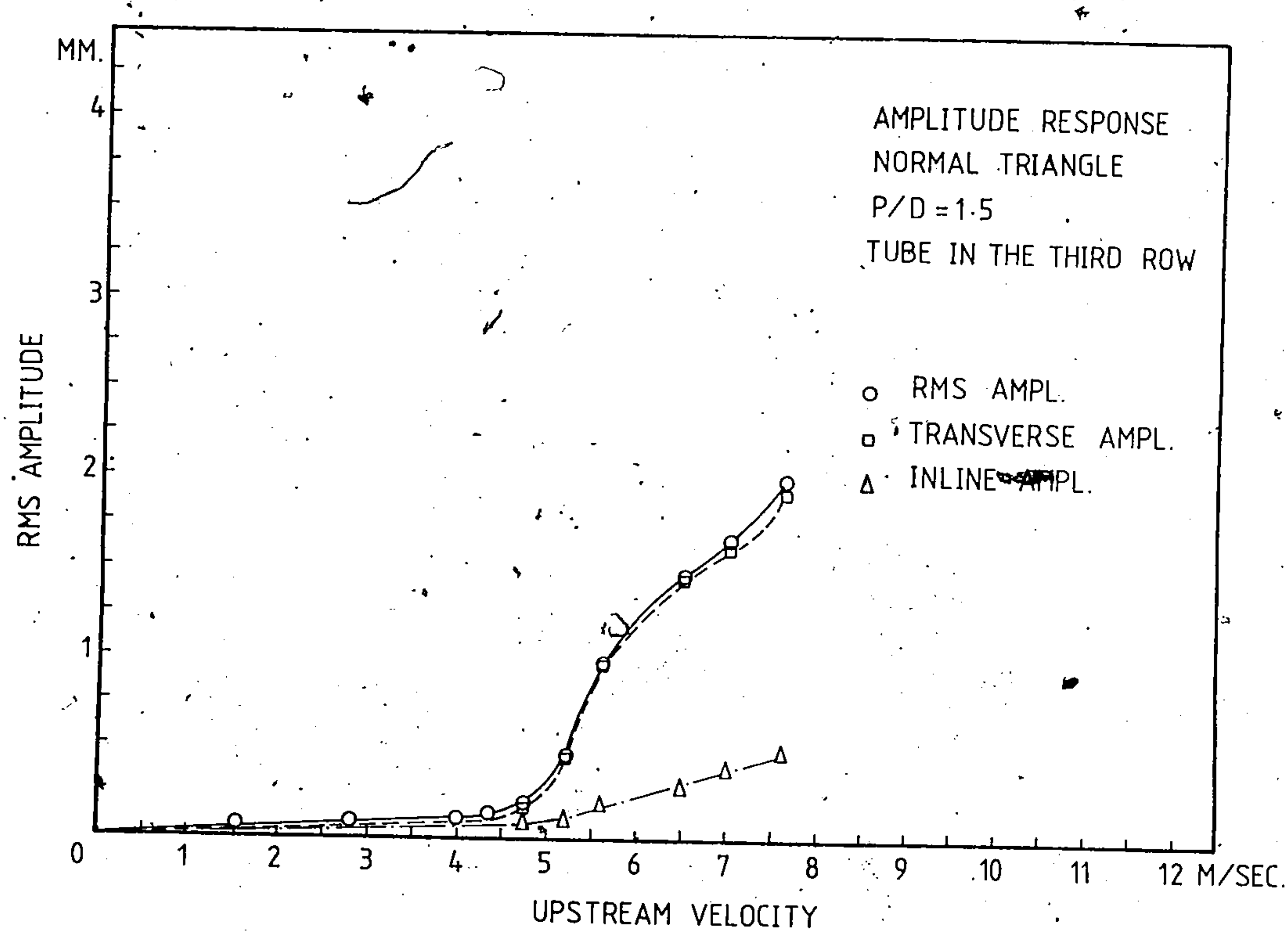
MM.
RMS AMPLITUDE
0
1
2
3
4
5
6
7
8
9
10
11
12 M/SEC.
UPSTREAM VELOCITY
AMPLITUDE RESPONSE
NORMAL TRIANGLE
P/D = 1·5
TUBE IN THE THIRD ROW
RMS AMPL.
TRANSVERSE AMPL.
INLINE AMPL.

FIGURE 4.53

for the normal triangular array with P/d = 1.33 is about one-half the critical velocity for the normal triangular array with P/d = 1.5. The increase in tube amplitudes in the post stable region is much steeper for the array with lower pitch-to-diameter ratio.

4.4.7 Parallel Triangular Array; P/d = 1.375

The first parallel triangular array tested had a pitch-to-diameter ratio of 1.375. The array is shown in Figure 4.33. Tubes marked 6 and 7 in the third and fourth rows respectively, are the instrumented tubes. The in-line, transverse, and RMS amplitudes obtained for tube No. 6 in the third row were plotted versus the upstream flow velocity as shown in Figure 4.54. In the region up to the critical velocity, the amplitudes in the in-line direction were slightly higher than those in the transverse direction. However as the tube became unstable, the amplitudes became higher in the transverse direction. The increase in tube amplitudes above the critical velocity was very rapid. This resulted in a well defined critical velocity for the present tube of V_{cr} = 3.70 m/sec. Tube amplitudes at the critical velocity were less than one-half percent of the tube diameter.

The amplitude-velocity curve obtained for the second monitored tube, tube No. 7 in the fourth row, was plotted as shown in Figure 4.55. This tube exhibited similar behaviour in the stable region, except that the amplitudes were slightly higher for this tube in the transverse direction, and remained higher in this direction into the

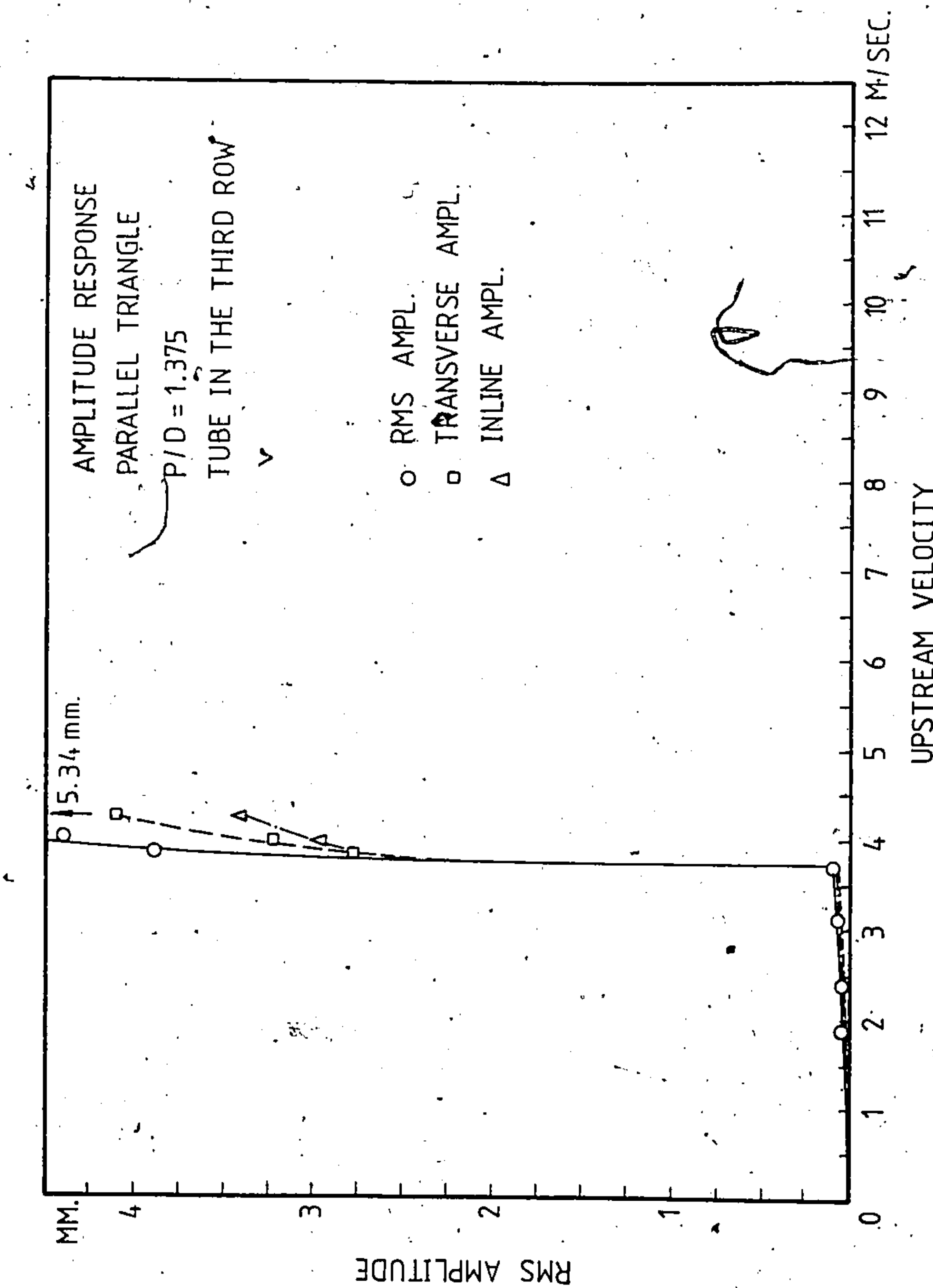
AMPLITUDE RESPONSE
PARALLEL TRIANGLE
P/D = 1.375
TUBE IN THE THIRD ROW
○ RMS AMPL.
□ TRANSVERSE AMPL.
△ INLINE AMPL.
5.34 mm.
RMS AMPLITUDE
MM.
4
3
2
1
0
1
2
3
4
5
6
7
8
9
10
11
12 M/SEC.
UPSTREAM VELOCITY

FIGURE 4.54

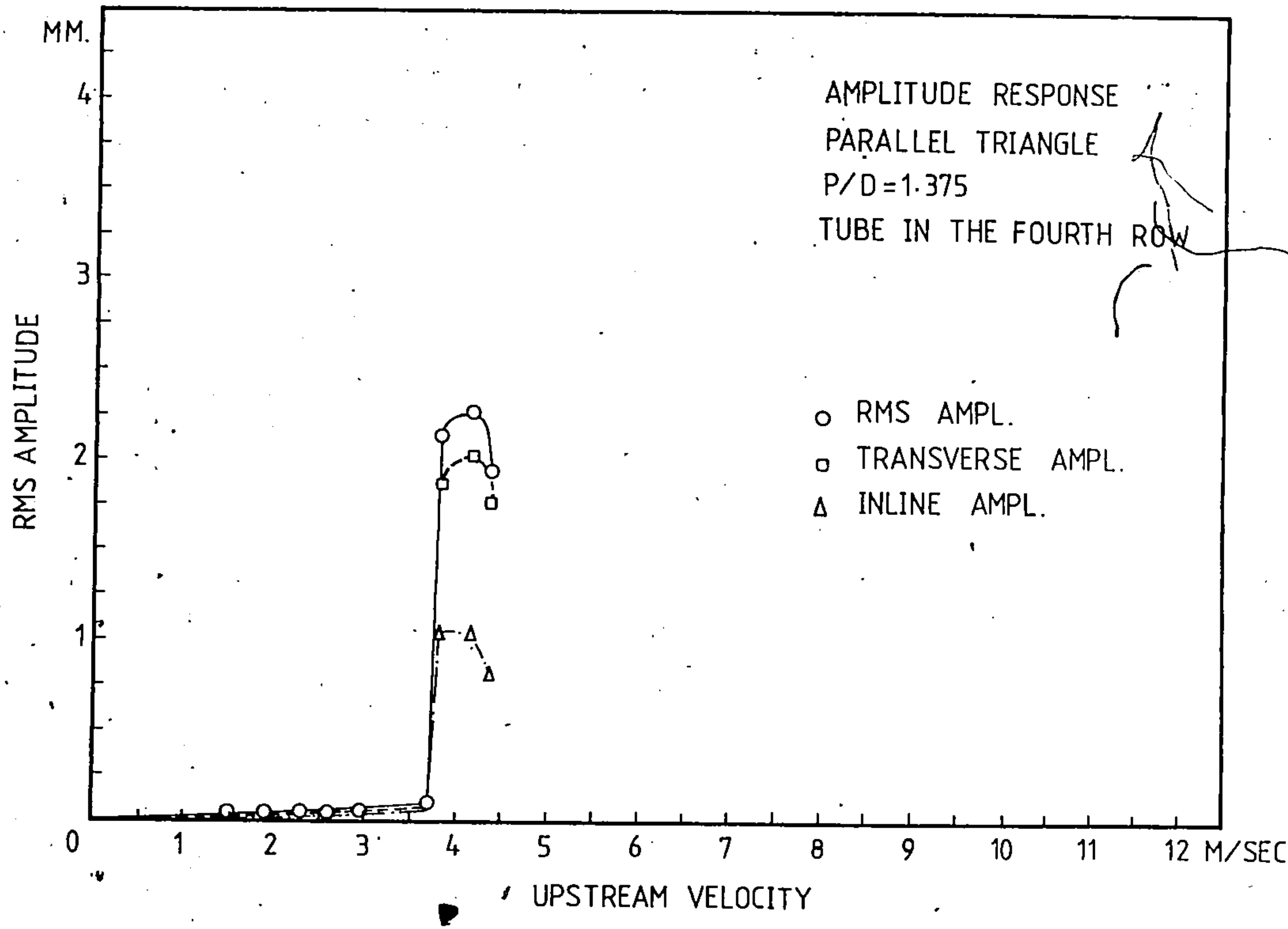
MM.
RMS AMPLITUDE
0
1
2
3
4
5
6
7
8
9
10
11
12 M/SEC.
UPSTREAM VELOCITY
AMPLITUDE RESPONSE
PARALLEL TRIANGLE
P/D = 1·375
TUBE IN THE FOURTH ROW
o RMS AMPL.
□ TRANSVERSE AMPL.
Δ INLINE AMPL.

FIGURE 4.55

unstable region. A well defined critical velocity having the same value of V_{cr} = 3.70 m/sec., as the tube in the third row, was obtained for the present tube. The sharp increase in tube amplitudes obtained at the critical velocity were found to decay after reaching a certain value. The reason behind this behaviour is not understood and is believed to be due to nonlinearities in the source of excitation. Unfortunately, the experiment was terminated at this point as it was observed that any further increase in the flow velocity could result in a tube-to-tube clashing of other tubes in the array.

4.4.8 Parallel Triangular Array; P/d = 1.73:

The second parallel triangular array used had a larger pitch-to-diameter ratio of 1.73. The layout of the tubes in this array was given previously in Figure 4.36. For the present array, tubes marked 6 and 7 in the third and fourth rows respectively, are the instrumented tubes.

The different tube tip amplitudes obtained for tube No. 6 in the third row were plotted versus the corresponding upstream flow velocities as shown in Figure 4.56. As can be seen from this figure, the increase in tube tip amplitudes with the flow velocity in the stable region is linear up to a point near the critical flow velocity. In this region, amplitudes were slightly higher in the in-line direction over those in the transverse direction. The sharp increase in tube amplitudes at 5.10 m/sec. gave a well defined critical flow velocity for the present tube. The large increase in the in-line

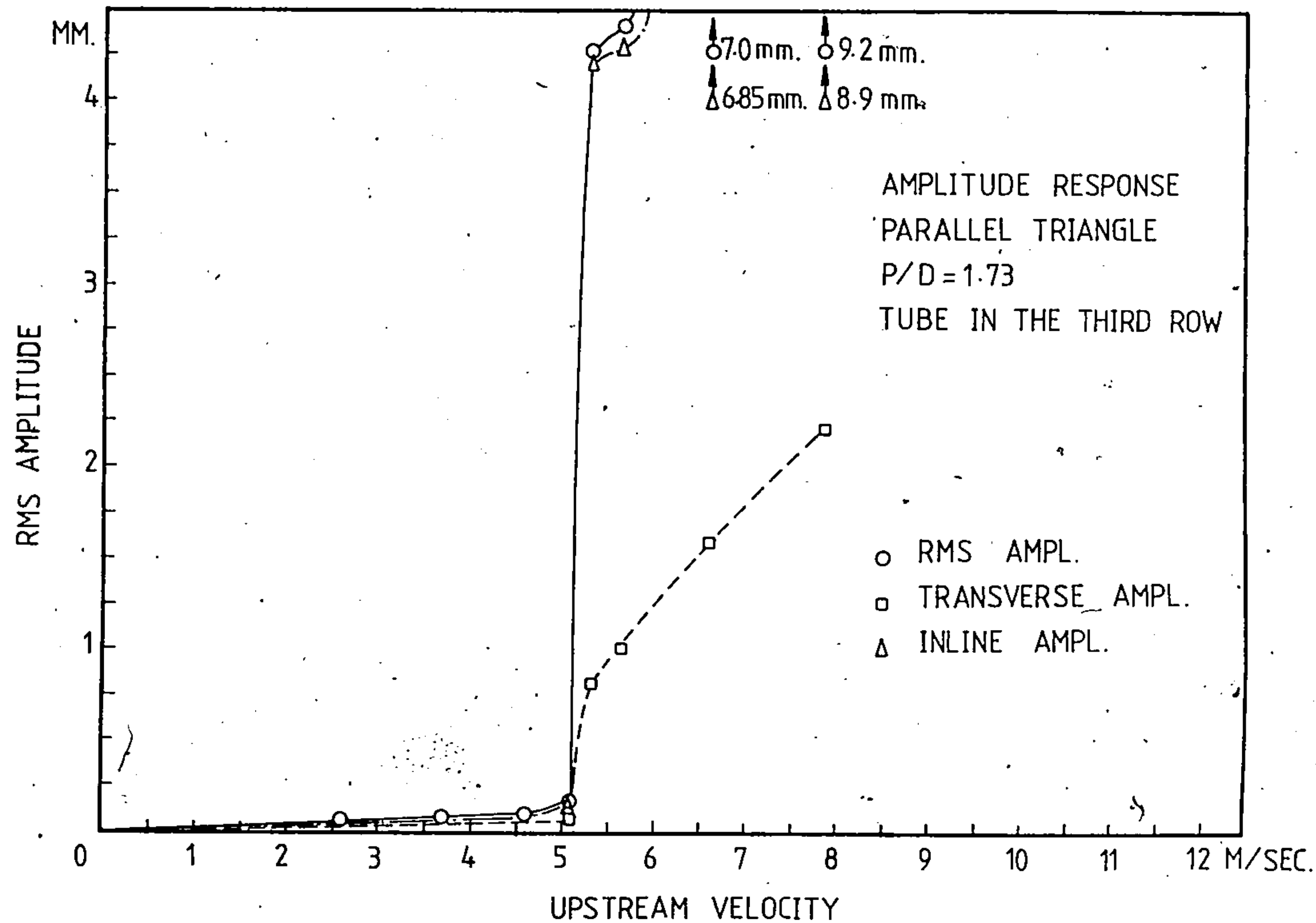

MM.
RMS AMPLITUDE
0
1
2
3
4
5
6
7
8
9
10
11
12 M/SEC.
UPSTREAM VELOCITY
7.0 mm.
9.2 mm.
6.85 mm.
8.9 mm.
AMPLITUDE RESPONSE
PARALLEL TRIANGLE
P/D = 1.73
TUBE IN THE THIRD ROW
RMS AMPL.
TRANSVERSE AMPL.
INLINE AMPL.

FIGURE 4.56

amplitudes above the critical velocity, i.e., in the unstable region, show that the tube was vibrating primarily in the in-line direction.

The tube tip amplitudes obtained for the second monitored tube, tube No. 7 in the fourth row, were plotted as shown in Figure 4.57. The tube exhibited essentially the same behaviour except a slightly lower critical velocity of V_{cr} = 5.00 m/sec. was found. Note that for both tubes, the RMS tube tip amplitudes at the critical velocity were less than 1% of the tube diameter. Also both tubes are whirling primarily in the streamwise direction.

In summary, two arrays of the parallel triangular configuration were tested, one with a relatively small pitch-to-diameter ratio of 1.375, and the second with a larger pitch-to-diameter ratio of 1.73. The critical velocity obtained for the array with small P/d is about 38% lower than the value for the array with large P/d. The amplitude increase above the critical velocity is very rapid for both arrays.

4.4.9 Discussion

The critical flow velocities for the four standard array geometries, with two values of the pitch-to-diameter ratio for each geometry, were determined. The results obtained are summarized in Table 4.10. As can be seen from this table, the tubes tested were varied in location for different array geometries from the second to the fourth row. For every array, the two instrumented tubes had essentially the same critical flow velocity. This is to be expected as it was found from a previous study by Weaver and ElKashlan [74] on

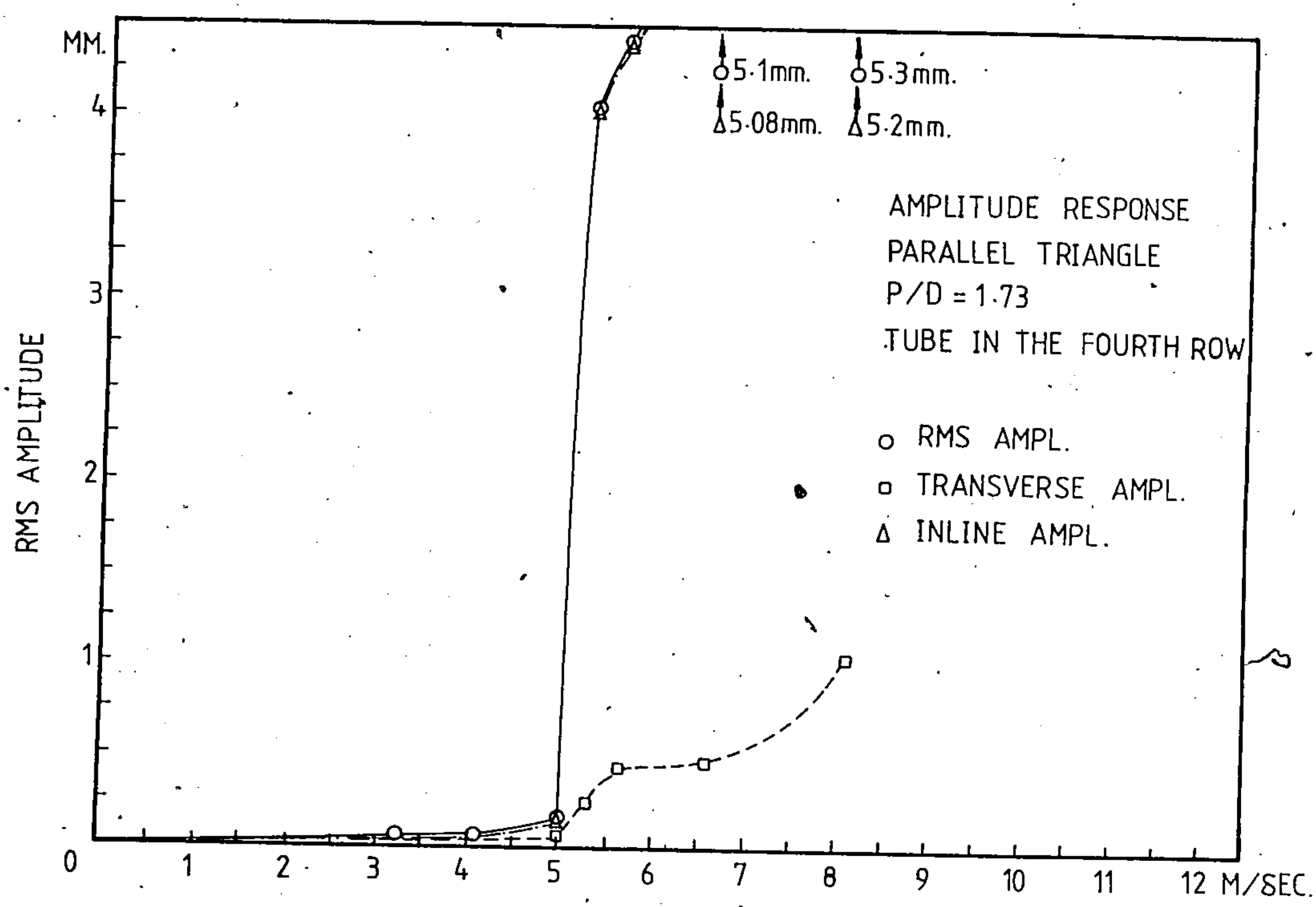

MM.
RMS AMPLITUDE
0
1
2
3
4
5
6
7
8
9
10
11
12 M/SEC.
UPSTREAM VELOCITY
5·1mm.
5·08mm.
5·3mm.
5·2mm.
AMPLITUDE RESPONSE
PARALLEL TRIANGLE
P/D = 1·73
TUBE IN THE FOURTH ROW
o RMS AMPL.
□ TRANSVERSE AMPL.
Δ INLINE AMPL.

FIGURE 4.57

TABLE 4.10

Fluidelastic instability results for the different tube arrays tested in the present study.

Array Geometry	Pitch-to-diameter ratio	Tube Location	Critical Flow velocity (m/sec)	Reduced Velocity
Normal	1.33	second row	3.70	23.48
Square		third row	3.70	23.48
	1.5	second row	3.50	16.54
		third row	3.35	15.83
Rotated	1.414	second row	6.10	23.20
Square		fourth row	6.10	23.20
	1.70	second row	16.90	45.70
		fourth row	17.10	46.24
Normal	1.33	second row	2.60	16.50
Triangle		third row	2.60	16.50
	1.50	second row	4.75	22.44
		third row	5.00	23.62
Parallel	1.375	third row	3.70	18.50
Triangle		fourth row	3.70	18.50
	1.73	third row	5.10	16.48
		fourth row	5.00	16.16

a parallel triangular array, that tubes in the second, third, and fourth rows are the most critical ones in the array, and their critical flow velocities are almost the same. The critical flow velocities for the present cantilevered tubes for the parallel triangular array with P/d = 1.375, were also compared with that obtained previously [20] for a rigid cylinder elastically mounted. According to the present results the value for the reduced pitch flow velocity is:

$$\frac{V_p}{fd} = 21.36 \qquad \text{(dimensionless)}$$

The expected value from [20] using the relationship

$$\frac{V_p}{fd} = \alpha \left(\frac{m}{\rho d^2}\right)^{0.29} (\delta)^{0.21}$$

will be:

$$\frac{V_p}{fd} = 13.00 \qquad \text{(dimensionless)}$$

This means that the value of the reduced velocity obtained for the present tube is 64% higher than that expected from a rigid cylinder elastically mounted. Such a difference was the reason behind the following analysis.

Critical flow velocities for tubes in a single row tube array was investigated originally by Connors [14]. The theoretical model is based on equating the energy input for a single tube to the energy dissipated by damping for that tube. Pettigrew et al. [47] generalized Connor's formulation to include tube arrays. The model as applied to simply supported tubes is as follows.

For a tube array subjected to non-uniform flow $V_r(x)$, the vibration response $y(x,t)$ at any time t and point x along the length ℓ of any tube may be generally expressed by

$$y(x,t) = Y_i(x) \sin \omega_i t$$

where

$Y_i(x)$ = the maximum amplitude of the ith mode,

ω_i = the angular natural frequency.

The fluid force component per unit length $P_f(x,t)$ that is in phase with the tube vibration velocity is normally formulated as:

$$\begin{aligned} P_f(x,t) &= 1/2\ \rho\ V_r^2(x)\ (ky(x,t+\pi/2)/d).d \\ &= 1/2\ \rho\ V_r^2(x)\ (kY_i(x) \sin \omega_i(t+\pi/2)) \\ &= 1/2\ \rho\ V_r^2(x)\ kY_i(x) \cos \omega_i t \end{aligned}$$

where

d = tube diameter

ρ = fluid density

k = fluid force/tube motion proportionality constant, and

$t + \pi/2$ = the phase

The differential energy input per unit length per unit time will be:

$$dE_i = P_f(x,t)\ dy(x,t)/dt$$
$$= 1/2\ \rho\ V_r^2(x).k.Y_i(x)\ \cos\ \omega_i t.Y_i(x).\omega_i\ \cos\ \omega_i t$$
$$= 1/2\ k\rho\omega_i\ V_r^2(x)\ Y_i^2(x)\ \cos^2\ \omega_i t$$

The total energy input due to the fluid forces over the length of the tube for one vibration cycle will be:

$$E_i = (k\rho\omega_i/2) \int_o^{\ell} \int_o^{2\pi/\omega_i} V_r^2(x)\ Y_i^2(x)\ \cos^2(\omega_i t)\ dt\ dx$$

$$= (K\rho\omega_i/2) \int_o^{\ell} V_r^2(x)\ Y_i^2(x)\ \left(\frac{2\pi}{\omega_i} \cdot \frac{1}{2} \right) dx$$

$$= \left(\frac{\pi k\rho}{2} \right) \int_o^{\ell} V_r^2(x)\ Y_i^2(x)\ dx \qquad (1)$$

The damping force per unit length $P_c(x,t)$ is

$$P_c(x,t) = c\ dy(x,t)/dt$$
$$= c\ \omega_i Y_i(x)\ \cos\ \omega_i t$$

where c = damping coefficient per unit length.

The differential stored vibration energy per unit length will be:

$$dE_s = P_c(x,t) \cdot dy(x,t)/dt$$
$$= c\,\omega_i^2\, Y_i^2(x)\, \cos^2 \omega_i t$$

The total energy dissipated by damping during one vibration cycle, assuming damping occurs over the whole length of the tube will be:

$$E_s = c\omega_i^2 \int_0^{\ell} \int_0^{2\pi/\omega_i} Y_i^{\,2}(x) \cos^2(\omega_i t)\, dt\, dx$$

$$= c\omega_i^2 \int_0^{\ell} Y_i^2(x) \cdot \frac{2\pi}{\omega_i} \cdot \frac{1}{2}\, dx$$

$$= \pi\, c\omega_i \int_0^{\ell} Y_i^2(x)\, dx \qquad (2)$$

Fluidelastic instabilities occur when $E_i \geq E_s$. Thus the critical velocity for fluidelastic instability is defined as when $E_i = E_s$, or from equations (1) and (2):

$$\pi\, c\omega_i \int_0^{\ell} Y_i^2(x)dx = \left(\frac{\pi k\rho}{2}\right) \int_0^{\ell} V_r^2(x)\, Y_i^2(x)dx$$

Since $Y_i(x)$ is directly proportional to the mode shape $\phi_i(x)$,

$$c\omega_i \int_0^{\ell} \phi_i^2(x)dx = \frac{k\rho}{2} \int_0^{\ell} V_r^2(x)\, \phi_i^2(x)dx$$

and since $c = 2\delta m f_i$ and $\omega_i = 2\pi f_i$

$$2\delta m f_i \cdot 2\pi f_i \int_o^\ell \phi_i^2(x)dx = \frac{k\rho}{2} \int_o^\ell V_r^2(x)\ \phi_i^2(x)dx$$

or

$$\frac{8\pi}{k} \cdot \frac{m\delta f_i^2}{\rho} \int_o^\ell \phi_i^2(x)dx = \int_o^\ell V_r^2(x)\ \phi_i^2(x)dx$$

Defining $K = \sqrt{8\pi/k}$ and $V_r(x)$ in terms of flow velocity distribution function $\psi(x)$ so that

$$V_r(x) = V_r \cdot \psi(x)$$

$$\therefore \quad K^2 \frac{m\delta}{\rho d^2} \int_o^\ell \phi_i^2(x)dx = \frac{V_r^2}{f_i^2 d^2} \int_o^\ell \psi^2(x)\phi^2(x)dx$$

If the mass of the tube is not uniformly distributed, then the equivalent mass per unit length is

$$m = \frac{\int_o^\ell m(x)\phi_i^2(x)dx}{\int_o^\ell \phi_i^2(x)dx}$$

Thus for non-uniform mass distribution

$$K^2 \frac{\delta}{\rho d^2} \int_o^{\ell} m(x)\phi_i^2(x)dx = \frac{V_r^2}{f_i^2 d^2} \int_o^{\ell} \psi^2(x)\ \phi_i^2(x)dx$$

or

$$\frac{V_r}{fd} = K \left[\frac{\delta \int_o^{\ell} m(x)\ \phi_i^{\ 2}(x)dx}{\rho d^2 \int_o^{\ell} \psi^2(x)\ \phi_i^2\ (x)dx} \right]^{1/2} \tag{3}$$

Case 1: Rigid Cylinder Elastically Mounted

For this case, the mass of the tube per unit length was uniform along the span ℓ, with a uniform flow velocity distribution, thus $\psi(x) = 1$. Since the mode shape for a rigid cylinder is $\phi(x) = 1$

$$\frac{V_r}{fd} = K \left(\frac{m\delta}{\rho d^2}\right)^{1/2}$$

The same relation as obtained by Connor's [14] and others. The constant K is to be calculated for every individual array.

Case 2: Cantilevered Cylinder

As can be seen from equation (3), for uniform mass, and flow velocity distributions, theoretically the mode shape is unimportant. However, for the cantilevered tube used in the present study, a solid acrylic tube was mounted on a stainless steel rod of smaller diameter.

If the length of the whole span is ℓ, the tube length is $3\ell/4$ and the rod length is $\ell/4$, and where:

$$(EI)_{tube} = 2.56\ (EI)_{rod}$$

Also, the flow was partially admitted over the tube length and not the whole span, i.e. $\psi(x) = 0$, over the rod length, while $\psi(x) = 1$, over the tube length (assuming uniform flow velocity distribution over tube length). Thus, if the effect of partial admission is only considered assuming uniform mass distribution and mode shape, equation (3) becomes:

$$\frac{V_r}{fd} = K \left(\frac{m\delta}{\rho d^2}\right)^{1/2} \left[\frac{\int_0^\ell \phi_i^2(x)\,dx}{0 + \int_{\ell/4}^{\ell} \psi^2(x)\phi_i^2(x)\,dx}\right]^{1/2} \quad (4)$$

Since, for a cantilevered tube vibrating in the first mode and with initial velocity = 0, the vibration response $y(x,t)$ at any time t and point x along the span ℓ of the tube, may be expressed by:

$$y(x,t) = A \sin \omega t\ [(\cos Bx - \cosh Bx) - 1.35\ (\sin Bx - \sinh Bx)]$$
$$= A\phi(x) \sin \omega t \quad (5)$$

Substituting $\phi(x)$ in equation (4) and integrating between the limits yields:

$$\frac{V_r}{fd} = 1.15\ K \left(\frac{m\delta}{\rho d^2}\right)^{1/2}$$

i.e., the partial admission of a uniform flow to a cantilevered tube with a uniform mass distribution over 75% of the span at the free end, will result in delaying the critical flow velocity by 15%. However, since the mass was not uniformly distributed, adding this effect, equation (3) becomes:

$$\frac{V_r}{fd} = K \left(\frac{\delta}{\rho d^2}\right)^{1/2} \left[\frac{\int_o^{\ell/4} m_1 \, \phi_i^2(x) \, dx + \int_{\ell/4}^{\ell} m \, \phi_i^2(x) \, dx}{\int_{\ell/4}^{\ell} \psi^2 (x) \, \phi_i^2 (x) \, dx} \right]^{1/2} \qquad (6)$$

where, m_1 = rod mass per unit length

m = tube mass per unit length.

Integrating equation (6) using equation (5) and knowing that $m_1 = 0.66$ m for the present tube, gives:

$$\frac{V_r}{fd} = 1.10 \ K \left(\frac{m\delta}{\rho d^2}\right)^{1/2}$$

Which means that considering both effects of the partial admission and the nonuniform mass distribution for the present cantilevered tube will result theoretically in only delaying the critical velocity by 10%. However, Franklin and Soper [62] studied the effect of partial admission on hollow cantilevered tubes. They found that when one third of the span measured from the tip was blocked off, the critical flow velocity will be twice its value without blockage. The theory overestimates the new critical velocity by 21% in this case. When the blockage was applied from the root, the theory underestimated the new critical velocity. Unfortunately, they did not provide any value for the new critical velocity. However the mass ratio is another important factor especially in air flow. If the critical velocity is more dependent on the mass ratio than previously estimated [20], the ratio between the results obtained from the cantilevered tube and the rigid cylinder will be less. However, due to the limited information regarding the effect of partial admission, only the 10% difference obtained above will be taken into consideration. On the basis of using this correction factor, the present results were compared with the most updated results of Lever [84] and Chen [85]. Unfortunately, the results for most of the arrays used in the present study were not given in [84], and the programme used by Lever, was used with the necessary data to obtain the graphs needed for such a comparison as shown in Figures 4.58, 4.59. As can be seen, most of the present results were higher than those predicted theoretically. The only results which agree with the theory given by Lever are those of the normal square array with P/d = 1.5 and the parallel triangular array with P/d = 1.73. The highest difference was with the rotated square arrays which showed experimentally that they are the least prone to fluidelastic instabilities. However, a better agreement was obtained when the present results were compared with the collected data for different array configurations published by Chen [85], as shown in Figure 4.60. The present results are seen to follow more closely the trend of other experimental results for different values of the mass damping parameter. However, although Chen represented a lower

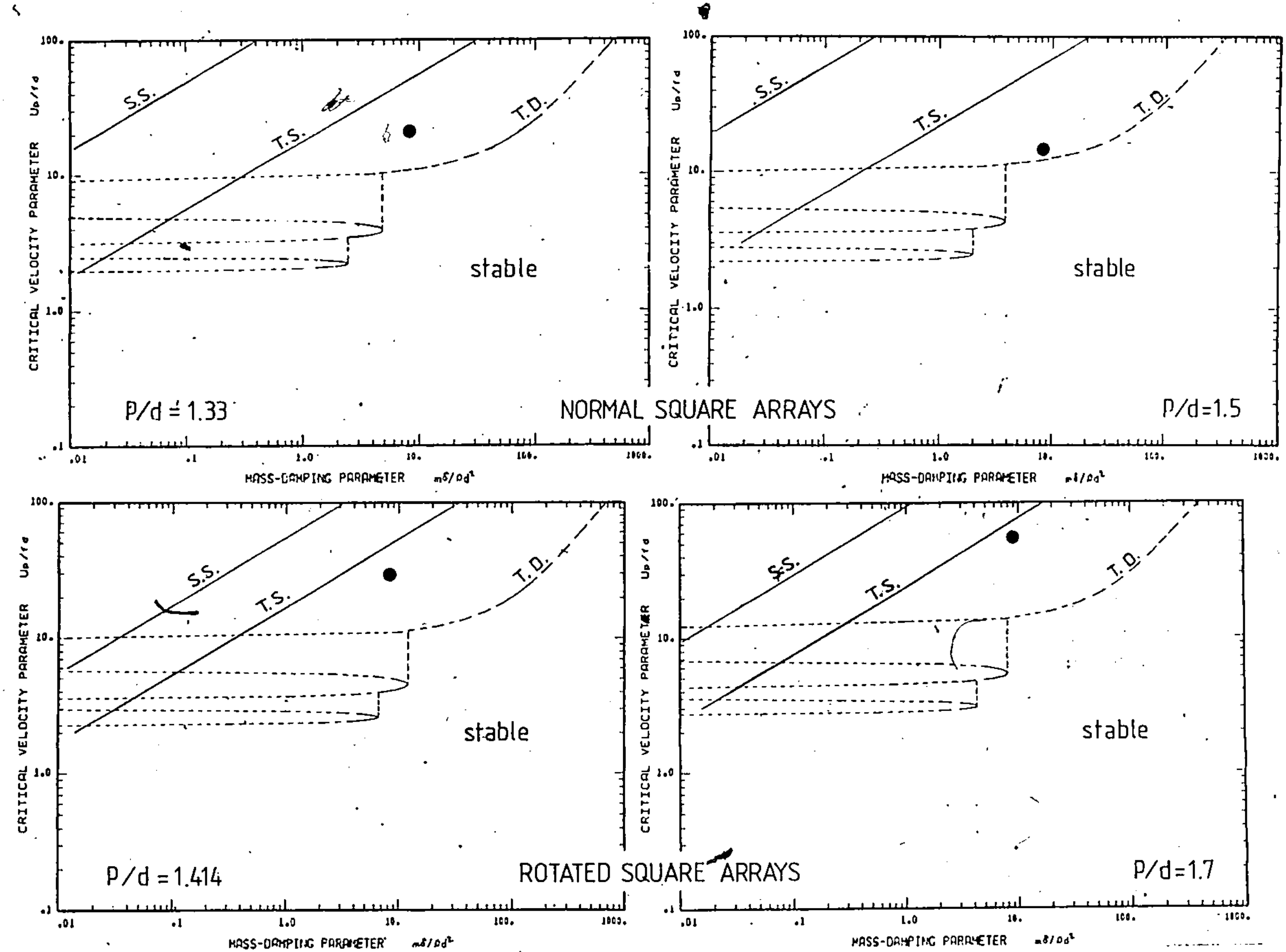

FIGURE 4.58: STABILITY DIAGRAMS DERIVED FROM [84];
● PRESENT RESULTS

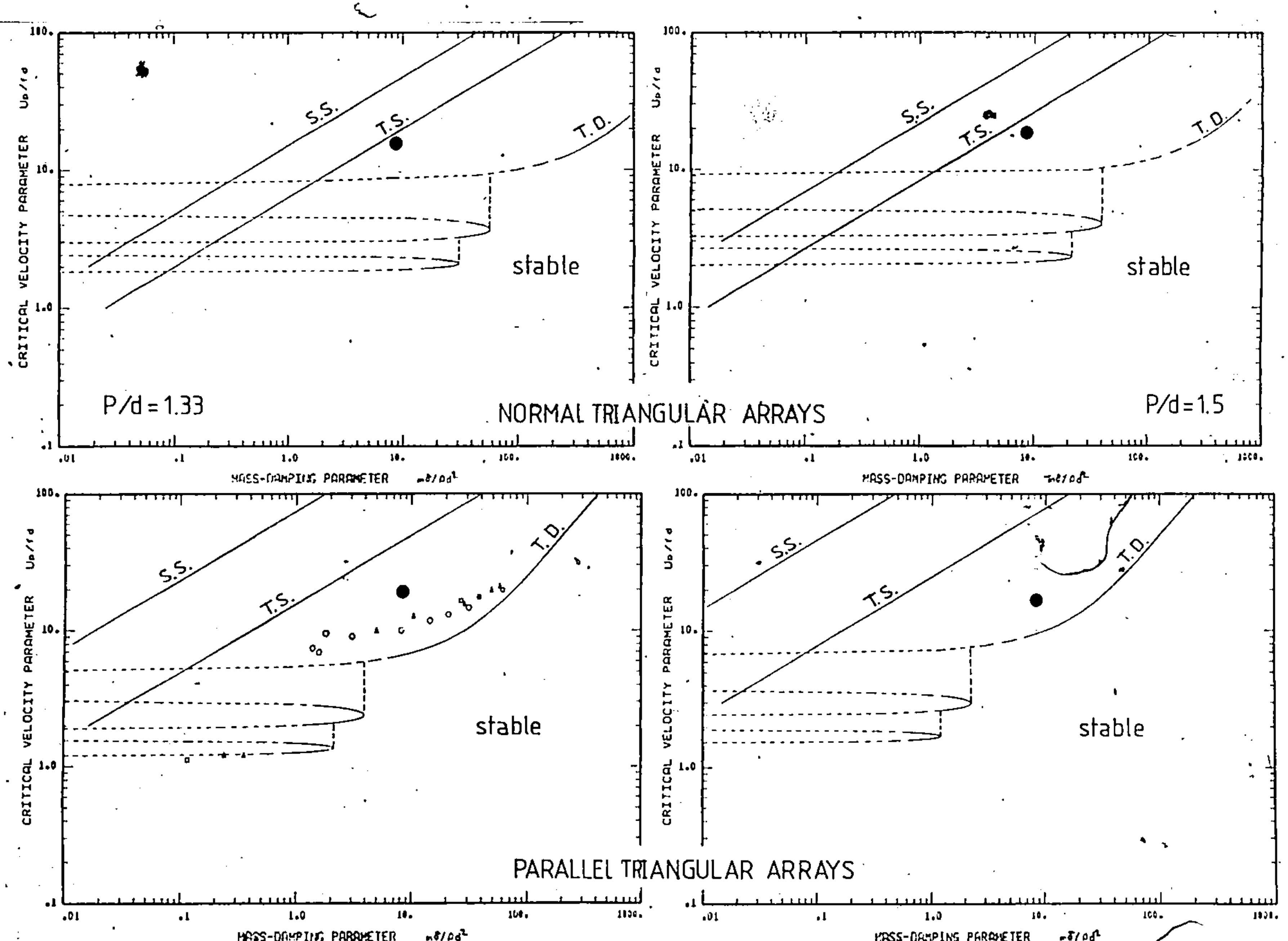

FIGURE 4.59: STABILITY DIAGRAMS DERIVED FROM [84];
● PRESENT RESULTS

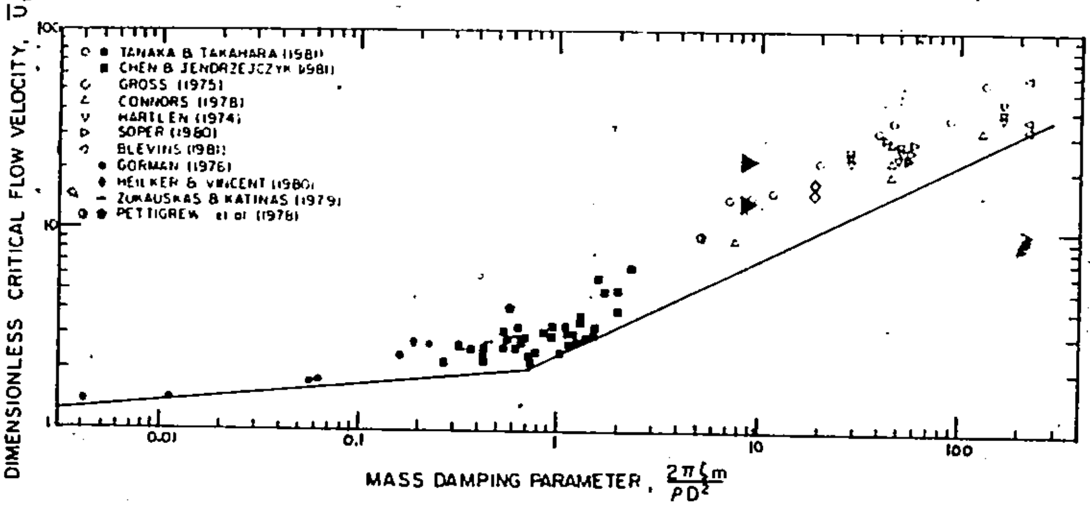

Stability diagram for square arrays

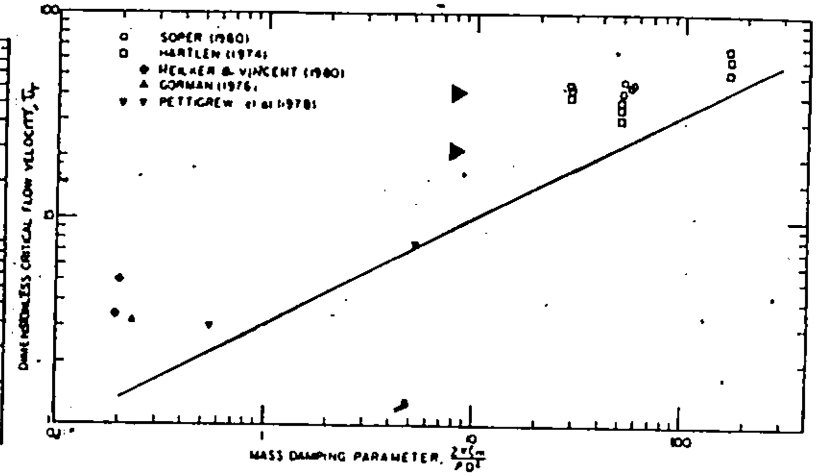

Stability diagram for rotated square arrays

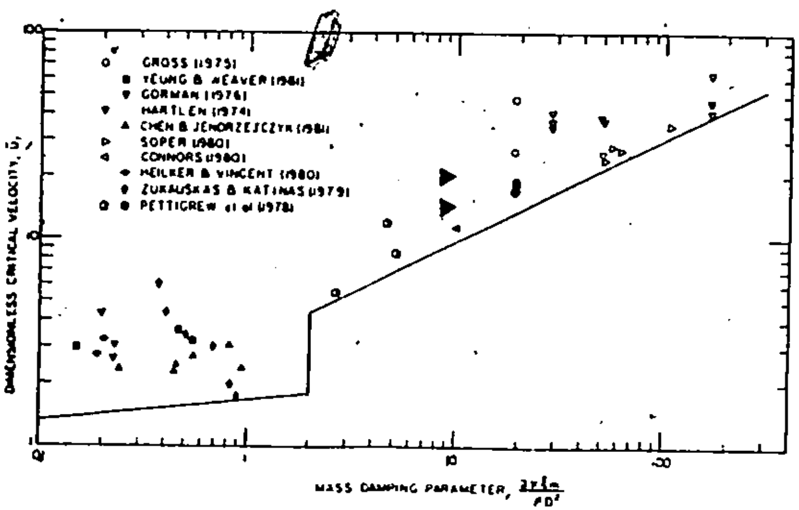

Stability diagram for triangular arrays

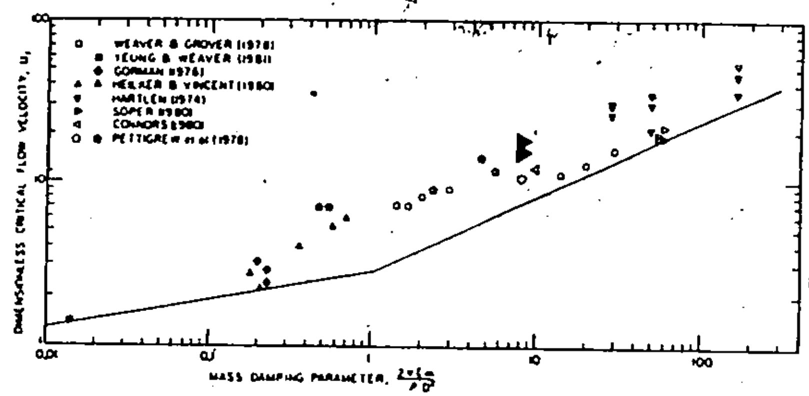

Stability diagram for rotated triangular arrays

FIGURE 4.60: STABILITY DIAGRAMS FROM [85];
▶ PRESENT RESULTS

boundary for instability, and which does not agree with Lever's theory, it is easy to see at this point that such a boundary is too conservative for arrays of different pitch-to-diameter ratios. Using different stability curves for different arrays as suggested by Lever's theory seems to be a very good idea.

The present results were also compared with the results of Hartlen [16] and Soper [17] for tube arrays of different pitch-to-diameter ratios. Although, most of their results were for arrays of pitch-to-diameter ratios other than the ones used in the present study, they represented trends for the present arrays. The results will be first compared on the basis on the instability factor K, defined as:

$$K = \frac{\left(\frac{V_g}{fd}\right)}{\left(\frac{m\delta}{\rho d^2}\right)^{0.5}}$$

The results are shown in Figures 4.61 to 4.64. The only difference between the present results and the results of Hartlen and Soper is that they were obtained for different mass damping parameters. It is evident from these figures that the instability factor seems to be a function of the mass damping parameter for the same array. Most of the arrays show that, the lower the mass damping parameter, the higher the value of the instability factor K. This confirms the theoretical predictions of Lever [84]. These figures also show that the value of K is expected to decrease with increasing the pitch-to-diameter ratio

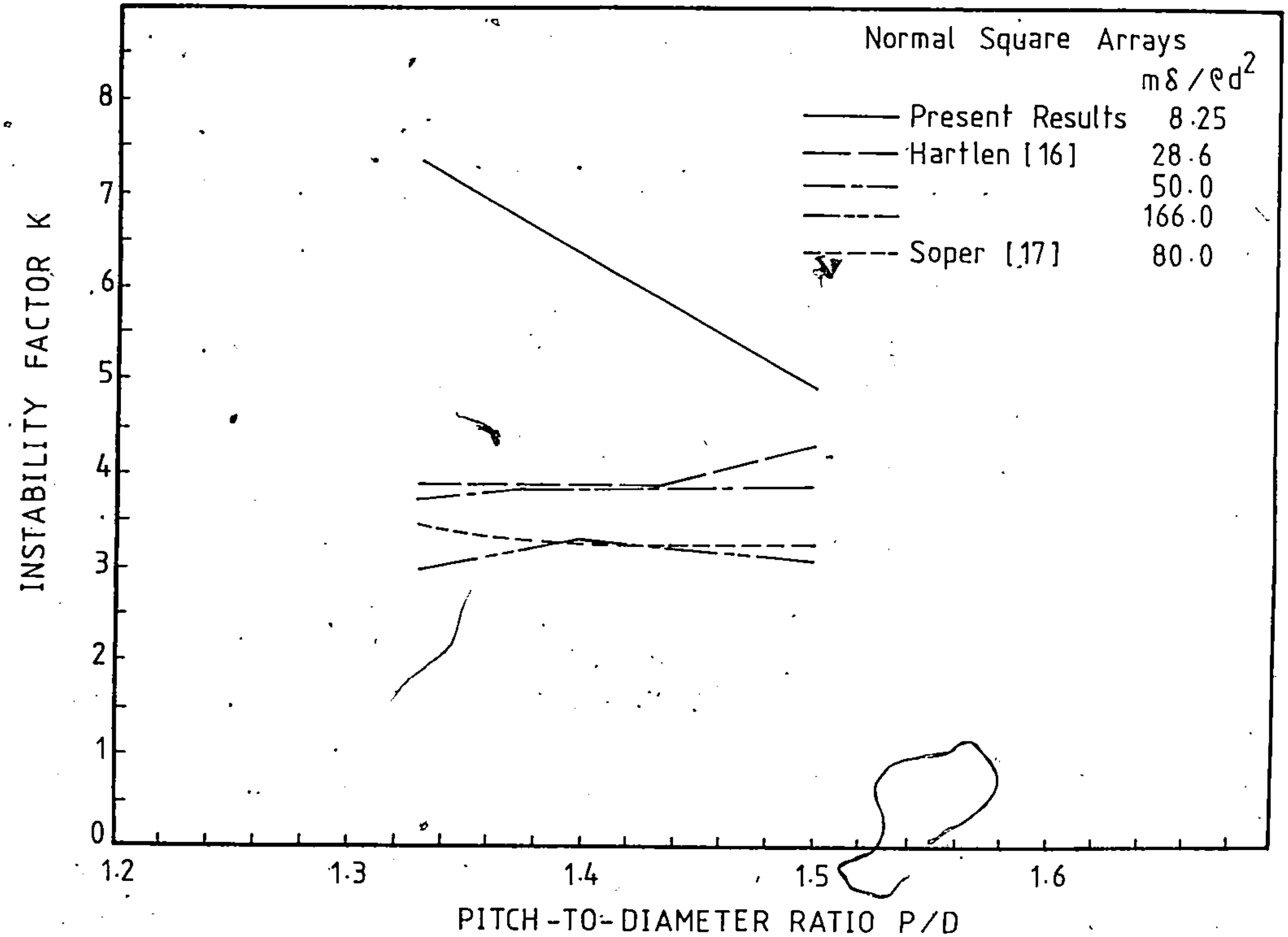
Normal Square Arrays
mδ/ρd²
Present Results 8.25
Hartlen [16] 28.6
50.0
166.0
Soper [17] 80.0
INSTABILITY FACTOR K
0
1
2
3
4
5
6
7
8
1.2
1.3
1.4
1.5
1.6
PITCH-TO-DIAMETER RATIO P/D

FIGURE 4.61

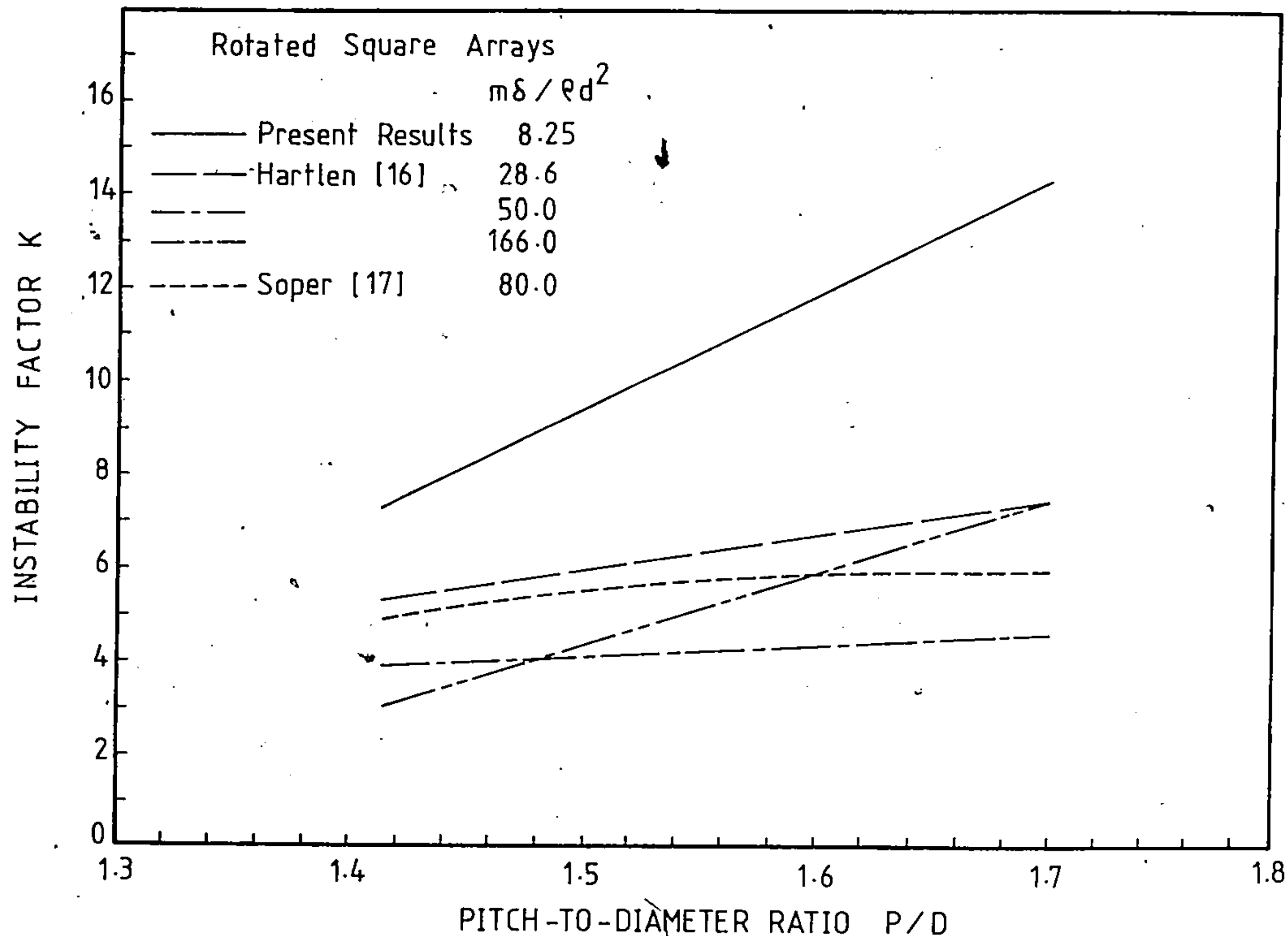
Rotated Square Arrays
$m\delta/\rho d^2$
Present Results 8.25
Hartlen [16] 28.6
50.0
166.0
Soper [17] 80.0
INSTABILITY FACTOR K
0
2
4
6
8
10
12
14
16
1.3
1.4
1.5
1.6
1.7
1.8
PITCH-TO-DIAMETER RATIO P/D

FIGURE 4.62

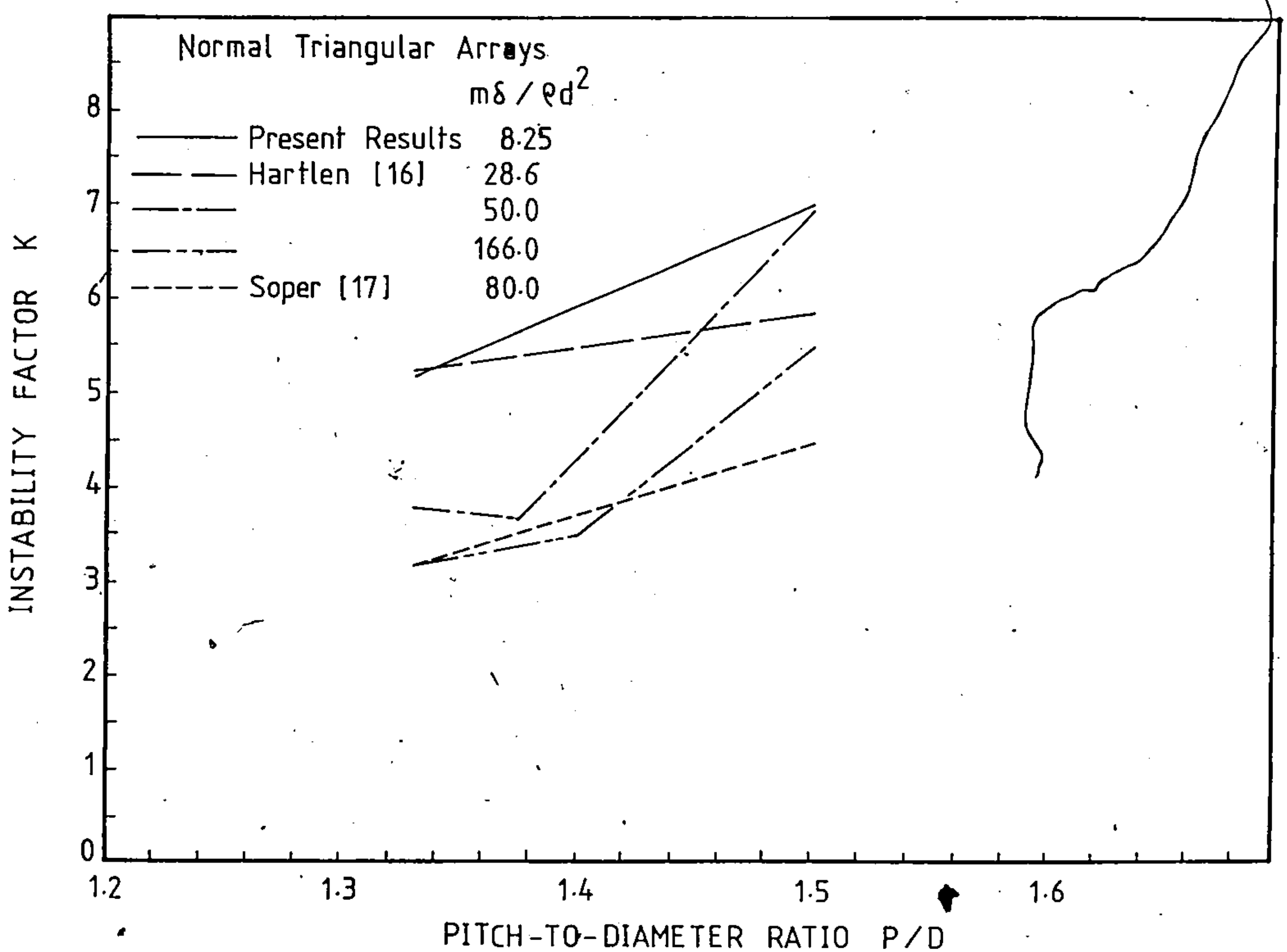

Normal Triangular Arrays
mδ / ρd²
Present Results 8·25
Hartlen [16] 28·6
50·0
166·0
Soper [17] 80·0
INSTABILITY FACTOR K
0
1
2
3
4
5
6
7
8
1·2
1·3
1·4
1·5
1·6
PITCH-TO-DIAMETER RATIO P/D

FIGURE 4·63

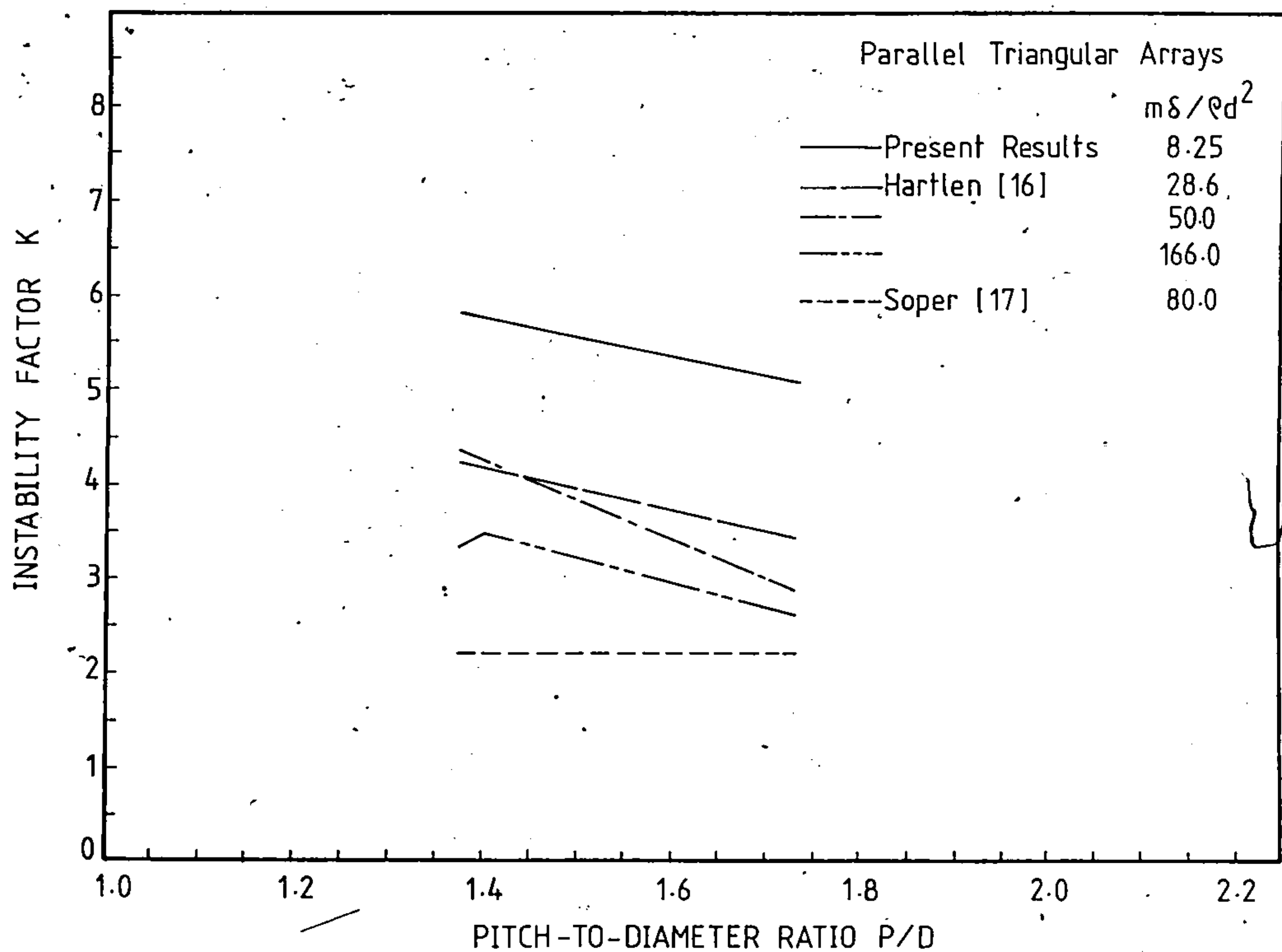
Parallel Triangular Arrays
mδ/ρd²
Present Results 8·25
Hartlen [16] 28·6
50·0
166·0
Soper [17] 80·0
INSTABILITY FACTOR K
0
1
2
3
4
5
6
7
8
1·0
1·2
1·4
1·6
1·8
2·0
2·2
PITCH-TO-DIAMETER RATIO P/D

FIGURE 4.64

for the normal square and parallel triangular configurations between the values of P/d shown in Figures 4.61 and 4.64, while for the rotated square and the normal triangular configurations, the value of K will increase with increasing P/d.

These results were also plotted for the reduced velocity V_g/fd versus the mass damping parameter $m\delta/\rho d^2$ for different arrays, as shown in Figures 4.65 to 4.72. A best fit through these data show that using one stability formula of the form:

$$\frac{V}{fd} = K \left(\frac{m\delta}{\rho d^2}\right)^n$$

with one value for K or n as suggested by Connors [14] and others seems invalid. These figures show that the exponent n will change as the mass damping parameter changes. Also, the increase in the reduced velocity is a function of the pitch-to-diameter ratio, the higher the value of P/d, the steeper the increase in the reduced velocity for different configurations except for the normal triangular arrays. The present results suggest the use of rotated square arrays in practical heat-exchangers as they showed that they are the least prone to fluidelastic instabilities.

It should be noted, as made clear by figures 4.65-4.72, that the data for specific arrays is still too sparse and scattered to derive reliable design formulae for individual array geometries. The scatter is likely the result of the different test configurations used and the different methods of determining critical flow velocities. More consistent tests are required over a broader range of mass-damping parameters.

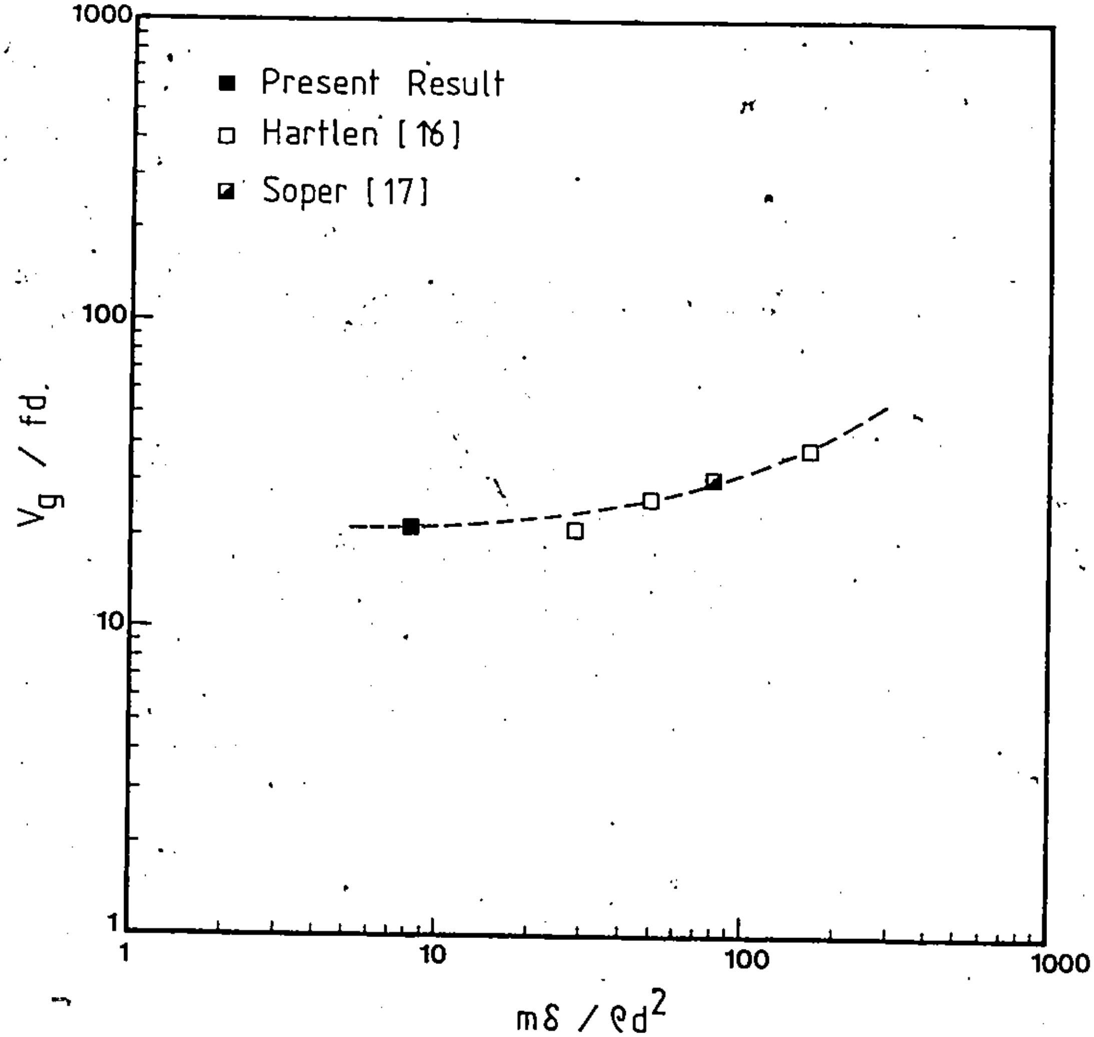

FIGURE 4.65: STABILITY DIAGRAM FOR THE NORMAL SQUARE ARRAY WITH P/d = 1.33.

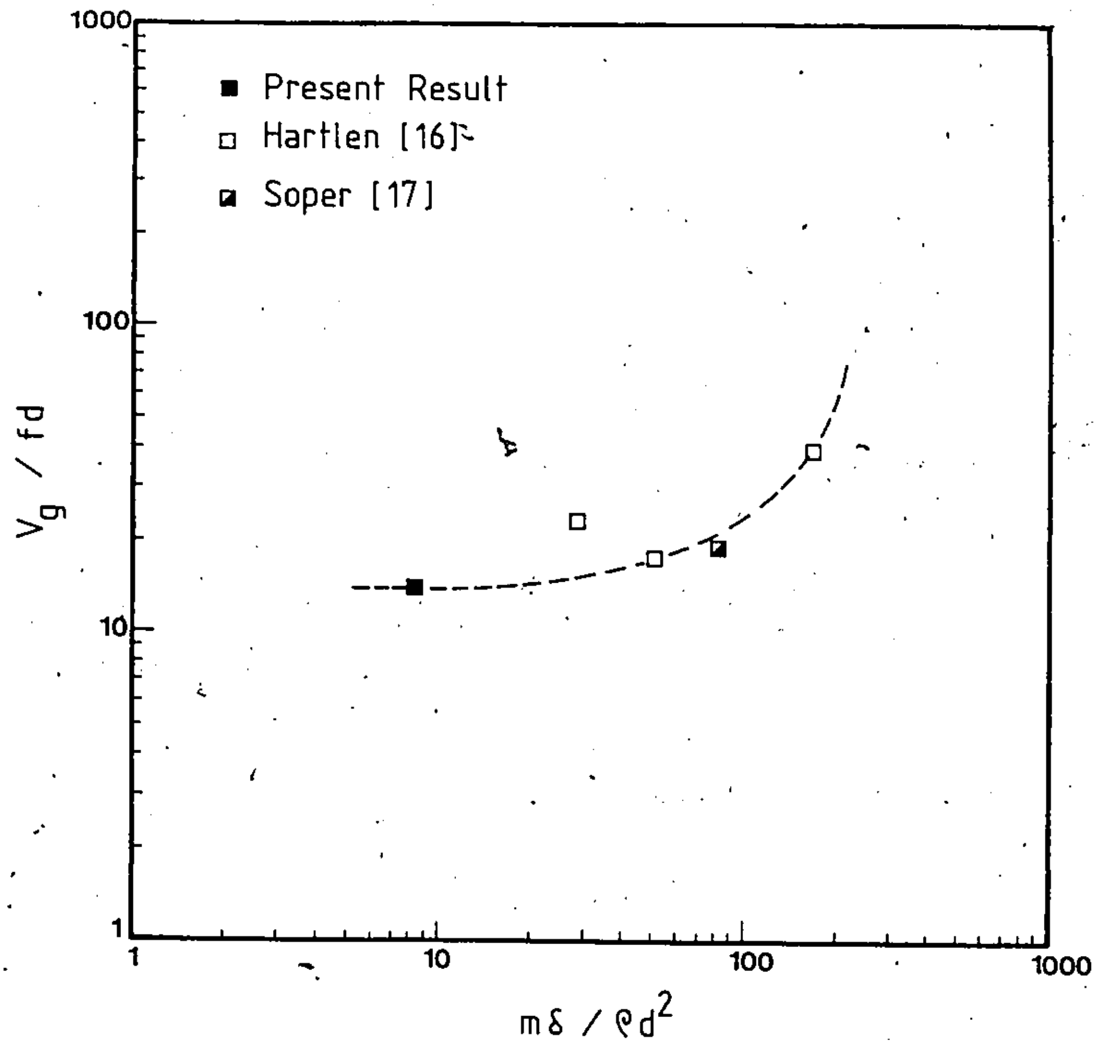

FIGURE 4.66: STABILITY DIAGRAM FOR THE NORMAL SQUARE ARRAY WITH P/d = 1.50.

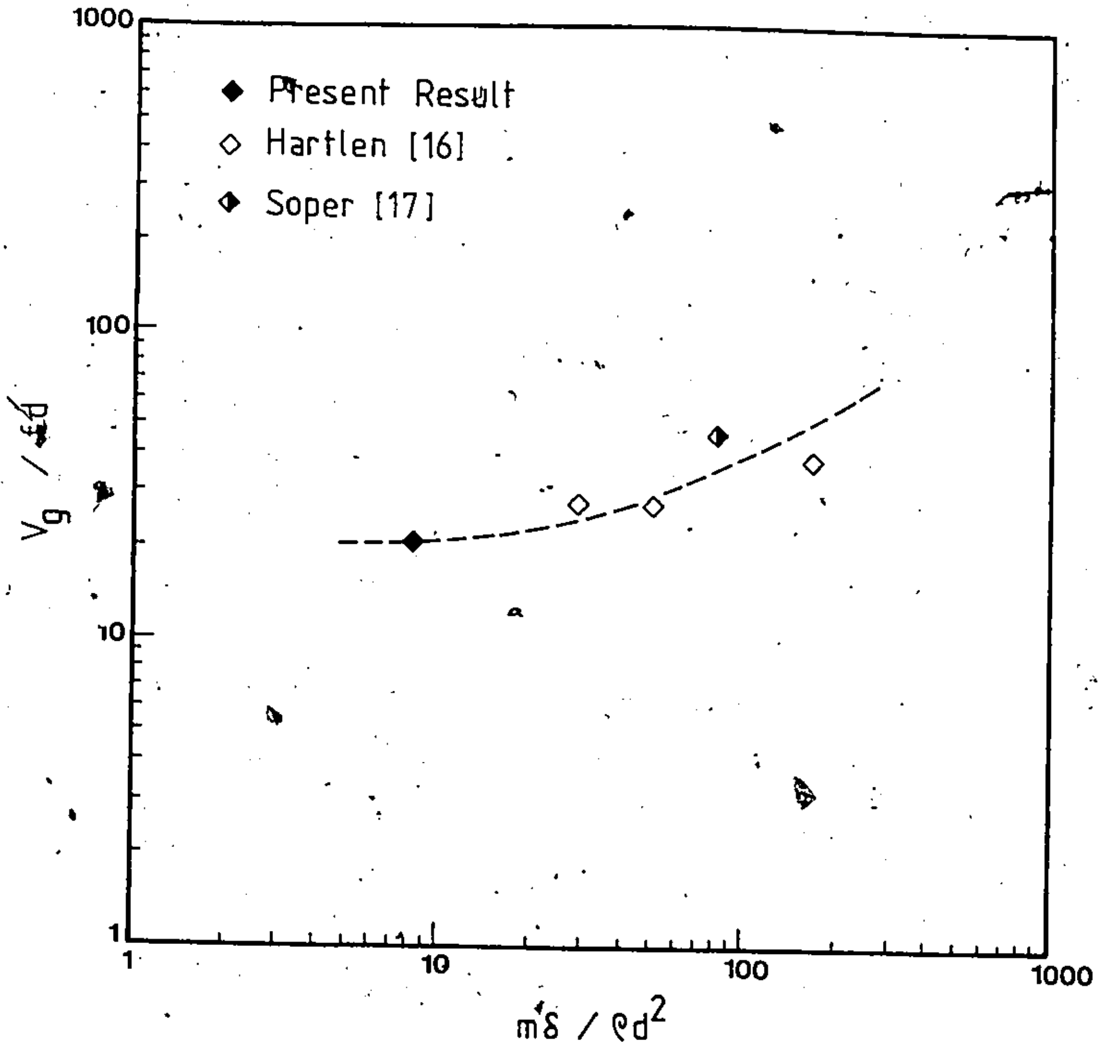

FIGURE 4.67: STABILITY DIAGRAM FOR THE ROTATED SQUARE ARRAY WITH P/d = 1.414.

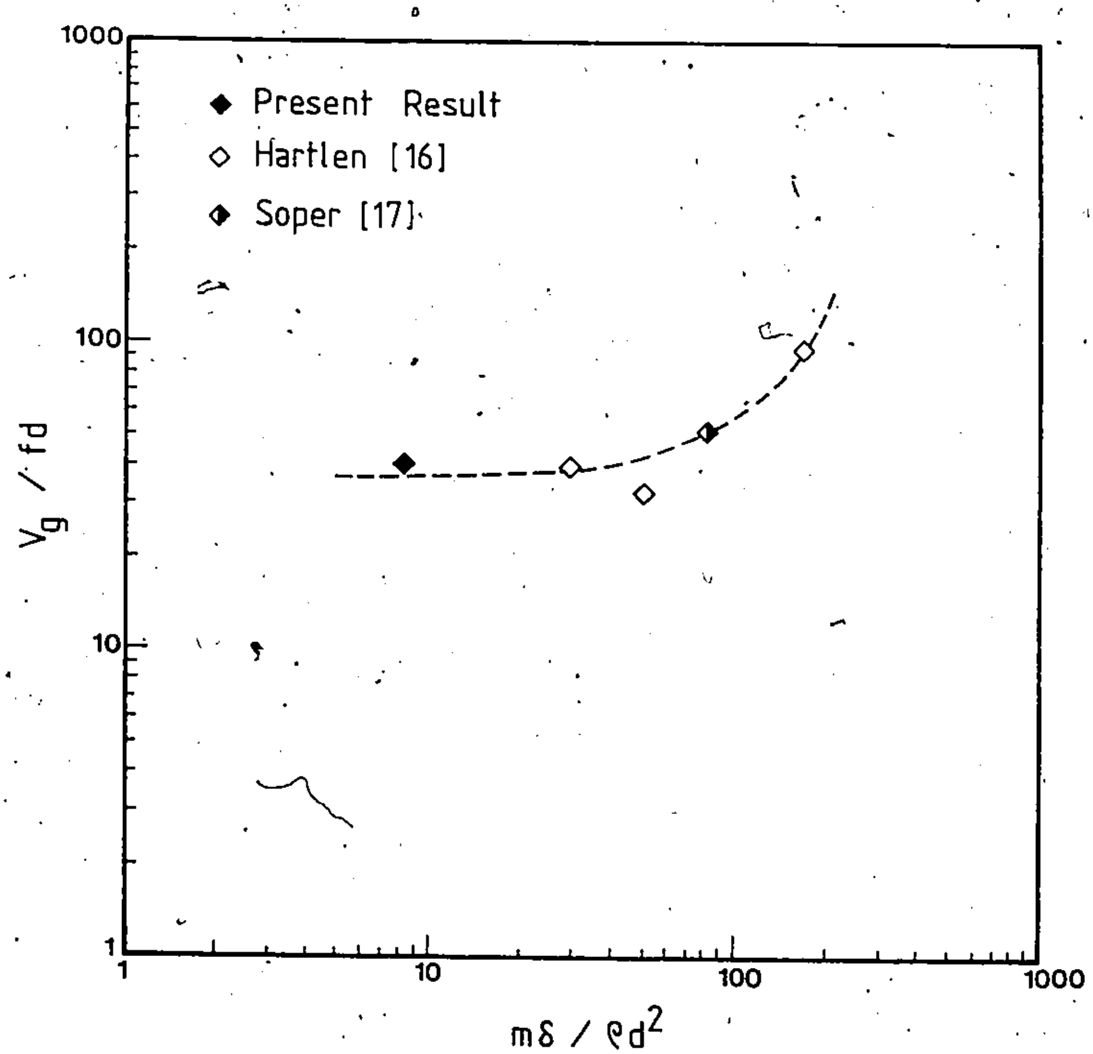

FIGURE 4.68: STABILITY DIAGRAM FOR THE ROTATED SQUARE ARRAY WITH P/d = 1.70.

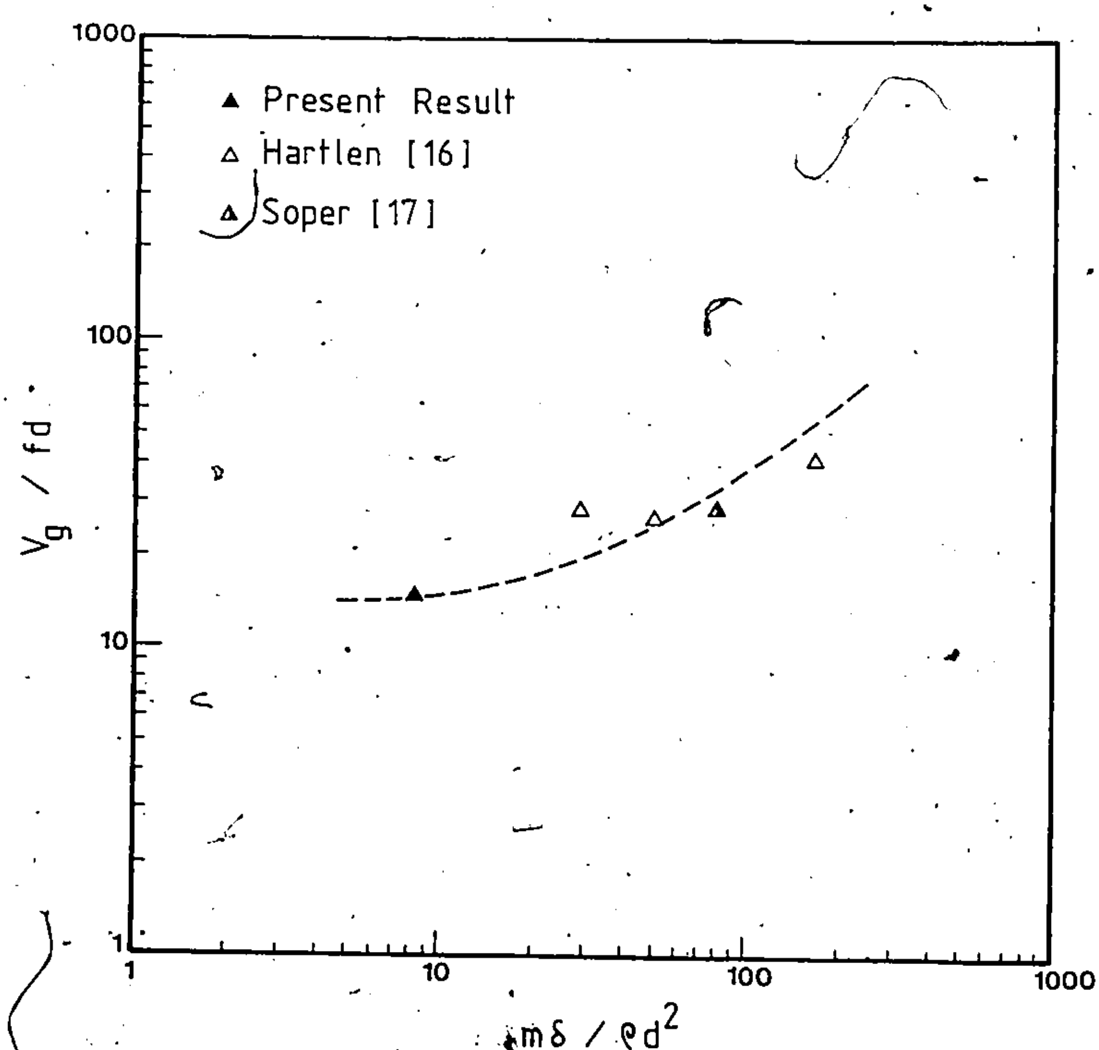

FIGURE 4.69: STABILITY DIAGRAM FOR THE NORMAL TRIANGULAR ARRAY WITH P/d = 1.33.

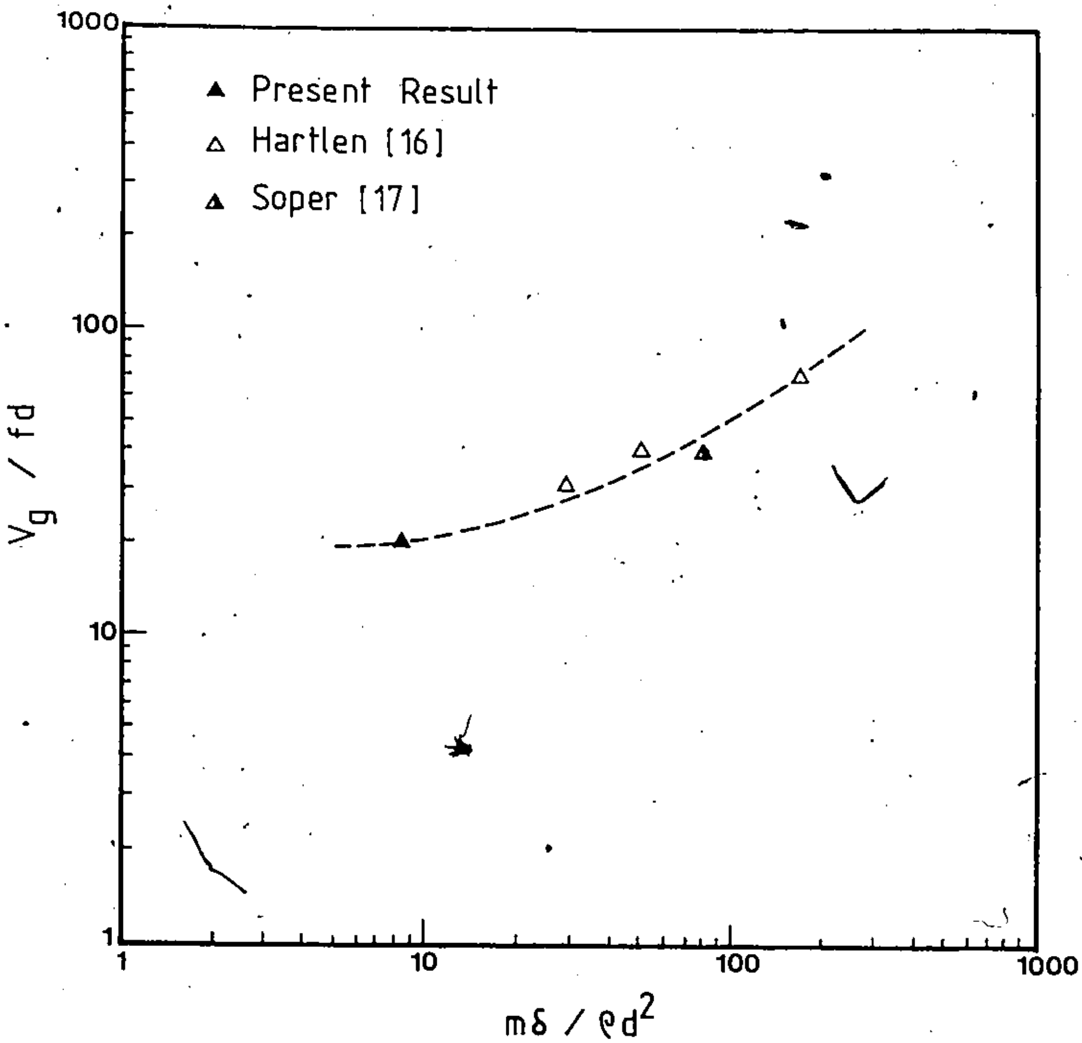

FIGURE 4.70: STABILITY DIAGRAM FOR THE NORMAL TRIANGULAR ARRAY WITH P/d = 1.50.

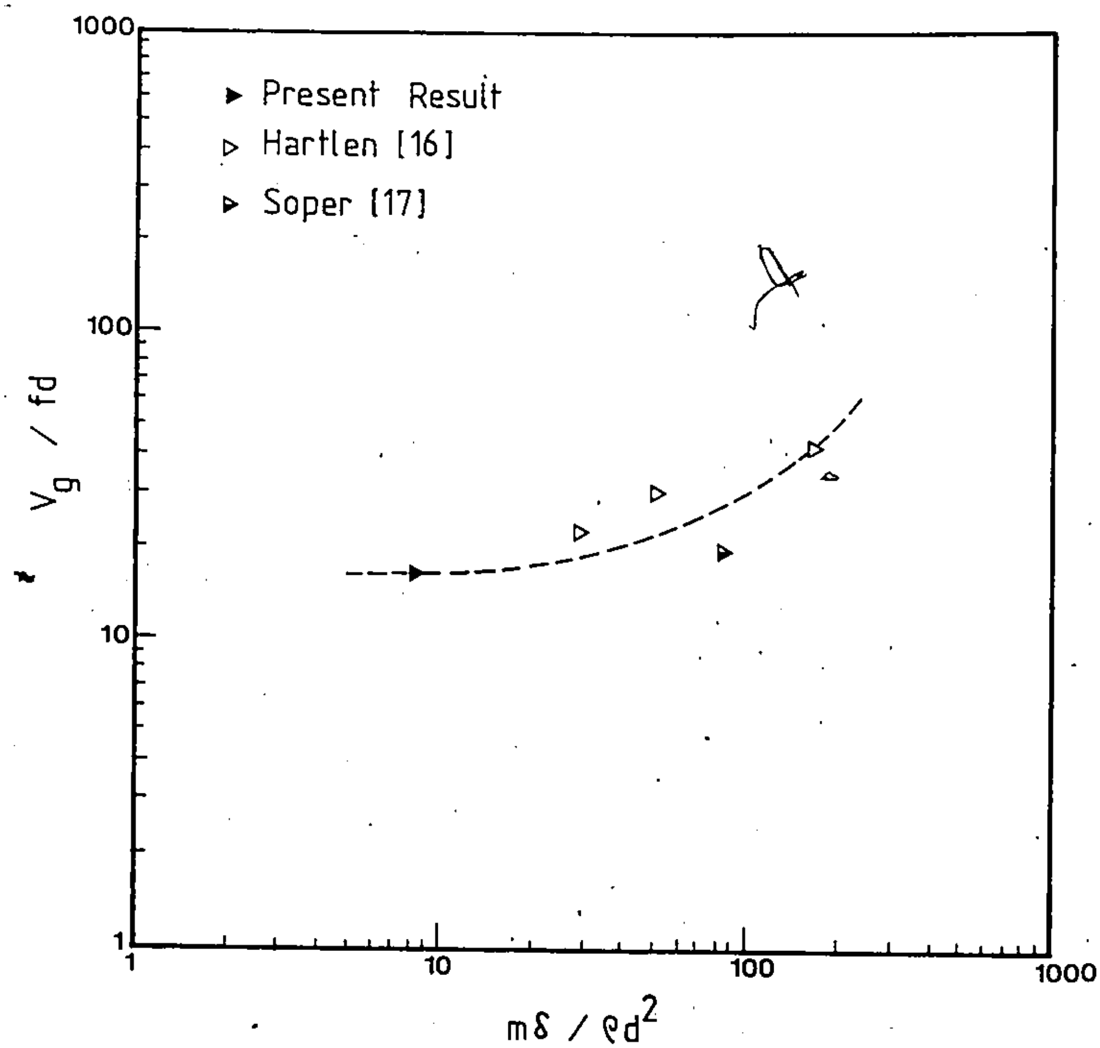

FIGURE 4.71: STABILITY DIAGRAM FOR THE PARALLEL TRIANGULAR ARRAY WITH P/d = 1.375.

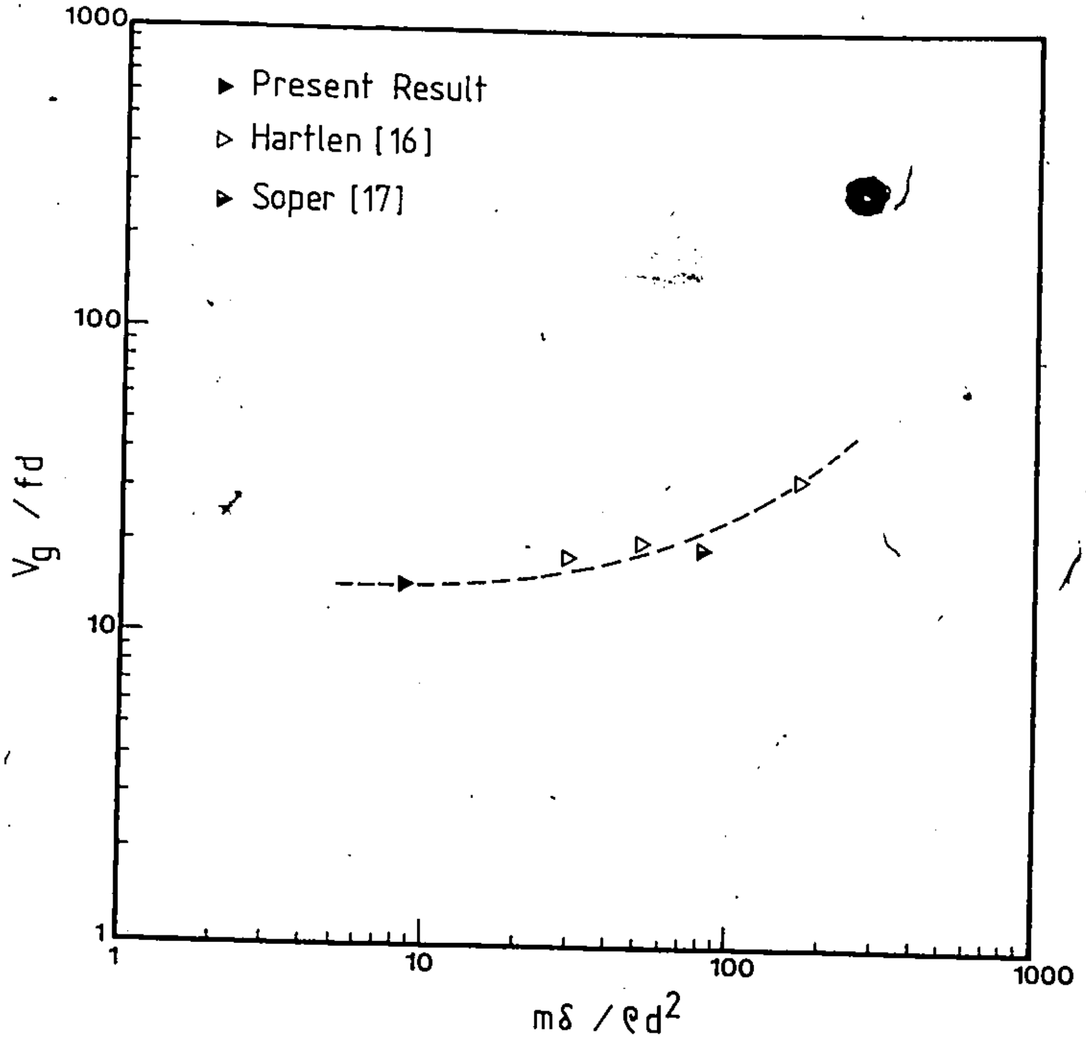

FIGURE 4.72: STABILITY DIAGRAM FOR THE PARALLEL TRIANGULAR ARRAY WITH P/d = 1.73.

CHAPTER 5

CONCLUSIONS

Eight tube arrays were tested in a low speed wind-tunnel having a 305 mm x 305 mm square test-section. The tube arrays were of the four standard configurations used in tube and shell heat exchangers and they are namely: normal square, rotated square, normal triangle, and parallel triangle. For each configuration, two arrays of different pitch-to-diameter ratio were tested. The design of the tube arrays and the test-section allowed changing the tube arrays without changing the test section. Vortex shedding from tubes in these arrays as well as the critical flow velocities which are associated with the fluidelastic instability mechanism were determined. Correlation of the Strouhal numbers obtained and the existing information in the literature were attempted. Vortex shedding frequencies from the tubes were determined by inserting a hot wire probe into the minimum gap between tubes for the different arrays. The probe's exact location depended on the number of tube rows used for each array. However, the results obtained are for tubes in the leading rows of a heat-exchanger, i.e. where the phenomenon is more critical. Tube amplitudes for the onset of fluidelastic instability were determined by using four strain gauges installed near the fixed end of the flexible tubes. Each pair of strain gauges represented a certain direction.

The results of the experimental work presented in this thesis suggest the following conclusions:

Vortex Shedding

1. Discrete frequencies due to regular vortex shedding from the tubes for the different tube arrays tested were observed at low Reynolds numbers. For higher values of Reynolds number the excess of energy of the vortices over the broad turbulence spectrum diminished and ultimately disappeared. The Reynolds number at which regular vortices in the flow disappear is a function of the array configuration and pitch-to-diameter ratio.

2. The height of the discrete peak in the velocity spectra, which is directly proportional to the level of energy associated with the vortices, showed the normal square array with pitch ratio of 1.33 to have the lowest level of energy of all the arrays tested in this study. However, both normal square and parallel triangular arrays showed an increase in the height of the vorticity peaks with increasing flow velocity. Further increase in flow velocity resulted in reduction in these peaks. While normal square arrays showed higher energy peaks for the higher pitch ratio, the parallel triangular arrays showed higher energy peaks for the lower pitch ratio. On the other hand, both the rotated square and normal triangular arrays indicated a continuous drop in the height of the peaks associated with the flow periodicity with

increasing flow velocity. For rotated square arrays the level of energy was higher for the lower pitch ratio, while normal triangular arrays showed the reverse. This shows that the energy content associated with the vortices is a function of array pattern and pitch ratio.

3. No vortex shedding resonance was observed for any of the tube arrays tested, even though the vortex shedding frequency coincided with the tube natural frequency at some flow velocity for most of the arrays. This suggests that vortex shedding resonance should not be a problem in practical heat exchanger tube arrays exposed to a gas flow.

4. There is evidence to show that laminar vortex shedding occurs for some arrays at low Reynolds numbers and is associated with very high Strouhal numbers. For the normal square arrays, a Strouhal number of 2.34 was obtained for the pitch ratio of 1.33 and of 1.44, 1.72 and 2.04 for the pitch ratio of 1.5. For the normal triangular array of 1.33 pitch ratio, the Strouhal number was 4.89. The appearance of Strouhal numbers which are almost double the results published in the literature for the normal square arrays tested in the present study warns of the fact that vortex shedding could be expected at half the flow velocities predicted from Strouhal numbers in the literature [7]. This is a potential problem for tube arrays exposed to liquid flows.

5. Strouhal numbers decrease with increasing pitch-to-diameter ratio. The decrease is gradual for normal and rotated square arrays and is sharp for normal and parallel triangular arrays.

6. The following formulae were obtained from a best fit through all the available Strouhal numbers at high Reynolds numbers.

$$S_u = -1 + \exp\left\{\frac{(P/d - 1)^{-0.66}}{2.5}\right\} \quad \text{for normal square arrays.}$$

$$S_u = -1 + \exp\left\{\frac{(P/d - 1)^{-0.75}}{2.38}\right\} \quad \text{for rotated square arrays.}$$

$$S_u = -1 + \exp\left\{\frac{(P/d - 1)^{-0.75}}{1.79}\right\} \quad \text{for parallel triangular arrays.}$$

No formula was obtained for the normal triangular arrays due to the large scatter in the data. These new formulae are believed to serve as reasonable design guidelines against vortex shedding response, especially in water flows where higher dynamic heads are more likely to induce significant tube response.

7. Of the arrays tested, five showed a single value of Strouhal number. For the normal square array with P/d = 1.50, rotated square array with P/d = 1.70, and the normal triangular array with P/d = 1.5, more than one value of Strouhal number was obtained. Generally these multiple values of Strouhal numbers show good agreement with comparable results in the literature. Multiple Strouhal numbers could be expected for arrays of pitch

ratios of around 1.5 and for the Reynolds number range 400 < Ru < 5000. It would appear that in cases where there are multiple Strouhal numbers, it is not valid to try to fit a single curve through the data ~~as~~ has been commonly attempted. Further research is necessary to define these curve branches and to determine which branches are likely to be more significant in terms of tube resonance or acoustic excitation.

8. There is now considerable evidence to show that a discrete phenomenon characteristic of vortex shedding exists for closely packed tube arrays. This excitation phenomenon is not broad band as suggested by Owen [8], at least in the early tube rows of an array. This implies that Owen's turbulent buffeting is not the correct excitation mechanism, contrary to the opinion expressed by Paidoussis [7]. The present results also show clearly, the incorrect flow velocity was used by Owen in his equation. The flow velocity upon which the Strouhal number is based must be used to correctly correlate his equation with experimental data.

9. Zukauskas and Katinas' formula [12] for normal triangular arrays showed good agreement for interpreting Strouhal numbers for rotated square and parallel triangular arrays.

Fluidelastic Instability

1. The effect of changing pitch-to-diameter ratio for different array geometries was determined experimentally for the first time at low damping parameter ($m\delta/\rho d^2 = 8.25$).

2. Critical flow velocities for fluidelastic instabilities for tubes in the second, third, and fourth rows are essentially the same for all the array geometries and pitch ratios tested.

3. The tube amplitudes at the critical flow velocities are less than 1% of tube diameter.

4. The increase in tube amplitudes above the critical flow velocities is very sharp for normal square arrays. Increasing the pitch-to-diameter ratios from 1.33 to 1.50 resulted in slightly lower critical velocities. This is contrary to the theoretical predictions.

5. Rotated square arrays are also associated with a sharp increase in tube amplitudes in the unstable region. The tubes become unstable mainly in the in-line direction for the high pitch-to-diameter ratio, contrary to the transverse direction normally observed. The critical velocity increased by a factor of 3 when the pitch-to-diameter ratio was increased from 1.414 to 1.70.

6. The critical flow velocity almost doubled for the normal triangular arrays as the pitch-to-diameter ratio was increased from 1.33 to 1.50. The increase in tube amplitude is more gradual around the stability threshold as compared with arrays of other geometries.

7. The critical flow velocity for the parallel triangular array with P/d = 1.375 is about 38% lower than for P/d = 1.73. The amplitude increase above the critical velocity is very rapid for both arrays. This is contrary to what Hartlen [16] reported. The implication is that the rate of increase in tube amplitude above the stability threshold may depend to some extent unknown and uncontrolled parameters.

8. Normal triangular arrays as compared with normal square arrays of the same P/d, showed that they are more prone to fluidelastic instability. However, the present results suggest the use of rotated square arrays for practical heat exchangers as they showed that they are the least prone to fluidelastic instability.

9. Comparison of the instability factor K from the present results and those of Hartlen [16] and Soper [17], showed that it is a function of the damping parameter, the lower the damping parameter, the higher the value K. Also, plots of the reduced velocity, V_g/fd, versus the damping parameter, $m\delta/\rho d^2$, for the different arrays tested in this study showed that using a one

parameter equation of the form suggested by Connors [14] and others for all arrays is invalid. The parametric relationship is expected to be nonlinear as suggested by Lever [84]. The results show even that the increase in the reduced velocity is a function of P/d, the higher the value of P/d, the steeper the increase in the reduced velocity for different configurations except for the normal triangular arrays.

It is hoped that the contribution of the present study will be helpful in understanding some of the controversy which exists in the literature and provide some direction towards the development of better design guidelines for heat-exchangers against flow induced vibrations. It has also been demonstrated that a great deal more research is required to develop a full understanding of fluid excitation phenomena in heat exchangers.

The following is recommended for future research:

1. Although good correlation for Strouhal numbers was obtained for normal and rotated square arrays, as well as parallel triangular arrays for high Reynolds numbers, the scatter in the Strouhal numbers for normal triangular arrays is very large and more tests are needed especially at low pitch-to-diameter ratios.

2. Some arrays showed that laminar vortex shedding occur at very low Reynolds numbers and is associated with very high Strouhal

numbers. More tests are necessary to show which other arrays may develop laminar vortex shedding.

3. There are some cases where arrays may produce multiple Strouhal numbers. Further research is necessary to show which other arrays may produce this kind of behaviour, and to determine if one of the Strouhal numbers is more dominant or if all are equally likely to excite acoustic or tube resonance.

4. Fluidelastic instabilities in water flows are expected to be different from those in air flows. More tests are needed to study the effect of changing pitch-to-diameter ratios for different geometries in water flows.

5. The effect of imposing different boundary conditions on the tubes, as well as partial flow admissions need to be studied. In practical heat exchangers, the tubes are multi-span with the flow velocity unevenly distributed along the spans. The vast majority of studies to date have treated single span bundles on idealized supports and subjected to uniform flows.

REFERENCES

1. Paidoussis, M.P., "Flow-induced Vibrations in Nuclear Reactors and Heat Exchangers, Practical Experience and State of Knowledge", Symposium on Practical Experiencies with Flow-induced Vibration, Karlsruhe, Germany, Preprints I, pp. 01-39, Sept. 3-6, 1979.

2. Proceedings UKAEA/NPL International Symposium on Vibration Problems in Industry, Keswick, U.K., April 1973.

3. Proceedings BNES International Conference on Vibration in Nuclear Plant, Keswick, U.K., May 1978.

4. Proceedings UKAEA/BNES Third Keswick International Conference on Vibration in Nuclear Plant, Keswick, U.K., May 1982.

5. Transactions 4th International Conference on Structural Mechanics in Reactor Technology, San Francisco, 1977.

6. Transactions 6th International Conference on Structural Mechanics in Reactor Technology, Paris 1981.

7. Paidoussis, M.P., "Flow-Induced Vibration of Cylindrical Structures: A Review of the State of the Art" to be represented at the Second International Topical Meeting on Nuclear Reactor Thermohydraulics, sponsored by ANS, ASME, and AIChemE, to be held in Santa Barbara, California, on 11-14 January 1983, under the title of, "A Review of Flow-Induced Vibrations in Reactors and Reactor Components".

8. Owen, P.R., "Buffeting Excitation of Boiler Tube Vibration", J. Mechanical Engineering Science, Vol. 7, pp. 431-439, Dec. 1965.

9. Pettigrew, M.J., and Gorman, D.J., "Vibration of Heat Exchanger Components in Liquid and Two-Phase Cross-Flow", Paper 2.3, Proceedings BNES International Conference on Vibration in Nuclear Plant, Keswick, U.K., May 1978.

10. Chen, Y.N., "Flow induced Vibration and Noise in Tube-Bank Heat Exchangers due to Von-Karman Streets", ASME J. Engineering for Industry, Series B, Vol. 90, No. 1, pp. 134-146, Feb. 1968.

11. Fitz-Hugh, J.S., "Flow Induced Vibrations in Heat-Exchangers", Proceedings of the UKAEA/NPL International Symposium on vibration Problems in Industry, Keswick, U.K., Paper 427, 1973.

12. Zukauskas, A., and Katinas, V., "Flow-Induced Vibration in Heat-Exchanger Tube Banks", Practical Experiences with Flow-Induced Vibrations, eds. Naudascher, E., and Rockwell, D., Springer-Verlag, Berlin, pp. 188-196, 1980.

13. Murray, B.G., Bryce, W.B., and Rae, G., "Strouhal Numbers in Tube Arrays", Paper 2.4, Proceedings UKAEA/BNES ~~Third~~ Keswick International Conference on Vibration in Nuclear Plant, Keswick, U.K., May 1982.

14. Connors, J.H., "Fluidelastic Vibration of Tube Arrays Excited by Cross Flow", Symposium on Flow Induced Vibration in Heat Exchangers, Winter Annual Meeting of ASME, New York, pp. 42-56, Dec. 1970.

15. Blevins, R.D., "Fluidelastic Whirling of a Tube Row", ASME, Journal of Pressure Vessel Technology, Vol. 96, Series J,4, pp. 263-267, November 1974.

16. Hartlen, R.T., "Wind Tunnel Determination of the Fluid Elastic Vibration Thresholds for Typical Heat-Exchanger Tube Patterns", Ontario Hydro Research Division Report No. 74-309-K, 1974.

17. Soper, B.M., "The Effect of Tube Layout on the Fluidelastic Instability of Tube Bundles in Cross Flow", Flow-Induced Heat Exchanger Tube Vibration, 1980, eds, Chenweth, J.M., and Stenner, J.R., HTD-Vol. 9, ASME, New York, pp. 1-9, 1980.

18. Gibert, R.J., Chabrerie, J., and Sagner, M., "Vibrations of Tube Arrays in Transversal Flow", Trans. 4th International Conference on Structural Mechanics in Reactor Technology, Series F, paper F4/h, San Francisco, 1977.

19. Weaver, D.S., and Grover, L.K., "Cross-Flow Induced Vibrations in a Tube Bank - Turbulent Buffeting and Fluid Elastic Instability", Journal of Sound and Vibration, Vol. 59, pp. 277-294, 1978.

20. Weaver, D.S., and ElKashlan, M., "The Effect of Damping and Mass Ratio on the Stability of a Tube Bank", Journal of Sound and Vibration, Vol. 76, pp. 283-294, 1981.

21. Weaver, D.S., and Yeung, H.C., "Approach Flow Direction Effects on the Cross-Flow Induced Vibrations of a Square Array of Tubes", to appear in the Journal of Sound and Vibration.

22. Yeung, H.C., and Weaver, D.S., "The Effect of Approach Flow Direction on the Flow Induced Vibrations of a Triangular Tube Array". ASME J. Vibration, Acoustics, Stress and Reliability, Vol. 105, No. 1, pp. 76-82, 1981.

23. Weaver D.S., and Yeung, H.C., "The Effect of Tube Mass on the Flow Induced Response of Various Tube Arrays in Water", Private communication.

24. Heilker, W.J., and Vincent, R.Q., "Vibration in Nuclear Heat Exchangers due to Liquid and Two-Phase Flow", Trans. of the ASME, Journal of Engineering for Power, Vol. 103, pp. 358-366, April 1981.

25. Weaver, D.S., and Koroyannakis, D., "Flow Induced Vibrations of Heat Exchanger U-tubes, A Simulation to Study the Effects of Asymmetric Stiffness", ASME Journal of Mechanical Design, Vol. 104, ASME Paper 81-DET-20, 1982.

26. Weaver, D.S., and Koroyannakis, D., "The Cross-Flow Response of a Tube Array in Water - A Comparison with the Same Array in Air", Flow-Induced Vibration of Circular Cylindrical Structures, ASME, PVP-Vol. 63, eds. Chen, S.S., Paidoussis, M.P., and Au-Yang, M.K., New York, pp. 71-85, 1982.

27. Lever, J.H., and Weaver, D.S., "A Theoretical Model for Fluid-Elastic Instability in Heat Exchanger Tube Bundles", Journal of Pressure Vessel Technology, Transactions of the ASME, Vol. 104, No. 3, pp. 147-158, August 1982.

28. Marris, A.W., "A Review on Vortex Streets, Periodic Wakes, and Induced Vibration Phenomena", Journal of Basic Engineering, pp. 185-196, June 1964.

29. Föppel, L., Sitzungsberieche d.k. bayer. Akad. d. Wissensch. zu Nunchen 1913, 1-17. Also given as an example in Milne-Thomson, "Theoretical Hydrodynamics", fourth edition, MacMillan, pp. 366, 1960.

30. Tritton, D.J., "Experiments on Flow Past a Circular Cylinder at Low Reynolds Numbers", Journal of Fluid Mechanics, Vol. 6, Part 4, p. 547, November 1959.

31. Roshko, A., "On the Development of Turbulent Wakes from Vortex Sheets", NACA Report 1191, p. 801, 1954.

32. Lienhard, J.H., "Synoposis of Lift, Drag and Vortex Frequency Data for Rigid Circular Cylinders", Bulletin 300, Washington State University, 1966.

33. Bishop, R.E.D., and Hassan, A.Y., "The Lift and Drag Forces on a Circular Cylinder in a flowing Fluid", Proc. royal Soc. London, Series A., Vol. 277, pp. 32-50, 1964.

34. Gerrard, J.H., "An Experimental Investigation of the Oscillating Lift and Drag of a Circular Cylinder Shedding Turbulent Vortices", J. Fluid Mechanics, Vol. 11, Part 2, pp. 244-256, September 1961.

35. Griffin, O.M., "Flow Near Self-Excited and Forced Vibrating Circular Cylinders", ASME paper No. 71, vib. 25, 1971.

36. Relf, E.F., and Simmons, L.F.G., "The Frequency of the Eddies Generated by the Motion of Circular Cylinders through a Fluid", Aeronautical Research Council, No. 917, 1924.

37. Fujino, "The Dynamic Behaviour of Stacks under the Action of Wind", Proceedings of the 7th National Congress of Applied Mechanics, Tokyo, pp. 387-392, 1957.

38. Spivack, H.M., "Vortex Frequency and Flow Pattern in the Wake of Two Parallel Cylinders at Varied Spacing Normal to an Air Stream", Journal of the Aeronautical Sciences, pp. 289-301, June 1946.

39. Landweber, L., "Flow About a Pair of Adjacent Parallel Cylinders Normal to a Stream", David Taylor Model Basin Report 485, 1942.

40. Grotz, B.J., and Arnold, F.R., "Flow-Induced Vibrations in Heat-Exchangers", Tech. Report No. 31 to Office of Naval Research from Stanford U., California, AD 104568, August 1956.

41. Bauly, J.A., "Vortex Shedding in Tube Banks", Symposium on Internal Flows, paper 25, Mech. Eng. Dept. of University of Salford, pp. 20-22, April 1971.

42. König, A., and Gregorig, R., "A Criterion for Vibration in Transverse Flow over a Tube", Part 3: Vibration Experiments in the Nest of Tubes. Chemie. Ing. Techn. Vol. 40, No. 13, pp. 645-650, 1968 (In German) English Translation ORNL-tr-2104.

43. Putnam, A.A., "Flow-Induced Noise and Vibration in Heat Exchangers", ASME paper No. 64-WA/HT-21, 1964.

44. Classen, P. and Gregorig, R., "A Criterion for Oscillations of a Tube Caused by Cross-Flow. Part 4. Oscillation Experiments with an Aligned Tube Bundle". Chemie. Ing. Techn., Vol. 43, No. 17, pp. 982-985, 1971, (In German, English Abstract).

45. Chen, Y.N., and Weber, M., "Flow-Induced Vibrations in Tube Bundle Heat Exchangers with Cross and Parallel Flow". Conf., Flow-Induced Vibration in Heat Exchangers, Winter Annual Meeting of ASME, New York, pp. 57-58, Dec. 1st, 1970.

46. Jaudet, A., and Hutzler, D., "Acoustic Pulsations and Vibratory Stresses in Heat Exchangers", Inst. of Fuel, Heat Exchangers Conf., Paris, paper 13, (in French), June 1971.

47. Pettigrew, M.J., Sylvestre, Y., and Campagna, A.O., "Vibration Analysis of Heat Exchanger and Steam Generator Designs", Nuclear Engineering and Design, Vol. 48, pp. 97-115, 1978.

48. Grover, L.K., and Weaver, D.S., "Cross-Flow Induced Vibrations in a Tube Bank - Vortex Shedding", Journal of Sound and Vibration, Vol. 59, pp. 263-276, 1978.

49. Weaver, D.S., and Lever, J., "Tube Frequency Effects on Cross Flow-Induced Vibrations in Arrays". Reprints for 5th Biennial Symposium on Turbulence, University of Missouri-Rolla, U.S.A., Paper IV.4, pp. IV.4-1 - IV.4-8, 3-5 October 1977.

50. Hill, R.S., and Armstrong, C., "Aerodynamic Sound in Tube Banks", Proc. Phys. Soc., 79, Part 1, pp. 225-227, January 1962.

51. Chen, Y.N., "Fluctuating Lift Forces of the Karman Vortex Streets on Single Circular Cylinders and in Tube Bundles", Trans. ASME J. Eng. Ind., 94, Series B, 2, pp. 623-628, May 1972.

52. Morse, P.M., "Vibration and Sound", 2nd ed., McGraw Hill, pp. 398, 1968.

53. Funakawa, M., and Umakoshi, R., "The Acoustic Resonance in Tube Bank", Bull. JSME, 13,57, pp. 348-355, March 1970.

54. Zdravkovich, M.M., and Nuttall, J.A., "On the Elimination of Aerodynamic Noise in a Staggered Tube Bank", J. of Sound and Vibration, 34(2), pp. 173-177, May 22, 1974.

55. Chen, Y.N., "Vibration in Tube Cluster due to Bernard-Karman Streets", C.R. des 8e Journ. de l Hydraul: Instability in Hydraulics and Fluid Mechanics, Lille, Soc. Hydrotech. de France, Vol. 1, pp. 238-246 (In French; English Summary Vol. 2, pp. 565), 8-10 June 1964.

56. Roberts, B.W., "Low Frequency, Aeroelastic Vibrations in a Cascade of Circular Cylinders", Mechanical Engineering Science Monograph, No. 4, Sept. 1966.

57. Chen, Y.N., "The Orbital Movement and the Damping of the Fluidelastic Vibration of Tube Banks due to Vortex Formation, Part 2, Criterion for the Fluidelastic Orbital Vibration of Tube Arrays", Trans. ASME, Vol. 96, Series B, No. 3, pp. 1065-1071, August 1974.

58. Chen, Y.N., "The Sensitive Tube Spacing Region of Tube Bank Heat Exchangers for Fluid-Elastic Coupling in Cross Flow", Fluid Structure Interaction Phenomena in Pressure Vessel and Piping Systems, ASME, ed. M.K. Au-Yang, and J. Brown, Jr., pp. 1-18, 1977.

59. Gross, H.G., "Untersuchung Aeroelastischer Schwingungsmechanismen und dureno Berucksichtigung bei der Auslegung von Rohrbundelwarmetauschern. Dissertation, Technical University of Hanover, 1975.

60. Blevins, R.D., "Fluidelastic Whirling of Tube Rows and Tube Arrays", ASME Journal of Fluids Engineering, Vol. 99, pp. 457-461, 1977.

61. Savkar, S.D., "A Note on the Phase Relationships Involved in the Whirling Instability in Tube Arrays", ASME Journal of Fluids Engineering, Dec. 1977/727.

62. Franklin, R.E., and Soper, B.M.H., "An Investigation of Fluidelastic Instabilities in Tube Bank Subjected to Fluid Cross-Flow", Trans. 4th International Conference on Structural Mechanics in Reactor Technology, San Francisco, 1977.

63. Mahrenholtz, O., "Vibrations of Tube Bundles", Practical Experiences with Flow-Induced Vibrations, eds. Naudascher, E., and Rockwell, D., Springer-Verlag, Berlin, 1980.

64. Chen, S.S., "A Mathematical Model for Cross-Flow Induced Vibrations of Tube Rows", 3rd International Conference on Pressure Vessel Technology, Part 1, pp. 415-426, 1977.

65. Chen, S.S., "Cross Flow Induced Vibrations of Heat Exchanger Tube Banks", Nuclear Engineering and Design, Vol. 47, pp. 67-86, 1978.

66. Tanaka, H., and Takahara, S., "Unsteady Fluid Dynamic Force on Tube Bundle and its Dynamic Effect on Vibration", Flow-Induced Vibration in Power Plant Components, ASME, PVP-vol. 41, ed. Au-Yang, M.K., New York, pp. 77-92, 1980.

67. Tanaka, H., and Takahara, S., "Fluid Elastic Vibration of Tube Array in Cross Flow", Journal of Sound and Vibration, Vol. 77, No. 1, pp. 19-37, 1981.

68. Tanaka, H., Takahara, S., and Ohta, K., "Flow -Induced Vibration of Tube Arrays with Various Pitch-to-Diameter Ratios", Journal of Pressure Vessel Technology, Transactions of the ASME, Vol. 104, No. 3, pp. 168-174, August 1982.

69. Chen, S.S., "Instability Mechanisms and Stability Criteria of a Group of Circular Cylinders Subjected to Cross Flow, Part I: Theory", ASME Journal of Mechanical Design, Vol. 104, ASME Paper No. 81-DET-21, 1982.

70. Chen, S.S., "Instability Mechanisms and Stability Criteria of a Group of Circular Cylinders Subjected to Cross-Flow; Part II: Numerical Results and Discussions", ASME Journal of Mechanical Design, Vol. 104, ASME Paper No. 81-DET-22, 1982.

71. Price, S.J., and Paidoussis, M.P., "Fluidelastic Instability of an Infinite Double Row of Circular Cylinders Subject to a Uniform Cross Flow", ASME Journal of Mechanical Design, Vol. 104, ASME Paper No. 81-DET-24, 1982.

72. Weaver, D.S., and Schneider, W., "The Effect of Flat Bar Supports on the Cross-Flow Induced Response of Heat Exchanger U-Tubes", ASME Paper No. 82-JPGC-NE-12, 1982.

73. Grover, L.K., "Cross Flow-Induced Vibration Deep Inside a Closely Packed Tube-Bank", Ph.D. Thesis, McMaster University, 1977.

74. Weaver, D.S., and ElKashlan, M., "On the Number of Tube Rows Required to Study Cross-Flow Induced Vibrations in Tube Banks", Journal of Sound and Vibration, Vol. 75, pp. 265-273, 1981.

75. Southworth, P.J., and Zdravkovich, M.M., "Effect of Grid-Turbulence on the Fluidelastic Vibrations of In-Line Tube Banks in Cross Flow", Journal of Sound and Vibration, 39 (4), pp. 461-469, 1975.

76. ElKashlan, M., "Tube Row and Damping Parameter Effects on Tube-Array Stability", M.Eng. Thesis, McMaster University, 1980.

77. Abd-Rabbo, A., "Flow Visualization and Dynamics of Heat Exchanger Tube Arrays in Water Cross-Flow", Ph.D. Thesis submitted August 1984, Dept. of Mechanical Engineering, McMaster University.

78. Dye, R.C.F., and Abrahams, C.G.M., "An Investigation of the Aerodynamic Stability of a Cross-Flow Type Finned Tube Heat-Exchanger", ASME Paper No. 68-WA/HT-19.

79. Walker, W.M., and Reising, G.F., "Flow-Induced Vibrations in Cross-Flow Heat-Exchangers", Chemical and Process Engineering, pp. 95-103, Nov. 1968.

80. Fitzpatrick, J.A., "A Study of Flow and Acoustic Phenomena in Tube Banks", Ph.D. Thesis, The Queen's University of Belfast, 1976.

81. Borges, A.R.J., "Vortex Shedding Frequencies of the Flow Through Two-Row Banks of Tubes", J. of Mechanical Engineering Science, 11, No. 5, pp. 498-502, 1969.

82. Heinecke, E., "Stationary and Instationary Flow Phenomena in and Behind Staggered and In-line Tube Banks", Proceedings of UKAEA/NPL International Symposium on Vibration Problems in Industry, Keswick, U.K., Paper No. 412, 1973.

83. Fitzpatrick, J.A., and Donaldson, I.J., "Row Depth Effects on Turbulence Spectra and Acoustic Vibrations in Tube Banks", Journal of Sound and Vibration, Volume 73 (2), pp. 225-237, 1980.

84. Lever, J.H., "A Theoretical Model for the Cross-Flow Induced Fluid-Elastic Instability in Heat Exchanger Tube Bundles", Ph.D. Thesis, McMaster University, 1983.

85. Chen, S.S., "The Instability Flow Velocity of Tube Arrays in Cross Flow", International Conference on Flow Induced Vibrations in Fluid Engineering, Reading, England, Paper F2, September 14-16, 1982.

APPENDIX A

SPECIFICATIONS OF THE INSTRUMENTS EMPLOYED

1. Tuning of a Flexible Tube in a Tube Array

(i) Capacitive Probe

M.T.I. Type ASP (Accumeasure System Probe) - 10.

(10 thou full scale range, 0.25 mm).

(ii) Distance and Vibration Meter

M.T.I. Type AS (Accumeasure System) 1000.

Supplier: The Mechanical Technology Incorporated Company, Latham, N.Y., U.S.A.

2. Vibration Pick-Up and Tuning of Instrumented Tube

(i) Strain gauges

Gauge type: CEA-09-032 UW-120

Resistance: 120 ± 0.3% Ω

Gauge factor at 75°F: 2.11 ± 1.0%

K_t: +1.2%

Temperature range: -100°F (-75°C) to +400°F (+205°C) for continuous use in static measurements.

Supplier: Micro-Measurements Division

Measurements Group

Raleigh, North Carolina, U.S.A.

(ii) Conditioning Amplifier

4-2310 Signal conditioning amplifier

Model 2360

Vishay instruments

Supplier: Intertechnology Limited

Box 219 Don Mills, Ontario

Canada, M3C 2S4

3. Fourier Analysis

Dynamic Analyzer II

Model SD 375-1

It employs the following sections (only a summary of important features, for more details refer to the user's manual):

1. Input section: A dual channel input with a maximum input of 50 Vrms, with a memory hold, frequency selection from 1 Hz to 100 kHz, level indication and overload LED.
2. Averager and storage memory section: Linear, exponential and peak.
3. System Functions Section.
4. Display Section: Built-in TV raster scan display.
5. Plotter Section: For use with an external X-Y plotter.

6. Cursor Section: Specified modes.
7. Parameters Section.
8. Output Section: On the rear panel, received on a video hard copy device, Type SD 422, for the results obtained in this thesis.

Supplier: Spectral Dynamics Corporation Company,
San Diego, California, U.S.A.

4. Oscilloscope

Tektronix, Type 564, Storage Oscilloscope with two Type 3A72 dual-trace amplifier and Oscilloscope Camera, Type C-27.

Suppliers: Tektronix, Inc., Portland, Oregon, U.S.A.

5. Recorder

Visicorder Oscillograph, Model 2106.

It is a direct writing 12-channel oscillograph that records at frequencies from D.C. to 13,000 Hz. The oscillograph uses a high-pressure mercury vapor lamp that emits high intensity ultra-violet light, which is reflected from miniature mirror galvanometers through a precision optical system into the recording paper.

Supplier: Honeywell Test Instruments Inc.,
Denver, Colorado, U.S.A.

6. Flow Measurements

(i) Pitot-Static Probe

Part No. PBC-18-G-16-KL

Supplier: United Electric Controls Ltd.,
Mississauga, Canada

(ii) Manometer

Alcohol 0.8 Sp.gr.

E8708

Supplier: R. Fuess, Berlin-Steglitz, Germany

(iii) 90° Miniature Hot-Wire Probes

DISA Type 55P14

Sensor resistance at 20°C, $R_{20} = 3.3\ \Omega$, $3.1\ \Omega$

Leads resistance, $R_L = 0.6\ \Omega$

Sensor TCR, $\alpha_{20} \simeq 0.36\%/^{\circ}C$

Measure total probe resistance, R_{TOT}, at ambient temperature, T_o, Select $T_{sensor} < 300^{\circ}C$ and calculate operating resistance, R:

$$R = R_{TOT} + \alpha_{20}\, R_{20}\, (T_{sensor} - T_o)$$

(iv) Hot-Wire Probe Support

DISA Type 55H21

(v) Constant Temperature Anemometer

DISA Type 55A01

Suppliers: DISA Elektronik A/S, DK2730,

Herlev, Denmark

(vi) Voltmeter

HP 3465A digital multimeter

Hewlett-Packard

7. Speed Control Unit

3-Phase Adjustable speed D.C. motor control systems (Ratiotrol unit)

Efficiency at maximum speed and load = 99%

System efficiency, including motor = 87%

HP = 10

Supplier: Boston Gear, Incom International Inc.

Using this system an excellent control over the entire speed range was obtained. The system consists of a control panel and a regulator.

APPENDIX B

INSTRUMENT CALIBRATION

It was necessary before conducting the experiments to check the calibration of the instruments used and to get calibration curves whenever needed. The Spectral Dynamics model SD375 Fourier Analyzer was calibrated using the following instruments:

1. Signal Generator
2. RMS Voltmeter
3. Oscillator
4. Frequency Counter
5. Band Pass Filter
6. Random Noise

The procedure for checking out the operation of the Model SD375 is well documented in the manual provided with the instrument. The instrument was found to satisfy the specifications given by the manufacturer. However, such a calibration has two fold value, as it at the same time makes the user familiar with the front and rear panels of the instrument and their operation.

On the other hand, for other instruments like the hot-wire probe, calibration is done using other instruments such as a pitot-static probe and a manometer. The calibration of the strain gauges required the use of a drill press and a strain indicator.

The following is a brief summary of the procedures followed for conducting the calibration of the strain gauges and the hot wire probes, and some of the calibration curves obtained.

1. Strain Gauge Calibration

Two strain gauges were connected together in a half bridge for the same direction on each of the instrumented tubes in order to double the sensitivity of the output.

After many trials to build a frame to perform the calibration, they all failed to give consistent results. Thus an arrangement was made using a drill press to perform the calibration. The array base was held tightly with the drill press table and a drill was used to hold the tube tip in a zero reference position. The length of the drill was small to prevent any bending of the drill and the strain gauges were balanced to zero strain in both directions. The drill press table was then used to push the tube in the specified direction and strain for that direction was recorded using the strain indicator. The output from the orthogonal direction was also recorded. This procedure was repeated for other tip positions with an increment of 0.5 mm and up to a maximum value of 4.0 mm. Higher values of displacement will mean tube-to-tube clashing with the low value of P/d used in this study. It was believed that this value is sufficient for checking the strain gauge performance. The calibration curves obtained were plotted as shown in Figure B-1. As can be seen from this Figure, motion in the x_1-direction gives output to X and Y oriented gauges. The same procedure was repeated for the motion of the same tube in the orthogonal direction (y_1-direction). The obtained values $X(y_1)$ and $Y(y_1)$ were plotted as shown in Figure B-2. In this way we were able to account for any angle difference between the position of locating the strain gauges and the direction of motion. It is clear that:

$$X(x_1) = X \cos\theta_x \quad ; \quad Y(x_1) = Y \sin\theta_y$$
$$X(y_1) = X \sin\theta_x \quad ; \quad Y(y_1) = Y \cos\theta_y$$

From the plots θ_x, θ_y were calculated, and the exact values of strain in both directions X, Y were calculated and plotted as shown in Figure B-3. No indication of major difference between both directions was noticed. The same procedure was repeated for the second instrumented tube and its calibration curves were plotted as shown in Figure B-4 to B-6.

It should be noticed that all calibration curves show a linear relation between the strain gauge output and the displacement of the tube tip, and this was the first conclusion of performing this calibration.

The small difference in the value of strain between both tubes was believed to be due to minor misalignment of strain gauges on both tubes. This output of strain was then obtained in volts using the

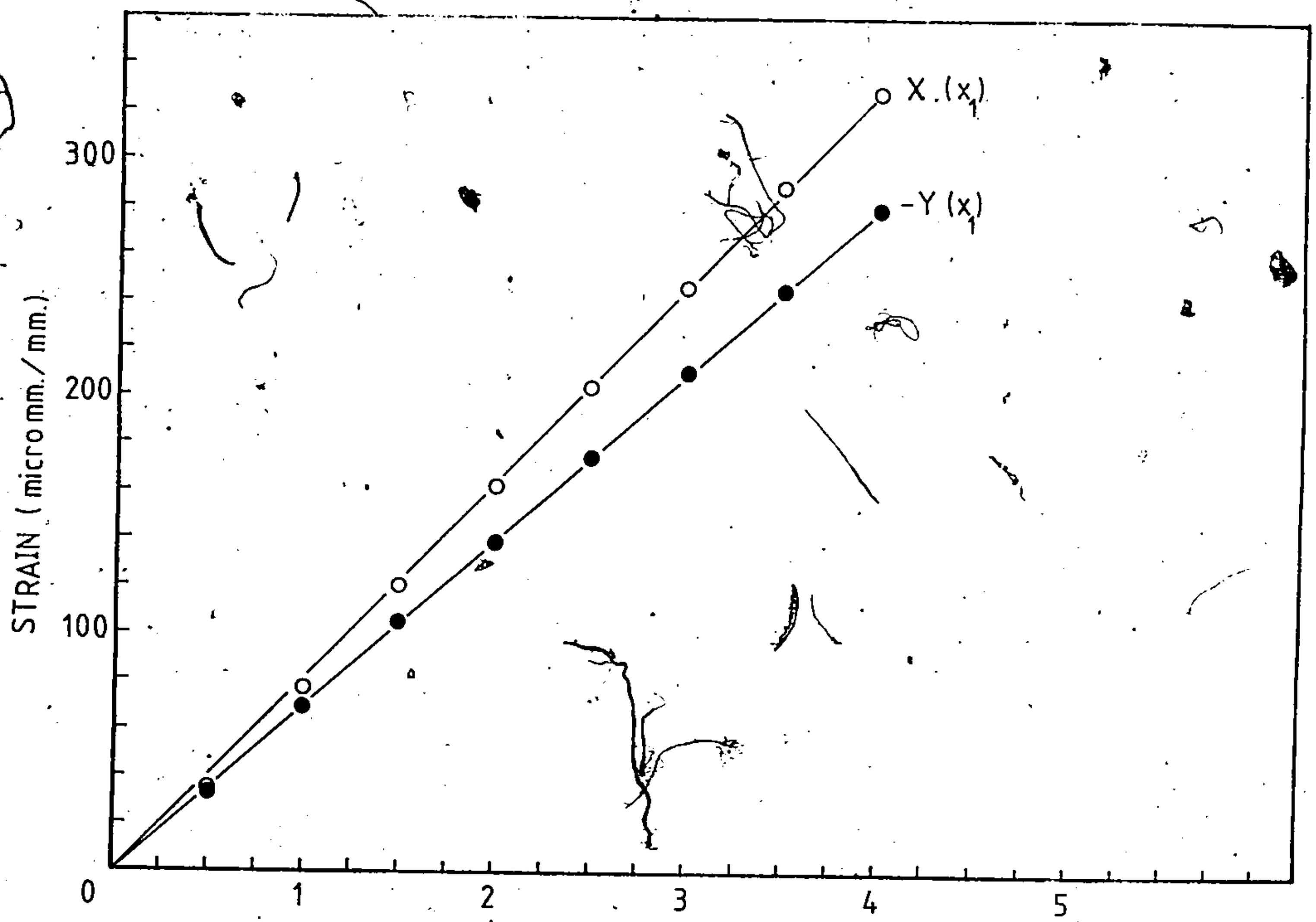
X.(x1)
-Y(x1)
STRAIN (micro mm./mm.)
300
200
100
0
1
2
3
4
5
TUBE TIP DISPLACEMENT (mm.)

FIGURE B-1

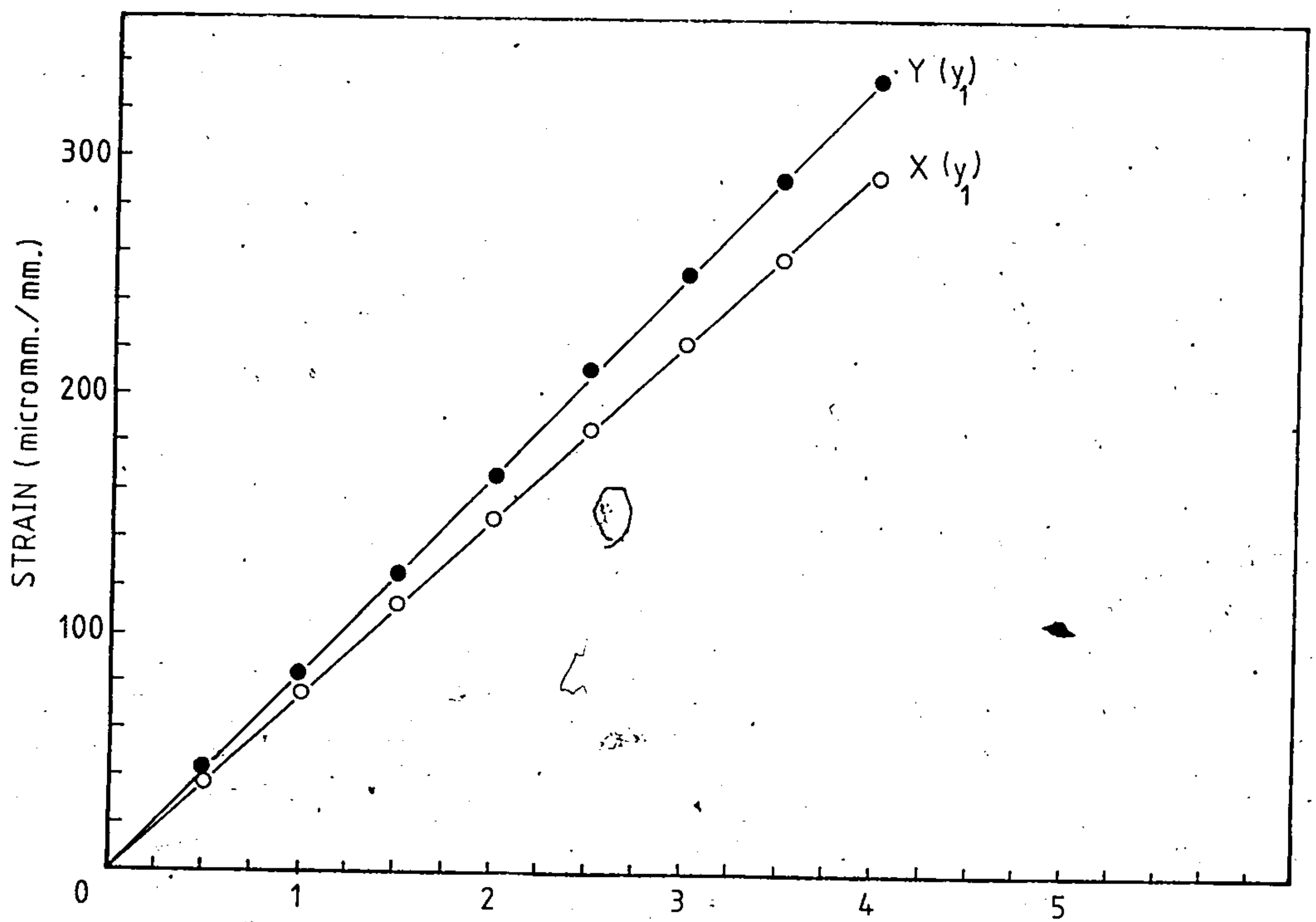

Y (y_1)
X (y_1)
STRAIN (micromm./mm.)
300
200
100
0
1
2
3
4
5
TUBE TIP DISPLACEMENT (mm.)

FIGURE B-2

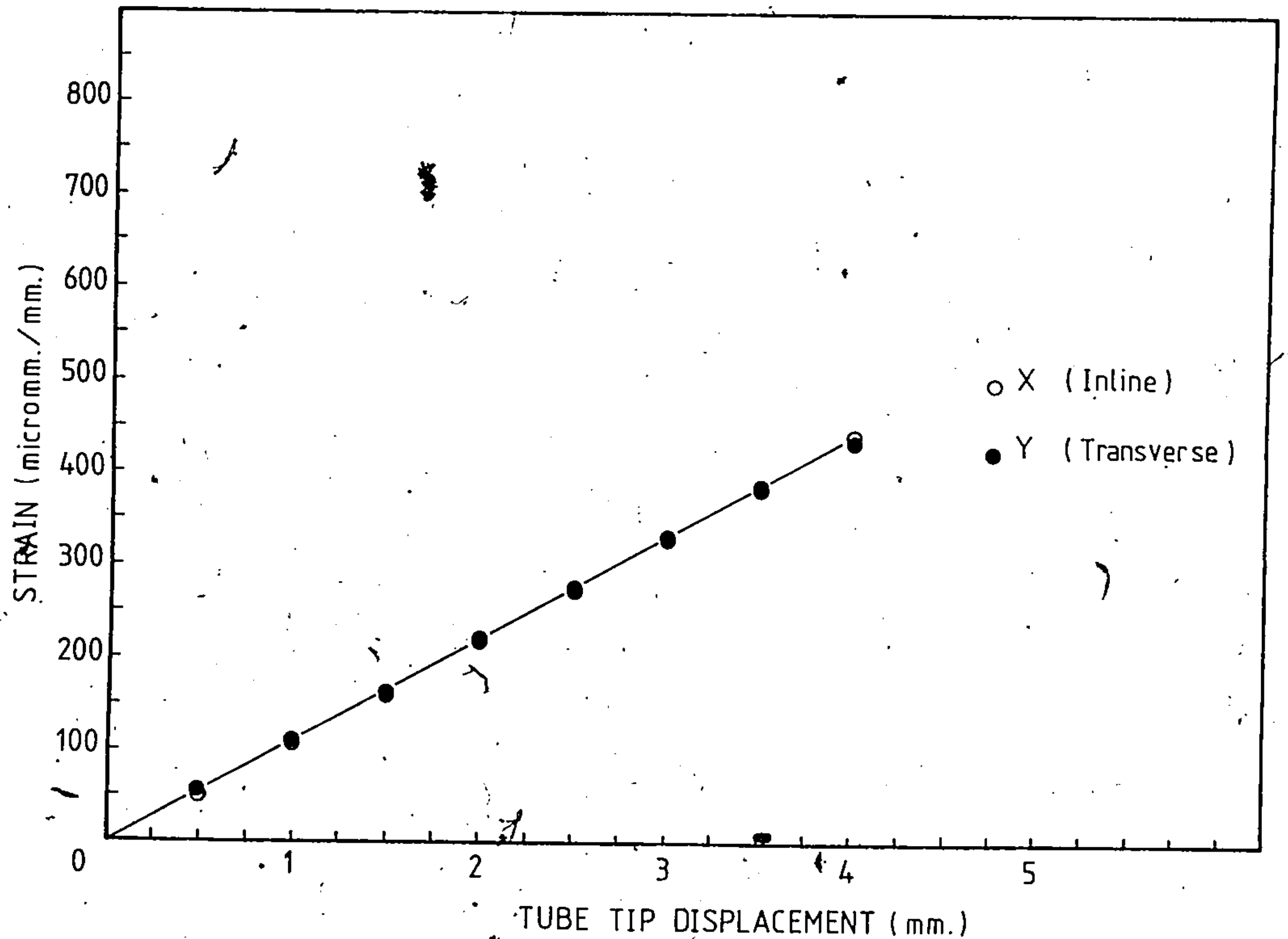
STRAIN (micromm./mm.)
800
700
600
500
400
300
200
100
0
1
2
3
4
5
TUBE TIP DISPLACEMENT (mm.)
X (Inline)
Y (Transverse)

FIGURE B - 3

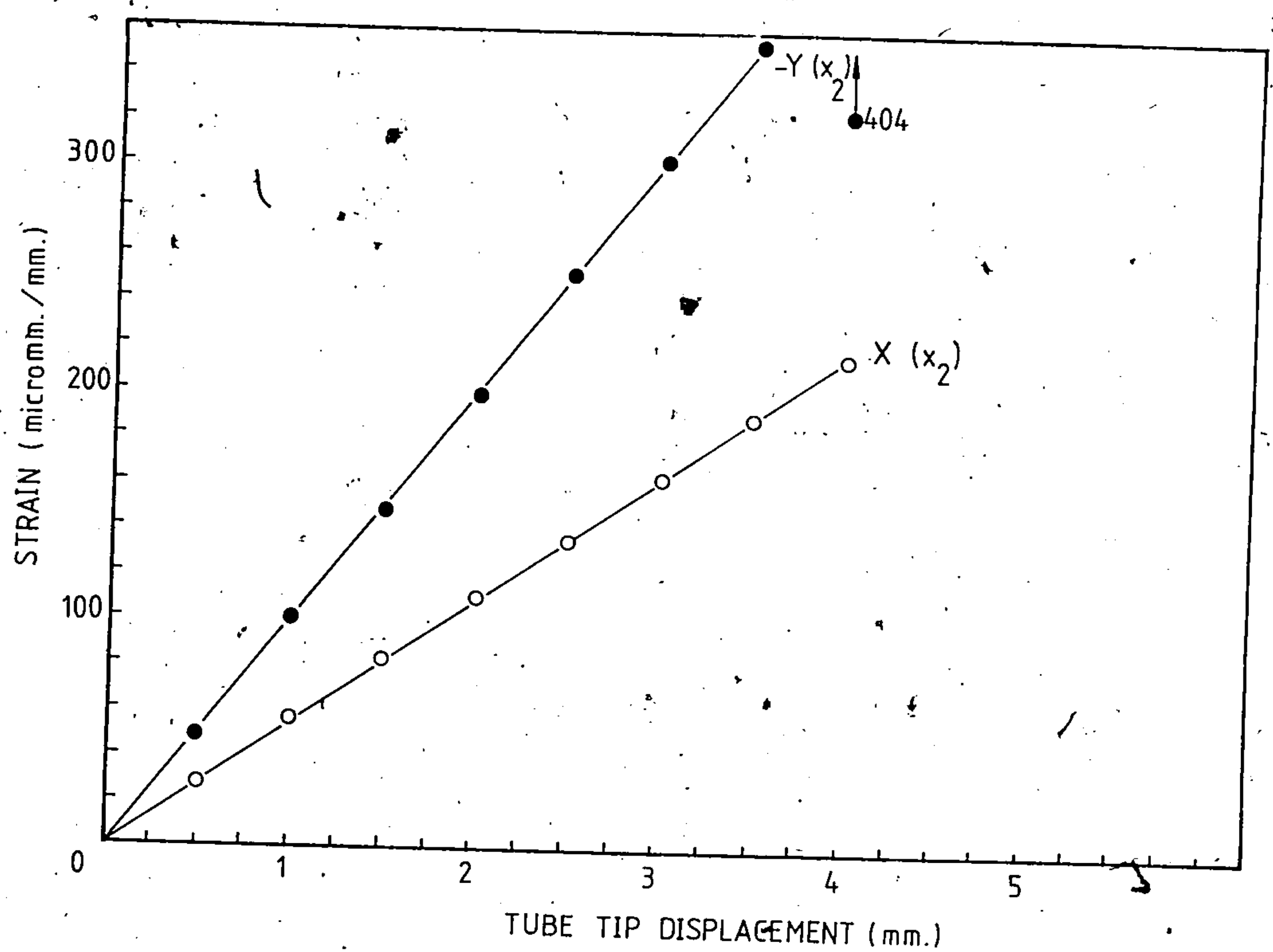
-Y (x_2)
404
X (x_2)
300
200
100
0
1
2
3
4
5
STRAIN (micromm. / mm.)
TUBE TIP DISPLACEMENT (mm.)

FIGURE B - 4

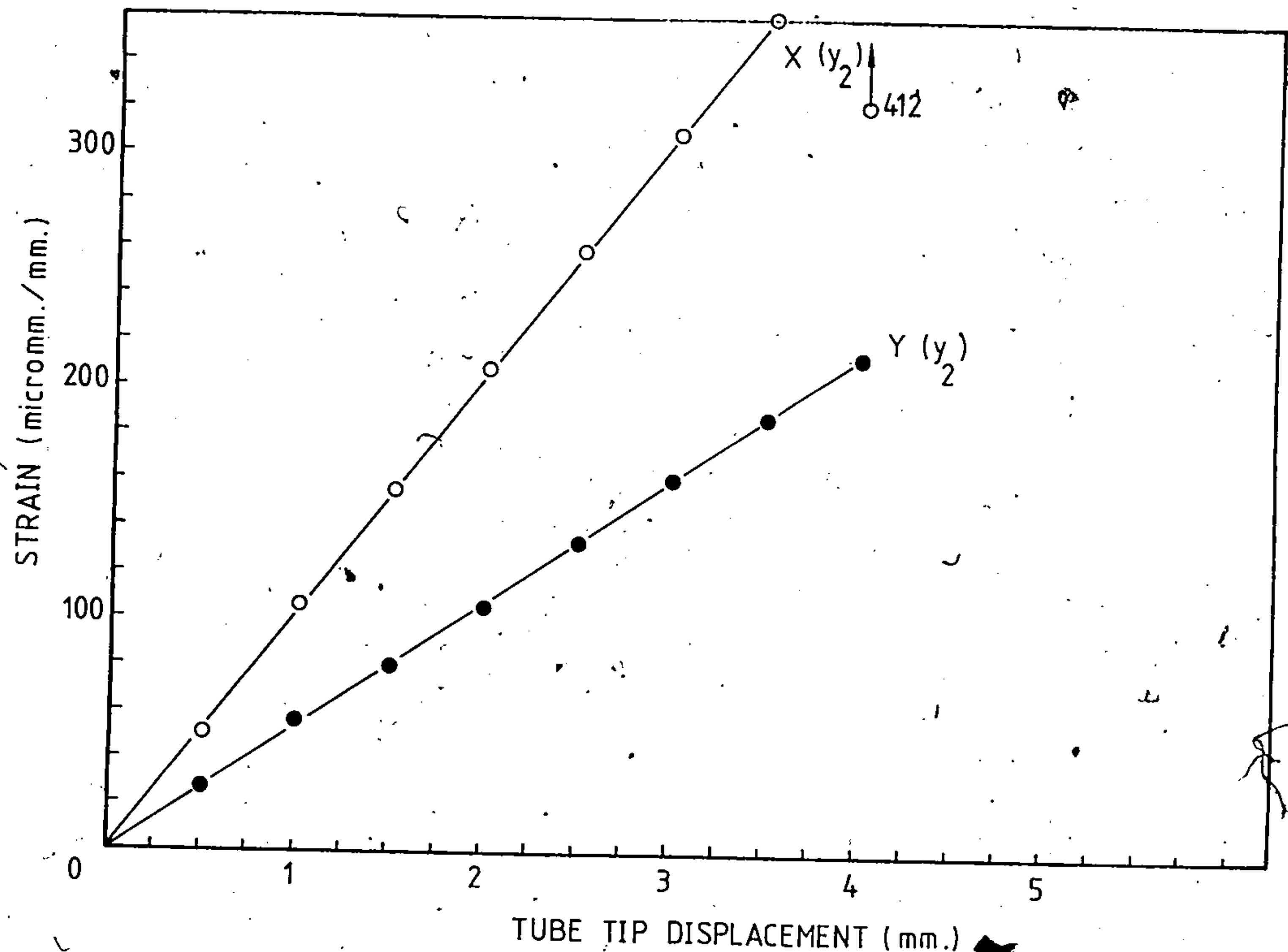

X (y_2)
412
Y (y_2)
STRAIN (micromm./mm.)
0
100
200
300
1
2
3
4
5
TUBE TIP DISPLACEMENT (mm.)

FIGURE B - 5

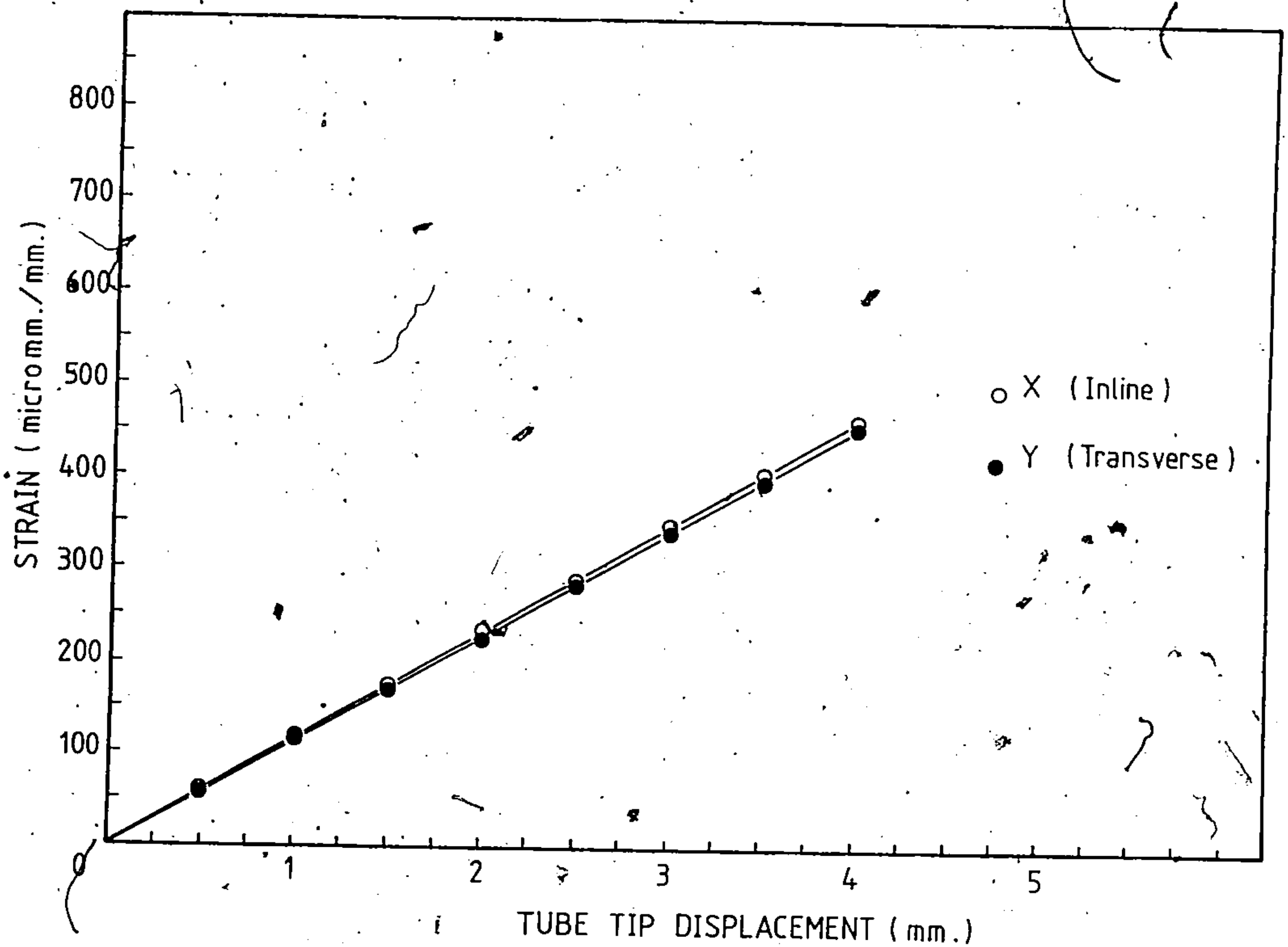
STRAIN (micromm./mm.)
800
700
600
500
400
300
200
100
0
1
2
3
4
5
TUBE TIP DISPLACEMENT (mm.)
○ X (Inline)
● Y (Transverse)

FIGURE B - 6

signal conditioning amplifier and a digital voltmeter for a few values of strain and it showed that every 2.54 cm = 0.063 volt.

It was most important to check the frequency of the flexible tubes and the alignment of the array before this calibration was started.

2. Hot-wire Probe Calibration

For the purpose of calibrating the hot-wire probes which are used for measuring the upstream flow velocity and the gap velocity between tubes in the air tunnel, an existing calibration nozzle which has a low turbulence potential core 2.0 cm. in diameter was used. A schematic view of the nozzle is shown in Figure B-7. The nozzle gives a uniform flow field of good accuracy and having a contour suitable for an air-tunnel contraction design with a curvature designed to give a flat velocity profile at the exit.

The specifications of the hot-wire probes are:

R_{20} = 3.3 and 3.1 Ω (sensor resistance at 20°C) respectively
R_L = 0.6 Ω (Lead resistance)
α_{20} = 0.36%/°C
T_{sensor} < 300°C (a value to be selected)
R_{Total} = 3.68 Ω (measured)
T_{actual} = 21.8°C (varies with time)

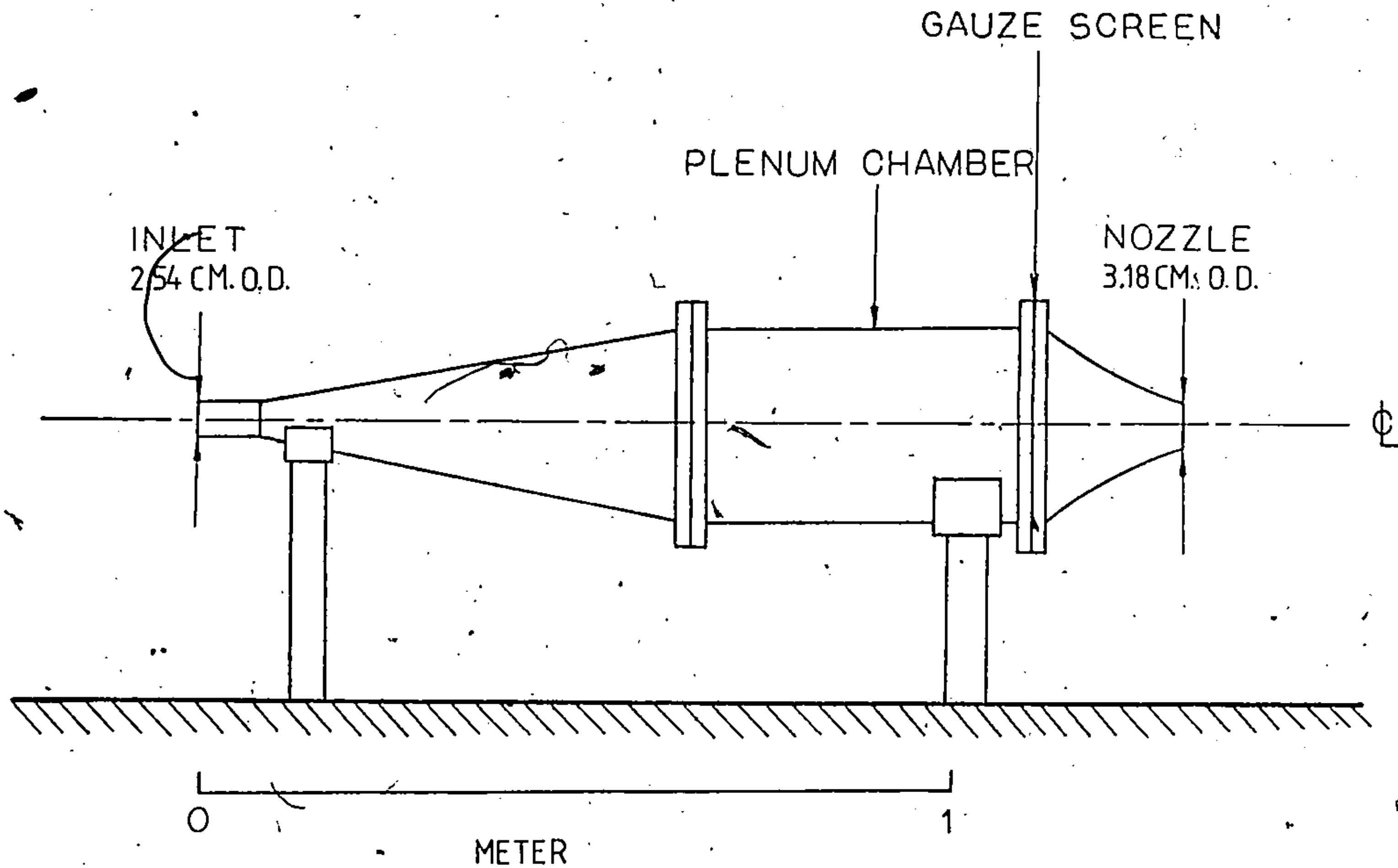

THE CALIBRATION NOZZLE

FIGURE B-7

The formula used for calculating the operating resistance is,

$$R = R_{TOT} + \alpha_{20} * R_{20} \; (T_{sensor} - T_{actual})$$

As can be seen from this formula, a constant value of 6.0 Ω for the operating resistance can be selected, provided that this resistance setting on the DISA constant temperature anemometer during the calibration is the same during the experiments. The output from the DISA constant temperature anemometer will be in volts and for accurate readings of this output a digital voltmeter is used.

A pitot-tube and the hot-wire probe were mounted side by side at the exit to the nozzle. An alcohol inclined manometer was used for measuring the flow velocity out of the pitot-probe together with the formula:

$$\text{flow velocity} \quad V = 11.47 \sqrt{\Delta h \text{ (cm of alcohol)}} \qquad \text{m./sec.}$$

A steady air flow through the calibration nozzle was established for each run of the blower. The output of the hot-wire probe (volts) and the flow velocity (m./sec.) were obtained for the range of blower speeds and a calibration curve was plotted as shown in Figure B-8. The linear relation between the square root of the pitot-static probe output (flow velocity) and the square of the hot-wire probe output was calculated and plotted as shown in Figure B-9. This line was used to obtain the flow velocities at low and high values of flow velocities and which could not be obtained during the course of

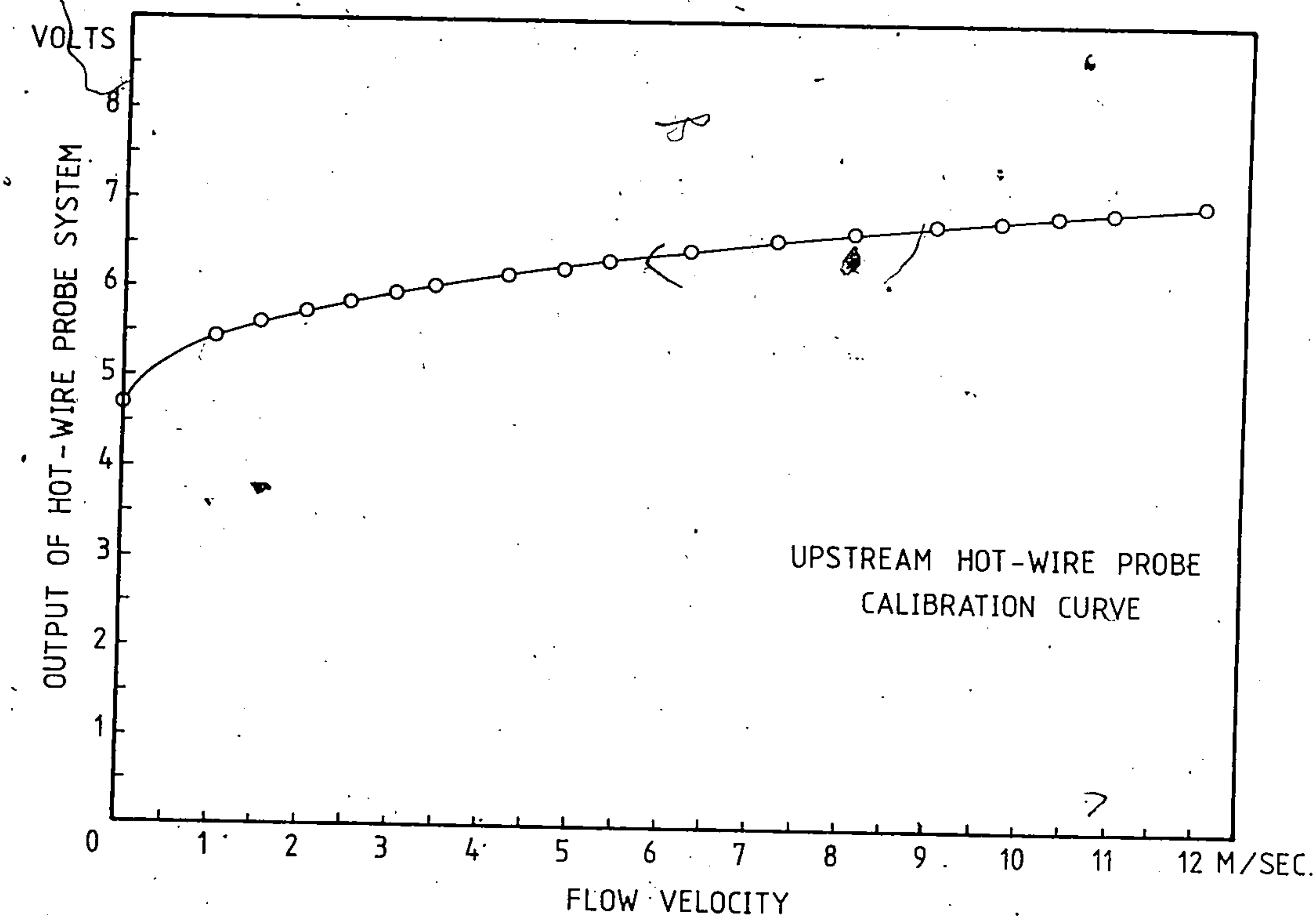
VOLTS
OUTPUT OF HOT-WIRE PROBE SYSTEM
0
1
2
3
4
5
6
7
8
9
10
11
12 M/SEC.
UPSTREAM HOT-WIRE PROBE
CALIBRATION CURVE
FLOW VELOCITY

FIGURE B-8

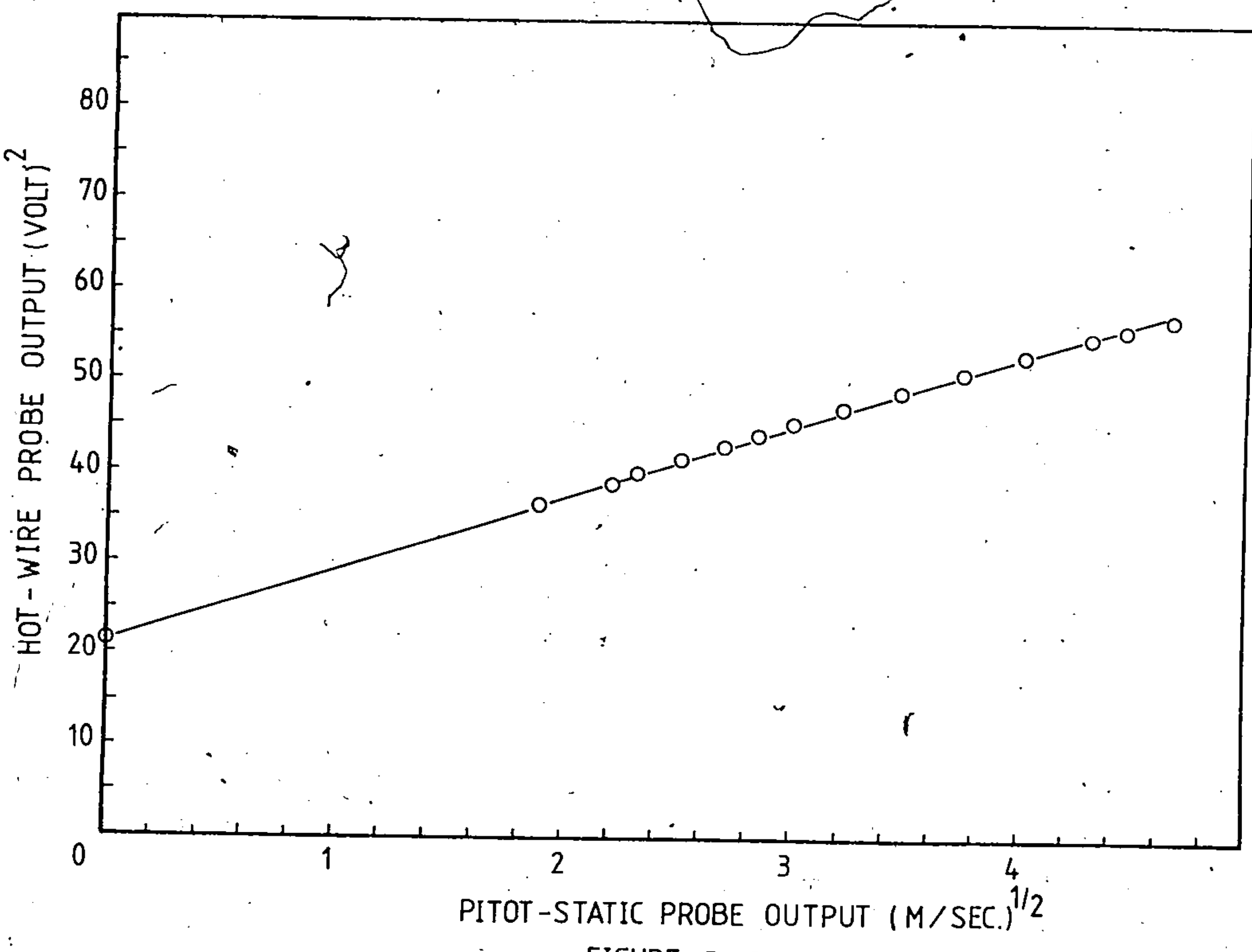
HOT-WIRE PROBE OUTPUT (VOLT)^2
80
70
60
50
40
30
20
10
0
1
2
3
4
PITOT-STATIC PROBE OUTPUT (M/SEC.)$^{1/2}$

FIGURE B-9

the calibration due to the limited capability of the instruments used. The same procedure was repeated with the hot-wire probe used for measuring the flow velocity in the gap between tubes. The results are shown in Figures B-10 and B-11.

The calibration of the hot-wire probes was checked many times during the course of the experiments and was found to be the same. A minor difference was noted in the hot-wire probes output readings with the flow velocity is zero and a new set of calibration curves was obtained. This difference was believed to be due to some change in room temperature. However, such a difference didn't affect the calibration very much. Also, due to the damage of one of the hot-wire probes during the course of the experiments, a new calibration curve was obtained.

The last set of these calibration curves is the one represented in this thesis.

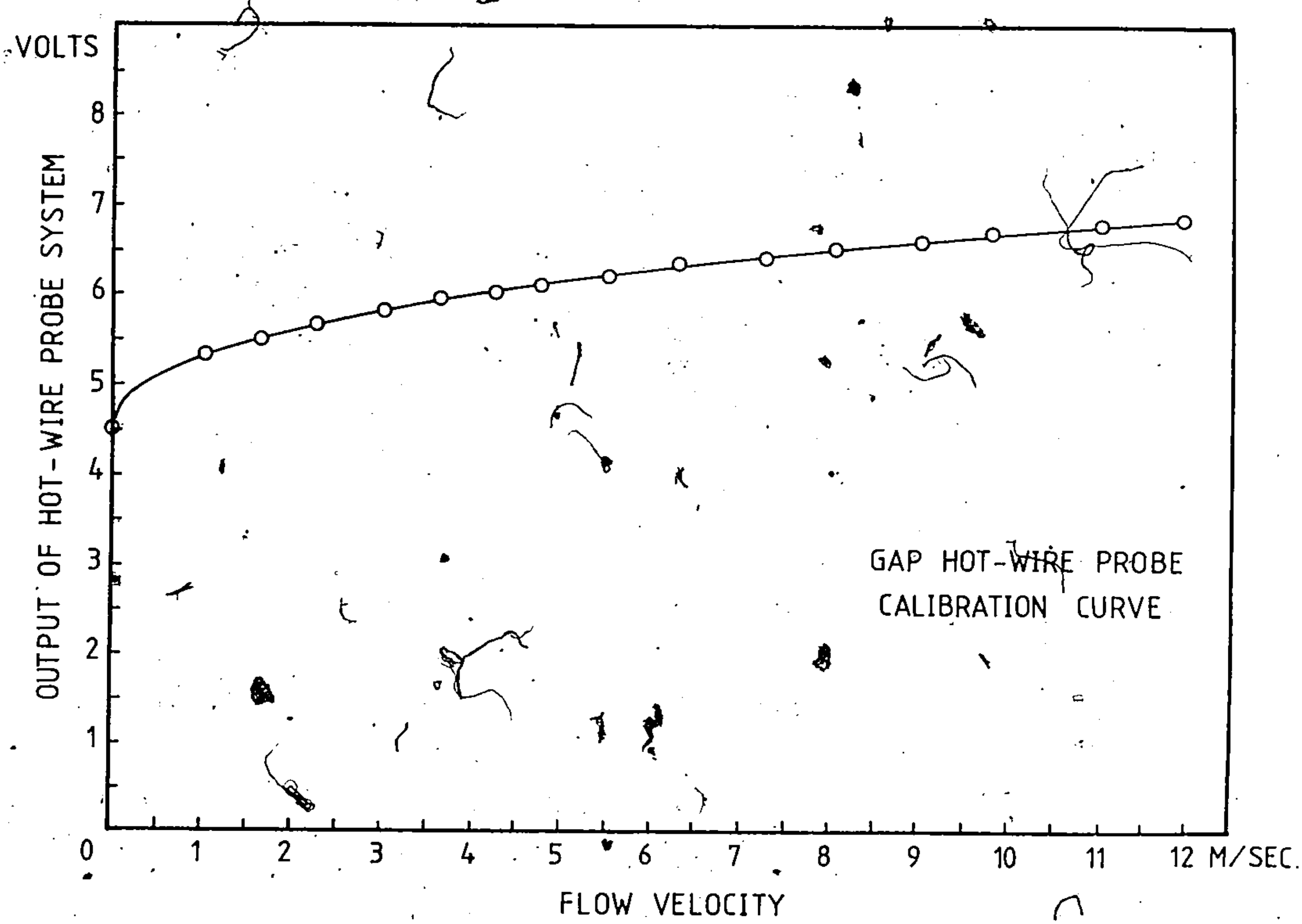
VOLTS
OUTPUT OF HOT-WIRE PROBE SYSTEM
8
7
6
5
4
3
2
1
0
1
2
3
4
5
6
7
8
9
10
11
12 M/SEC.
FLOW VELOCITY
GAP HOT-WIRE PROBE
CALIBRATION CURVE

FIGURE B-10

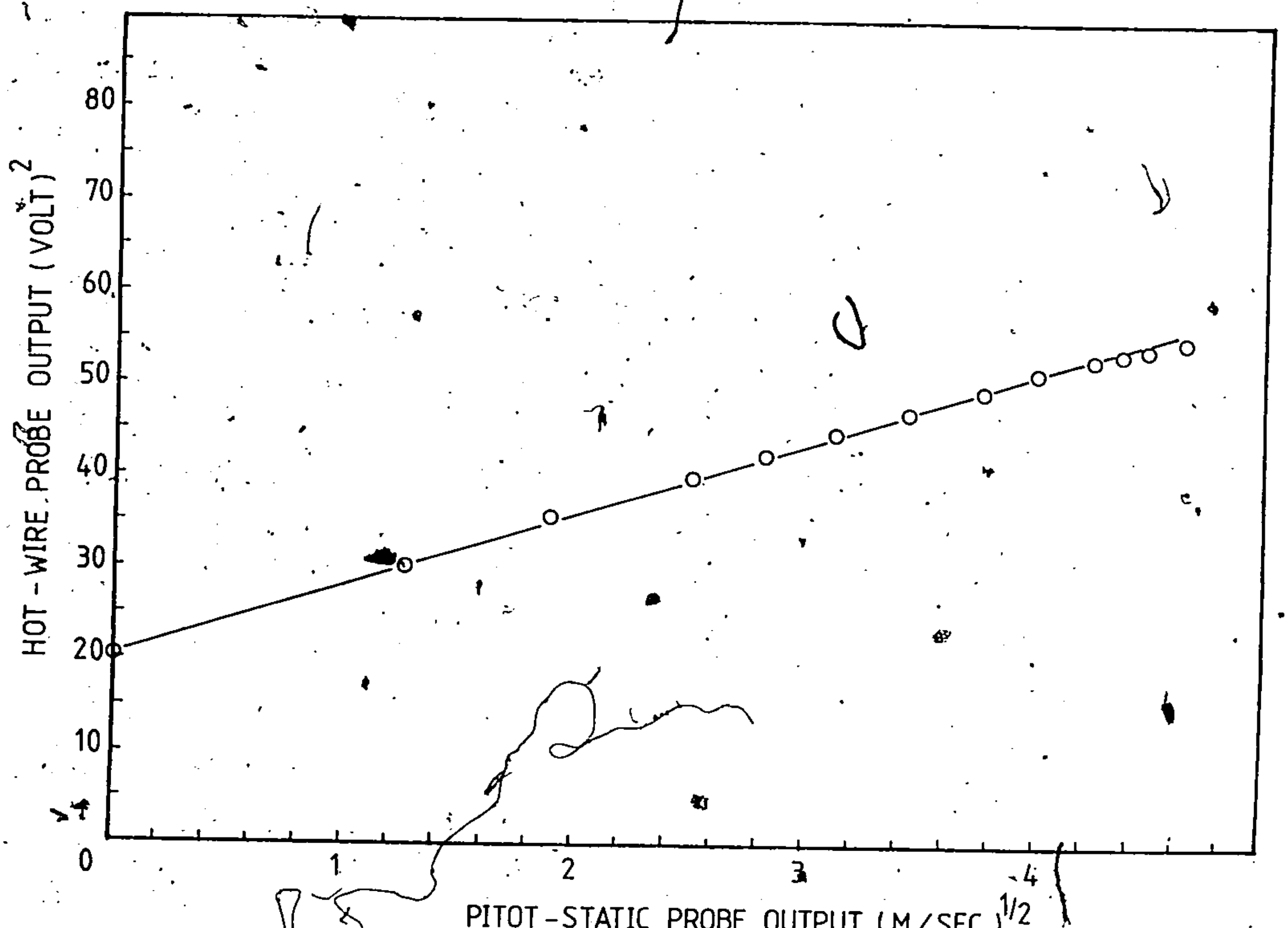

HOT - WIRE PROBE OUTPUT (VOLT)^2
80
70
60
50
40
30
20
10
0
1
2
3
4
PITOT - STATIC PROBE OUTPUT (M / SEC.)$^{1/2}$

FIGURE B - 11

APPENDIX C

RATIOS BETWEEN GAP AND UPSTREAM FLOW VELOCITIES

One of the problems which face researchers who are trying to compare their results with other available experimental results is the exact flow velocity on which the results are based. Usually, the results are not based on the upstream flow velocity, measured upstream of the tube array as this does not reflect the real velocity exposed to the tubes. Rather the flow velocity in the gap between tubes is used. There are various definitions for obtaining the gap flow velocity used by different groups of researchers. The following is intended to clarify the various definitions and demonstrate one of the reasons for not having a consistent comparison between different available results for arrays having the same geometry and dimensions. The comparison between different definitions is limited only to the arrays used in this thesis.

1. Pitch Velocity, V_p:

The pitch velocity defining the velocity in the gap between tubes is defined as:

$$V_p = \frac{P}{P-d} V_u$$

where P is the pitch, d is the tube outside diameter, and V_u is the upstream flow velocity. The definition for pitch velocity is used for all arrays regardless of their geometry. Values of different ratios for arrays used in this thesis are given in Table C-1.

2. Theoretical Gap Velocity, V_g:

This definition is based on the theoretical mean velocity in the smallest gap between tubes for the different geometries of tube arrays.

(i) $V_g = \frac{P}{P-d} V_u$ for normal square arrays,

(ii) $V_g = \frac{\sqrt{2}}{2} \frac{P}{P-d} V_u$ for rotated square arrays,

(iii) $V_g = \frac{P}{P-d} V_u$ for normal triangular arrays,

(iv) $V_g = \frac{\sqrt{3}}{2} \frac{P}{P-d} V_u$ for parallel triangular arrays.

It is easy to see that for rotated square and parallel triangular arrays, the gap velocity is less than that defined by the pitch velocity. Ratios are given in Table C-1.

TABLE C-1

Ratios between gap and upstream flow velocities.

Geometry	Pitch Ratio	V_p/V_u	V_g/V_u	V_{gm}/V_u
Normal Square	1.33	4.03	4.03	4.00
	1.50	3.00	3.00	3.42
Rotated Square	1.414	3.42	2.41	2.86
	1.70	2.43	1.72	2.08
Normal Triangle	1.33	4.03	4.03	4.84
	1.50	3.00	3.00	3.04
Parallel Triangle	1.375	3.67	3.17	3.70
	1.73	2.37	2.05	2.28

3. <u>Experimental Gap Velocity, V_{gm}:</u>

This represents the flow velocity measured experimentally using the hot-wire probe in the minimum gap between tubes. Those values given in Table C-1, are the result of the present research and have never been published before. The exact locations for the hot-wire probe are those used for measuring the interstitial flow frequency spectra. The results obtained are plotted in Figures C-1 to C-8. Large fluctuations were noticed in the gap flow velocity especially at low flow velocities. The higher values of flow velocities measured experimentally over those determined theoretically are believed to be due to the velocity profiles being parabolic rather than flat. It should be noted that most of these arrays showed higher gap flow velocities at low Reynolds numbers than those represented by the linear relationship given. This is probably due to the shape of the velocity profile. At low Reynolds numbers, the velocity profile is expected to be more parabolic in shape with a peak velocity considerably higher than the theoretical average velocity. At higher Reynolds numbers, turbulence becomes fully developed and the velocity profile is expected to flatten out somewhat. While the measured gap flow velocity may be physically significant, it is not known for most arrays. Therefore, the experimental average velocity was used for calculating the ratio V_{gm}/V_u and the gap Strouhal numbers S_{gm}.

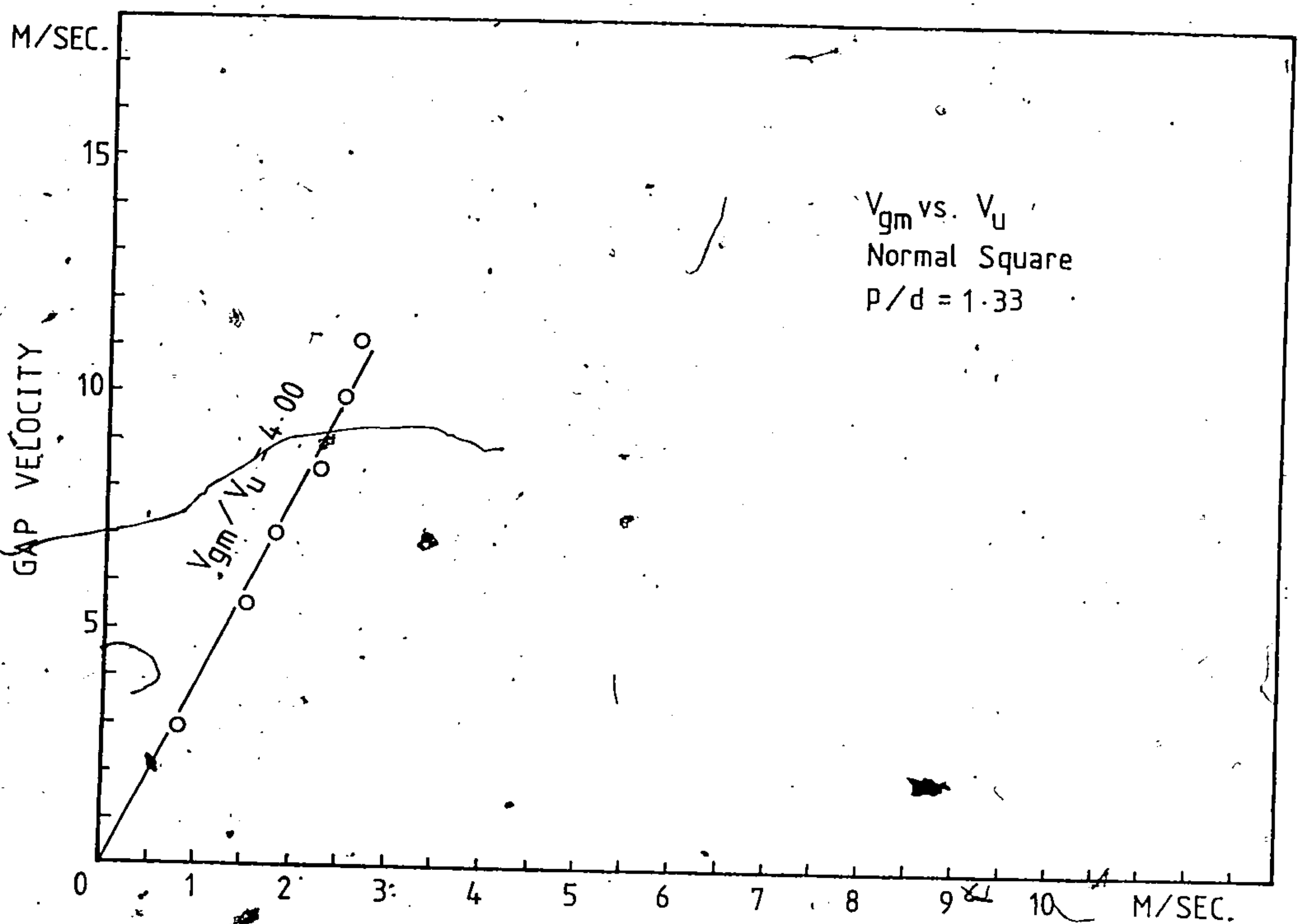
M/SEC.
15
10
5
0
GAP VELOCITY
1
2
3
4
5
6
7
8
9
10
M/SEC.
UPSTREAM VELOCITY
$V_{gm}/V_u = 4.00$
V_{gm} vs. V_u
Normal Square
P/d = 1·33

FIGURE C-1

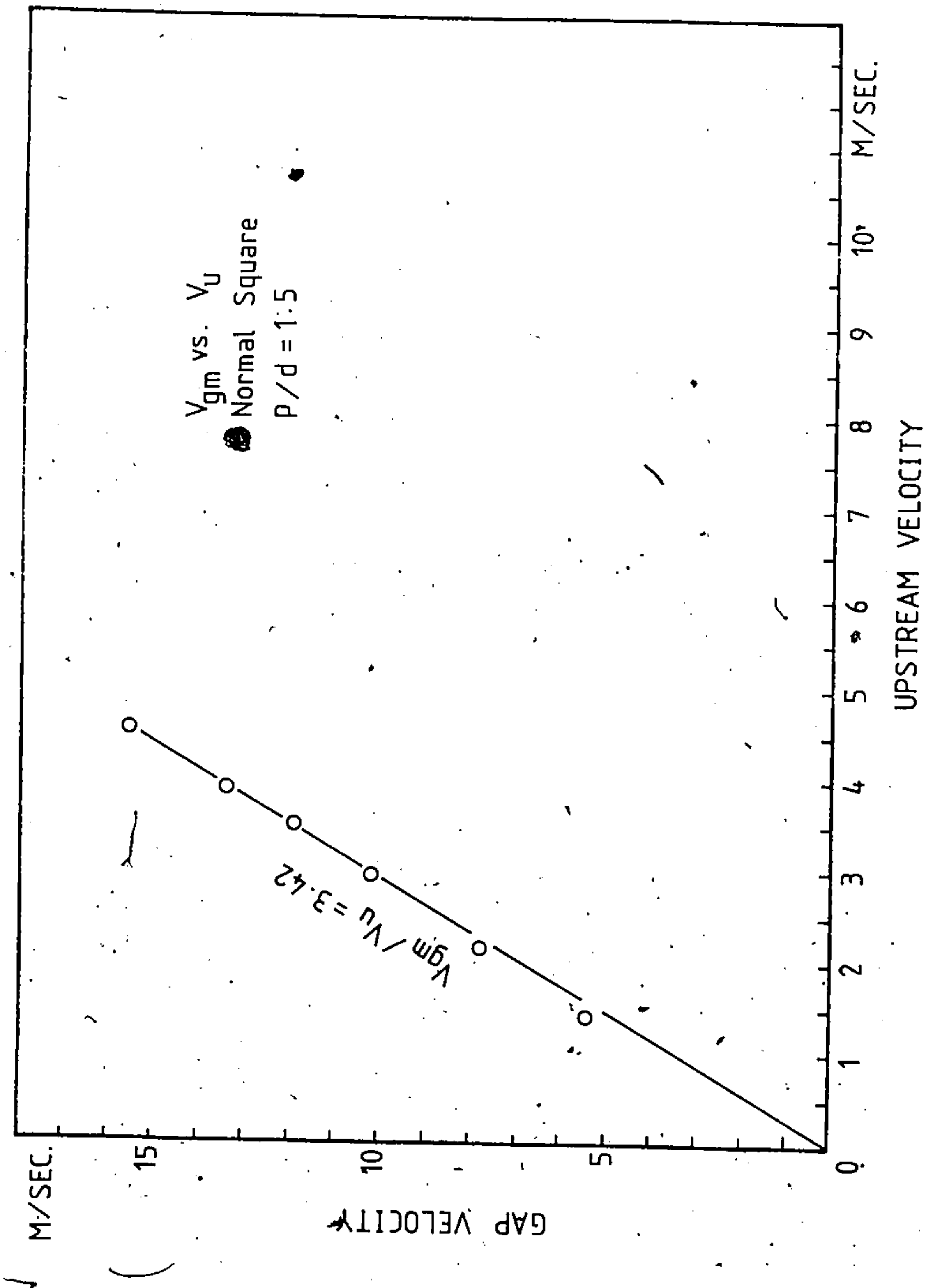

V_{gm} vs. V_U
Normal Square
P/d = 1:5
$V_{gm}/V_u = 3.42$
GAP VELOCITY
M/SEC.
UPSTREAM VELOCITY
M/SEC.
0
5
10
15
1
2
3
4
5
6
7
8
9
10

FIGURE C -2

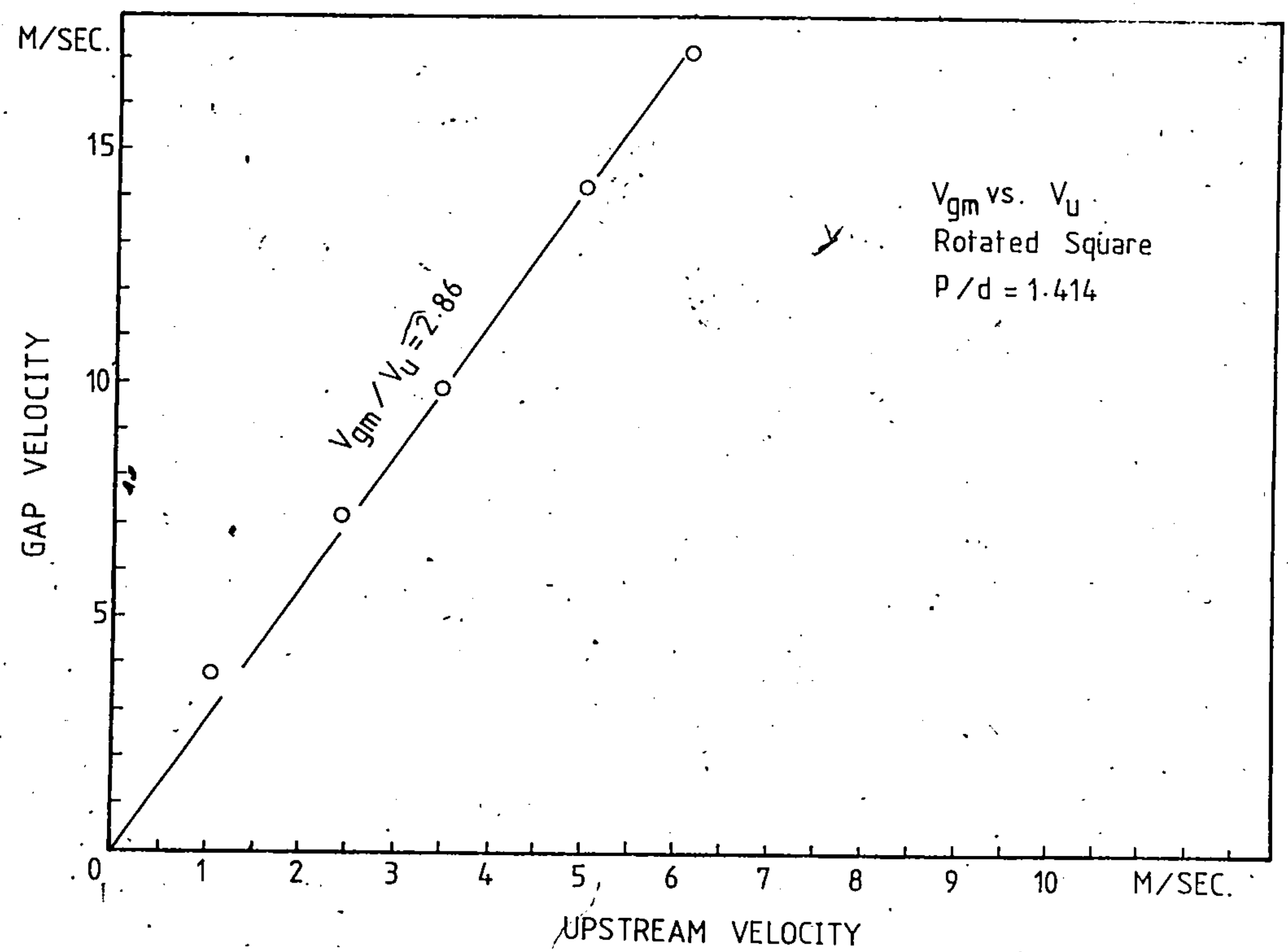
M/SEC.
15
10
5
0
GAP VELOCITY
1
2
3
4
5
6
7
8
9
10
M/SEC.
UPSTREAM VELOCITY
$V_{gm}/V_u = 2.86$
V_{gm} vs. V_u
Rotated Square
P / d = 1.414

FIGURE C-3

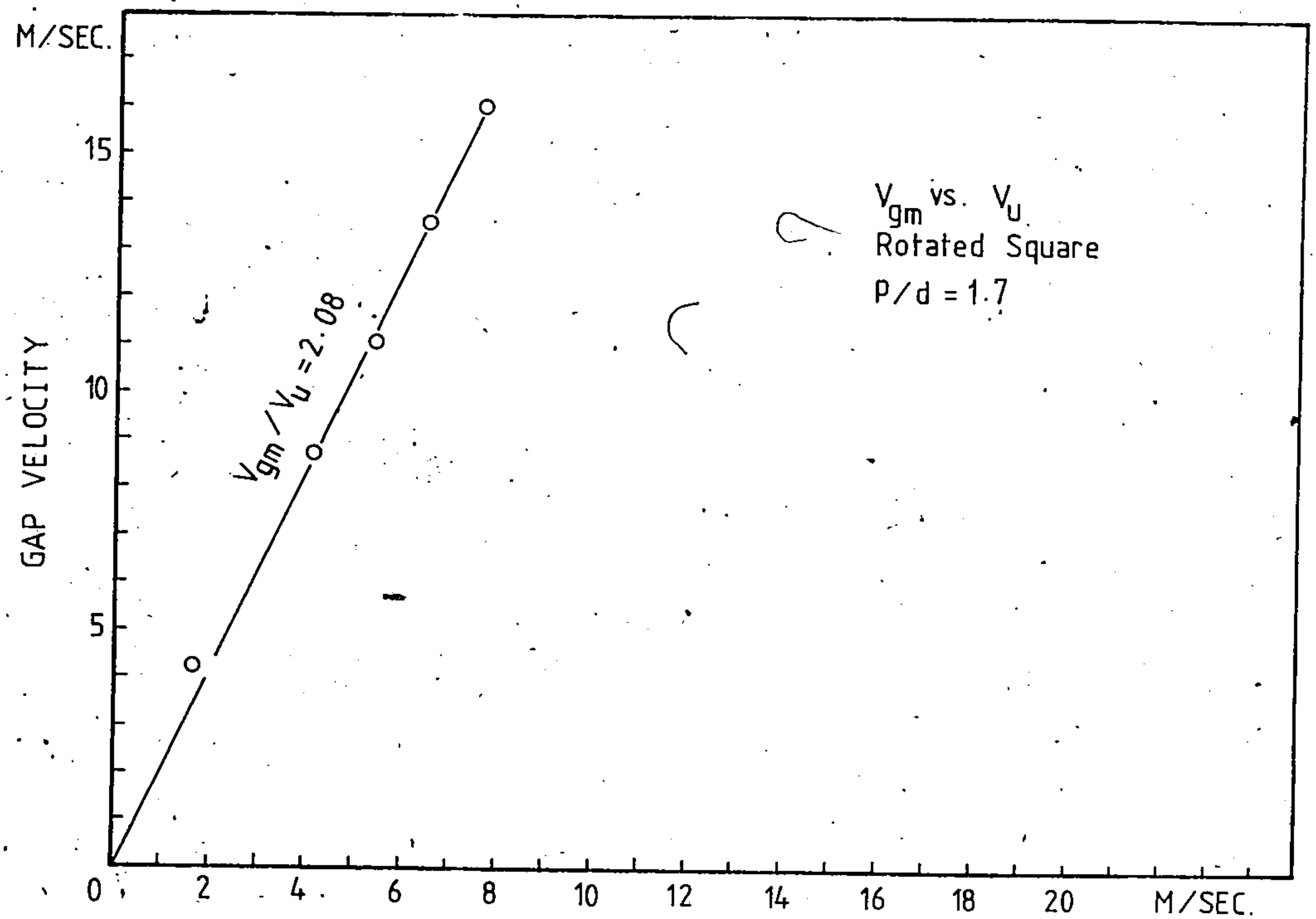

UPSTREAM VELOCITY

FIGURE C-4

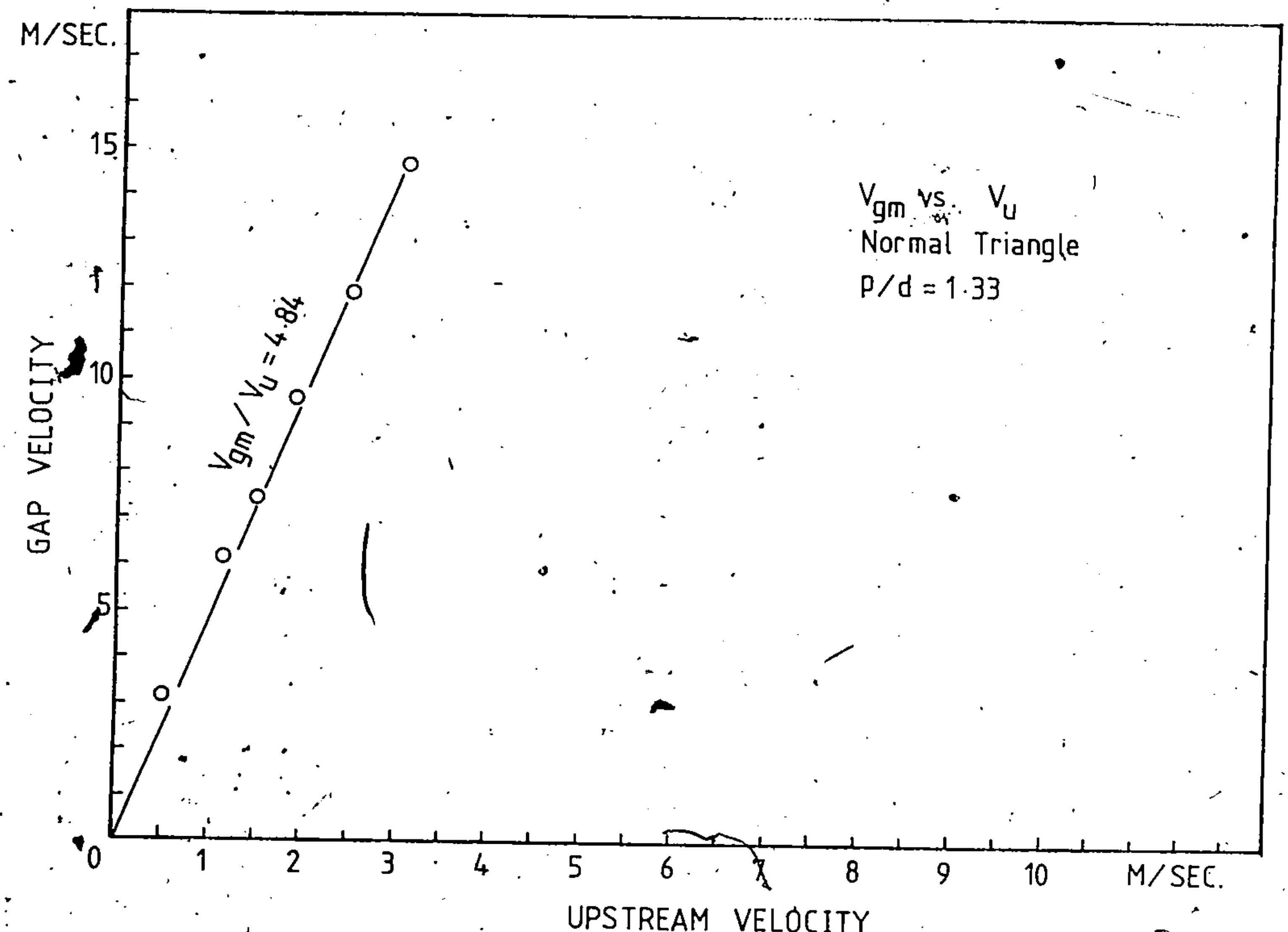
M/SEC.
15
10
5
0
GAP VELOCITY
$V_{gm}/V_u = 4.84$
V_{gm} vs. V_u
Normal Triangle
P/d = 1.33
1
2
3
4
5
6
7
8
9
10
M/SEC.
UPSTREAM VELOCITY

FIGURE C-5

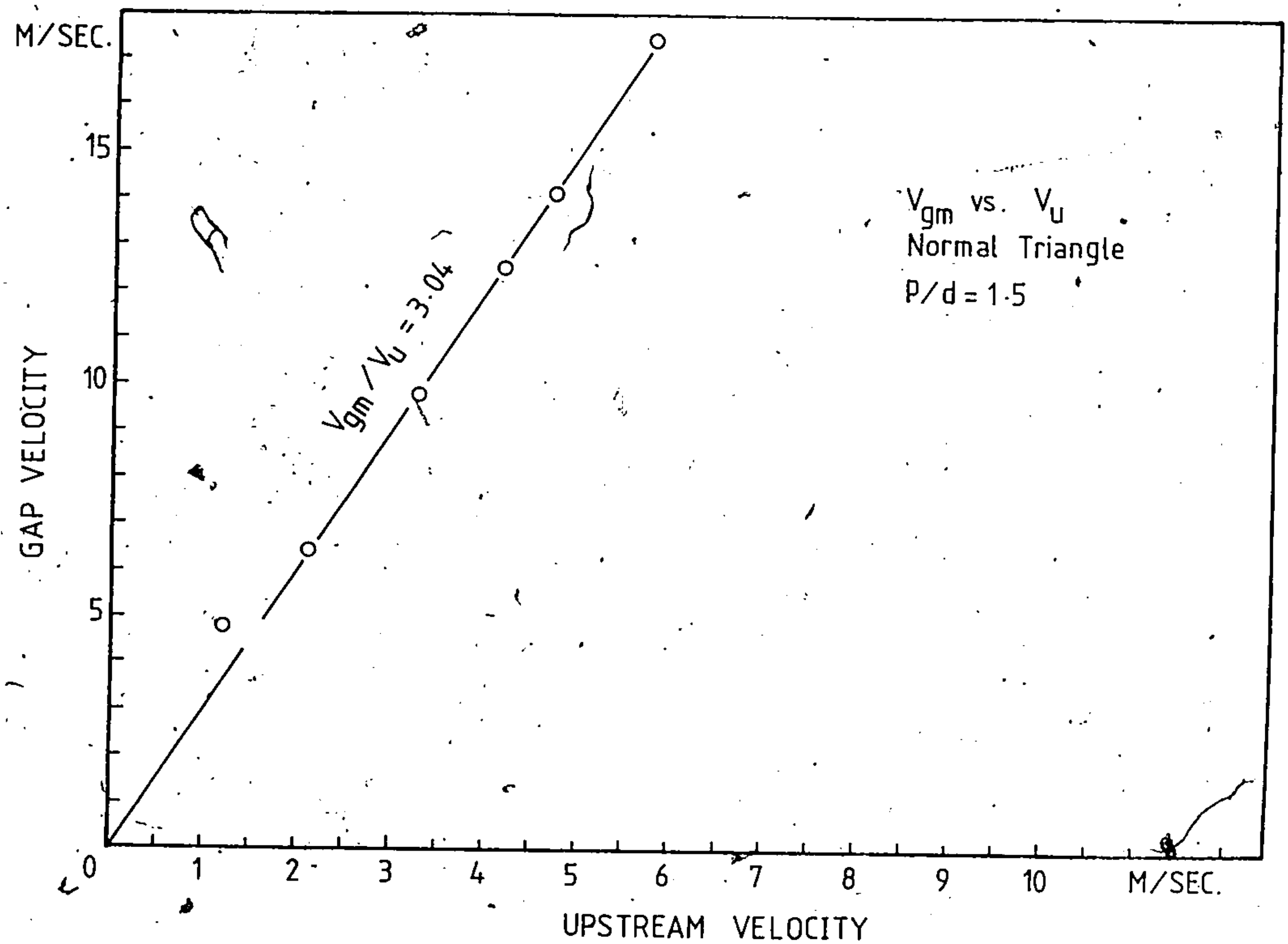
M/SEC.
15
10
5
0
GAP VELOCITY
V_{gm} vs. V_u
Normal Triangle
P/d = 1.5
$V_{gm}/V_u = 3.04$
1
2
3
4
5
6
7
8
9
10
M/SEC.
UPSTREAM VELOCITY

FIGURE, C-6

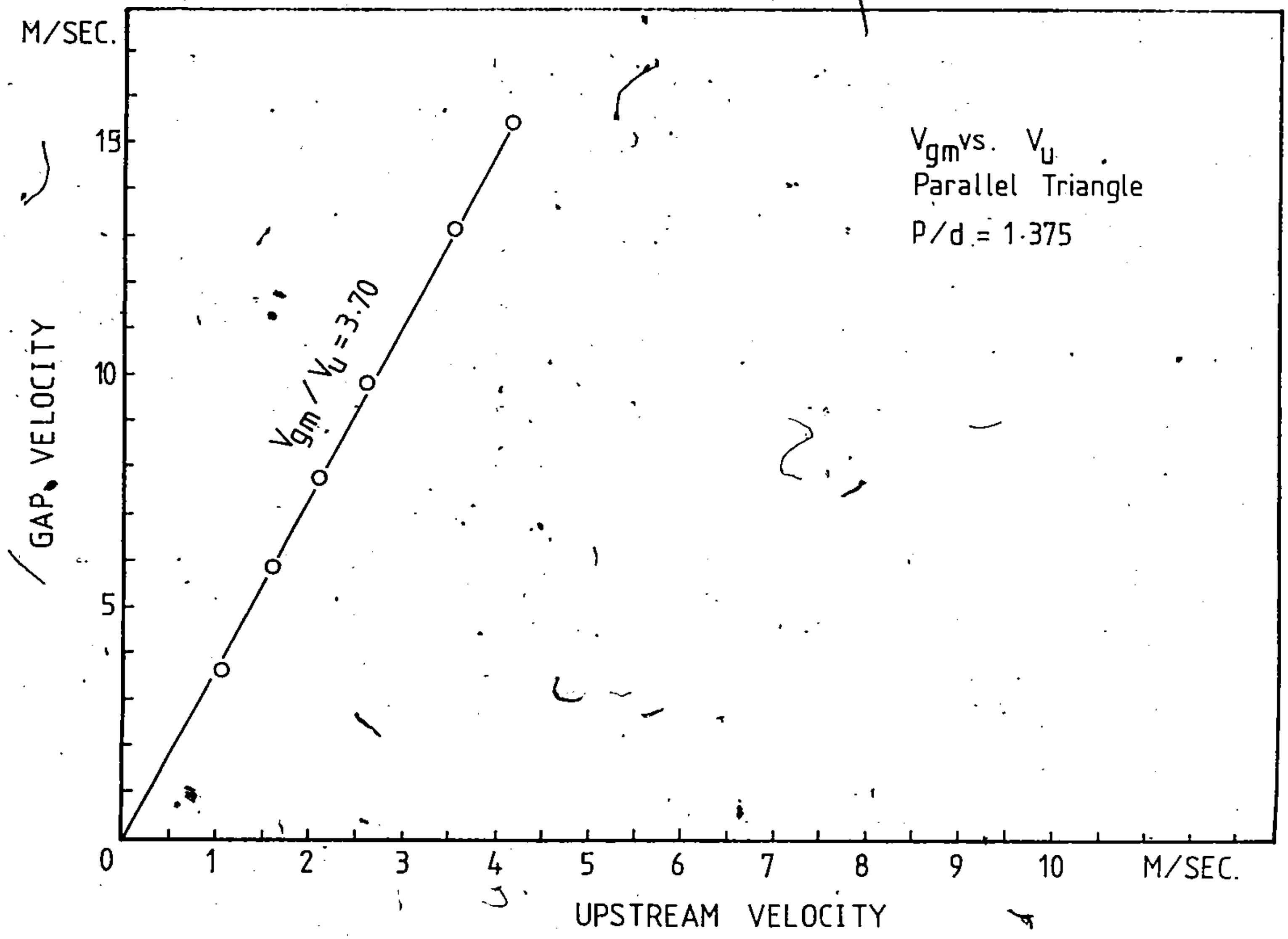

M/SEC.
GAP VELOCITY
V_{gm} vs. V_u
Parallel Triangle
P/d = 1·375
$V_{gm} / V_u = 3.70$
0
1
2
3
4
5
6
7
8
9
10
15
M/SEC.
UPSTREAM VELOCITY

FIGURE C - 7

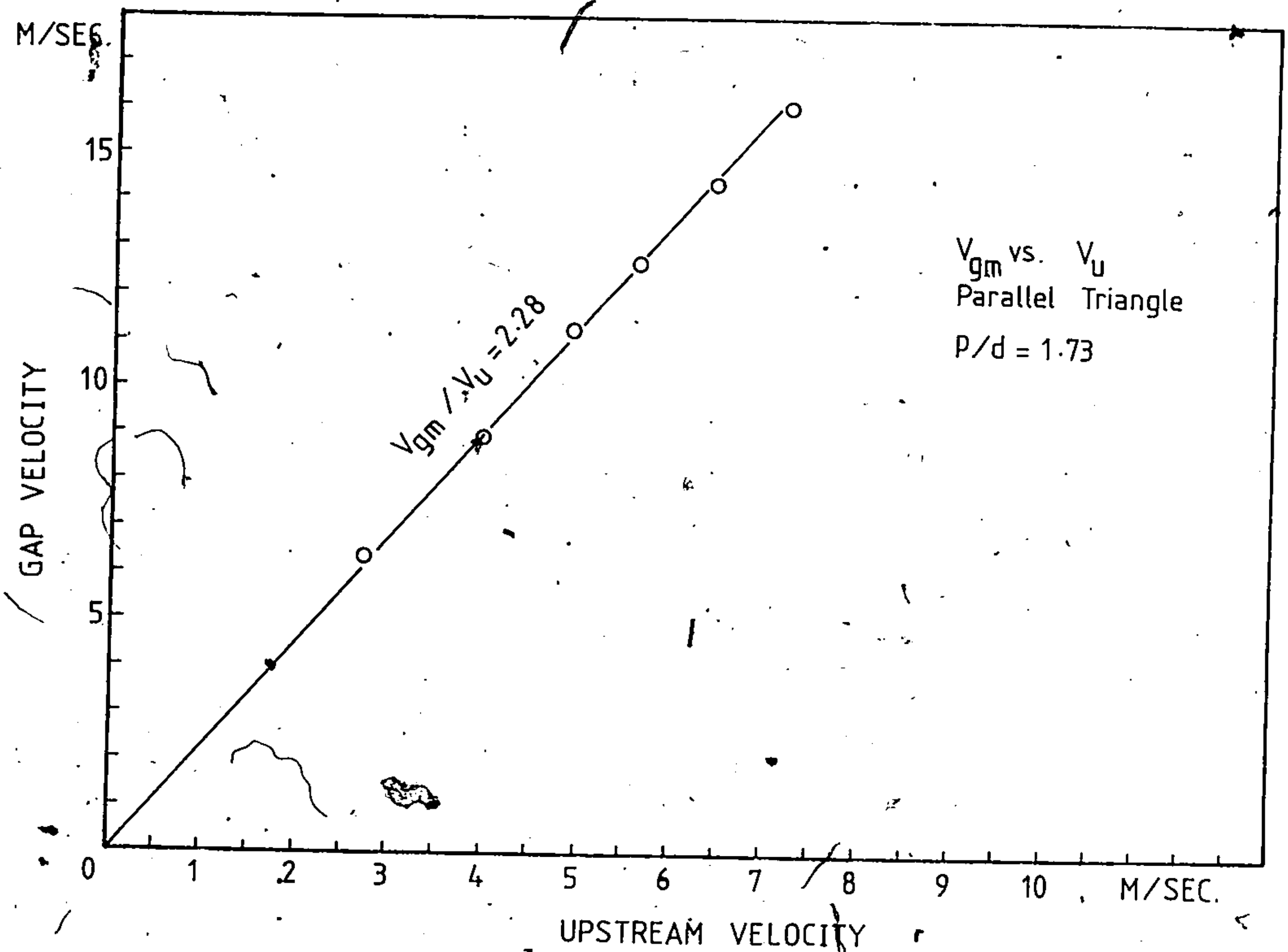

M/SEC.
GAP VELOCITY
15
10
5
0
1
2
3
4
5
6
7
8
9
10
M/SEC.
UPSTREAM VELOCITY
$V_{gm} / V_u = 2.28$
V_{gm} vs. V_u
Parallel Triangle
P/d = 1.73

FIGURE C-8